The transport of integral membrane proteins across the nuclear pore complex

Meinema, Anne Cornelis

The transport of integral membrane proteins across the nuclear pore complex

Cover: An artist impression of a membrane protein in transit through the nuclear pore complex.
Artwork by Graham Johnson, grahamj.com.
Design by Eduard Madrid, dsign-ed.com.
Model of nuclear pore complex: Alber et al., 2007.

Printed by: BOXPress BV/proefschriftmaken.nl
Oisterwijk

ISBN: 978-90-367-5517-7 (printed version)
978-90-367-5518-4 (electronic version)

The work published in this thesis was carried out in the Biochemistry department of the Groningen Biomolecular Sciences and Biotechnology Institute (GBB) of the University of Groningen, The Netherlands. The research was financially supported by the Netherlands Organization for Scientific Research (NWO).

rijksuniversiteit
groningen

The transport of integral membrane proteins across the nuclear pore complex

Proefschrift

ter verkrijging van het doctoraat in de
Wiskunde en Natuurwetenschappen
aan de Rijksuniversiteit Groningen
op gezag van de
Rector Magnificus, dr. E. Sterken,
in het openbaar te verdedigen op
vrijdag 25 mei 2012
om 16:15 uur

door

Anne Cornelis Meinema

geboren op 26 november 1982

te Noordoostpolder

Promotor:	Prof. dr. B. Poolman
Copromotor:	Dr. L.M. Veenhoff
Beoordelingscommissie:	Prof. dr. M. Fornerod Prof. dr. P.M. Lansdorp Prof. dr. P. van Haastert

ISBN: 978-90-367-5517-7

- Laat geslacht na geslacht van uw schepping verhalen... -
Psalm 145:4

- Heb een open oor en een open geest voor kennis -
Spreuken 23:12

- Het vermogen je te verwonderen is belangrijker dan genialiteit -
Naar: De wereld van Sofie, Jostein Gaarder

Table of contents

Chapter 1

The nuclear envelope, the NPC and the transport of membrane proteins into the nucleus

- An introduction -

Anne C. Meinema and Liesbeth M. Veenhoff

Abstract

The nucleus is one of the largest organelles in eukaryotic cells, it contains most of the cells genome and keeps the DNA segregated from the cytoplasm. The development of the membrane-bound structure of the nucleus, the nuclear envelope (NE), was the evolutionary event that gave rise to eukaryotes. From that point on, the nuclear envelope-embedded nuclear pore complexes (NPCs), formed the selective barrier to the flow of information that represents the central dogma in molecular biology – DNA makes RNA makes proteins –. The nuclear envelope also protects and organizes the genome and as such has fundamental impact on cellular organization and complexity. A growing list of integral membrane proteins of the nuclear envelope are described to function in the organization of the genome as well as the assembly of the NPCs. In this thesis, we studied how the nuclear pore complex sorts these proteins between the nuclear and cytoplasmic compartments to obtain a specific protein composition of the inner membrane.

Proteins of the inner nuclear membrane

The NE consists of two phospholipid bilayers, called the inner and the outer nuclear membrane (INM, ONM), with the lumenal space in between (Fig. 1.1). The INM faces the nucleoplasm and contains proteins that are involved in chromatin organization and the maintenance of nuclear stability via interactions with the nuclear lamina (Dechat *et al.*, 2008). The nuclear lamina is a network of filaments present in metazoan nuclei that aligns with the INM (Gruenbaum *et al.*, 2005). Baker's yeast lack the lamina, but have an INM-associated protein called Esc1 (Enhancer of silent chromatin 1), that shares features with components of the lamina in metazoans (Taddei *et al.*, 2004). The ONM is continuous with the endoplasmic reticulum (ER) of the cell and has partially overlapping functions in the transport, synthesis and folding of proteins, and the synthesis of lipids (Voeltz *et al.*, 2002). While the NE is a cisternal membrane structure, the ER forms cisternae (flattend membrane disks) as well as tubules (tube structures) (West *et al.*, 2011). In mammalian cells, most of the ER network lies around the nucleus, while in baker's yeast most of the ER aligns the plasma membrane (Fig. 1.1).

Historically, the NE was viewed as little more than a diffusion barrier between the cytoplasm and the nucleoplasm. But nowadays, the nuclear envelope is known to have a function in the genome architecture, epigenetics, transcription, splicing, DNA replication and control of the cell cycle. Also cytoskeletal stability, cell migration, and nuclear positioning are dependent on nuclear envelope function. In all of these aspects integral membrane proteins of the INM play a crucial role [reviewed in (Heessen and Fornerod, 2007;Gruenbaum *et al.*, 2005;Wilson and Foisner, 2010;Hetzer and Wente, 2009;Zuleger *et al.*, 2008)]. Using a proteomic study, Schirmer and coworkers identified initially ~80 nuclear envelope transmembrane proteins (NETs) in liver cells (Schirmer *et al.*, 2003;Zuleger *et al.*, 2011b) and later dozens unique hits were found in different other cell types (Korfali *et al.*, 2010;Wilkie *et al.*, 2011;Schirmer and Gerace, 2005). Apart from the membrane proteins of the NPC, only a small fraction of NETs is well studied. The vast

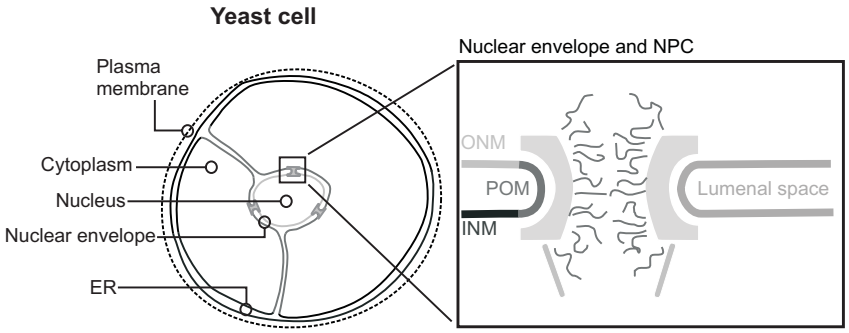

Figure 1.1: Simplified scheme of the geometry of the NE-ER network. The yeast endoplasmic reticulum (ER) adheres to the plasma membrane, while the mammalian ER is positioned throughout the cytosol and around the nucleus. The ER is continuous with the ONM. Insets: the outer nuclear membrane (ONM) is continuous with the inner nuclear membrane (INM) via the pore membrane (POM). The nuclear pore complex (NPC) is anchored at POM in the nuclear envelope (NE).

majority are lamina-associated proteins (LAPs), including LAP1, LAP2, LBR, Emerin, MAN1, Nurim, SUN1, SUN2, Unc-84, LEM2/NET25. Mutations in the lamins or in the LAPs are linked to many diseases which range from muscular dystrophies to lipodystrophies, neuropathy, osteopoikilosis, and premature aging syndromes (Dauer and Worman, 2009;Wilkie and Schirmer, 2006;Worman *et al*., 2010).

Different families or domains can be recognized among the proteins of the inner nuclear membrane. One of these families is the SUN (*Schizosaccharomyces pombe* Sad1 and *Caenorhabditis elegans* Unc-84 homology)-protein family, which is conserved among the eukaryotes and includes also the human SUN1 and SUN2 and the yeast Mps3 proteins. The SUN-proteins are localized at in INM and form a stable bridge with members of the KASH (*Drosophila* Klarsicht, *C. elegans* ANC-1, and the mammalian paralogs Syne/Nesprin-1 and -2)-protein family, which are exclusively localized at the ONM. While bridged in the lumenal space, the SUN-proteins interacts with the lamina and the KASH proteins with the cellular cytoskeleton. The SUN-KASH interaction, also referred to as the linker of nucleoskeleton and cytoskeleton (LINC) complex, is important to the position the nucleus in the cell and to transfer signals and forces across the NE (reviewed in (Starr and Fridolfsson, 2010)).

Many lamina associated proteins share the LEM (LAP2, Emerin, MAN)-domain of ~40 – 50 conserved residues at or near their N-terminus (Laguri *et al*., 2001;Lin *et al*., 2000). The LEM domains bind chromatin via a 10 kDa small protein named BAF (Barrier-to-autointegration factor), which is conserved in different species (Margalit *et al*., 2007;Cai *et al*., 1998;Cai *et al*., 2001;Furukawa, 1999;Lee and Craigie, 1998). While the majority of characterized NET interacts with chromatin-associated proteins, some NETs bind directly to chromatin. MAN1 and LEM2 for example binds directly to DNA via their conserved C-terminal winged helix domain (Caputo *et al*., 2006), later called the Man1/Src1 C-terminal domain (MCS) (Grund *et al*., 2008) or Man1 C-terminal homology domain (MCHD) (Yewdell *et al*., 2011). LAP2β binds DNA using a domain on its N-terminus (Cai *et al*., 2001). Transcriptional regulation by inner membrane proteins occurs

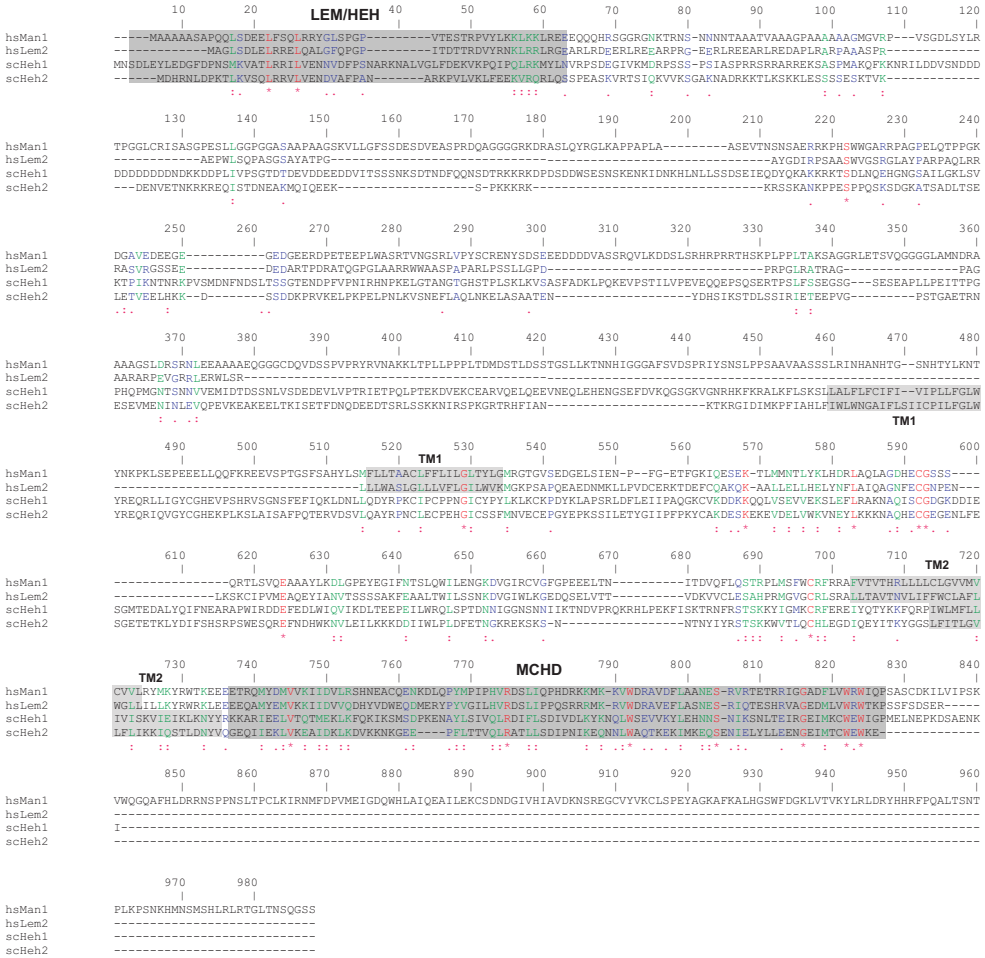

Figure 1.2: Sequence alignment shows conservation of the HEH/LEM-domain and the Man1 C-terminal homology domain. The amino acid sequence alignment of the saccharomyces cerevisiae Heh1 and Heh2 (scHeh1, scHeh2) and the human Man1 and Lem2 (hsMan1, hsLem2) was performed with Clustal W (Thompson *et al.*, 1994). Similarity was found in the HEH/LEM-domain, the MAN1 C-terminal homology domain (MCHD) and some in the lumenal domain between the first (TM1) and the second transmembrane segment (TM2). An asterisk (*) and red colored residue indicates identical amino acids, whereas the dots (: and .) and green colored residue indicate a decreased similarity.

via the tethering of particular chromosome regions to the NE and orchestrating the recruitment of transcriptional activators or silencers. For example, MAN1 was found to interact with the Smad transcription factors, which are crucial regulators for growth factors (transforming growth factor β or bone morphogenic proteins). Histone deacetylases, that are associated with promoter repression in general, interact with Emerin (Holaska and Wilson, 2007) and Lap2β (Nili *et al.*, 2001;Somech *et al.*, 2005) and as such may explain partly how NE tethering induces repression (Egecioglu and Brickner, 2011). The INM localized protein Lamin B Receptor (LBR) features a sterol reductase domain at its extralumenal domain (Silve *et al.*, 1998). The presence of LBR in

the INM is required to maintain the size and shape of the NE (Hoffmann *et al.*, 2002). Mutations in LBR or loss of function cause malformation of the nucleus and lead to different disorders (Hoffmann *et al.*, 2007).

In *Saccharomyces cerevisiae* several INM-localized proteins have been studied: Doa10 is a transmembrane ubiquitin ligase that targets nuclear proteins for degradation (Deng and Hochstrasser, 2006). Src1/Heh1 and Heh2 are actively transported to the INM and show homology with MAN1 and LEM2 ((King *et al.*, 2006), Fig 1.2). They have a role in NPC assembly (Yewdell *et al.*, 2011), and Src1/Heh1 has a role in subtelomeric gene expression, mRNA export and chromatin segregation (Grund *et al.*, 2008;Rodriguez-Navarro *et al.*, 2002). Nur1 together with Heh1, tethers the ribosomal DNA to the INM in order to stabilize the highly repetitive sequence of the rDNA (King *et al.,* 2006;Mekhail *et al.*, 2008). Mps3 is a component of the spindle pole body (Gardner *et al.*, 2011), and Asi1, Asi2 and Asi3 are involved in the regulation of the transcription factors Stp1 and Stp2 (species-specific tRNA processing protein), which control the cellular import of amino acids (Zargari *et al.*, 2007;Boban *et al.*, 2006). Altogether, the INM-localized proteins have essential roles in the spatial organization of the chromatin and the regulation of gene-expression, as well as maintaining the general architecture and stability of the nucleus.

The structure of the NPC

All transport between the cytoplasm and nucleus occurs through highly selective gates, called nuclear pore complexes. The NPCs are embedded in the NE and the ONM is connected with the INM in the NPC via a highly curved pore membrane (POM) (Fig. 1.1). The NPC is likely the largest molecular 'machine' in the cell, composed of ~30 different proteins (Cronshaw *et al.*, 2002;Rout *et al.*, 2000), of which in fact only a core subset is stably attached to the NPC (Rabut *et al.*, 2004). In yeast, each of the NPC proteins is present in multiple copies, totaling to 456 proteins per NPC (Alber *et al.*, 2007b) and a mass of ~50 MDa. The proteins that form the NPC are collectively named nucleoporins (Nups). The overall structure of the NPC has been extensively studied by electron microscopy and proteomic approaches, and its overall 8-fold rotational symmetric shape (Fig. 1.3A, B) is conserved over the species (reviewed in (Brohawn *et al.*, 2009). 3-dimensional electron microscopy of *Dictyostelium discoideum* nuclei and *Xenopus* oocytes nuclear envelope spreads showed that the diameter of the NPC ranges from 100 to 150 nm and the thickness from 35 to 70 nm in the different species; the aqueous central channel is about 30 to 50 nm wide (Beck *et al.*, 2007;Frenkiel-Krispin *et al.*, 2010;Stoffler *et al.*, 1999;Beck *et al.*, 2004). Besides the typical octagonal circular symmetry around the transport axis in the center, the scaffold of the NPCs also shows symmetry in the plane of the membrane (Fig. 1.3C), and the copy number of Nups in the NPC is likely a factor of eight (8, 16 or 32).

The peripheral components of the NPC differ at both sides. The nuclear side contains the nuclear basket structure that protrudes 90 – 120 nm into the nucleoplasm and is involved in mRNA export, spindle pole body assembly and chromatin organization. At the other side, approximately 35 – 50 nm long fibrils extent out into the cytoplasm, and these function in protein entry to the NPC (reviewed in: (Schwartz, 2005)).

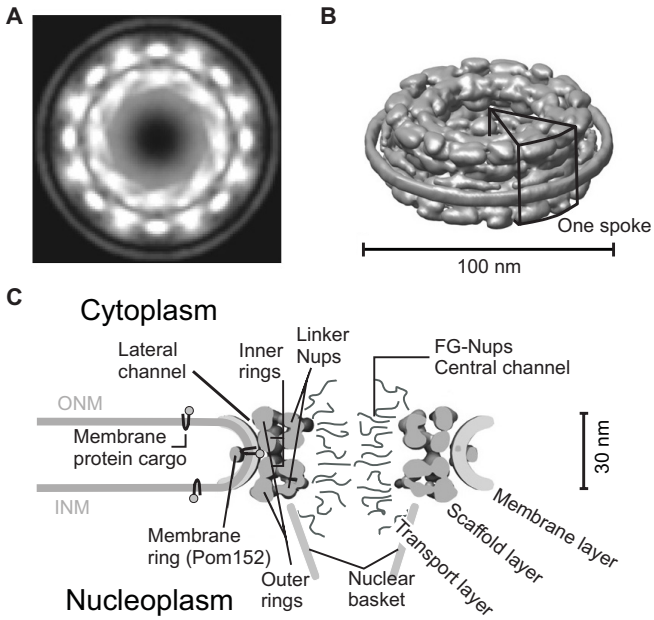

Figure 1.3: The structure of the NPC. (A) The distribution of the nucleoporin mass density (white) within the yeast NPC shows the eigth-fold rotational symmetry, projected from the cytoplasmic side (Alber *et al.*, 2007a;Alber *et al.*, 2007b) **(B)** A model of the yeast NPC was made on the basis of a large array of experimental data and subsequent computational modeling (Alber *et al.*, 2007a;Alber *et al.*, 2007b); one symmetry unit (spoke) is indicated. **(C)** A schematic vertical cross section of the NPC shows the different layers in the NPC and the scaffold symmetry about the plane of the NE. The ~10 nm wide lateral channels and the ~50 nm wide central channel are indicated. This schematic is based on the model of the NPC from (Alber *et al.*, 2007a;Alber *et al.*, 2007b). The models and images are reproduced with permission.

When looking at the position of the individual Nups within the NPC one can distinguish 3 co-axial layers: A) a membrane layer, B) a scaffold layer and C) a barrier or transport layer, each composed of separate sets of Nups (Table 1, Fig. 1.3C) (Alber *et al.*, 2007b;Hoelz *et al.*, 2011;Onischenko and Weis, 2011). The yeast components and their vertebrate counterparts are indicated in Tabel 1; they have similar domain compositions, as far as studied they have a similar position within the NPC and perform similar functions. The membrane layer consists of integral membrane proteins anchoring the NPC to the POM. The scaffold layer is the spoke-ring complex of the two outer rings, one at the nuclear side and one at the cytoplasmic side, sandwiching the two inner rings. The transport layer consists of linker Nups and FG-Nups (Fig. 1.3C). The function of components of the NPC in recruiting protein, RNA and DNA components to regulate silencing, transcription, mRNA quality control and export, cell cycle control and diverse other functions are not discussed in this chapter. We will focus in more detail on the structure of the NPC and its function in nuclear transport.

A) At the sharply curved POM, where the ONM joins the INM, the membrane layer is formed by three integral membrane proteins. These pore membrane proteins, Pom152

Table 1.1

Composition of the NPC	
Yeast	*Vertebrate*
A) Membrane layer	
Ndc1	Ndc1
Pom34	-
Pom152	-
Nup53	Nup35
Nup59	Nup35
-	gp210
-	Pom121
Pom33	-
B) Scaffold layer, outer ring	
Nup84	Nup107
Nup85	Nup75/Nup85
Nup120	Nup160
Nup133	Nup133
Nup145C	Nup96
Sec13	Sec13
Seh1	Seh1
-	Nup37
-	Nup43
-	ALADIN
B) Scaffold layer, inner ring	
Nup157	Nup155
Nup170	Nup155
Nup188	Nup188
Nup192	Nup205

Composition of the NPC	
Yeast	*Vertebrate*
C) Transport layer, linker Nups	
Nic96	Nup93
Nup82	Nup88
C) Transport layer, FG-Nups	
Nup1	Nup153
Nup42	NLP1/hCG1
Nup49	Nup58/Nup45
Nsp1	Nup62
Nup57	Nup54
Nup53	Nup35
Nup59	Nup35
Nup60	-
Nup100	Nup98
Nup116	Nup98
Nup145N	Nup98
Nup159	Nup214/CAN
NPC-associated components	
Mlp1	Tpr
Mlp2	Tpr
-	Nup358

Table 1. The composition of the NPC (adapted from (Alber *et al.*, 2007b;Hoelz *et al.*, 2011;Onischenko *et al.*, 2011)).

(Wozniak *et al.*, 1994), Pom34 (Miao *et al.*, 2006) and Ndc1 (Chial *et al.*, 1998) anchor the NPC at the NE (Alber *et al.*, 2007b). The large soluble domains of Pom152 form a stable ring-structure in the lumenal space of the NE (Strambio-de-Castillia *et al.*, 1995) (Fig. 1.3B, C). The three integral membrane proteins form a stable complex with each other (Onischenko *et al.*, 2009).

B) The architectural model by Alber *et al.* (Fig. 1.3), generated by a combined experimental and computational approach, shows that the spoke-ring scaffold layer consists of inner and outer rings (Alber *et al.*, 2007a;Alber *et al.*, 2007b). The outer rings are composed of the seven Nups that constitute the Nup84-subcomplex. This complex

has been extensively studied by the Hurt, Schwartz, Blobel/Hoelz laboratories (Alber *et al.*, 2007b;Amlacher *et al.*, 2011;Brohawn *et al.*, 2009;Hoelz *et al.*, 2011), and high resolution structures are available of several of the Nups. The other essential core complex is composed of Nup157, Nup170, Nup188 and Nup192, which directly connects to Nic96, Nup53 and Nup59 and as such bridges the membrane proteins and the transport layer (Amlacher *et al.*, 2011). Nup157, Nup170, Nup188 and Nup192 form the inner rings in the architectural model (Alber *et al.*, 2007b). α-Solenoids and β-propellers form the building blocks of the NPC scaffold in an arrangement similar to that of clathrin-coats, reflecting the shared function in stabilizing sharply curved membranes (Devos *et al.*, 2004). Between the scaffold layer and the pore membrane are peripheral or lateral channels (Fig. 1.3C), which have been proposed to allow membrane proteins to diffuse across the NPC. These lateral channels have been reported to be 10 nm in diameter and would allow membrane proteins with a soluble domain of ~50 – 60 kDa to diffuse from the ONM to the INM (Worman and Courvalin, 2000;Frenkiel-Krispin *et al.*, 2010;Hinshaw *et al.*, 1992;Soullam and Worman, 1995).

C) The transport layer facilitates the movement of cargo across the NPC, while it blocks the translocation of non-cargo. It is thus both a transport channel and a selective barrier (reviewed e.g. in (Peters, 2009). The transport layer consists of a subset of Nups, having a small terminus that is well-folded and anchored to the scaffold of the NPC while the other terminus is long, unstructured and rich of phenylalanine-glycine repeats (FGs) (Strawn *et al.*, 2004). These FG-Nups protrude their disordered FG-domains into the 30 – 50 nm wide central channel of the NPC. The transport channel is thus filled with the long unstructured filaments, yielding an effective pore radius of 3 – 4 nm to restrict the free diffusion across to NPC to small molecules (Keminer and Peters, 1999;Pante and Kann, 2002). As discussed below, the transport of cargo is facilitated by transport factors binding to the FG-repeats while the movement of other proteins across the NPC is repelled by the unfolded FG-Nups (Terry and Wente, 2009). Individual FG-Nup proteins may consist of up to 50 FG repeats, separated by hydrophilic linkers of 5 – 50 residues. Taking into account the stoichiometry of FG-Nups per NPC (Rout *et al.*, 2000), there are in total about 190 FG-Nups and about 2700 FG-motifs per NPC. Some Nups that are listed as part of the transport layer have few (Nup59, Nup53) or none (Nic96, Nup82) of these unfolded FG-repeats and function as a bridge between the different subcomplexes.

Despite more than 50 years of research on the structure and function of the NPC (Watson, 1959), many new insights are still presented each year (Hoelz *et al.*, 2011;Kahms *et al.*, 2011;Strambio-de-Castillia *et al.*, 2010;Wente and Rout, 2010). It remains intriguing, that the architecture of the NPC forms a sophisticated complex that stabilizes an opening in the NE by maintaining the sharp curvature of the POM and facilitates the transport of cargo to the nucleus while obstructing the passage of non-cargo.

Nuclear transport of soluble proteins

The NPC handles large amounts of proteins; the capacity of the NPC is estimated at 500 – 1000 molecules per second (Görlich *et al.*, 1996;Smith *et al.*, 2002;Dange *et al.*, 2008;Yang *et al.*, 2004). It also transports rather large structures such as ribosomal subunits (Johnson *et al.*, 2001;Yao *et al.*, 2007;Zemp and Kutay, 2007) and messenger RNA-protein complexes (mRNPs, (Mehlin *et al.*, 1992)). Even virus capsids of 32 and 36 nm in diameter or gold particles up to 39 nm in diameter are transported across the NPC (Pante and Kann, 2002). Small molecules, like water, ions, peptides and small proteins, are able to diffuse freely through the central channel of the NPC. In general, it is accepted that macromolecules bigger than ~40 kDa or having a Stokes radius larger than ~5 nm require active import to overcome the selective permeability barrier of the NPC at an appreciable rate (Keminer and Peters, 1999). The defining feature of cargo is the nuclear localization signal (NLS) or nuclear export signal (NES). The well-exposed transport signals are recognized and bound by transport receptors, which shuttle the cargo across the permeability barrier of the NPC (Pemberton and Paschal, 2005). There are 15 identified nuclear transport receptors in yeast (and 20 in human cells), which are collectively named as karyopherins (Kaps) (Quan *et al.*, 2008). In the 'classical import pathway', the Kapα transport factors, one in baker's yeast and six in human cells, recognize NLSs on cargo and bind to a family member of the larger Kapβ-family (Conti and Izaurralde, 2001;Gorlich and Kutay, 1999;Tran *et al.*, 2007;Weis, 2003). In other cases, the transport can be independent of Kapα and mediated by direct recognition of the NLS or NES by a Kapβ. The availability of different Kaps enables the cell to regulate the transport of different types of cargo (Terry *et al.*, 2007).

The 'classical import pathway' is the best-studied and is mediated by the cooperation of Kapα and Kapβ (Kap60 and Kap95 in yeast). Proteins imported via this pathway have an NLS resembling the classical NLS (cNLS), identified in the semian virus 40 (SV40) large T-antigen (PKKKRKV) (Dingwall *et al.*, 1982;Dingwall and Laskey, 1991). The general principles of nuclear transport are the same for the different transport pathways, and we will explain the classical import cycle as an example for nuclear import and export. The nuclear transport can be divided in four steps: I) the cargo is recognized and bound by karyopherins in the cytoplasm, II) the karyopherins transport the cargo across the NPC, III) the complex is dissociated in the nucleus and the cargo remains here, and IV) the Kaps are shuttled back to the cytoplasm. Essential for driving nuclear transport is V) the Ran-cycle, which maintains the asymmetric localization of RanGTP in the nucleus and RanGDP in the cytoplasm to provide a concentration gradient across the NPC (Fig. 1.4 and reviewed in (Stewart, 2007)).

I. The transport cycle of cargo via the classical pathway starts with the binding between the basic residues of the cNLS and Kapα, followed by the subsequent binding of Kapα to Kapβ1. Proteins bearing a cNLSs need a Kapα as an adapter protein for Kapβ binding, other cargos are directly bound by Kapβ (Goldfarb *et al.*, 2004). For stronger interaction with Kapα, some proteins bear a bipartite NLS, consisting of two clusters of basic residues separated by a linker (Lange *et al.*, 2010;Robbins *et al.*, 1991).

The first cluster binds the Armadillo (ARM)-repeats 1-4 in the first binding groove of Kapα and the second cluster binds the ARM-repeats 6-8 in the second groove (Conti and Kuriyan, 2000).

The N-terminus of Kapα binds to Kapβ1 and is known as the importin-β binding (IBB)-domain (Gorlich *et al.*, 1996). The IBB-domain has a cluster of basic residues that resembles an NLS and binds one of the NLS-binding grooves on Kapα (Kobe, 1999). Cargo competes with the IBB-domain for the same binding site on Kapα. Upon cargo binding, the IBB of Kapα gets exposed and the affinity for Kapβ1 is increased.

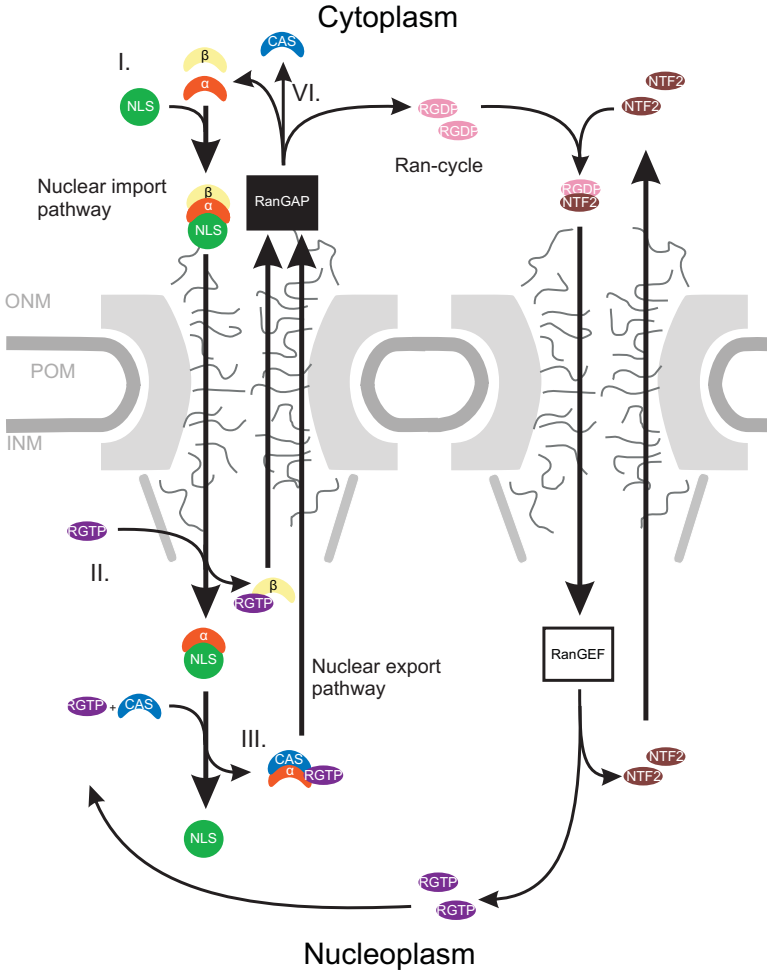

Figure 1.4: Overview of the components of nuclear transport. The nuclear import complex is formed between NLS-bearing cargo (NLS), karyopherin-α (α) and karyopherin-β (β). After passing the NPC, RanGTP (RGTP) dissociates karyopherin-β from the complex and shuttles back to the cytosol. Karyopherin-α is displaced from the complex by the exportin CAS and RanGTP. The cargo remains in the nucleus and karyopherin-α is exported back to the cytoplasm. The Ran GTPase activating protein (RanGAP) in the cytoplasm hydrolyzes the export complex-associated RanGTP to RanGDP (RGDP) to release karyopherin-β, karyopherin-α and CAS. To reset the Ran-cycle, the RanGDP is re-imported to the nucleus by NTF2 and converted to RanGTP by the Ran Guanine nucleotide exchange factor (RanGEF). The figure is based on (Stewart, 2007).

In turn, Kapβ1 interacts with the FG-repeats in the NPC to transport the Kapα-cargo complex into the nucleus (reviewed in (Stewart, 2007)). This auto-inhibitory mechanism of Kapα prevents binding to Kapβ1 when no cargo is bound and thus prevents futile cycling of empty Kapα across the NPC. For an overview of the molecular role played by the IBB domain in orchestrating nucleocytoplasmic transport see (Lott and Cingolani, 2011).

II. How exactly the complex is translocated across the pore is under fierce debate. Although the transport across the NPC can be mimicked *in silico* and *in vitro* (Smith *et al.*, 2002;Zilman *et al.*, 2010;Cai *et al.*, 2001;Jovanovic-Talisman *et al.*, 2009;Kowalczyk *et al.*, 2011), it remains still controversial how the cargo is exactly transported. In the recent years, different models are proposed to describe the mechanism of the actual transport. They have in common that the interactions between Kapβ1 and the FG-repeats are needed, and that the trimeric complex diffuses through the FG-Nup meshwork according to a random walk to cross the NPC (Peters, 2009;Stewart, 2007;Weis, 2007). The models aim to explain the selectivity of the NPC, i.e. the discrimination between cargo and non-cargo, while taking in account that cargo can cross the NPC within 10-20 ms (Cardarelli and Gratton, 2010;Yang *et al.*, 1998). We will discuss the four most prominent models:

a. The Brownian-affinity gating or virtual gating model (Rout *et al.*, 2000) describes the NPC as an entropic barrier for diffusion of non-cargo into the nucleus. The high concentration of FG-Nups in the central channel prevent cargo entering the NPC and facilitates the entrance of cargo. The binding energy from the interaction between Kap-cargo and FG-Nups lowers the overall free energy barrier and enables passage. The FG-Nups extend into the central channel and are highly dynamic. As long as the interactions between Kap and FGs are not too strong, and binding and unbinding are fast, efficient transport across the NPC is assured (Rout *et al.*, 2000). One variant on this model predicts an affinity gradient for the Kap-cargo complex in the central channel, promoting the direction of nuclear transport (Ben-Efraim and Gerace, 2001). Another variant, the reversible FG-domain collapse model, explains a higher selectivity of the NPC. This model predicts that upon cargo interaction, the FG-domain at the cytoplasmic side of the NPC collapse and pull specifically the Kap-cargo complex into the transport channel, where it undergoes the cycles of random binding and unbinding as predicted by the virtual gating model (Lim *et al.*, 2006).

b. The selective phase model describes that the FG-repeats of Nups are interconnected by weak hydrophobic interactions to form a hydrogel (Ribbeck and Gorlich, 2002). This hydrogel fills the central channel of the NPC and acts like

a sieve with a small pore sizes so that only proteins smaller than 40 kDa can pass through. Kap-cargo complexes can form hydrophobic interactions with the FG-Nups and thus dissolve into the hydrogel (Ribbeck and Gorlich, 2002). A hydrogel of a concentrated solution of single FG-Nups was formed *in vitro* (Frey *et al*., 2006) and fast diffusion into the gel was demonstrated (Frey and Gorlich, 2007).

c. To explain fast diffusion across the NPC, the reduction of dimensionality model predicts that the FG-Nups form one coherent hydrophobic layer that coats the walls of the central channel. Kap-cargo complexes can interact with the hydrophobic layer, while a hole of 8 – 10 nm is left open for diffusion of small proteins. This predicted organization in the NPC allows Kap-cargo to diffuse in 2-dimensions along the walls of the channel, which would increase the transport rate (Peters, 2005;Peters, 2009).

d. The Forest-model is a merge of the virtual gate and the hydrogel models. It describes that some Nups adopt a globular or collapsed conformation, while others are more dynamic extended coil structure. These two types of Nups form two distinct traffic zones in the interior of the NPC, of which zone 1 in the center would allow diffusion of larger proteins and could act as the virtual gate. Zone 2 consists of a thin hydrogel along the walls of the channel and small cargo could dissolve in this layer (Yamada *et al*., 2010).

III. Once the Kap-cargo complex reaches the nuclear side of the NPC, Kapβ gets bound by the small molecule RanGTP and its conformation changes so that it is no longer able to bind the cargo-Kapα dimer. The cargo-Kapα dissociates from Kapβ and is released into the nucleus. This dissociation is dependent on RanGTP and occurs specifically at the nuclear side of the NPC, because the RanGTP concentration is highest in the nucleus. The binding of Kapβ by RanGTP promotes the interaction between Kapβ and the FG-Nups, which facilitates the diffusion of Kapβ back to the cytoplasm (Görlich *et al*., 1996;Rexach and Blobel, 1995). Kapα is bound by the exportin CAS (or Cse1 in yeast) and RanGTP (Kutay *et al*., 1997) and exported back to the cytoplasm through the NPC, while interacting with the FG-Nups. The export of Kapα is mechanistically similar to the export of NES-bearing cargos with the use of CAS instead of the nuclear export receptor CRM1 (Fornerod *et al*., 1997).

IV. Once the dimeric complex of Kapβ-RanGTP and the trimeric complex of Kapα-RanGTP-CAS are translocated across the NPC and enters the cytoplasm, RanGAP (Ran GTPase activating protein or RCC1 in vertebrates) stimulates, together with the accessory protein RanBP1, the hydrolysis of RanGTP to RanGDP (Bischoff and

Gorlich, 1997;Görlich *et al.*, 1996). The complexes are dissociated, to set Kapβ and Kapα free for another import cycle. CAS is unable to bind Kapα in the absence of RanGTP; this will thus not happen in the cytoplasm. CAS diffuses back to the nucleus through the NPC.

V. RanGDP needs NTF2, a small factor of 15 kDa for its transport back to the nucleus (Ribbeck *et al.*, 1998;Smith *et al.*, 1998). Here, RanGDP is phosphorylated to RanGTP by RanGEF (Ran guanine exchange factor) at the expense of one ATP. Note that two RanGTP molecules are needed to dissociate the cargo from the trimeric import complex, and thus two molecules of ATP are consumed to import one cargo molecule to the nucleus(Bischoff and Ponstingl, 1995;Stewart, 2007). RanGEF is bound to chromatin, thus it is only found in the nucleus, while RanGAP exists exclusively in the cytoplasm. The asymmetric localization of RanGEF in the nucleus and RanGAP in the cytosol creates a gradient of RanGTP across the NE. This gradient assures that the import complexes are dissociated in the nucleus, while the export complexes are dissociated in the cytoplasm, giving directionality to nuclear transport.

Membrane protein insertion into the ER

INM-localized membrane proteins are synthesized and inserted into the ER. Like for other membrane proteins, the mRNA is translated at the ribosomes and the nascent polypeptide is inserted in the membranes of the ER via a protein translocation machinery. The vast majority of membrane proteins are co-translationally inserted into the ER via the Sec61 translocon. However, the insertion of some proteins, like the small C-terminal tail-anchored proteins, is post-translational and here the GET pathway is employed (reviewed in (Renthal, 2010;Schuldiner *et al.*, 2008;Hegde and Keenan, 2011)).

The targeting of most integral membrane proteins into the ER occurs via the Sec61 translocon and starts when the first hydrophobic segment emerges from the ribosome during translation. This hydrophobic segment, either a cleavable N-terminal signal sequence or the first transmembrane sequence, is recognized by the signal recognition particle (SRP) (Walter and Blobel, 1980) on the translating ribosome to slow down temporally the translation (Halic *et al.*, 2004). The SRP brings the ribosome to the ER via the interaction with the SRP receptor (SR) and transfers the complex to the Sec61 translocon (Meyer *et al.*, 1982). The ribosome docks at the translocon, and the hydrophobic segment of the nascent polypeptide chain is transferred from the SRP into the Sec61 translocon. If the hydrophobic element is a signal peptide, the soluble domain is translocated into the lumen of the ER and the signal peptide is cleaved off. On the contrary, a transmembrane domain is released into the membrane of the ER via the lateral gate of the translocon (reviewed in (Cross *et al.*, 2009;Osborne *et al.*, 2005;du Plessis *et al.*, 2011)). The topology of the membrane protein is defined by the insertion of the first transmembrane segment and depends

mainly on the charge distribution within the flanking sides of the transmembrane segments, but the folded state of translated domains and other factors may also influence the orientation of the protein in the membrane (reviewed in (van Klompenburg *et al.*, 1997)). For multispanning (or polytopic) membrane proteins, the adjacent transmembrane segments are subsequently inserted into the ER with alternating topology.

Tail-anchored proteins are small single-spanning membrane proteins having their transmembrane segment within ~40 residues of the C-terminus (Renthal, 2010). The transmembrane segment is so close to the C-terminus, that the translation is terminated before the transmembrane segment can be exposed in the cytoplasm. The tail-anchored protein is thus released from the ribosome before it could be recognized by the SRP (Kutay *et al.*, 1993). Post-translational insertion into the ER is needed to get the tail-anchored protein in the membranes. This pathway of targeting tail-anchored proteins has recently been studied in yeast, but it is not yet fully understood. The transmembrane segment is recognized by Sgt2 and transferred by the aid of Get4 and Get5 in an ATP-dependent manner to Get3 (Wang *et al.*, 2010). A homodimer of Get3 stabilizes the membrane protein and targets the molecule to the membrane receptor formed by Get1 and Get2, which integrate the tail-anchored membrane protein into the ER (Mariappan *et al.*, 2011;Hegde and Keenan, 2011).

Membrane protein transport to the INM

Two different mechanisms exist to target integral membrane proteins to the INM in cells that undergo an open mitosis: one occurring during the interphase and the second during the open mitosis. The NE of higher eukaryotes breaks down during mitoses, and the membranes of the NE, including INM proteins, are absorbed into the mitotic ER (Ellenberg *et al.*, 1997;Yang *et al.*, 1997). During the telophase, a new NE is formed around the decondensing chromatin. The membranes that will give rise to the INM are segregated from other membranes by the interaction of INM proteins to chromatin (Anderson *et al.*, 2009;Pyrpasopoulou *et al.*, 1996;Ulbert *et al.*, 2006). These INM proteins may thus be captured in the INM during the reformation of the NE and do not necessarily cross the NPC. A different targeting mechanism must apply in cells with a closed mitosis, like baker's yeast, and in higher eukaryotic cells during the interphase. Here, sorting of INM proteins relies on the transport of membrane proteins across the NPC. Once inserted into the ER, membrane proteins are able to diffuse freely between ER and ONM, and destined for the INM they need to cross the NPC via the pore membrane that connects the INM and ONM (reviewed in (Antonin *et al.*, 2011;Lusk *et al.*, 2007;Zuleger *et al.*, 2008)). In this thesis we will focus on the second mechanism.

Initially it was shown by Powel and Burke in heterokaryons (cells with two nuclei) that the INM-located integral membrane protein p55 was able to diffuse from one nucleus via the ER to the other. This showed in the first place that the ONM and INM are connected via the NPC and suggested that nuclear transport of membrane proteins is a diffusive process (Powell and Burke,

1990). Later, Soullam and Worman found that the N-terminal domain of LBR was essential for its targeting to the INM (Soullam and Worman, 1993). They demonstrated that this domain lacked an NLS and reasoned that the proteins accumulated in the INM "by diffusion and ligand binding". Subsequently, it was shown that the lateral diffusion rate of GFP-labeled LBR was reduced in the INM compared to the diffusion in the ER, probably due to specific and functional interactions with nuclear components (Ellenberg *et al.*, 1997). This led to the diffusion-retention model: a membrane protein is able to diffuses across the NPC and is retained in the nucleus by intranuclear interactions (Worman and Courvalin, 2000), like the binding to the lamina or heterochromatin. Thus, the transmembrane domain(s) remain in the pore membrane during the transport across the NPC, while the soluble domains pass through the lateral channel (Fig. 1.3C). The intra nuclear interactions are important for the localization of several membrane proteins, as was demonstrated that e.g. LBR, Emerin, MAN1 and SUN1 were tethered in the nucleus in different organisms (Wu *et al.*, 2002;Ellenberg *et al.*, 1997;Graumann *et al.*, 2007;Ostlund *et al.*, 1999;Worman and Courvalin, 2000;Ostlund *et al.*, 2006;Lu *et al.*, 2008;Zuleger *et al.*, 2011a).

Similar to the nuclear transport of soluble proteins, an upper size limit of 60 – 75 kDa was found, above which membrane proteins would not cross the NPC to reach the INM (Soullam and Worman, 1995;Wu *et al.*, 2002;Ohba *et al.*, 2004). As discussed by Hinshaw *et al.* and later by Soullam *et al.*, the narrow lateral channel in the NPC is about 10 nm wide and this is large enough to provide access for cytosolic domains up to 60 – 75 kDa (Hinshaw *et al.*, 1992;Soullam and Worman, 1995). Specifically in yeast, Deng and Hochstrasser determined that Doa10 (Ssm4), a yeast transmembrane ubiquitin ligase, accumulated in the INM by diffusion and retention (Deng and Hochstrasser, 2006). Interestingly, Doa10 could accumulate in the INM by diffusion across the NPC while having the soluble domain of an ER-localized protein Hrd1 (Der3), with a mass of 38 kDa plus one GFP copy of 28 kDa. Replacing this Hrd1-domain for a larger globular protein Pgk1 (~45 kDa), the cytoplasmic domain increased from ~66 to ~73 kDa, and nuclear accumulation was attenuated. This is consistent with the proposed upper size limit based on earlier studies in higher eukaryotes (Soullam and Worman, 1995).

However, some observations of Ohba *et al.* did not match the simple diffusion-retention model. It was found that nuclear transport of a membrane reporter based on Lap2β was dependent on metabolic energy; after ATP-depletion, the reporter did not accumulate at the INM but remained in the ER (Ohba *et al.*, 2004). The reporter did not have an NLS and so there was no reason to think that nuclear transport was dependent on Kaps. They argued that electron microscopic and tomographic studies of the NPC in the NE of *Xenopus laevis* had in fact not provided strong evidence for lateral channels in the NPC. They suggested that energy-dependent restructuring of the NPC could be needed for the diffusion of membrane proteins across the NPC. A model of the NPC was proposed, where "the NPC undergoes continuous, energy dependent restructuring…" which "…would create transient channels through the NPC at the nuclear pore membrane, thereby permitting lateral diffusional movement of integral proteins in the lipid bilayer between the INM and ONM" (Ohba *et al.*, 2004).

In the same year, another targeting mechanism for INM proteins was presented by Braunagel *et al.* They reported the finding of a sorting motif in the occlusion-derived virus (ODV) protein E66, which would target the membrane protein towards the NPC immediately after its synthesis (Braunagel *et al.*, 2004;Saksena *et al.*, 2004). A cluster of positively charged residues at the cytoplasmic site, immediately next to the predicted transmembrane segment, was marked as the INM sorting motif. This cluster would be recognized by an isoform of p10, the homologue of importin-α (Kapα) in *Spodoptera frugiperda*. They hypothesized that this isoform could target the protein through the ER to the NPC and even across the NPC (Saksena *et al.*, 2006).

In 2006, two proteins, Src1/Heh1 and Heh2, caught our attention in a proteomics study of yeast nuclear envelopes. They had predicted LEM-domains indicating localization at the INM and they featured putative NLSs (L.M. Veenhoff, unpublished). This raised the exciting possibility that these proteins may be imported by a mechanism alike that of soluble cargo and involving Kaps. Solid evidence, that Kap60 and Kap95 and RanGTP were needed for the INM-localization of these two yeast proteins, was published that same year (King *et al.*, 2006). Three other membrane proteins featuring an NLS were later found: the human Pom121 (Funakoshi *et al.*, 2011;Yavuz *et al.*, 2010), which is a component of the membrane layer and essential for NPC-assembly (Antonin *et al.*, 2005;Talamas and Hetzer, 2011) and two members of the SUN family, the human SUN2 and the *C. elegans* Unc-84 (Tapley *et al.*, 2011;Turgay *et al.*, 2010). However, critics rightfully pointed out that the prevalence of these sequences within INM proteins, which are rich of positively charged residues, could be a contribution to their chromatin binding function (Antonin *et al.*, 2011). Hypothetically, these putative chromatin-binding motifs could in principle support the capture of INM proteins by chromatin-binding and their retention at the INM. The best proof to distinguish the function of these sequences as being an NLS or a chromatin-binding motif, is to study if the nuclear localization is karyopherin and RanGTP dependent and if it can redirect a non-nuclear protein into the nucleus. Such experiments have not been successfully performed, adding to the doubts in the field. Further complications arrived as it was actually shown that location of Unc-84 in the INM of *C. elegans* cells requires multiple targeting signals, namely two NLSs plus an INM sorting motif and a SUN-nuclear envelope localization signal (Tapley *et al.*, 2011). SUN2 targeting is also complicated, as in addition to a classical NLS, two other elements are needed for its proper INM localization (Turgay *et al.*, 2010). One element is an arginine cluster that serves to recruit COPI components to retrieve SUN2 from the Golgi to the ER, i.e. in the case it escapes via the secretory pathway. The other element is a SUN domain which is located within the luminal space between ONM and INM, interacting with a KASH-domain and tethering SUN2 at the INM. Many INM-localized proteins do not have predicted NLSs, and their nuclear targeting depends on intranuclear interactions. For example the yeast INM-localization of Mps3 depends on binding to the histone variant H2A.Z homologue Htz1 (Gardner *et al.*, 2011). Finally, in a screen on the dependence of INM targeting on ATP and/or the RanGTP-gradient, it was observed that different NETs respond differently (Zuleger *et al.*, 2011a). Thus, in summary, there are probably multiple rather than one single import mechanisms.

Aim of the project

At the start of the project, we were far from understanding how NPC passage of INM proteins is accomplished. Focusing on the Kap and NLS-dependent transport of membrane proteins across the NPC in baker's yeast, we set out to answer the following questions:

I. The first question relates to the transport mechanism in general. We wanted to know if the requirement of karyopherins and RanGTP is directly needed to maintain the nuclear localization of Heh1 and Heh2, or is their localization still due to nuclear tethering. In other words, is the accumulation of membrane proteins in the INM maintained by just the transport kinetics, similar as the accumulation of soluble cargo?

II. The next question concerned the transport mechanism and pathway. While membrane proteins traverse the NPC, the transmembrane domain remains in the pore membrane and the soluble domain was thought to move through the 10 nm wide peripheral or lateral channel (Hinshaw *et al.*, 1992;Soullam and Worman, 1995). Despite the critical note by Ohba *et al.* about the presence and role of the lateral channel (Ohba *et al.*, 2004), they were widely referred to as the gate for membrane proteins transport to the nucleus (Deng and Hochstrasser, 2006;Kutay *et al.*, 1997;Worman and Courvalin, 2000;Zuleger *et al.*, 2008). Moreover, the lateral channels are clearly observed in high-resolution electron microscopic images of the *Xenopus* oocytes NPCs (Frenkiel-Krispin *et al.*, 2010). With the finding of an NLS and the Kap-dependent targeting mechanism, the question was raised if and where the NLS-bound Kaps would interact with the FG-Nups.

III. Ohba *et al.* claimed that energy was needed for continuous NPC restructuring to allow membrane proteins to diffuse across the NPC (Ohba *et al.*, 2004). King *et al* showed that the RanGTP-gradient was needed to actively transport two yeast membrane proteins to the INM (King *et al.*, 2006). The question remained if indeed an ATP-dependent restructuring of the NPC would be needed for membrane protein diffusion across the NPC.

IV. The question why only some proteins need an NLS for targeting to the INM was answered by Lusk *et al.*: membrane proteins with a small extralumenal domain (<25 kDa) are allowed to diffuse freely across the NPC but membrane proteins with larger domains (up to 70 kDa) need Kap-mediated transport to access the nucleus (Lusk *et al.*, 2007). Clearly, there was room for testing and fine-tuning of this model as Doa10 did accumulate at the INM while having a soluble domain of ~66 kDa and no NLS (Deng and Hochstrasser, 2006). Also, Kap60 and Kap95 together make up a rather voluminous complex of ~155 kDa; it is difficult to envision how this complex together with a membrane protein would pass through the ~10 nm wide channels. We thus raised the question about the size-exclusion limits of membrane protein transport to the nucleus.

V. The last questions relate to the dynamics of the NE composition. If membrane proteins are imported, (how) do they leave again if no longer needed at the INM? What determines their concentration at the INM: can it be determined by the kinetics of import and leak, alike that of soluble proteins?

Outline of the thesis

To answer the above questions, we first developed methods to study and quantify nuclear transport of soluble proteins in yeast (chapter 2). In chapter 3, we use these methods to show that membrane reporter proteins in yeast can accumulate at the INM without nuclear retention and that high-affinity binding to Kap60 of the cargo's NLSs is essential for efficient nuclear accumulation. In chapter 4, we provide evidence that a long intrinsically-disordered linker between the NLS and the transmembrane domain in integral membrane proteins is required for nuclear transport. Our data indicate that the intrinsically-disordered linker slices through the scaffold of the NPC, facilitating the Kap-bound terminus to interact with the FG-Nups while the transmembrane domains remain in the POM. Chapter 5 provides the methods we developed to study and quantify the nuclear transport of integral membrane proteins to the INM. In chapter 6, we determined the kinetics of transport of membrane protein to the INM and showed that membrane proteins with large soluble domains (up to 174 kDa) can pass the NPC. We also discuss how Kap-independent nuclear efflux of membrane proteins dependents on ATP. In chapter 7, we discuss our model of membrane protein transport across the NPC and hypothesize that the proposed mechanisms also holds for the nuclear transport of membrane proteins in human cells.

References

1. Alber, F., S.Dokudovskaya, L.M.Veenhoff, W.Zhang, J.Kipper, D.Devos, A.Suprapto, O.Karni-Schmidt, R.Williams, B.T.Chait, M.P.Rout, and A.Sali. 2007a. Determining the architectures of macromolecular assemblies. *Nature* **450**:683-694.
2. Alber, F., S.Dokudovskaya, L.M.Veenhoff, W.Zhang, J.Kipper, D.Devos, A.Suprapto, O.Karni-Schmidt, R.Williams, B.T.Chait, A.Sali, and M.P.Rout. 2007b. The molecular architecture of the nuclear pore complex. *Nature* **450**:695-701.
3. Amlacher, S., P.Sarges, D.Flemming, N.van, V, R.Kunze, D.P.Devos, M.Arumugam, P.Bork, and E.Hurt. 2011. Insight into structure and assembly of the nuclear pore complex by utilizing the genome of a eukaryotic thermophile. *Cell* **146**:277-289.
4. Anderson, D.J., J.D.Vargas, J.P.Hsiao, and M.W.Hetzer. 2009. Recruitment of functionally distinct membrane proteins to chromatin mediates nuclear envelope formation in vivo. *J. Cell Biol.* **186**:183-191.
5. Antonin, W., C.Franz, U.Haselmann, C.Antony, and I.W.Mattaj. 2005. The integral membrane nucleoporin pom121 functionally links nuclear pore complex assembly and nuclear envelope formation. *Mol. Cell* **17**:83-92.
6. Antonin, W., R.Ungricht, and U.Kutay. 2011. Traversing the NPC along the pore membrane: targeting of membrane proteins to the INM. *Nucleus.* **2**:87-91.
7. Beck, M., F.Forster, M.Ecke, J.M.Plitzko, F.Melchior, G.Gerisch, W.Baumeister, and O.Medalia. 2004. Nuclear pore complex structure and dynamics revealed by cryoelectron tomography. *Science* **306**:1387-1390.
8. Beck, M., V.Lucic, F.Forster, W.Baumeister, and O.Medalia. 2007. Snapshots of nuclear pore complexes in action captured by cryo-electron tomography. *Nature* **449**:611-615.
9. Ben-Efraim, I. and L.Gerace. 2001. Gradient of increasing affinity of importin beta for nucleoporins along the pathway of nuclear import. *J. Cell Biol.* **152**:411-417.
10. Bischoff, F.R. and D.Gorlich. 1997. RanBP1 is crucial for the release of RanGTP from importin beta-related nuclear transport factors. *FEBS Lett.* **419**:249-254.
11. Bischoff, F.R. and H.Ponstingl. 1995. Catalysis of guanine nucleotide exchange of Ran by RCC1 and stimulation of hydrolysis of Ran-bound GTP by Ran-GAP1. *Methods Enzymol.* **257**:135-144.
12. Boban, M., A.Zargari, C.Andreasson, S.Heessen, J.Thyberg, and P.O.Ljungdahl. 2006. Asi1 is an inner nuclear membrane protein that restricts promoter access of two latent transcription factors. *J. Cell Biol.* **173**:695-707.
13. Braunagel, S.C., S.T.Williamson, S.Saksena, Z.Zhong, W.K.Russell, D.H.Russell, and M.D.Summers. 2004. Trafficking of ODV-E66 is mediated via a sorting motif and other viral proteins: facilitated trafficking to the inner nuclear membrane. *Proc. Natl. Acad. Sci. U. S. A* **101**:8372-8377.
14. Brohawn, S.G., J.R.Partridge, J.R.Whittle, and T.U.Schwartz. 2009. The nuclear pore complex has entered the atomic age. *Structure.* **17**:1156-1168.
15. Cai, M., Y.Huang, R.Ghirlando, K.L.Wilson, R.Craigie, and G.M.Clore. 2001. Solution structure of the constant region of nuclear envelope protein LAP2 reveals two LEM-domain structures: one binds BAF and the other binds DNA. *EMBO J.* **20**:4399-4407.
16. Cai, M., Y.Huang, R.Zheng, S.Q.Wei, R.Ghirlando, M.S.Lee, R.Craigie, A.M.Gronenborn, and G.M.Clore. 1998. Solution structure of the cellular factor BAF responsible for protecting retroviral DNA from autointegration. *Nat. Struct. Biol.* **5**:903-909.
17. Caputo, S., J.Couprie, I.Duband-Goulet, E.Konde, F.Lin, S.Braud, M.Gondry, B.Gilquin, H.J.Worman, and S.Zinn-Justin. 2006. The carboxyl-terminal nucleoplasmic region of MAN1 exhibits a DNA binding winged helix domain. *J. Biol. Chem.* **281**:18208-18215.
18. Cardarelli, F. and E.Gratton. 2010. In vivo imaging of single-molecule translocation through nuclear pore complexes by pair correlation functions. *PLoS. One.* **5**:e10475.
19. Chial, H.J., M.P.Rout, T.H.Giddings, and M.Winey. 1998. Saccharomyces cerevisiae Ndc1p is a shared component of nuclear pore complexes and spindle pole bodies. *J. Cell Biol.* **143**:1789-1800.
20. Conti, E. and E.Izaurralde. 2001. Nucleocytoplasmic transport enters the atomic age. *Curr. Opin. Cell Biol.* **13**:310-319.
21. Conti, E. and J.Kuriyan. 2000. Crystallographic analysis of the specific yet versatile recognition of distinct nuclear localization signals by karyopherin alpha. *Structure.* **8**:329-338.
22. Cronshaw, J.M., A.N.Krutchinsky, W.Zhang, B.T.Chait, and M.J.Matunis. 2002. Proteomic analysis of the mammalian nuclear pore complex. *J. Cell Biol.* **158**:915-927.
23. Cross, B.C., I.Sinning, J.Luirink, and S.High. 2009. Delivering proteins for export from the cytosol. *Nat. Rev. Mol. Cell Biol.* **10**:255-264.
24. Dange, T., D.Grunwald, A.Grunwald, R.Peters, and U.Kubitscheck. 2008. Autonomy and robustness of translocation through the nuclear pore complex: a single-molecule study. *J. Cell Biol.* **183**:77-86.
25. Dauer, W.T. and H.J.Worman. 2009. The nuclear envelope as a signaling node in development and disease. *Dev. Cell* **17**:626-638.

26. Dechat, T., K.Pfleghaar, K.Sengupta, T.Shimi, D.K.Shumaker, L.Solimando, and R.D.Goldman. 2008. Nuclear lamins: major factors in the structural organization and function of the nucleus and chromatin. *Genes Dev.* **22**:832-853.
27. Deng, M. and M.Hochstrasser. 2006. Spatially regulated ubiquitin ligation by an ER/nuclear membrane ligase. *Nature* **443**:827-831.
28. Devos, D., S.Dokudovskaya, F.Alber, R.Williams, B.T.Chait, A.Sali, and M.P.Rout. 2004. Components of coated vesicles and nuclear pore complexes share a common molecular architecture. *PLoS. Biol.* **2**:e380.
29. Dingwall, C. and R.A.Laskey. 1991. Nuclear targeting sequences--a consensus? *Trends Biochem. Sci.* **16**:478-481.
30. Dingwall, C., S.V.Sharnick, and R.A.Laskey. 1982. A polypeptide domain that specifies migration of nucleoplasmin into the nucleus. *Cell* **30**:449-458.
31. du Plessis, D.J., N.Nouwen, and A.J.Driessen. 2011. The Sec translocase. *Biochim. Biophys. Acta* **1808**:851-865.
32. Egecioglu, D. and J.H.Brickner. 2011. Gene positioning and expression. *Curr. Opin. Cell Biol.* **23**:338-345.
33. Ellenberg, J., E.D.Siggia, J.E.Moreira, C.L.Smith, J.F.Presley, H.J.Worman, and J.Lippincott-Schwartz. 1997. Nuclear membrane dynamics and reassembly in living cells: targeting of an inner nuclear membrane protein in interphase and mitosis. *J. Cell Biol.* **138**:1193-1206.
34. Fornerod, M., M.Ohno, M.Yoshida, and I.W.Mattaj. 1997. CRM1 is an export receptor for leucine-rich nuclear export signals. *Cell* **90**:1051-1060.
35. Frenkiel-Krispin, D., B.Maco, U.Aebi, and O.Medalia. 2010. Structural analysis of a metazoan nuclear pore complex reveals a fused concentric ring architecture. *J. Mol. Biol.* **395**:578-586.
36. Frey, S. and D.Gorlich. 2007. A saturated FG-repeat hydrogel can reproduce the permeability properties of nuclear pore complexes. *Cell* **130**:512-523.
37. Frey, S., R.P.Richter, and D.Gorlich. 2006. FG-rich repeats of nuclear pore proteins form a three-dimensional meshwork with hydrogel-like properties. *Science* **314**:815-817.
38. Funakoshi, T., M.Clever, A.Watanabe, and N.Imamoto. 2011. Localization of Pom121 to the inner nuclear membrane is required for an early step of interphase nuclear pore complex assembly. *Mol. Biol. Cell* **22**:1058-1069.
39. Furukawa, K. 1999. LAP2 binding protein 1 (L2BP1/BAF) is a candidate mediator of LAP2-chromatin interaction. *J. Cell Sci.* **112 (Pt 15)**:2485-2492.
40. Gardner, J.M., C.J.Smoyer, E.S.Stensrud, R.Alexander, M.Gogol, W.Wiegraebe, and S.L.Jaspersen. 2011. Targeting of the SUN protein Mps3 to the inner nuclear membrane by the histone variant H2A.Z. *J. Cell Biol.* **193**:489-507.
41. Goldfarb, D.S., A.H.Corbett, D.A.Mason, M.T.Harreman, and S.A.Adam. 2004. Importin alpha: a multipurpose nuclear-transport receptor. *Trends Cell Biol.* **14**:505-514.
42. Gorlich, D., P.Henklein, R.A.Laskey, and E.Hartmann. 1996. A 41 amino acid motif in importin-alpha confers binding to importin-beta and hence transit into the nucleus. *EMBO J.* **15**:1810-1817.
43. Gorlich, D. and U.Kutay. 1999. Transport between the cell nucleus and the cytoplasm. *Annu. Rev. Cell Dev. Biol.* **15**:607-660.
44. Görlich, D., N.Pante, U.Kutay, U.Aebi, and F.R.Bischoff. 1996. Identification of different roles for RanGDP and RanGTP in nuclear protein import. *EMBO J.* **15**:5584-5594.
45. Graumann, K., S.L.Irons, J.Runions, and D.E.Evans. 2007. Retention and mobility of the mammalian lamin B receptor in the plant nuclear envelope. *Biol. Cell* **99**:553-562.
46. Gruenbaum, Y., A.Margalit, R.D.Goldman, D.K.Shumaker, and K.L.Wilson. 2005b. The nuclear lamina comes of age. *Nat. Rev. Mol. Cell Biol.* **6**:21-31.
47. Gruenbaum, Y., A.Margalit, R.D.Goldman, D.K.Shumaker, and K.L.Wilson. 2005a. The nuclear lamina comes of age. *Nat. Rev. Mol. Cell Biol.* **6**:21-31.
48. Grund, S.E., T.Fischer, G.G.Cabal, O.Antunez, J.E.Perez-Ortin, and E.Hurt. 2008. The inner nuclear membrane protein Src1 associates with subtelomeric genes and alters their regulated gene expression. *J. Cell Biol.* **182**:897-910.
49. Halic, M., T.Becker, M.R.Pool, C.M.Spahn, R.A.Grassucci, J.Frank, and R.Beckmann. 2004. Structure of the signal recognition particle interacting with the elongation-arrested ribosome. *Nature* **427**:808-814.
50. Heessen, S. and M.Fornerod. 2007. The inner nuclear envelope as a transcription factor resting place. *EMBO Rep.* **8**:914-919.
51. Hegde, R.S. and R.J.Keenan. 2011. Tail-anchored membrane protein insertion into the endoplasmic reticulum. *Nat. Rev. Mol. Cell Biol.*
52. Hetzer, M.W. and S.R.Wente. 2009. Border control at the nucleus: biogenesis and organization of the nuclear membrane and pore complexes. *Dev. Cell* **17**:606-616.
53. Hinshaw, J.E., B.O.Carragher, and R.A.Milligan. 1992. Architecture and design of the nuclear pore complex. *Cell* **69**:1133-1141.
54. Hoelz, A., E.W.Debler, and G.Blobel. 2011. The structure of the nuclear pore complex. *Annu. Rev. Biochem.* **80**:613-643.
55. Hoffmann, K., C.K.Dreger, A.L.Olins, D.E.Olins, L.D.Shultz, B.Lucke, H.Karl, R.Kaps, D.Muller, A.Vaya, J.Aznar,

R.E.Ware, C.N.Sotelo, T.H.Lindner, H.Herrmann, A.Reis, and K.Sperling. 2002. Mutations in the gene encoding the lamin B receptor produce an altered nuclear morphology in granulocytes (Pelger-Huet anomaly). *Nat. Genet.* **31**:410-414.

56. Hoffmann, K., K.Sperling, A.L.Olins, and D.E.Olins. 2007. The granulocyte nucleus and lamin B receptor: avoiding the ovoid. *Chromosoma* **116**:227-235.
57. Holaska, J.M. and K.L.Wilson. 2007. An emerin "proteome": purification of distinct emerin-containing complexes from HeLa cells suggests molecular basis for diverse roles including gene regulation, mRNA splicing, signaling, mechanosensing, and nuclear architecture. *Biochemistry* **46**:8897-8908.
58. Johnson, A.W., J.H.Ho, G.Kallstrom, C.Trotta, E.Lund, L.Kahan, J.Dahlberg, and J.Hedges. 2001. Nuclear export of the large ribosomal subunit. *Cold Spring Harb. Symp. Quant. Biol.* **66**:599-605.
59. Jovanovic-Talisman, T., J.Tetenbaum-Novatt, A.S.McKenney, A.Zilman, R.Peters, M.P.Rout, and B.T.Chait. 2009. Artificial nanopores that mimic the transport selectivity of the nuclear pore complex. *Nature* **457**:1023-1027.
60. Kahms, M., J.Huve, R.Wesselmann, J.C.Farr, V.Baumgartel, and R.Peters. 2011. Lighting up the nuclear pore complex. *Eur. J. Cell Biol.* **90**:751-758.
61. Keminer, O. and R.Peters. 1999. Permeability of single nuclear pores. *Biophys. J.* **77**:217-228.
62. King, M.C., C.P.Lusk, and G.Blobel. 2006. Karyopherin-mediated import of integral inner nuclear membrane proteins. *Nature* **442**:1003-1007.
63. Kobe, B. 1999. Autoinhibition by an internal nuclear localization signal revealed by the crystal structure of mammalian importin alpha. *Nat. Struct. Biol.* **6**:388-397.
64. Korfali, N., G.S.Wilkie, S.K.Swanson, V.Srsen, D.G.Batrakou, E.A.Fairley, P.Malik, N.Zuleger, A.Goncharevich, H.J.de las, D.A.Kelly, A.R.Kerr, L.Florens, and E.C.Schirmer. 2010. The leukocyte nuclear envelope proteome varies with cell activation and contains novel transmembrane proteins that affect genome architecture. *Mol. Cell Proteomics.* **9**:2571-2585.
65. Kowalczyk, S.W., L.Kapinos, T.R.Blosser, T.Magalhaes, N.P.van, R.Y.Lim, and C.Dekker. 2011. Single-molecule transport across an individual biomimetic nuclear pore complex. *Nat. Nanotechnol.* **6**:433-438.
66. Kutay, U., F.R.Bischoff, S.Kostka, R.Kraft, and D.Gorlich. 1997. Export of importin alpha from the nucleus is mediated by a specific nuclear transport factor. *Cell* **90**:1061-1071.
67. Kutay, U., E.Hartmann, and T.A.Rapoport. 1993. A class of membrane proteins with a C-terminal anchor. *Trends Cell Biol.* **3**:72-75.
68. Laguri, C., B.Gilquin, N.Wolff, R.Romi-Lebrun, K.Courchay, I.Callebaut, H.J.Worman, and S.Zinn-Justin. 2001. Structural characterization of the LEM motif common to three human inner nuclear membrane proteins. *Structure.* **9**:503-511.
69. Lange, A., L.M.McLane, R.E.Mills, S.E.Devine, and A.H.Corbett. 2010. Expanding the definition of the classical bipartite nuclear localization signal. *Traffic.* **11**:311-323.
70. Lee, M.S. and R.Craigie. 1998. A previously unidentified host protein protects retroviral DNA from autointegration. *Proc. Natl. Acad. Sci. U. S. A* **95**:1528-1533.
71. Lim, R.Y., N.P.Huang, J.Koser, J.Deng, K.H.Lau, K.Schwarz-Herion, B.Fahrenkrog, and U.Aebi. 2006. Flexible phenylalanine-glycine nucleoporins as entropic barriers to nucleocytoplasmic transport. *Proc. Natl. Acad. Sci. U. S. A* **103**:9512-9517.
72. Lin, F., D.L.Blake, I.Callebaut, I.S.Skerjanc, L.Holmer, M.W.McBurney, M.Paulin-Levasseur, and H.J.Worman. 2000. MAN1, an inner nuclear membrane protein that shares the LEM domain with lamina-associated polypeptide 2 and emerin. *J. Biol. Chem.* **275**:4840-4847.
73. Lott, K. and G.Cingolani. 2011. The importin beta binding domain as a master regulator of nucleocytoplasmic transport. *Biochim. Biophys. Acta* **1813**:1578-1592.
74. Lu, W., J.Gotzmann, L.Sironi, V.M.Jaeger, M.Schneider, Y.Luke, M.Uhlen, C.A.Szigyarto, A.Brachner, J.Ellenberg, R.Foisner, A.A.Noegel, and I.Karakesisoglou. 2008. Sun1 forms immobile macromolecular assemblies at the nuclear envelope. *Biochim. Biophys. Acta* **1783**:2415-2426.
75. Lusk, C.P., G.Blobel, and M.C.King. 2007. Highway to the inner nuclear membrane: rules for the road. *Nat. Rev. Mol. Cell Biol.* **8**:414-420.
76. Margalit, A., A.Brachner, J.Gotzmann, R.Foisner, and Y.Gruenbaum. 2007. Barrier-to-autointegration factor--a BAFfling little protein. *Trends Cell Biol.* **17**:202-208.
77. Mariappan, M., A.Mateja, M.Dobosz, E.Bove, R.S.Hegde, and R.J.Keenan. 2011. The mechanism of membrane-associated steps in tail-anchored protein insertion. *Nature* **477**:61-66.
78. Mehlin, H., B.Daneholt, and U.Skoglund. 1992. Translocation of a specific premessenger ribonucleoprotein particle through the nuclear pore studied with electron microscope tomography. *Cell* **69**:605-613.
79. Mekhail, K., J.Seebacher, S.P.Gygi, and D.Moazed. 2008. Role for perinuclear chromosome tethering in maintenance of genome stability. *Nature* **456**:667-670.
80. Meyer, D.I., E.Krause, and B.Dobberstein. 1982. Secretory protein translocation across membranes-the role of the "docking protein'. *Nature* **297**:647-650.

81. Miao, M., K.J.Ryan, and S.R.Wente. 2006. The integral membrane protein Pom34p functionally links nucleoporin subcomplexes. *Genetics* **172**:1441-1457.
82. Nili, E., G.S.Cojocaru, Y.Kalma, D.Ginsberg, N.G.Copeland, D.J.Gilbert, N.A.Jenkins, R.Berger, S.Shaklai, N.Amariglio, F.Brok-Simoni, A.J.Simon, and G.Rechavi. 2001. Nuclear membrane protein LAP2beta mediates transcriptional repression alone and together with its binding partner GCL (germ-cell-less). *J. Cell Sci.* **114**:3297-3307.
83. Ohba, T., E.C.Schirmer, T.Nishimoto, and L.Gerace. 2004. Energy- and temperature-dependent transport of integral proteins to the inner nuclear membrane via the nuclear pore. *J. Cell Biol.* **167**:1051-1062.
84. Onischenko, E., L.H.Stanton, A.S.Madrid, T.Kieselbach, and K.Weis. 2009. Role of the Ndc1 interaction network in yeast nuclear pore complex assembly and maintenance. *J. Cell Biol.* **185**:475-491.
85. Onischenko, E. and K.Weis. 2011. Nuclear pore complex-a coat specifically tailored for the nuclear envelope. *Curr. Opin. Cell Biol.* **23**:293-301.
86. Osborne, A.R., T.A.Rapoport, and B.B.van den. 2005. Protein translocation by the Sec61/SecY channel. *Annu. Rev. Cell Dev. Biol.* **21**:529-550.
87. Ostlund, C., J.Ellenberg, E.Hallberg, J.Lippincott-Schwartz, and H.J.Worman. 1999. Intracellular trafficking of emerin, the Emery-Dreifuss muscular dystrophy protein. *J. Cell Sci.* **112**:1709-1719.
88. Ostlund, C., T.Sullivan, C.L.Stewart, and H.J.Worman. 2006. Dependence of diffusional mobility of integral inner nuclear membrane proteins on A-type lamins. *Biochemistry* **45**:1374-1382.
89. Pante, N. and M.Kann. 2002. Nuclear pore complex is able to transport macromolecules with diameters of about 39 nm. *Mol. Biol. Cell* **13**:425-434.
90. Pemberton, L.F. and B.M.Paschal. 2005. Mechanisms of receptor-mediated nuclear import and nuclear export. *Traffic.* **6**:187-198.
91. Peters, R. 2005. Translocation through the nuclear pore complex: selectivity and speed by reduction-of-dimensionality. *Traffic.* **6**:421-427.
92. Peters, R. 2009. Translocation through the nuclear pore: Kaps pave the way. *Bioessays* **31**:466-477.
93. Powell, L. and B.Burke. 1990. Internuclear exchange of an inner nuclear membrane protein (p55) in heterokaryons: in vivo evidence for the interaction of p55 with the nuclear lamina. *J. Cell Biol.* **111**:2225-2234.
94. Pyrpasopoulou, A., J.Meier, C.Maison, G.Simos, and S.D.Georgatos. 1996. The lamin B receptor (LBR) provides essential chromatin docking sites at the nuclear envelope. *EMBO J.* **15**:7108-7119.
95. Quan, Y., Z.L.Ji, X.Wang, A.M.Tartakoff, and T.Tao. 2008. Evolutionary and transcriptional analysis of karyopherin beta superfamily proteins. *Mol. Cell Proteomics.* **7**:1254-1269.
96. Rabut, G., V.Doye, and J.Ellenberg. 2004. Mapping the dynamic organization of the nuclear pore complex inside single living cells. *Nat. Cell Biol.* **6**:1114-1121.
97. Renthal, R. 2010. Helix insertion into bilayers and the evolution of membrane proteins. *Cell Mol. Life Sci.* **67**:1077-1088.
98. Rexach, M. and G.Blobel. 1995. Protein import into nuclei: association and dissociation reactions involving transport substrate, transport factors, and nucleoporins. *Cell* **83**:683-692.
99. Ribbeck, K. and D.Gorlich. 2002. The permeability barrier of nuclear pore complexes appears to operate via hydrophobic exclusion. *EMBO J.* **21**:2664-2671.
100. Ribbeck, K., G.Lipowsky, H.M.Kent, M.Stewart, and D.Gorlich. 1998. NTF2 mediates nuclear import of Ran. *EMBO J.* **17**:6587-6598.
101. Robbins, J., S.M.Dilworth, R.A.Laskey, and C.Dingwall. 1991. Two interdependent basic domains in nucleoplasmin nuclear targeting sequence: identification of a class of bipartite nuclear targeting sequence. *Cell* **64**:615-623.
102. Rodriguez-Navarro, S., J.C.Igual, and J.E.Perez-Ortin. 2002. SRC1: an intron-containing yeast gene involved in sister chromatid segregation. *Yeast* **19**:43-54.
103. Rout, M.P., J.D.Aitchison, A.Suprapto, K.Hjertaas, Y.Zhao, and B.T.Chait. 2000. The yeast nuclear pore complex: composition, architecture, and transport mechanism. *J. Cell Biol.* **148**:635-651.
104. Saksena, S., Y.Shao, S.C.Braunagel, M.D.Summers, and A.E.Johnson. 2004. Cotranslational integration and initial sorting at the endoplasmic reticulum translocon of proteins destined for the inner nuclear membrane. *Proc. Natl. Acad. Sci. U. S. A* **101**:12537-12542.
105. Saksena, S., M.D.Summers, J.K.Burks, A.E.Johnson, and S.C.Braunagel. 2006. Importin-alpha-16 is a translocon-associated protein involved in sorting membrane proteins to the nuclear envelope. *Nat. Struct. Mol. Biol.* **13**:500-508.
106. Schirmer, E.C., L.Florens, T.Guan, J.R.Yates, III, and L.Gerace. 2003. Nuclear membrane proteins with potential disease links found by subtractive proteomics. *Science* **301**:1380-1382.
107. Schirmer, E.C. and L.Gerace. 2005. The nuclear membrane proteome: extending the envelope. *Trends Biochem. Sci.* **30**:551-558.
108. Schuldiner, M., J.Metz, V.Schmid, V.Denic, M.Rakwalska, H.D.Schmitt, B.Schwappach, and J.S.Weissman. 2008. The GET complex mediates insertion of tail-anchored proteins into the ER membrane. *Cell* **134**:634-645.

109. Schwartz, T.U. 2005. Modularity within the architecture of the nuclear pore complex. *Curr. Opin. Struct. Biol.* **15**:221-226.

110. Silve, S., P.H.Dupuy, P.Ferrara, and G.Loison. 1998. Human lamin B receptor exhibits sterol C14-reductase activity in Saccharomyces cerevisiae. *Biochim. Biophys. Acta* **1392**:233-244.

111. Smith, A., A.Brownawell, and I.G.Macara. 1998. Nuclear import of Ran is mediated by the transport factor NTF2. *Curr. Biol.* **8**:1403-1406.

112. Smith, A.E., B.M.Slepchenko, J.C.Schaff, L.M.Loew, and I.G.Macara. 2002. Systems analysis of Ran transport. *Science* **295**:488-491.

113. Somech, R., S.Shaklai, O.Geller, N.Amariglio, A.J.Simon, G.Rechavi, and E.N.Gal-Yam. 2005. The nuclear-envelope protein and transcriptional repressor LAP2beta interacts with HDAC3 at the nuclear periphery, and induces histone H4 deacetylation. *J. Cell Sci.* **118**:4017-4025.

114. Soullam, B. and H.J.Worman. 1993. The amino-terminal domain of the lamin B receptor is a nuclear envelope targeting signal. *J. Cell Biol.* **120**:1093-1100.

115. Soullam, B. and H.J.Worman. 1995. Signals and structural features involved in integral membrane protein targeting to the inner nuclear membrane. *J. Cell Biol.* **130**:15-27.

116. Starr, D.A. and H.N.Fridolfsson. 2010. Interactions between nuclei and the cytoskeleton are mediated by SUN-KASH nuclear-envelope bridges. *Annu. Rev. Cell Dev. Biol.* **26**:421-444.

117. Stewart, M. 2007. Molecular mechanism of the nuclear protein import cycle. *Nat. Rev. Mol. Cell Biol.* **8**:195-208.

118. Stoffler, D., B.Fahrenkrog, and U.Aebi. 1999. The nuclear pore complex: from molecular architecture to functional dynamics. *Curr. Opin. Cell Biol.* **11**:391-401.

119. Strambio-de-Castillia, C., G.Blobel, and M.P.Rout. 1995. Isolation and characterization of nuclear envelopes from the yeast Saccharomyces. *J. Cell Biol.* **131**:19-31.

120. Strambio-de-Castillia, C., M.Niepel, and M.P.Rout. 2010. The nuclear pore complex: bridging nuclear transport and gene regulation. *Nat. Rev. Mol. Cell Biol.* **11**:490-501.

121. Strawn, L.A., T.Shen, N.Shulga, D.S.Goldfarb, and S.R.Wente. 2004. Minimal nuclear pore complexes define FG repeat domains essential for transport. *Nat. Cell Biol.* **6**:197-206.

122. Taddei, A., F.Hediger, F.R.Neumann, C.Bauer, and S.M.Gasser. 2004. Separation of silencing from perinuclear anchoring functions in yeast Ku80, Sir4 and Esc1 proteins. *EMBO J.* **23**:1301-1312.

123. Talamas, J.A. and M.W.Hetzer. 2011. POM121 and Sun1 play a role in early steps of interphase NPC assembly. *J. Cell Biol.* **194**:27-37.

124. Tapley, E.C., N.Ly, and D.A.Starr. 2011. Multiple mechanisms actively target the SUN protein UNC-84 to the inner nuclear membrane. *Mol. Biol. Cell* **22**:1739-1752.

125. Terry, L.J., E.B.Shows, and S.R.Wente. 2007. Crossing the nuclear envelope: hierarchical regulation of nucleocytoplasmic transport. *Science* **318**:1412-1416.

126. Terry, L.J. and S.R.Wente. 2009. Flexible gates: dynamic topologies and functions for FG nucleoporins in nucleocytoplasmic transport. *Eukaryot. Cell* **8**:1814-1827.

127. Thompson, J.D., D.G.Higgins, and T.J.Gibson. 1994. CLUSTAL W: improving the sensitivity of progressive multiple sequence alignment through sequence weighting, position-specific gap penalties and weight matrix choice. *Nucleic Acids Res.* **22**:4673-4680.

128. Tran, E.J., T.A.Bolger, and S.R.Wente. 2007. SnapShot: nuclear transport. *Cell* **131**:420.

129. Turgay, Y., R.Ungricht, A.Rothballer, A.Kiss, G.Csucs, P.Horvath, and U.Kutay. 2010. A classical NLS and the SUN domain contribute to the targeting of SUN2 to the inner nuclear membrane. *EMBO J.* **29**:2262-2275.

130. Ulbert, S., M.Platani, S.Boue, and I.W.Mattaj. 2006. Direct membrane protein-DNA interactions required early in nuclear envelope assembly. *J. Cell Biol.* **173**:469-476.

131. van Klompenburg, W., I.Nilsson, G.von Heijne, and K.B.de. 1997. Anionic phospholipids are determinants of membrane protein topology. *EMBO J.* **16**:4261-4266.

132. Voeltz, G.K., M.M.Rolls, and T.A.Rapoport. 2002. Structural organization of the endoplasmic reticulum. *EMBO Rep.* **3**:944-950.

133. Walter, P. and G.Blobel. 1980. Purification of a membrane-associated protein complex required for protein translocation across the endoplasmic reticulum. *Proc. Natl. Acad. Sci. U. S. A* **77**:7112-7116.

134. Wang, F., E.C.Brown, G.Mak, J.Zhuang, and V.Denic. 2010. A chaperone cascade sorts proteins for posttranslational membrane insertion into the endoplasmic reticulum. *Mol. Cell* **40**:159-171.

135. Watson, M.L. 1959. Further observations on the nuclear envelope of the animal cell. *J. Biophys. Biochem. Cytol.* **6**:147-156.

136. Weis, K. 2003. Regulating access to the genome: nucleocytoplasmic transport throughout the cell cycle. *Cell* **112**:441-451.

137. Weis, K. 2007. The nuclear pore complex: oily spaghetti or gummy bear? *Cell* **130**:405-407.

138. Wente, S.R. and M.P.Rout. 2010. The nuclear pore complex and nuclear transport. *Cold Spring Harb. Perspect. Biol.*

2:a000562.

139. West, M., N.Zurek, A.Hoenger, and G.K.Voeltz. 2011. A 3D analysis of yeast ER structure reveals how ER domains are organized by membrane curvature. *J. Cell Biol.* **193**:333-346.
140. Wilkie, G.S., N.Korfali, S.K.Swanson, P.Malik, V.Srsen, D.G.Batrakou, H.J.de las, N.Zuleger, A.R.Kerr, L.Florens, and E.C.Schirmer. 2011. Several novel nuclear envelope transmembrane proteins identified in skeletal muscle have cytoskeletal associations. *Mol. Cell Proteomics.* **10**:M110.
141. Wilkie, G.S. and E.C.Schirmer. 2006. Guilt by association: the nuclear envelope proteome and disease. *Mol. Cell Proteomics.* **5**:1865-1875.
142. Wilson, K.L. and R.Foisner. 2010. Lamin-binding Proteins. *Cold Spring Harb. Perspect. Biol.* **2**:a000554.
143. Worman, H.J. and J.C.Courvalin. 2000. The inner nuclear membrane. *J. Membr. Biol.* **177**:1-11.
144. Worman, H.J., C.Ostlund, and Y.Wang. 2010. Diseases of the nuclear envelope. *Cold Spring Harb. Perspect. Biol.* **2**:a000760.
145. Wozniak, R.W., G.Blobel, and M.P.Rout. 1994. POM152 is an integral protein of the pore membrane domain of the yeast nuclear envelope. *J. Cell Biol.* **125**:31-42.
146. Wu, W., F.Lin, and H.J.Worman. 2002. Intracellular trafficking of MAN1, an integral protein of the nuclear envelope inner membrane. *J. Cell Sci.* **115**:1361-1371.
147. Yamada, J., J.L.Phillips, S.Patel, G.Goldfien, A.Calestagne-Morelli, H.Huang, R.Reza, J.Acheson, V.V.Krishnan, S.Newsam, A.Gopinathan, E.Y.Lau, M.E.Colvin, V.N.Uversky, and M.F.Rexach. 2010. A bimodal distribution of two distinct categories of intrinsically disordered structures with separate functions in FG nucleoporins. *Mol. Cell Proteomics.* **9**:2205-2224.
148. Yang, L., T.Guan, and L.Gerace. 1997. Integral membrane proteins of the nuclear envelope are dispersed throughout the endoplasmic reticulum during mitosis. *J. Cell Biol.* **137**:1199-1210.
149. Yang, Q., M.P.Rout, and C.W.Akey. 1998. Three-dimensional architecture of the isolated yeast nuclear pore complex: functional and evolutionary implications. *Mol. Cell* **1**:223-234.
150. Yang, W., J.Gelles, and S.M.Musser. 2004. Imaging of single-molecule translocation through nuclear pore complexes. *Proc. Natl. Acad. Sci. U. S. A* **101**:12887-12892.
151. Yao, W., D.Roser, A.Kohler, B.Bradatsch, J.Bassler, and E.Hurt. 2007. Nuclear export of ribosomal 60S subunits by the general mRNA export receptor Mex67-Mtr2. *Mol. Cell* **26**:51-62.
152. Yavuz, S., R.Santarella-Mellwig, B.Koch, A.Jaedicke, I.W.Mattaj, and W.Antonin. 2010. NLS-mediated NPC functions of the nucleoporin Pom121. *FEBS Lett.* **584**:3292-3298.
153. Yewdell, W.T., P.Colombi, T.Makhnevych, and C.P.Lusk. 2011. Lumenal interactions in nuclear pore complex assembly and stability. *Mol. Biol. Cell* **22**:1375-1388.
154. Zargari, A., M.Boban, S.Heessen, C.Andreasson, J.Thyberg, and P.O.Ljungdahl. 2007. Inner nuclear membrane proteins Asi1, Asi2, and Asi3 function in concert to maintain the latent properties of transcription factors Stp1 and Stp2. *J. Biol. Chem.* **282**:594-605.
155. Zemp, I. and U.Kutay. 2007. Nuclear export and cytoplasmic maturation of ribosomal subunits. *FEBS Lett.* **581**:2783-2793.
156. Zilman, A., T.S.Di, T.Jovanovic-Talisman, B.T.Chait, M.P.Rout, and M.O.Magnasco. 2010. Enhancement of transport selectivity through nano-channels by non-specific competition. *PLoS. Comput. Biol.* **6**:e1000804.
157. Zuleger, N., D.A.Kelly, A.C.Richardson, A.R.Kerr, M.W.Goldberg, A.B.Goryachev, and E.C.Schirmer. 2011a. System analysis shows distinct mechanisms and common principles of nuclear envelope protein dynamics. *J. Cell Biol.* **193**:109-123.
158. Zuleger, N., N.Korfali, and E.C.Schirmer. 2008. Inner nuclear membrane protein transport is mediated by multiple mechanisms. *Biochem. Soc. Trans.* **36**:1373-1377.
159. Zuleger, N., M.I.Robson, and E.C.Schirmer. 2011b. The nuclear envelope as a chromatin organizer. *Nucleus.* **2**:339-349.

Chapter 2

Transport of soluble cargo and non-cargo through the nuclear pore complex

Anne C. Meinema[1], Geert van den Bogaart[1¥], Bert Poolman[1] and Liesbeth M. Veenhoff[1,2]

1 Department of Biochemistry, Groningen Biomolecular Sciences and Biotechnology Institute, Netherlands Proteomics Centre, Zernike Institute for Advanced Materials, University of Groningen, Nijenborgh 4, 9747 AG, Groningen, The Netherlands.

2 Department of Neuroscience, European Research Institute on the Biology of Ageing, University Medical Centre Groningen, Groningen, The Netherlands

¥ Present address: Department of Neurobiology, Max Planck Institute for Biophysical Chemistry, Am Faßberg 11, 37077 Göttingen, Germany

Partly published in:

van den Bogaart G*, Meinema AC*, Krasnikov V, Veenhoff LM, Poolman B. Nuclear transport factor directs localization of protein synthesis during mitosis. *Nat Cell Biol.* 2009 Mar; **11**(3):350-6.

* These authors contributed equally to this work

Abstract

Cellular cargo destined for the nucleus bears a nuclear localization signal (NLS) that is recognized by karyopherins, the nuclear transport factors. The cargo is actively imported across the nuclear pore complex (NPC) into the nucleus. The NPCs, however, are leaky, and accumulated cargo can efflux back to the cytosol but with a lower rate constant than during active import (Timney *et al.*, 2006). In this study, we quantified nuclear import and the passive efflux of GFP-NLS reporter proteins with a FRAP-based method. Consistent with the nuclear pore complex being a crowded environment that hinders efflux and facilitates import, we observed that the import rate constant was less dependent on the cargo size than the efflux rate constant. Interestingly, we observed that the difference in nuclear accumulation of GFP-tcNLS, Pho4NLS-GFP and rgNLS-GFP, mediated by respectively Kap60/95, Kap121 and Kap104, were due to differences in the efflux rate constant. Lastly, at high expression levels of cargo, we see that the nuclear accumulation is reduced, which could reflect saturation of the import pathway.

Introduction

Transport of macromolecules into the nucleus is mediated by the nuclear pore complex (NPC). In *Saccharomyces cerevisiae,* the NPC is a large assembly of ~30 different proteins, called nucleoporins or Nups, each present in multiple copies (Rout *et al.*, 2000). This complex is embedded in the nuclear envelope and connects the nucleus with the cytoplasm. Proteins bearing a nuclear localization signal (NLS) or nuclear export signal (NES) are actively transported into or out of the nucleus (reviewed in (Stewart, 2007;Wente and Rout, 2010)). The NPC functions as a barrier for large proteins without an NLS or NES, while smaller cargos, proteins up to 25 – 60 kDa, have been reported to diffuse freely across the NPC (Gorlich and Kutay, 1999;Keminer and Peters, 1999;Mohr *et al.*, 2009;Paine *et al.*, 1975). Import typically starts with the binding between the NLS on the cargo and a soluble transport factor, which is called a karyopherin (Kap, or Importin in human cells). Most members of the Kapβ-family bind their cargo directly, only Kapβ1 (Kap95 in yeast) complexes with cargo via the adaptor protein Kapα (Kap60 in yeast)(Pemberton and Paschal, 2005). Associated with the cargo, Kapβ interacts with the phenylalanine-glycine (FG) repeats of the FG-Nups that fill the central channel of the NPC (reviewed in (Terry and Wente, 2009)). The interactions between the Kap and the FG-Nups facilitate the diffusion of Kap-cargo through this dense and dynamic network of filaments into the nucleus. The cargo is released in the nucleus upon binding of the Kaps to RanGTP (Görlich *et al.*, 1996;Kutay *et al.*, 1997). Together with RanGTP are the Kaps shuttled back to the cytoplasm where RanGEF hydrolyses RanGTP to RanGDP which releases Kapα and Kapβ and makes them available for another round of import. The small molecule RanGDP is translocated by NTF2 across the NPC to the nucleoplasm, where it is converted to RanGTP by the nucleotide exchange factor RCC1 (RanGEF) at the expense of an ATP (Bischoff and Ponstingl, 1995). The specific localization of RCC1 in the nucleus and RanGAP in the cytoplasm generates the gradient of RanGTP over the nuclear envelope as the motive force to drive nuclear transport.

In higher eukaryotic cells, nuclear transport has been studied by the use of isolated nuclei (Siebrasse and Peters, 2002), by permeabilization of cells (Yang *et al.*, 2004;Ribbeck *et al.*, 1999) and after microinjection of cargo into the cytoplasm (Smith *et al.*, 2002). More recently, single molecule imaging methods have contributed to our understanding of the kinetics and the path of transport (Yang *et al.*, 2004;Grunwald *et al.*, 2011;Dange *et al.*, 2008;Tokunaga *et al.*, 2008). In yeast cells, metabolic poisons have been used to measure nuclear transport rates *in vivo* (Leslie *et al.*, 2006;Timney *et al.*, 2006). In this poison assay, the yeast cells were treated with 2-deoxyglucose plus sodium azide to deplete the cells of ATP and GTP, which disrupts the RanGTP gradient (as shown in (Schwoebel *et al.*, 2002;Shulga *et al.*, 1996)). Without a RanGTP gradient, nuclear import is abolished and the nuclear accumulated cargo equilibrates over the nucleus and cytoplasm. After the poisons are washed away, the RanGTP-gradient quickly recovers and nuclear import can be monitored. A pump-leak model for nuclear transport has been postulated, where the cargo flux into the nucleus is in equilibrium with leakage out of the nucleus. As import rate constants are higher than efflux rate constants, it results in a net accumulation of cargo in the nucleus (Timney *et al.*, 2006).

In the present study, we developed a fluorescence after photo-bleaching (FRAP)-based method to quantify nuclear transport in *Saccharomyces cerevisiae in vivo*. Photobleaching of fluorescent cargo in the nucleus and monitoring of the recovery as a result of nuclear transport has been used before in mammalian cells (Koster *et al.*, 2005). This technique, called selective-FRAP (sFRAP, reviewed in (Goodwin and Kenworthy, 2005)), is non-invasive and enables the study of nuclear transport under native conditions, provided that photo-damage is not occurring over the time period of the measurement (Koster *et al.*, 2005;Lippincott-Schwartz *et al.*, 2001).

We measured transport kinetics of import via the classical import pathway mediated by Kap60 and Kap95 (i.e. Kapα and Kapβ1 in metazoans), with a GFP reporter linked to the classical NLS (cNLS) from the simian virus 40 large-T antigen (Dingwall *et al.*, 1982). We compared the transport of cargo bearing a cNLS to cargo bearing the NLS of Nab2 (rgNLS) imported by Kap104 (Lee and Aitchison, 1999) or bearing the NLS of Pho4 (Pho4NLS) and imported by Kap121 (Kaffman *et al.*, 1998). We thus performed similar experiments as carried out by Timney *et al* (Timney *et al.*, 2006) but using sFRAP instead of the poison-method. We observed that these reporters accumulated in the nucleus to different levels as a result of differences in efflux rate constants, rather than differences in import rate constants. The efflux rate constants were lower for larger molecules, reinforcing the notion that the NPC is a crowded environment where competition for available space contributes to the selectivity of transport. The efflux rates were also different for the different cargos, and we discuss possible explanations for this observation. Lastly, at the highest expression levels of cargo, we see that the nuclear accumulation drops which could reflect saturation of the import pathway.

Results

We measured nuclear transport of fluorescent cargo with different NLSs and having different sizes in the yeast strain *S. cerevisiae* BY4742 using sFRAP. We imaged cells expressing the

following cargos: GFP fused to a tandem of cNLS (GFP-tcNLS), GFP-tcNLS-GFP, Pho4NLS-GFP, and rgNLS-GFP, and we compared their localization to that of the non-cargo GFP. All cargos were accumulated in the nucleus, while GFP was distributed approximately equally over the cytoplasm and nucleus (Fig. 2.1A, B (pre-bleach)). The laser was focused for ~5 – 10 s in the nucleus until the fluorescence signal in the nucleus was reduced to ~40% of the initial fluorescence signal (Fig. 2.1B, t = 0). The ratio of fluorescence intensity in the nucleus over the cytoplasm (N/C ratio) was decreased during this photobleach pulse. A small fraction (<20%) of the fluorescent cargo located in the cytoplasm was also photobleached while the laser was focused in the nucleus. This is partly caused by the continuous flux of cargo across the NPC during the bleaching pulse, and partly because the laser beam also photobleaches some cytosol around the nucleus. Subsequently, we monitored the recovery of fluorescence in the nucleus by recording a time-series of images during 30 – 40 seconds (Fig. 2.1B). The reduced N/C ratio recovered to the original value, because photobleached and non-photobleached GFP-tcNLS redistributed over the nucleus and cytoplasm due to continuous nuclear import and leakage.

For the analysis of the sFRAP data a method was developed to determine the fluorescence intensities of the nucleus and the cytoplasm, based on a pixel analysis (Fig. 2.2A, B). A mask overlay was used to distinguish the nucleus from the cytoplasm and the background fluorescence (Fig. 2.2A). The fluorescence intensity of the entire cell was plotted in a histogram and the regions of the mask could be set with thresholds (Fig. 2.2B). The peak fluorescence intensity for each region was obtained from the histogram, and the area under the graph defined the surface area of the cross-section through the nucleus and cytoplasm. The fluorescence intensities were converted to

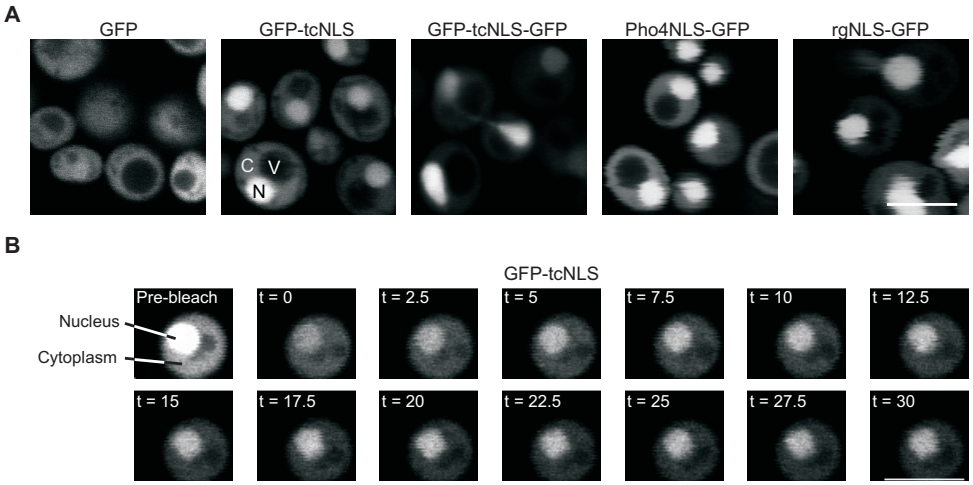

Figure 2.1: Selective-FRAP to study nuclear transport. A) Confocal images of yeast cells show the localization GFP, GFP-tcNLS, GFP-tcNLS-GFP, Pho4NLS-GFP and rgNLS-GFP. The cytoplasm (C), nucleus (N) and vacuole (V) are indicated, scale bar is 5 μm. **B)** The laser was focused for 5 – 10 seconds in the nucleus of a yeast cell expressing GFP-tcNLS to photobleach the fluorescent cargo in the nucleus. The level of fluorescence in the nucleus is more decreased than in the cytoplasm, resulting in a reduced nuclear accumulation of fluorescent cargo (t = 0). A time series of images was recorded to follow the recovery of the accumulation of fluorescent cargo in the nucleus. Scale bar is 5 μm.

cellular concentrations using the count-rate per molecule, as was determined from fluorescence correlation spectroscopy (FCS)-measurements (Fig. 2.2C). We performed FCS on crude cell extracts of cells expressing GFP (Fig. 2.2C) and assumed that the fluorescent quantum yield of the fluorescent proteins in live cells was the same as in these extracts. We found a fluorescence count-rate per molecule of 0.75 ± 0.08 kHz/molecule for GFP, measured in a confocal volume of ~0.2 fL (Veldhuis *et al.*, 2006). We measured the average diameter of the cell, the nucleus and the vacuole, and we assumed that these structures are spherical. We estimated the volume of the nucleus to be 4.2 ± 0.19 fL (Fig. 2.2D) and the cytoplasm 49.1 ± 2.1 fL (n = 381) (Fig. 2.2E). The volumes determined with this method are similar to those calculated with more sophisticated 3-dimensional imaging methods, like 3D reconstructions based on multiple confocal slices (Leslie *et al.*, 2006;Timney *et al.*, 2006).

Using this method the concentration of GFP reporters in the nucleus and cytoplasm (Fig. 2.3A) and the NC-ratios were calculated from a large population of cells under steady state conditions (Fig. 2.3B, C). The concentration of GFP in the cytoplasm and nucleus was similar as apparent from an N/C ratio of ~1. GFP-tcNLS accumulated 4.2 fold in the nucleus and GFP-tcNLS-GFP accumulated 10.4 fold. rgNLS-GFP and Pho4NLS-GFP showed an N/C ratio of more than 10-fold and their nuclear accumulation was thus substantially higher than that

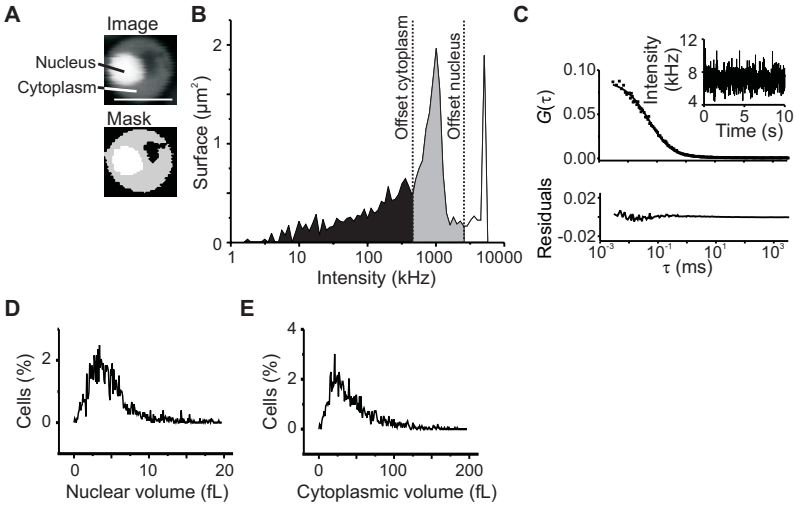

Figure 2.2: Image analysis to determine the fluorescent cargo concentration and the volumes of the nucleus and cytoplasm. A) A confocal image of a yeast cell expressing GFP-tcNLS and a mask overlay of the yeast cell are shown. The overlay was used to distinguish the nucleus (white) and the cytoplasm (gray) from the vacuole and background (black). Scale bar is 5 μm. **B)** The offset to define regions in the mask overlay was set in the histogram, where the pixel intensities of the confocal image are plotted to the surface area of the region. The peak intensities in the nucleus and cytoplasm were used to determine the concentrations. **C)** FCS measurement (■) and fit (solid line) on a cell-free lysate from yeast cells expressing GFP. The residuals from the fit are presented in the lower graph and the fluorescence trace in the inset. The number of particles in the focal volume was 11.5 ± 1.8, the diffusion constant was 82 ± 14 μm²/s and the count-rate per molecule was 0.75 ± 0.08 kHz/molecule. The focal volume for the green channel of our setup was ~0.2 fL (Veldhuis *et al.*, 2006). **D, E)** The distributions of the nuclear and cytoplasmic volumes are plotted for cells expressing GFP-tcNLS.

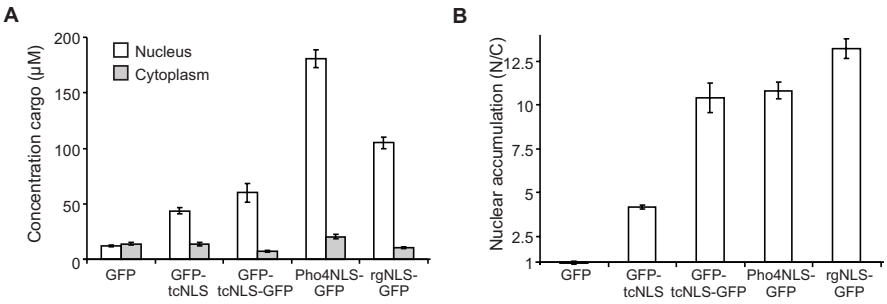

C

	Mass (kD)	$[X]_{cyt}$ (μM)	$[X]_{nucl}$ (μM)	$[X]_{total}$ (μM)	NC-ratio	V_{cyto} (fL)	V_{nucl} (fL)	*n*
GFP	29.6	12.9 ± 1.0	12.2 ± 0.8	12.8 ± 1.0	1.0 ± 0.1	53.4 ± 2.4	3.9 ± 0.2	63
GFP-tcNLS	31.2	13.6 ± 1.7	43.5 ± 2.9	15.9 ± 1.9	4.2 ± 0.1	48.7 ± 1.5	4.1 ± 0.1	222
GFP-tcNLS-GFP	58.2	7.33 ± 0.8	60.0 ± 8.5	11.1 ± 1.3	10.4 ± 0.8	55.1 ± 4.0	4.2 ± 0.3	54
Pho4NLS-GFP	34.1	20.1 ± 2.0	180 ± 8.2	32.3 ± 3.0	10.8 ± 0.5	46.0 ± 1.9	3.8 ± 0.1	302
rgNLS	32.5	10.3 ± 0.8	105 ± 5.0	20.6 ± 1.6	13.2 ± 0.6	36.9 ±1.1	4.5 ± 0.2	149

Figure 2.3: The cellular cargo concentration in the nucleus and cytoplasm. A) The cytoplasmic and nuclear concentrations of various cargos is plotted in a column chart. SEM is indicated. **B)** The ratio of fluorescence intensity in the nucleus over the cytoplasm (N/C ratio) for various cargos is plotted as a measure of the nuclear accumulation. SEM is indicated. **C)** Table listing for various cargos the molecular masses (Mass, (kDa)), the cytoplasmic ($[X]_{cyt}$ (μM)), the nuclear ($[X]_{nucl}$ (μM)), the total cellular cargo concentrations ($[X]_{total}$ (μM)), and the N/C ratio, as well as the cytosolic (V_{cyto} (fL)) and nuclear volumes (V_{nucl} (fL)), and the number of cells analyzed (*n*). Average values are indicated with SEM.

of GFP-tcNLS (Fig. 2.3C). Similarly, we quantified the cargo concentration of the nucleus and cytoplasm during the sFRAP experiments (Fig. 2.1B) and fitted the recovery kinetics (Fig. 2.4A and see materials and methods section). For the calculations, we assumed that the NPC density in the nuclear envelope is 12 per μm^2 (Leslie *et al.*, 2006;Timney *et al.*, 2006;Winey *et al.*, 1997). The flux is defined as the number of molecules per second that is transported across a singele NPC (molecules/s·NPC). The speed of nuclear transport is defined by the import and efflux rate constants and these are expressed per μM of cargo in the cytoplasm or nucleoplasm, respectively (expressed as molecules/s·NPC·μM). For all cargos, the import rate constants were higher than the efflux rate constants (Fig. 2.4B), resulting in a higher concentration in the nucleus than in the cytoplasm (Fig. 2.3B). Indeed, the nuclear accumulation (the N/C ratio) is determined by the ratio of the import and efflux rate constants, and at steady state the flux into the nucleus equals the flux out of the nucleus (Fig. 2.4C).

The efflux rate constant of Kap-unbound (naked) GFP-tcNLS did not significantly differ from both the influx and the efflux rate constants of GFP without NLS (Fig. 2.4B). This indicated that the leakage of GFP-tcNLS across the NPC to the cytosol is a diffusive process, which is consistent with the earlier proposal of the pump-leak model (Timney *et al.*, 2006). The import rate constant of GFP-tcNLS is ~4-fold higher than the efflux rate constant as apparent from an N/C ratio of 4.1. A 4-fold higher import speed of GFP-tcNLS compared to GFP, together with

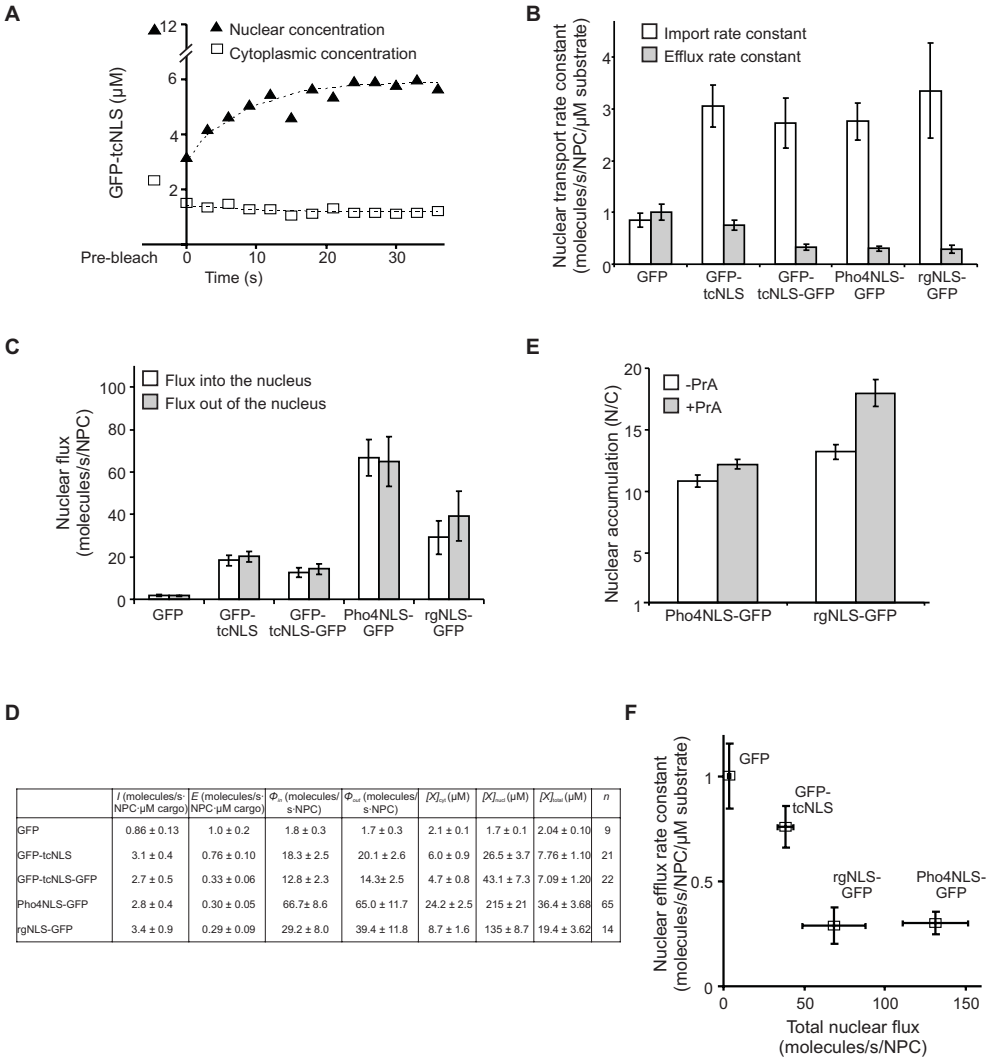

	I (molecules/s·NPC·μM cargo)	*E* (molecules/s·NPC·μM cargo)	Φ_{in} (molecules/s·NPC)	Φ_{out} (molecules/s·NPC)	$[X]_{cyt}$ (μM)	$[X]_{nucl}$ (μM)	$[X]_{total}$ (μM)	*n*
GFP	0.86 ± 0.13	1.0 ± 0.2	1.8 ± 0.3	1.7 ± 0.3	2.1 ± 0.1	1.7 ± 0.1	2.04 ± 0.10	9
GFP-tcNLS	3.1 ± 0.4	0.76 ± 0.10	18.3 ± 2.5	20.1 ± 2.6	6.0 ± 0.9	26.5 ± 3.7	7.76 ± 1.10	21
GFP-tcNLS-GFP	2.7 ± 0.5	0.33 ± 0.06	12.8 ± 2.3	14.3± 2.5	4.7 ± 0.8	43.1 ± 7.3	7.09 ± 1.20	22
Pho4NLS-GFP	2.8 ± 0.4	0.30 ± 0.05	66.7± 8.6	65.0 ± 11.7	24.2 ± 2.5	215 ± 21	36.4 ± 3.68	65
rgNLS-GFP	3.4 ± 0.9	0.29 ± 0.09	29.2 ± 8.0	39.4 ± 11.8	8.7 ± 1.6	135 ± 8.7	19.4 ± 3.62	14

Figure 2.4: Import and efflux rate constants and fluxes over the NPC are obtained by selective FRAP. A) The concentration of tcNLS-GFP in the cytoplasm (□) and nucleus (▲) during the sFRAP measurements (as in Fig. 2.1) were plotted. After photobleaching of GFP in the nucleus , the N/C ratio relaxed to initial value as a result of net import of fluorescent GFP-tcNLS and a net efflux of photobleached GFP-tcNLS. The dashed lines show a fit with equation 2 (materials and methods). **B)** The import and efflux rate constants and **C)** the flux into and out of the nucleus are plotted in column charts. SEM is indicated. **D)** A table listing the import (*I* (molecules/s·NPC· μM cargo)) and efflux rate constants (*E* (molecules/s·NPC· μM cargo)), the fluxes into (Φ_{in} (molecules/s·NPC)) and the out of the nucleus (Φ_{out} (molecules/s·NPC)), the cytoplasmic ($[X]_{cyt}$ (μM)), the nuclear ($[X]_{nucl}$ (μM)), the total cellular cargo concentrations ($[X]_{total}$ (μM)) and the number of cells analyzed (*n*). Average values are indicated with SEM. **E)** The nuclear accumulation of Pho4NLS-GFP and rgNLS-GFP is plotted without (white bar) or with an additional PrA-tag of 6.4 kDa (gray bar). **F)** The nuclear efflux rate constant (B) decreases with larger flux across the NPC. This flux is the sum of the flux into and out of the nucleus (D, E).

a ~3-fold higher concentration of cargo in the cytoplasm thus leads to a ~12 fold larger flux across the NPC (Fig. 2.4C) and thus a ~12 fold higher concentration in the nucleus (Fig. 2.4D).

We addressed the effects of cargo size on the transport kinetics by comparing the speed of transport of GFP-tcNLS-GFP of 58.2 kDa and GFP-tcNLS of 31.2 kDa. The cellular concentrations were similar (Fig. 2.4D), enabling us to compare the transport parameters directly. The efflux rate constant for GFP-tcNLS-GFP (0.3 molecules/s·NPC·μM cargo) was reduced compared to GFP-tcNLS (0.8 molecules/s·NPC·μM cargo), while the import rate constants were similar (Fig. 2.4B). This results in higher nuclear accumulation (Fig. 2.3C) of GFP-tcNLS-GFP compared to GFP-tcNLS. These data reinforce earlier findings that in *S. cerevisiae* passive nuclear efflux of small cargos across the NPC is hindered at the NPC in a size-dependent manner (Leslie *et al.*, 2006) and two-fold changes in molecular mass already significantly affected the accumulation levels. Consistently, nuclear accumulation of Pho4NLS-GFP and rgNLS-GFP were lower than those of the same proteins but with an additional 6.4 kDa Protein A-repeat sequence of 58 residues (Fig 4E). Together, we conclude that a relatively small increase in molecular mass of the protein already reduces the efflux speed and thereby decreases nuclear accumulation. Our sFRAP assay can detect such subtle differences in nuclear transport.

As discussed in more detail below, if the barrier function of the NPC would be similar for cargos of a given mass, one would expect the average efflux rate constants of the GFP cargos with or without NLS to be similar. However, we observe that they are different (Fig. 2.4B). Comparing the fluxes of the three GFP-NLS cargos and GFP we see that they correlate with the efflux rate constants: the larger the flux over the NPC, the lower the efflux rate constant (Fig. 2.4F). Larger fluxes are achieved at higher cellular cargo concentrations. When we thus plot the N/C ratio of Pho4NLS-GFP, rgNLS-GFP and GFP-tcNLS of a large population of cells as a function of the cellular cargo concentration, we see in the concentration range up to ~30 μM a trend of increased nuclear accumulation with increasing cellular concentrations of Pho4NLS-GFP, rgNLS-GFP and GFP-tcNLS (Fig. 2.5A, C, E). The increase in nuclear accumulation can indicate a decreased efflux rate constant or, less likely, an increased import rate constant. In turn, at highest concentrations, we observed that the N/C ratio decreases again (Fig. 2.5A, C, E), indicating a decreased import rate constant or, less likely, an increased efflux rate constant. Plotting the nuclear cargo concentration versus the cytoplasmic cargo concentration showed that at the highest concentrations, the N/C ratio of rgNLS-GFP and Pho4NLS-GFP deviated from the average NC-ratio as represented by the dotted line (Fig. 2.5B, D, F). The trends are less apparent for GFP-tcNLS, possibly because the cellular cargo concentrations were much lower.

Discussion

We studied the nuclear transport of fluorescent cargos featuring an rgNLS, a tcNLS or a Pho4NLS in *S. cerevisiae,* using the selective-FRAP assay, where we quantified both the import and efflux rate constants. The efflux of naked cargo is passive and hindered by the permeability barrier of the NPC, while import is facilitated by Kap-FG-nup interactions. In the cell, nuclear import

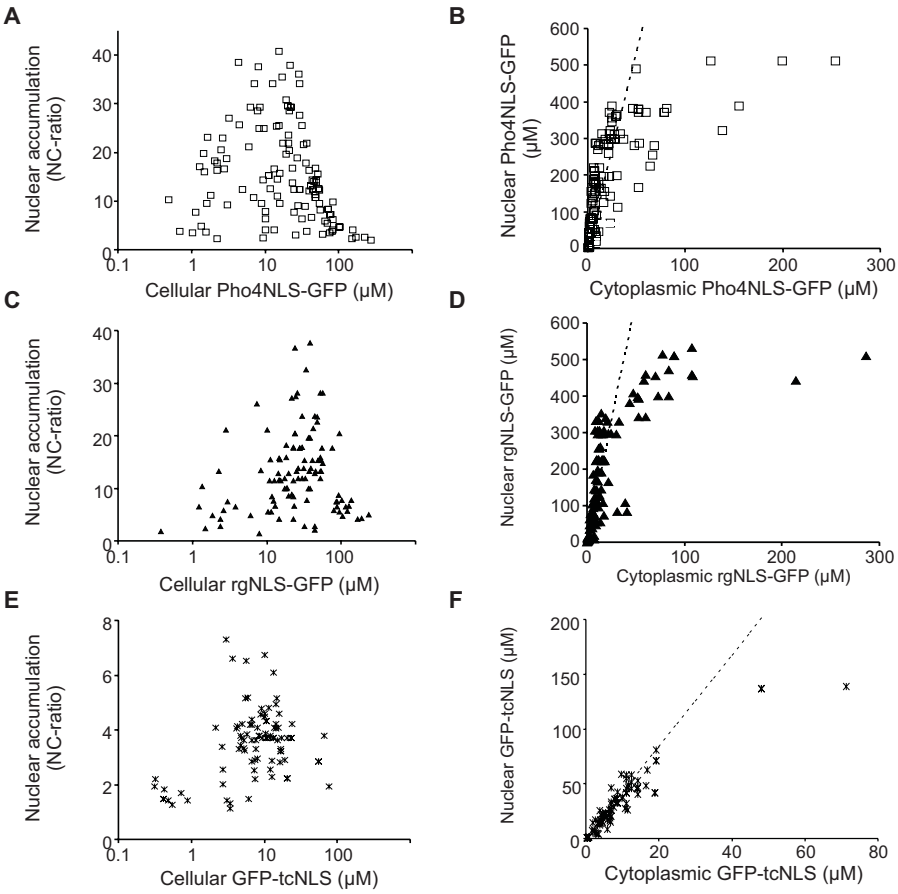

Figure 2.5: Variation in import rate constants and efflux rate constant. A) The N/C ratio of Pho4NLS-GFP of individual cells is as function ofthe cellular concentration is plotted on a logarithmic scale (n = 128). **B)** The nuclear concentration of Pho4NLS-GFP as a function of the cytoplasmic concentration. **C, E)** As (A) for rgNLS-GFP (n = 125) and GFP-tcNLS (n = 91). **D, F)** As (B) for rgNLS-GFP and GFP-tcNLS. The dotted lines present the average N/C ratio.

and efflux are parallel processes; as soon as cargo enters the nucleus and the Kaps are stripped off, it becomes naked-cargo ready to efflux back to the cytoplasm. We measured import rate constants of ~3 molecules/s·NPC·μM for different cargos, while the efflux rate constants ranged between 0.3 to 1 molecules/s·NPC·μM. The nuclear import rate constants of rgNLS-GFP and Pho4NLS-GFP measured previously were lower, namely 0.07 and 1.2 molecule/s·NPC·μM cargo, respectively (Timney *et al.*, 2006). These transport rate constants were obtained with an assay based on the use of metabolic poisons; their low import rate constants compared to our values may reflect the slow recovery from the metabolic poisoning (Schwoebel *et al.*, 2002) rather than slow transport. Our transport rate constants in yeast fall within the range of import kinetics from ~4 to ~100 molecules/s·NPC·μM cargo measured in different eukaryotic systems, using a variety

of assays (Smith *et al.*, 2002;Yang *et al.*, 2004;Ribbeck *et al.*, 1999;Siebrasse and Peters, 2002). The sFRAP allowed measurement of subtle differences in *in vivo* nuclear transport kinetics, such as the differences in passive nuclear efflux for cargo of different size. Our observation that passive nuclear efflux of small cargos across the NPC is size-dependent has been suggested before in *S. cerevisiae* (Leslie *et al.*, 2006). Also for artificial nanopores, mimicking the dimensions of the NPC, it was shown that the fluxes of naked cargo through the nanopore are dependent on protein size (Jovanovic-Talisman *et al.*, 2009).

We observed that the nuclear accumulation levels correlated with the efflux rate constants rather than the import rate constants. One possible explanation for this observation is that the NPC could be differently permeable for different GFP-NLS proteins, meaning that passive efflux through the NPC is dependent on the type of NLS present on the cargo. Alternatively, the efflux rate constants may depend on the total amount of cargo in transit, thus that is present in (travelling through) the pore. We observed that the efflux rate constants correlated with the total flux: the larger the total flux across the NPC, the lower the efflux rate constant (Fig. 2.4F). An increased import flux results in a higher concentration of NPC-resident cargo, and in principle this could affect the permeability barrier in two ways. First, the presence of Kap-cargo complexes may result in altered physicochemical properties of the transport barrier, like the induction of a different conformation of the FG-Nups (Lim *et al.*, 2006). Second, the flux of GFP may represent a significant fraction of the total flux through the NPC and thus have contributed to an increased molecular crowding in the pore. At average cellular concentrations of 10 – 20 μM, we measured a net flux into the NPC of about 35 – 60 molecules/s·NPC (Fig. 2.3F); the total flux was thus 70 – 120 molecules/s/NPC. Estimates of the fluxes across the NPC range from 200 to 1000 parallel transport events per pore per second in diverse metazoan systems (Dange *et al.*, 2008;Ribbeck and Gorlich, 2001;Smith *et al.*, 2002;Tokunaga *et al.*, 2008;Yang *et al.*, 2004). Assuming that the maximum cargo flux in *S. cerevisiae* cells is in the same range, then the flux of GFP-cargo would indeed be relative substantial contribution to the total flux of endogenous cargos.

Cargo in transit contributing to the passive permeability has been described previously for NPC-mimics where was found that the presence of cargo in the NPC inhibits the passage of non-cargo (Jovanovic-Talisman *et al.*, 2009;Zilman *et al.*, 2010). A decreased permeability by saturation of the NPCs seems a likely cause for the decrease in efflux rate constant at increased cargo concentration, but we cannot provide a definitive explanation, and further studies should be performed. The implication of a flux/crowding-dependent permeability barrier is that the NPCs would have a differential permeability, depending on the physiological state of a cell. This may be relevant for instance in the context of maintaining a permeability barrier in quiescent cells.

Finally, we found that the N/C ratio dropped at high cellular cargo concentrations, despite lower efflux rate constants under these conditions. One explanation could be that, at these high cargo concentrations, components of the import machinery becomes limiting, such as the transport factors or the capacity of RCC1 to convert RanGDP to RanGTP (Smith *et al.*, 2002). We measured for rgNLS-GFP and Pho4NLS-GFP that the saturation of the import pathway started at a cytoplasmic cargo concentration of ~25 μM or ~700,000 copies per cell. At these concen-

trations the total flux per NPC is larger than 150 molecules/s and this may indeed represent a significant increase compared to the endogenous flux.

Overall our transport data support that transport of proteins through the NPC can be explained by a simple pump-leak with high crowding in the pore contributing to the overall transport kinetics. Our data also demonstrates that sFRAP is a powerful tool to measure quantitatively the nuclear import and efflux rate constants.

Materials and methods

Plasmids and strains

The plasmids (listed in table 2.1) were obtained with conventional techniques, as follows: The construct coding for GFP was present on pUG34(Niedenthal *et al.*, 1996). The plasmid coding for tcNLS-GFP, pACM068-GFP-tcNLS, was constructed by ligating a tandem version of the *SV40-NLS* (tcNLS: PKKKRKVDPKKKRKV(Dingwall and Laskey, 1991)) in the multiple cloning site of pUG34. The *tcNLS* was ligated into the *Bam*HI and *Eco*RI sites as hybridized oligonucleotides (5'-GATCC CCAAA AAAGA AGAGA AAGGT AGATC CAAAA AAGAA GAGAA AGGTA GCTAG CG and 5'-AATTC GCTAG CTACCT TTCTC TTCTT TTTTG GATCT ACCTT TCTCT TCTTT TTTGG G). The constructs coding for Pho4NLS-GFP and rgNLS-GFP were obtained by removing the PrA coding sequence from respectively pBT018-Pho4NLS-GFP-PrA or pBT016-Nab2NLS-GFP-PrA (Timney *et al.*, 2006), using restriction enzymes *Hind*III and *Xho*I and ligation (T4 Ligase, Fermentas, Burlington, Canada) of the vector after filling in the complementary overhangs with the Klenow fragment of DNA polymerase I. All constructs were confirmed by sequencing.

All experiments were performed in yeast strain BY4742 ((Brachmann *et al.*, 1998) *MATa his3⊿1 leu2⊿0 lys2⊿0 ura3⊿0*, Invitrogen), grown in (low fluorescent) synthetic-dropout medium complete (SDC, Sigma-Aldrich, St Louis, MO) at pH 5.4, supplemented with 2% (w/v) glucose and without histidine or leucine.

Table 2.1 Plasmids

Name	Description	Source
pUG34	*Met25* promoter, *His3* selection marker, *CEN, GFP*	(Niedenthal et al., 1996)
pBT018-Pho4NLS-GFP-PrA	*TPI1*-promoter, *Leu2* selection marker, *2μ*, *Pho4NLS-GFP-PrA*	(Timney et al., 2006)
pBT016-Nab2NLS-GFP-PrA	*TPI1*-promoter, *Leu2* selection marker, *2μ*, *Nab2NLS-GFP-PrA*	(Timney et al., 2006)
pACM068-GFP-tcNLS	pUG34 where *tcNLS* and *GFP* were inserted	This study
pACM052-GFP-tcNLS-GFP	pACM068-tcNLS-GFP where an extra *GFP* was inserted	(Meinema et al., 2011)
pACM069-Pho4NLS-GFP	pBT018-Pho4NLS-GFP-PrA without *PrA*	This study
pACM070-Nab2NLS-GFP	pBT016-Nab2NLS-GFP-PrA without *PrA*	This study

Microscopy

Microscopy and selective FRAP were performed with a laser scanning confocal microscope, as described before (van den Bogaart *et al.*, 2007). Exponentially growing cells were kept in the minimal growth medium at 30 °C. The dwell times for laser scanning confocal microscopy were between 0.1 and 0.3 ms, the pixel steps were 50 nm and the focal volume was 0.2 fL (Veldhuis *et al.*, 2006). For each of the images, a pixel analysis was used to determine the volumes and fluorescence intensities of the various cell compartments (nucleus and cytoplasm; Fig. 2). To determine volumes, the surface areas of the confocal cross sections of the nucleus, vacuole and cytoplasm were measured and converted to a 3D volumes, assuming spherical shapes of these

compartments. The fluorescence intensities were converted into absolute GFP-concentrations, using the count rate per molecule estimated from fluorescence correlation spectroscopy (FCS) measurements on crude cell extracts. The fluorescence quantum yield in these cell extracts was assumed similar to that in cells.

Selective FRAP

Selective FRAP, also called selective photobleaching (reviewed in (Goodwin and Kenworthy, 2005)), was performed to determine the kinetics of nucleocytoplasmic transport. For selective FRAP, a confocal image of a yeast cell was recorded and the laser was focused on the nucleus for 5–10 s, resulting in partial (about 40–50%) photobleaching of the GFP. Because nucleocytoplasmic transport still occurred during this photobleaching step, the signal from the cytoplasm was also decreased by about 20–30%. The ratio of the GFP concentration in the nucleus to that in the cytoplasm (the N/C ratio) was decreased by the selective photobleaching and subsequently recovered to the steady-state N/C ratio through a net nuclear import of fluorescent molecules. The import of intact GFP was followed by recording a time series of images, using the same laser intensity as for photobleaching (less than 10 μW at the back aperture of the objective). Additional photobleaching during imaging was less than 3% and was neglected. The changes in the concentrations of cargo-GFP in the cytoplasm and the nucleus were fitted by using a model based on the assumption that diffusion of cargo in the cytoplasm and nucleus is much faster than the import and efflux rates and therefore these rate constants depend linearly on the cytoplasmic and nuclear concentrations of cargo. For the concentration change in the nucleus:

$$\frac{\mathrm{d}C_{\mathrm{N}}}{\mathrm{d}t} = \frac{IC_{\mathrm{C}}(t) - EC_{\mathrm{N}}(t)}{A} \tag{1}$$

where $C_{\mathrm{N}}(t)$ and $C_{\mathrm{C}}(t)$ are the concentrations in the nucleus and cytoplasm, respectively; I and E are the influx and efflux rate constants and $A = V_{\mathrm{N}}$, where V_{N} is the volume of the nucleus. For the concentration change in the cytoplasm, the solution is similar but now $A = -V_{\mathrm{C}}$, where V_{C} is the volume of the cytoplasm. The analytical solution for equation (1) for $C_{\mathrm{N}}(t)$ is given by

$$C_{\mathrm{N}}(t) = B\frac{C_{\mathrm{N}}(0)V_{\mathrm{N}} + C_{\mathrm{C}}(0)V_{\mathrm{C}}}{EV_{\mathrm{C}} + IV_{\mathrm{N}}} + C\frac{EC_{\mathrm{N}}(0) - IC_{\mathrm{C}}(0)}{EV_{\mathrm{C}} + IV_{\mathrm{N}}}\exp\left[-\left(\frac{E}{V_{\mathrm{N}}} + \frac{I}{V_{\mathrm{C}}}\right)t\right] \tag{2}$$

where $B = I$, $C = V_{\mathrm{C}}$ and $C_{\mathrm{N}}(0)$ and $C_{\mathrm{C}}(0)$ are the initial concentrations of cargo. For $C_{\mathrm{C}}(t)$, the solution is similar, but now $B = E$ and $C = -V_{\mathrm{N}}$. The rates from equation (2) were converted to the turnover of the NPC by assuming a constant density of 12 NPCs/μm^2, as reported in (Leslie *et al.*, 2006;Timney *et al.*, 2006;Winey *et al.*, 1997). Equation (3) and (4) were used to calculate the fluxes into (Φ_{in}) or out of the nucleus (Φ_{out}) across the NPC:

$$\Phi_{\mathrm{in}} = IC_{\mathrm{C}} \tag{3}$$

$$\Phi_{\mathrm{out}} = EC_{\mathrm{N}} \tag{4}$$

Acknowledgements

We thank B. L. Timney, C. Strambio-de-Castillia and J. J. Schuringa, for strains and plasmids. We thank V. Krasnikov for help with confocal microscopy. Financial support was provided by the Netherlands Science Foundation NWO (ALW grant number 814.02.002; VENI fellowship to L.M.V.; Top-subsidy grant 700.56.302 to B.P.).

References

1. Bischoff, F.R. and H.Ponstingl. 1995. Catalysis of guanine nucleotide exchange of Ran by RCC1 and stimulation of hydrolysis of Ran-bound GTP by Ran-GAP1. *Methods Enzymol.* **257**:135-144.
2. Brachmann, C.B., A.Davies, G.J.Cost, E.Caputo, J.Li, P.Hieter, and J.D.Boeke. 1998. Designer deletion strains derived from Saccharomyces cerevisiae S288C: a useful set of strains and plasmids for PCR-mediated gene disruption and other applications. *Yeast* **14**:115-132.
3. Dange, T., D.Grunwald, A.Grunwald, R.Peters, and U.Kubitscheck. 2008. Autonomy and robustness of translocation through the nuclear pore complex: a single-molecule study. *J. Cell Biol.* **183**:77-86.
4. Dingwall, C. and R.A.Laskey. 1991. Nuclear targeting sequences--a consensus? *Trends Biochem. Sci.* **16**:478-481.
5. Dingwall, C., S.V.Sharnick, and R.A.Laskey. 1982. A polypeptide domain that specifies migration of nucleoplasmin into the nucleus. *Cell* **30**:449-458.
6. Goodwin, J.S. and A.K.Kenworthy. 2005. Photobleaching approaches to investigate diffusional mobility and trafficking of Ras in living cells. *Methods* **37**:154-164.
7. Gorlich, D. and U.Kutay. 1999. Transport between the cell nucleus and the cytoplasm. *Annu. Rev. Cell Dev. Biol.* **15**:607-660.
8. Görlich, D., N.Pante, U.Kutay, U.Aebi, and F.R.Bischoff. 1996. Identification of different roles for RanGDP and RanGTP in nuclear protein import. *EMBO J.* **15**:5584-5594.
9. Grunwald, D., R.H.Singer, and M.Rout. 2011. Nuclear export dynamics of RNA-protein complexes. *Nature* **475**:333-341.
10. Jovanovic-Talisman, T., J.Tetenbaum-Novatt, A.S.McKenney, A.Zilman, R.Peters, M.P.Rout, and B.T.Chait. 2009. Artificial nanopores that mimic the transport selectivity of the nuclear pore complex. *Nature* **457**:1023-1027.
11. Kaffman, A., N.M.Rank, and E.K.O'Shea. 1998. Phosphorylation regulates association of the transcription factor Pho4 with its import receptor Pse1/Kap121. *Genes Dev.* **12**:2673-2683.
12. Keminer, O. and R.Peters. 1999. Permeability of single nuclear pores. *Biophys. J.* **77**:217-228.
13. Koster, M., T.Frahm, and H.Hauser. 2005. Nucleocytoplasmic shuttling revealed by FRAP and FLIP technologies. *Curr. Opin. Biotechnol.* **16**:28-34.
14. Kutay, U., F.R.Bischoff, S.Kostka, R.Kraft, and D.Gorlich. 1997. Export of importin alpha from the nucleus is mediated by a specific nuclear transport factor. *Cell* **90**:1061-1071.
15. Lee, D.C. and J.D.Aitchison. 1999. Kap104p-mediated nuclear import. Nuclear localization signals in mRNA-binding proteins and the role of Ran and Rna. *J. Biol. Chem.* **274**:29031-29037.
16. Leslie, D.M., B.Timney, M.P.Rout, and J.D.Aitchison. 2006. Studying nuclear protein import in yeast. *Methods* **39**:291-308.
17. Lim, R.Y., N.P.Huang, J.Koser, J.Deng, K.H.Lau, K.Schwarz-Herion, B.Fahrenkrog, and U.Aebi. 2006. Flexible phenylalanine-glycine nucleoporins as entropic barriers to nucleocytoplasmic transport. *Proc. Natl. Acad. Sci. U. S. A* **103**:9512-9517.
18. Lippincott-Schwartz, J., E.Snapp, and A.Kenworthy. 2001. Studying protein dynamics in living cells. *Nat. Rev. Mol. Cell Biol.* **2**:444-456.
19. Meinema, A.C., J.K.Laba, R.A.Hapsari, R.Otten, F.A.Mulder, A.Kralt, G.van den Bogaart, C.P.Lusk, B.Poolman, and L.M.Veenhoff. 2011. Long unfolded linkers facilitate membrane protein import through the nuclear pore complex. *Science* **333**:90-93.
20. Mohr, D., S.Frey, T.Fischer, T.Guttler, and D.Gorlich. 2009. Characterisation of the passive permeability barrier of nuclear pore complexes. *EMBO J.* **28**:2541-2553.
21. Niedenthal, R.K., L.Riles, M.Johnston, and J.H.Hegemann. 1996. Green fluorescent protein as a marker for gene expression and subcellular localization in budding yeast. *Yeast* **12**:773-786.
22. Paine, P.L., L.C.Moore, and S.B.Horowitz. 1975. Nuclear envelope permeability. *Nature* **254**:109-114.
23. Pemberton, L.F. and B.M.Paschal. 2005. Mechanisms of receptor-mediated nuclear import and nuclear export. *Traffic.* **6**:187-198.
24. Ribbeck, K. and D.Gorlich. 2001. Kinetic analysis of translocation through nuclear pore complexes. *EMBO J.* **20**:1320-1330.
25. Ribbeck, K., U.Kutay, E.Paraskeva, and D.Gorlich. 1999. The translocation of transportin-cargo complexes through nuclear pores is independent of both Ran and energy. *Curr. Biol.* **9**:47-50.
26. Rout, M.P., J.D.Aitchison, A.Suprapto, K.Hjertaas, Y.Zhao, and B.T.Chait. 2000. The yeast nuclear pore complex: composition, architecture, and transport mechanism. *J. Cell Biol.* **148**:635-651.
27. Schwoebel, E.D., T.H.Ho, and M.S.Moore. 2002. The mechanism of inhibition of Ran-dependent nuclear transport by cellular ATP depletion. *J. Cell Biol.* **157**:963-974.
28. Shulga, N., P.Roberts, Z.Gu, L.Spitz, M.M.Tabb, M.Nomura, and D.S.Goldfarb. 1996. In vivo nuclear transport kinetics in Saccharomyces cerevisiae: a role for heat shock protein 70 during targeting and translocation. *J. Cell Biol.*

135:329-339.

29. Siebrasse, J.P. and R.Peters. 2002. Rapid translocation of NTF2 through the nuclear pore of isolated nuclei and nuclear envelopes. *EMBO Rep.* **3**:887-892.
30. Smith, A.E., B.M.Slepchenko, J.C.Schaff, L.M.Loew, and I.G.Macara. 2002. Systems analysis of Ran transport. *Science* **295**:488-491.
31. Stewart, M. 2007. Molecular mechanism of the nuclear protein import cycle. *Nat. Rev. Mol. Cell Biol.* **8**:195-208.
32. Terry, L.J. and S.R.Wente. 2009. Flexible gates: dynamic topologies and functions for FG nucleoporins in nucleocytoplasmic transport. *Eukaryot. Cell* **8**:1814-1827.
33. Timney, B.L., J.Tetenbaum-Novatt, D.S.Agate, R.Williams, W.Zhang, B.T.Chait, and M.P.Rout. 2006. Simple kinetic relationships and nonspecific competition govern nuclear import rates in vivo. *J. Cell Biol.* **175**:579-593.
34. Tokunaga, M., N.Imamoto, and K.Sakata-Sogawa. 2008. Highly inclined thin illumination enables clear single-molecule imaging in cells. *Nat. Methods* **5**:159-161.
35. van den Bogaart, G., N.Hermans, V.Krasnikov, A.H.de Vries, and B.Poolman. 2007. On the decrease in lateral mobility of phospholipids by sugars. *Biophys. J.* **92**:1598-1605.
36. Veldhuis, G., M.Hink, V.Krasnikov, B.G.van den, J.Hoeboer, A.J.Visser, J.Broos, and B.Poolman. 2006. The oligomeric state and stability of the mannitol transporter, EnzymeII(mtl), from Escherichia coli: a fluorescence correlation spectroscopy study. *Protein Sci.* **15**:1977-1986.
37. Wente, S.R. and M.P.Rout. 2010. The nuclear pore complex and nuclear transport. *Cold Spring Harb. Perspect. Biol.* **2**:a000562.
38. Winey, M., D.Yarar, T.H.Giddings, Jr., and D.N.Mastronarde. 1997. Nuclear pore complex number and distribution throughout the Saccharomyces cerevisiae cell cycle by three-dimensional reconstruction from electron micrographs of nuclear envelopes. *Mol. Biol. Cell* **8**:2119-2132.
39. Yang, W., J.Gelles, and S.M.Musser. 2004. Imaging of single-molecule translocation through nuclear pore complexes. *Proc. Natl. Acad. Sci. U. S. A* **101**:12887-12892.
40. Zilman, A., T.S.Di, T.Jovanovic-Talisman, B.T.Chait, M.P.Rout, and M.O.Magnasco. 2010. Enhancement of transport selectivity through nano-channels by non-specific competition. *PLoS. Comput. Biol.* **6**:e1000804.

Chapter 3

A high affinity NLS is essential for strong accumulation of membrane proteins at the inner nuclear membrane

Anne C. Meinema[1], Justyna K. Laba[1], Rizqiya A. Hapsari[1], Geert van den Bogaart[1‡], C. Patrick Lusk[3], Bert Poolman[1], Liesbeth M. Veenhoff[1,2]

1 Department of Biochemistry, Groningen Biomolecular Sciences and Biotechnology Institute, Netherlands Proteomics Centre, Zernike Institute for Advanced Materials, University of Groningen, Nijenborgh 4, 9747 AG, Groningen, The Netherlands.

2 Department of Neuroscience, European Research Institute on the Biology of Ageing, University Medical Centre Groningen, Groningen, The Netherlands

3 Department of Cell Biology, Yale School of Medicine, New Haven, CT, USA, 06519

‡ Present address: Department of Neurobiology, Max Planck Institute for Biophysical Chemistry, Am Faßberg 11, 37077 Göttingen, Germany

Published in:

Meinema AC*, Laba JK*, Hapsari RA*, Otten R, Mulder FA, Kralt A, van den Bogaart G, Lusk CP, Poolman B, Veenhoff LM. Long unfolded linkers facilitate membrane protein import through the nuclear pore complex. *Science*. 2011 Jul 1; **333**(6038):90-3.

* These authors contributed equally to this work

Abstract

Nuclear pore complexes (NPCs) and soluble transport factors control the highly selective passage of macromolecules across the nuclear envelope (NE). The mechanism of import of membrane proteins from the endoplasmic reticulum (ER) to the inner nuclear membrane (INM) is not well characterized. For efficient targeting to the INM, a subset of *Saccharomyces cerevisiae* integral INM proteins require the soluble transport factors Kap60/Kap95 and the Ran GTPase (King *et al*., 2006). To further explore this transport mechanism through the NPC, we constructed a GFP-tagged transmembrane domain-containing reporter, having the minimal features required for nuclear targeting. This reporter protein consist of the NLS-containing domain and the first transmembrane segment of Heh2 and suffice for INM targeting in a Kap95-, Nup170- and RanGTP-dependent manner, alike Heh2. We confirmed the its localization at the INM and established assays to measure the nuclear accumulation. The reporters were mobile within the NE-ER network and their accumulation at the INM was the result of reversible import and efflux, and independent of selective retention at the INM. The NLS encoded on Heh2, is a high affinity NLS (K_D < 1 nM) compared to the classical NLS and other bipartite NLS's, and it is required for the strong nuclear accumulation.

Introduction

Proteins are transported across the nuclear pore complex (NPC) to reach the nucleus and to accumulate there. Proteins require a nuclear localization signal (NLS) for active nuclear transport, while small molecules are thought to diffuse freely across the NPC. The smaller a protein the more difficult it is to maintain large concentration gradients across the nuclear envelope as diffusion down the concentration gradient becomes more prominent. (Keminer and Peters, 1999). The NLS is recognized by a family of soluble transport factors called karyopherins (Kaps or importins and exportins). The Kap binds the NLS on the cargo protein and the Kap-cargo complex associates with a specific subset of proteins in the NPC, called nucleoporins (Nups) (Pemberton and Paschal, 2005). These Nups are enriched in Phe-Gly (FG) amino acid residues and interactions between Kaps and these FG-repeats are central to the transport mechanism (reviewed in (Wente and Rout, 2010)). In the nucleus, the Kap-cargo complex is dissociated by the binding of the small Ras-related nuclear protein in its GTP-bound form (RanGTP). The predominantly nuclear localization of RanGTP provides a directional cue to the transport cycle. The hydrolysis of GTP during Kap recycling to the cytoplasm provides the metabolic energy for nuclear transport (reviewed in (Stewart, 2007)). Although it is assumed that most of the cellular cargo that is imported into the nucleus interacts with intranuclear complexes or structures, the import machinery is capable to accumulate cargo that is not trapped. These cargos are actively imported into the nucleus and are able to leak back to the cytoplasm when the RanGTP gradient is dissipated or Kaps are no longer available (Timney *et al*., 2006).

To enrich membrane proteins at the inner nuclear membrane (INM), they travel from their point of synthesis and insertion in the endoplasmic reticulum (ER) to the outer nuclear membrane (ONM) and finally across the NPCs along the pore membrane (POM) that connects the INM and outer nuclear membrane (ONM) (see Fig. 3.1A, reviewed in (Lusk *et al.*, 2007;Zuleger *et al.*, 2008)). In EM analyses of the NPC, channels with a diameter of ~10 nm have been observed close to the POM (Frenkiel-Krispin *et al.*, 2010;Hinshaw *et al.*, 1992), and it has been suggested that they act as conduits for the diffusion of membrane proteins with soluble domains up to ~60 kDa (Ellenberg *et al.*, 1997;Soullam and Worman, 1995;Worman and Courvalin, 2000). In a number of cases, interactions with the nuclear lamina are required for the accumulation of specific membrane proteins at the INM (Graumann *et al.*, 2007;Lu *et al.*, 2008;Ostlund *et al.*, 1999;Ostlund *et al.*, 2006;Wu *et al.*, 2002;Zuleger *et al.*, 2011). Cumulatively, these data have contributed to a model in which the localization of integral INM proteins is a result of diffusion across the POM and selective retention at the INM.

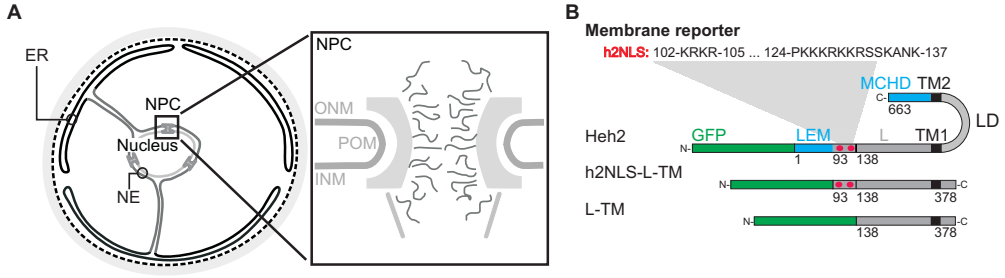

Figure 3.1: Heh2-based reporter proteins in a yeast cell. A) The geometry of a yeast cell. The nucleus is surrounded by the nuclear envelope (NE), consisting of an inner nuclear membrane (INM) and an outer nuclear membrane (ONM). The ONM is continuous with endoplasmic reticulum (ER). The INM is continuous with the ONM via the pore membrane (POM), which bends through the nuclear pore complex (NPC). **B)** Representation of Heh2-based GFP reporter proteins. LEM: domain with homology to members of the LEM (Lap2, emerin, MAN1)-family of integral INM proteins, MCHD: the MAN1-C-terminal Homology Domain, TM: transmembrane spanning segment, LD: lumenal domain, L: linker domain. The bipartite-like NLS is represented by two red dots and the amino acid sequence is indicated. Numbers correspond to the amino acids in full-length Heh2.

More recent work suggests that, similar to transport of soluble molecules, the targeting of membrane proteins to the INM is mediated by Kaps (Funakoshi *et al.*, 2011;King *et al.*, 2006;Tapley *et al.*, 2011;Turgay *et al.*, 2010). Specifically, the two *Saccharomyces cerevisiae* proteins Src1/Heh1 and Heh2 are identified to have an NLS and their localization was confirmed at the INM. Heh1 and Heh2 are homologues of the metazoan MAN1 and LEM2 (Fig. 1.2). They contain the well conserved helix-extension-helix (HEH)-motif in the LAP2-Emerin-MAN (LEM)-homology-domain at the N-terminus and the MAN1 C-terminal homology domain (MCHD) at the C-terminus (Grund *et al.*, 2008;King *et al.*, 2006;Lusk *et al.*, 2007). The LEM-domain is reported to bind chromatin via a small protein barrier-to-autointegration factor (BAF) (Margalit *et al.*, 2007), and MAN1 would bind directly to DNA via the positively charged helix in the conserved C-terminus (Caputo *et al.*, 2006). Heh1 and Heh2 bear also a bipartite NLS, consisting of two clusters of positive residues, required for INM-targeting by Kap60/Kap95 to the INM

(King *et al*., 2006). For other bipartite NLSs was shown that the first cluster binds in the first binding groove of Kap60 and the second cluster in the second groove (Conti and Kuriyan, 2000). Consequently, the interaction with a bipartite NLS is stronger than with a monopartite NLS (Hodel *et al*., 2006). The lumenal domain between the two transmembrane segments (TMs) of Heh1 and Heh2 is exposed in the lumenal region between the INM and the ONM and might have a role in NPC-assembly (Yewdell *et al*., 2011).

A greater level of control over the targeting of integral membrane proteins to the INM might exist than previously thought. We have set out to investigate the mechanism and path of nuclear transport of integral INM proteins. We constructed a membrane reporter protein having the minimal features for nuclear transport which turned out to consist of consecutively: (i) a high affinity NLS, (ii) a linker domain and (iii) a transmembrane domain. Similar to the full length protein Heh2, the reporter was efficiently targeted to the INM. But unlike Heh2, the reporter was able to leak back to the endoplasmic reticulum when the import step was disrupted. We found that the binding between the NLS and the transport factor Kap60 was strong (K_D < 1 nM), and this high affinity NLS was needed for strong accumulation of the reporter at the INM. We postulated that the nuclear accumulation of the reporter was thus solely based on the equilibrium of the rates of import and export kinetics and independent of intranuclear tethering.

Results

Heh2-based membrane protein reporters

We designed membrane reporters on the basis of Heh2, an integral membrane protein in yeast. To generate the membrane reporter with the features minimally needed for INM-targeting, we removed the homology domains LEM/HEH and MCHD at the N- and C-terminus, to prevent possible intranuclear interactions. In addition the second transmembrane segment (TM) and a major part of the lumenal domain (LD) were deleted. The reporter, named h2NLS-L-TM, consisted of GFP fused to amino acids 93-378 of Heh2 and comprised the bipartite NLS (Lange *et al*., 2010) (hereafter called h2NLS), a linker region (L) and one TM (Fig. 3.1B). Similar to Heh2, the reporter protein h2NLS-L-TM, accumulated specifically at the NE (Fig. 3.2). A control lacking the h2NLS, named L-TM, distributed over the NE and peripheral or plasma membrane-associated ER (ER) (Fig. 3.2). Thus, the h2NLS is essential for nuclear accumulation, whereas the MAN1 and LEM homology domains as well as the second TM are not required for NE localisation (King *et al*., 2006).

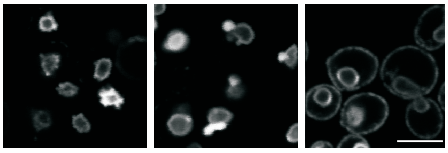

Figure 3.2: Localization of the membrane reporters in yeast cells. Confocal fluorescence images of a wild type (W303) strain expressing the reporters shown in figure 3.1. h2NLS-L-TM localizes exclusively to the NE, like Heh2. On the other hand, L-TM localizes throughout the NE-ER network. The average NE/ER ratios are shown with the standard error of the mean (SEM), scale bar is 5 μm.

The import pathways of h2NLS-L-TM and Heh2 are similar

For Heh2 it has been shown that its nuclear targeting is dependent on functional Kap95, the presence of Nup170 in the NPC and the concentration gradient of RanGTP over the NE (King *et al.*, 2006). To determine whether or not the membrane reporter h2NLS-L-TM had similar transport characteristics as Heh2, we tested the dependence of h2NLS-L-TM on Kap95, Nup170 and RanGTP. First, we examined the distribution of h2NLS-L-TM in a Kap95 (Karyopherin-β/Importin-β) "anchor away" strain (KAP95-AA) (Haruki *et al.*, 2008). KAP95-AA expresses an allele of *KAP95* fused to the *FRB* fragment of *TOR1* and a plasma membrane 'anchor' fused to FKB12 (PMA1-FKB12). The addition of rapamycin (RAP) yields a ternary complex of FKBP12 with FRB with nanomolar affinity (Chen *et al.*, 1995). After the formation of this complex, the cell is depleted of functional Kap95 and all Kap95-mediated nuclear transport is abolished (Fig. 3.3A). This enabled us to conditionally deplete the cells of functional Kap95 and thereby disrupt Kap95-mediated transport to the nucleus. Importantly, in the absence of RAP, the KAP95-AA strain has similar nuclear transport characteristics as the isogenic wild-type, because we found that the localization and nuclear accumulation of the reporters is similar (Fig. 3.3B and 3.2). In the presence of RAP the nuclear accumulation of h2NLS-L-TM is reduced dramatically (+RAP, Fig. 3.4A). Secondly, we found that h2NLS-L-TM is also mislocalized to the ER in a *nup170*Δ strain (Fig. 3.4B), suggesting that Nup170 plays a role in the nuclear accumulation of h2NLS-L-TM, like it does for Heh2. The deletion of Nup170 specifically disrupts nuclear transport of membrane proteins (King *et al.*, 2006) while it stimulates that of soluble proteins (Shulga *et al.*, 2000). Thirdly, we used a RanGEF mutant strain (*mtr1-1*) to determine the RanGTP-dependency of h2NLS-L-TM targeting to the NE. At the non-permissive temperature of 37°C, RanGEF is unable to convert RanGDP to RanGTP and the concentration gradient of RanGTP is readily dissipated

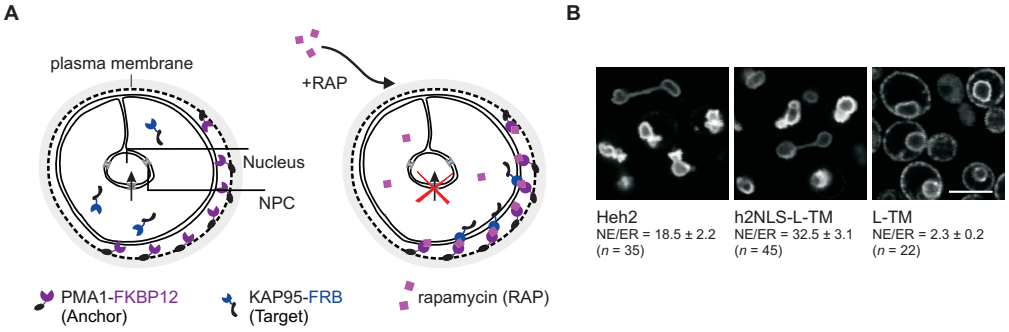

Figure 3.3: The KAP95-AA strain has similar transport properties as the wild-type strain. A) The cells in the KAP95-AA strain are depleted of functional Kap95 upon addtion of rapamycin. Schematic representation of the trapping of Kap95-FRB (Target) to Pma1-FKBP (Anchor) at the plasma membrane upon addition of rapamycin (RAP). Without rapamycin, Kap95-FRB facilitates nuclear import, whereas upon addition of rapamycin a ternary (nanomolar affinity) complex of FKBP12 and the FRB is formed (Chen *et al.*, 1995). The cell is then depleted of functional Kap95-FRB, and all Kap95 mediated cargo import to the nucleus is abolished. **B)** Confocal fluorescence images of the KAP95-AA strain expressing the reporter proteins Heh2, h2NLS-L-TM and L-TM tagged with GFP. The localization and the accumulation at the INM of these reporters were similar to that in wild-type cells (Fig. 3.2): Heh2 and h2NLS-L-TM were accumulated at the NE, while L-TM was localized throughout the NE-ER network. The average NE/ER ratios are shown with the SEM, scale bar is 5 μm.

(Kadowaki *et al.*, 1994). We found that h2NLS-L-TM was mislocalized in *mtr1-1* at the non-permissive temperature (Fig. 3.4C). Taken collectively, we conclude that the import pathway of Heh2 and h2NLS-L-TM are similar and thus independent of the presence of the LEM-domain, the MCHD or the second TM in the reporter.

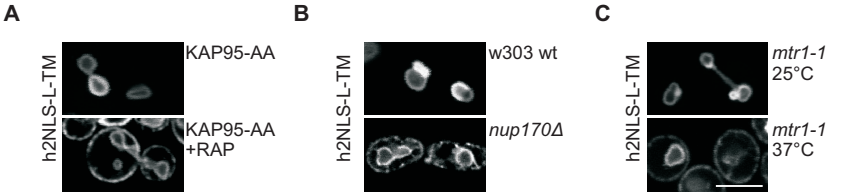

Figure 3.4: h2NLS-L-TM has similar nuclear transport properties as Heh2. A) Confocal fluorescence images show that h2NLS-L-TM mislocalizes when the cells are depleted of functional Kap95 (in the Kap95-AA strain in the presence of rapamycin (RAP)), **B)** when Nup170 is knocked out (*nup170⊿*) or **C)** when the RanGTP gradient across the NE is dissipated [in a RanGEF mutant strain (*mtr1-1*) at non-permissive temperature]. The scale bar is 5 μm.

h2NLS-L-TM accumulates at the INM

To validate if h2NLS-L-TM is indeed localized in the INM, we performed immuno- electron microscopy (immuno-EM) and the theta-assay. For the immuno-EM, we used anti-GFP antibodies and gold-conjugated secondary antibodies on cells expressing h2NLS-L-TM. The primary antibody binds to the reporter, while the secondary antibody labels the complex with a 10 nm large gold antibody. Significantly more gold particles were observed at the INM than at the ONM (Fig. 3.5A). Quantification of the gold particles' location showed 64% of the particles localized at the INM, 21% at the ONM and 15% in the lumen between the INM and ONM and/or the localization was ambiguous (Fig. 3.5B).

The theta assay was used as an additional proof that h2NLS-L-TM localizes at the INM. The theta assay is based on the phenomenon that over-expression of the nucleoporins Nup53 specifically causes INM proliferation (Marelli *et al.*, 2001), and this approach was previously used to discriminate between localisation of proteins in the INM or ONM. The extra intranuclear membrane lamellae are generally aligned with the INM, but often they also cut across the nucleus and then form typical nuclear envelope shapes resembling the Greek letter theta (θ)(Deng and Hochstrasser, 2006). If a fluorescent protein is localized at the INM, the proliferated membranes in the interior of the nucleus are visible as thetas in fluorescence microscopy; when the reporter is excluded from the INM, only the circular outline of the ONM is observed. We could see theta shaped nuclei in cells expressing Heh2 and h2NLS-L-TM, but also for L-TM (Fig. 3.5C). We quantified the number of the cells having theta-nuclei and found a fraction of 0.35 ± 0.07 for Heh2 expressing cells and a fraction of 0.35 ± 0.09 for h2NLS-L-TM expressing cells (Fig. 3.5D). This is consistent with about 30% of the cell population having theta-shaped nuclei as was reported for the INM-localised protein Doa10 and its interaction partners (Deng and Hochstrasser, 2006). The fraction of cells expressing L-TM with theta nuclei was significantly lower: 0.14 ± 0.08. This fraction was not as low (5-6%) as reported for proteins that are excluded from the INM (Deng and Hochstrasser, 2006). We reasoned that L-TM may be small enough to reach

the INM by diffusion across the NPC. The cause for more theta's with h2NLS-L-TM than with L-TM may be related to the strong nuclear accumulation of INM-resident proteins, which give rise to a more pronounced changes in the NE-morphology (e.g. h2NLS-L-TM, Fig. 3.2 and 3.3B) than ONM-ER reporters do (L-TM, Fig. 3.2 and 3.3B). The overexpression of Nup53 is thus a double stimulus to form theta nuclei for h2NLS-L-TM. Based on both the immuno-EM and the theta assay, we conclude that the h2NLS-containing reporter is indeed accumulated at the INM.

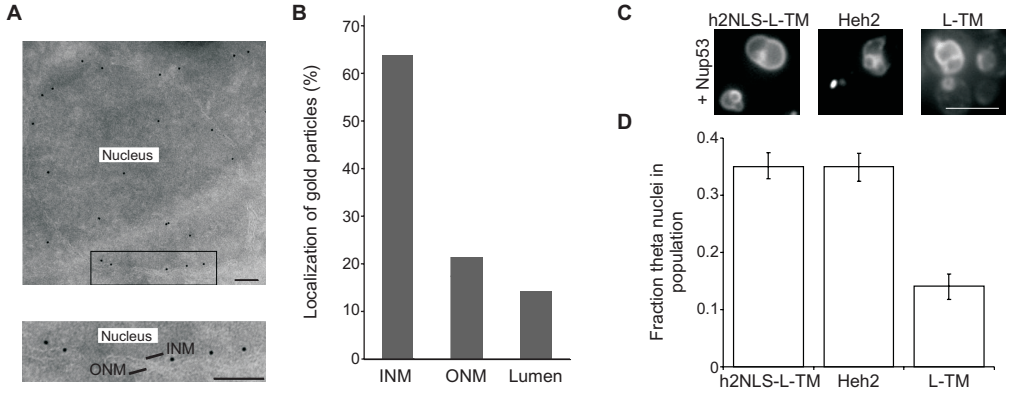

Figure 3.5: h2NLS-L-TM is imported to the INM as shown by ImmunoEM and the theta assay. A) Immunoelectron micrograph of h2NLS-L-TM in the KAP95-AA strain labelled with anti-GFP antibodies, followed by binding of a 10-nm diameter gold-conjugated secondary antibody. Scale bar is 250 nm. **B)** The localization of gold particles in the immuno-electron micrographs was quantified and plotted. Gold particles were localized closely to the inner nuclear membrane (INM), outer nuclear membrane (ONM) or ambiguous/between the membranes (Lumen) (n = 350). **C)** Representative wide-field microscope images of the KAP95-AA strain expressing the membrane reporters in combination with the overproduction of Nup53. The typical theta-shaped nuclei were visible for all three reporters. Scale bar is 5 μm. **D)** The fraction of cells having theta-shaped nuclei. A fraction of 0.3 has been reported for INM accumulated proteins (Deng and Hochstrasser, 2006).

Quantification of nuclear accumulation

To quantify the accumulation of the reporter proteins at the INM, we used the average pixel intensities at the NE and ER (NE/ER ratio) (Fig. 5.2), since the INM cannot be resolved from the ONM by standard light microscopy (Fig. 3.2 and 3.3B). The reporters were expressed from low-copy plasmids under the control of the *GAL1* promoter, and their subcellular distribution was monitored by confocal fluorescence microscopy. For each cell, the average pixel intensities at the NE and at the ER was determined from which the NE/ER ratio was calculated. The average NE/ER ratio was calculated over multiple cells (n > 18 for each point).

We measured the NE/ER ratios in time after inducing the expression of the reporter proteins. Over three hours of induction the h2NLS-L-TM accumulated ~35-fold at the NE, the full length Heh2 protein accumulated at somewhat lower levels. The reporter L-TM showed a significant lower nuclear accumulation with only 2 to 4-fold enrichment at the NE. This low level of L-TM at the NE is consistent with the inability of the reporter to be efficiently targeted to the INM. The small nuclear accumulation of L-TM is likely due to the different morphology of the

membranes of the NE compared to the ER (West *et al.*, 2011) and/or inaccuracies in the estimation of the ER area. The NE is a continuous cisternael membrane with low curvature, consisting of relatively flat parallel membrane bilayers separated by the perinuclear space. In contrast, the large ER is composed of both cisternae and membrane tubules with high membrane curvature and only 20 – 40% of the plasma membrane is covered with ER (West *et al.*, 2011). Moreover, optical microscopy does not resolve these details and we considered the ER as a continuous membrane, aligned with the plasma membrane. Thus in fact may have overestimated the area of the ER. We infer that deviation from 1× may thus be due to the higher density of membranes at the NE. Despite the inaccuracies in estimating the membrane areas, we can use the NE/ER ratio as a relative measure for nuclear accumulation of membrane proteins.

The NE/ER ratios were plotted against the average fluorescence intensity in the cell (Fig. 3.6). The NE/ER ratios of the reporters were stable between 1 and 3 hours after induction, corresponding to 35-100% of maximal expression. The NE/ER ratios are thus independent of the expression levels within this timeframe, allowing reproducible measurements.

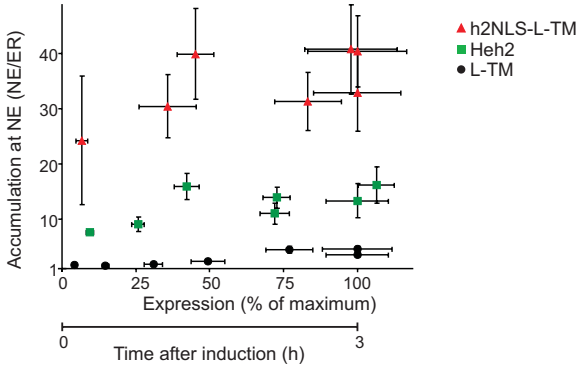

Figure 3.6: The nuclear accumulation of the reporters as a function of expression levels. The average accumulation at the NE was quantified at different levels of h2NLS-L-TM (red ▲), L-TM (black ●) and Heh2 (green ■), with the proteins expressed in the KAP95-AA strain (see Fig. 3.5). The NE-accumulation levels of the reporters are plotted against the normalized fluorescence of the cell during 3 hours. SEM is indicated and for each point: $n \geq 18$.

The nuclear accumulation of h2NLS-L-TM in the INM is independent of nuclear tethering

Using the Kap95-AA strain, we are able to conditionally deplete the cells of Kap95 and monitor the redistribution of the INM-localized h2NLS-L-TM to the ONM-ER network upon blocking of the import (Fig. 3.3A). We induced h2NLS-L-TM in the Kap95-AA cells for 2 hours and imaged the localization of the reporter. At time point zero, we added RAP to anchor Kap95 at the plasma membrane and quantified the fluorescence intensity in the nucleus and ER. Upon the addition of rapamycin, the nuclear accumulation dropped with a half-time of 14 ± 2.7 minutes (Fig. 3.7A). In contrast, the fluorescence intensity of Heh2 at the NE remained unaltered for over 90 min. The reduction of fluorescence intensity at the INM is not caused by protein degradation since the average overall fluorescence intensity of the cell remained constant for both h2NLS-L-TM and Heh2 during the course of the experiment (Fig. 3.7B). We conclude that, while Heh2 is bound to nuclear factors, h2NLS-L-TM is fully mobile within the NE-ER network. The LEM and MAN1 homology domains of Heh2 likely bind to interaction partners in the nucleus, as was reported for their homologues (Caputo *et al.*, 2006;King *et al.*, 2006;Margalit *et al.*, 2007). The lo-

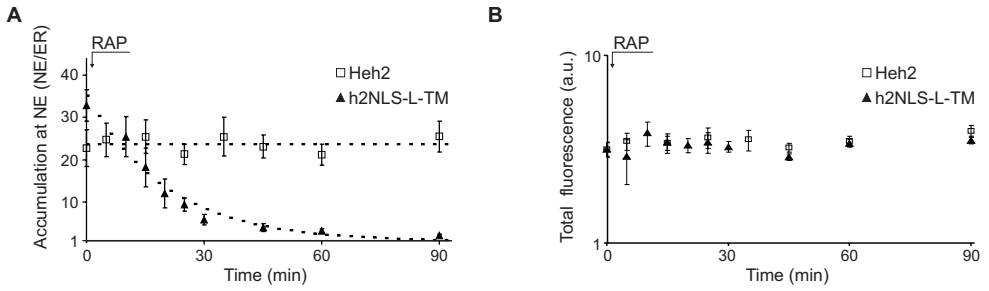

Figure 3.7: The nuclear accumulation of h2NLS-L-TM is based on faster import than efflux. **A)** The nuclear accumulation of h2NLS-L-TM (▲) and Heh2 (□) in the KAP95-AA strain as function of time after the anchoring of Kap95 at the plasma membrane (RAP at $t = 0$, $n \geq 13$). The decrease of nuclear accumulation of h2NLS-L-TM indicates its mobility over the NPC, while Heh2 is tethered to nuclear proteins or other INM structures. **B)** Addition of rapamycin did not affect the cellular reporter levels. The average fluorescence of a cell is plotted for Heh2 (□) and h2NLS-L-TM (▲) after addition of rapamycin. The total average fluorescence of a cell is the weighted average of the intensities at the surface of the NE and the ER. To calculate the surface of the double membrane of the NE (~16 μm^2) and ER (~150 μm^2), the diameter of the nucleus and the ER was obtained as described previously (van den Bogaart *et al.*, 2009) and is consistent with earlier results (Timney *et al.*, 2006). The volumes bounded by the ER and the nuclear membranes were assumed to be spherical. The fluorescence intensities were normalized to time zero, i.e. before the addition of rapamycin. The SEM is indicated.

calization of h2NLS-L-TM at the INM is thus independent on nuclear retention and the nuclear import is faster than efflux. We show for the first time that the Kap and RanGTP-dependent nuclear accumulation of membrane proteins is the resultant of fully reversible import and efflux.

The h2NLS promotes strong nuclear accumulation

We compared the transport characteristics of a soluble GFP-reporter containing the h2NLS with that of a soluble reporter with a tandem of the SV-40 classical NLS (tcNLS) (Dingwall *et al.*, 1982;Dingwall and Laskey, 1991). For this purpose, we constructed a reporter containing the h2NLS and the full length linker domain (L), consisting of 176 residues (GFP-h2NLS-L), a similar reporter with a truncated linker of 33 residues (GFP-h2NLS-L(33)), a reporter containing two copies of GFP having tcNLS in between (GFP-tcNLS-GFP), and one with GFP without an NLS as a negative control. Interestingly, the h2NLS-containing constructs had 15× higher nuclear accumulation levels than GFP-tcNLS-GFP (Fig. 3.8A).

These high accumulation levels were measured irrespective of the presence of the linker domain, suggesting that the linker region does not contribute directly to Kap60/95 binding or interactions with the FG-Nups. The high accumulation is not caused by retention in the nucleus, because the accumulation of h2NLS-L-TM and GFP-tcNLS-GFP dropped with comparable half-times in the Kap95-AA assay (Fig. 3.8B). The higher import rate might be caused by a higher affinity of the Kap60/Kap95 complex for h2NLS than for tcNLS. The fraction of karyopherin-cargo will be higher and consequently the import rate. The role of the linker domain will be discussed in Chapter 4.

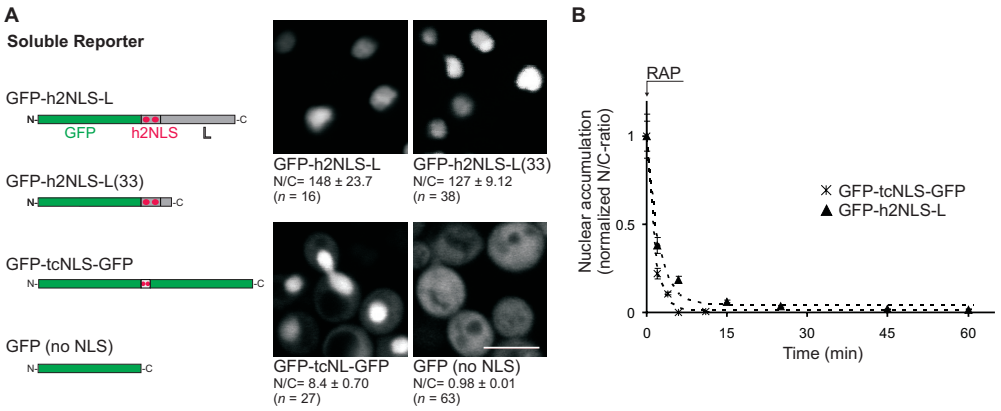

Figure 3.8: The h2NLS provokes a strong nuclear accumulation of soluble proteins. A) Representation of soluble reporters (i) GFP-h2NLS-L, (ii) GFP-h2NLS-L(33) (L is truncated to 33 residues) and (iii) GFP-tcNLS-GFP (tandem SV-40 classical NLS, fused to two copies of GFP) and (iv) GFP alone. The confocal fluorescence images show the localization of the reporters in live cells. We quantified the concentration of reporter in the nucleus (N) and in the cytosol (C) and calculated the N/C ratio as described in (Chapter 2, Fig. 2.2). The cytosolic fluorescence signal in cells expressing h2NLS-L and h2NLS-L(33) was close to the cellular auto-fluorescence levels, for which we did not correct. The N/C-ratios are thus somewhat underestimated. The scale bar is 5 μm. **B)** The accumulation of both reporters, GFP-h2NLS-L (53 kDa) and GFP-tcNLS-GFP (56 kDa), was measured after adding rapamycin (RAP) in the KAP95-AA strain to evaluate the nuclear efflux. The accumulation was normalized to $t = 0$, i.e. before addition of rapamycin. Regardless of the high accumulation of GFP-h2NLS-L (N/C ratio of 148, panel A), the efflux could be fitted to a mono-exponential decay function. The efflux of GFP-h2NLS-L was a slightly slower than that of GFP-tcNLS-GFP (i.e. half-times $t_{0.5}$ = 89 ± 10 s and 56 ± 4 s, respectively) ($n \geq 14$). The SEM is indicated.

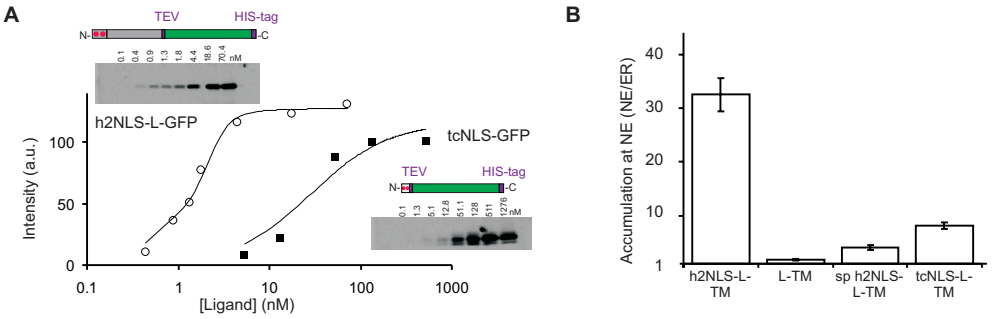

Figure 3.9: The high-affinity interaction between Kap60 and h2NLS allows high-level accumulation of membrane reporters at the INM. A) An *in vitro* solid-phase binding assay was performed, using purified Kap60 lacking the Importin-β binding domain, Kap60ΔIBB, and purified tcNLS-GFP (○) and h2NLS-L-GFP (■). Beads with Kap60ΔIBB were incubated with different concentrations of fluorescent cargo (ligand). The binding (intensity) was determined from in-gel fluorescence (inset) and fitted with a simple one-site model for binding to yield dissociation constants of 27 nM for tcNLS-GFP and <1 nM for h2NLS-L-GFP. **B)** The accumulation at the INM of reporter containing a bipartite h2NLS (h2NLS-L-TM), without NLS (L-TM), with single partite NLS (sp h2NLS-L-TM), or with tandem cNLS (tcNLS-L-TM) (n ≥ 32) was measured *in vivo* in the KAP95-AA strain. The high-affinity NLS is clearly needed for a strong nuclear accumulation. The SEM is indicated.

High affinity binding between Kap60 and h2NLS

Using an *in vitro* assay, we estimated the dissociation constant of Kap60ΔIBB for the h2NLS. The importin-β binding (IBB)-domain and NLS-cargo compete for the same NLS-binding groove on Kap60. This auto-inhibitory effect prevents futile cycling of Kap60/Kap95 across the NPC in the absence of cargo but also reduces the binding of NLS-containing cargo protein if Kap95 is not present (reviewed in (Lott and Cingolani, 2010)). NLS-binding affinities measured with Kap60ΔIBB resemble those in the presence of both Kap60 and Kap95 (Hahn *et al.*, 2008). We conjugated beads with Kap60ΔIBB and incubated them with purified tcNLS-GFP or h2NLS-L-GFP (Chapter 5). Amounts of bound cargo were estimated from in-gel fluorescence and fitted to yield dissociation constants (Lanfermeijer *et al.*, 1999). Although the data did not allow accurate determination of the dissociation constant, we estimated that the dissociation constant of Kap60ΔIBB for tcNLS-GFP was ~27 nM and for h2NLS-L-GFP <1 nM (Fig 3.9A). The affinity of Kap60 for h2NLS is thus an order of magnitude higher than for tcNLS.

The high affinity interaction between Kap60 and h2NLS is essential for nuclear accumulation

To assess whether this high affinity is actually required for the import of h2NLS-L-TM and thus for the import of membrane proteins, we replaced the bipartite h2NLS by a lower affinity NLS: either a single-partite version of the h2NLS, lacking the first KRKR basic region (sp h2NLS), or a tandem classical NLS (tcNLS). Both membrane reporters still accumulated at the INM, but the NE/ER ratios were significant lower (8.1 and 4.0, respectively) than for h2NLS-L-TM (Fig. 3.9B). The data indicates a correlation between the affinity of Kap60 for an NLS and the nuclear accumulation of membrane proteins.

Conclusion and discussion

The INM-localized integral membrane protein Heh2 was minimized to delineate the details of nuclear transport of membrane proteins into the nucleus. The LEM/HEH and MCHD homology-domains at the N- and C-terminus, which are thought to bind chromatin, were removed to prevent intranuclear binding (Caputo *et al.*, 2006;King *et al.*, 2006;Margalit *et al.*, 2007). One of the two TMs and the lumenal domain, which could interact with components of the NPC (Yewdell *et al.*, 2011), were deleted as well. This minimal reporter, h2NLS-L-TM, contained the h2NLS, a linker domain and the first TM. Immuno-EM and the theta-assay indicated that the reporter localization in the NE corresponds to accumulation at the INM. Its accumulation in the INM was dependent on Kap95, the RanGTP gradient and Nup170. We thus infer that the nuclear transport of h2NLS-L-TM was, like Heh2, mediated by the cells nuclear transport machinery and its import pathway across the NPC is via the pore membrane.

The membrane reporter h2NLS-L-TM leaked out of the nucleus and diffused back to the ER across the NPC, after the cells were depleted of Kap95 upon the addition of rapamycin to the strain Kap95-AA. The diffusion of h2NLS-L-TM across the NPC indicates that the path

of efflux tolerates soluble domains of at least 51 kDa. This is consistent with the observation of L-TM localization at the INM in the theta-nucleated cells and published data (Ellenberg *et al.*, 1997;Soullam and Worman, 1995;Worman and Courvalin, 2000).

The observation that h2NLS-L-TM leaked out of the nucleus, unlike Heh2, showed that h2NLS-L-TM was not tethered in the INM. The nuclear accumulation of membrane proteins is thus possible without selective nuclear retention. The nuclear accumulation of membrane proteins can be maintained by only transport kinetics. This allows the cell to control the levels of membrane proteins in the nucleus, independent of the concentration of cargo-retention sites.

The h2NLS provokes very efficient nuclear targeting of soluble proteins. The dissociation constant of Kap60ΔIBB for h2NLS was at least one order of magnitude higher than for tcNLS. The here reported dissociation constants are in line with published data (Hodel *et al.*, 2006;Lange *et al.*, 2010). The dissociation constant of Kap60 for h2NLS-L-GFP is among the highest measured for any yeast cargo (Hahn *et al.*, 2008;Lange *et al.*, 2010). The strong interaction between Kap60 and h2NLS-L-TM promotes a high accumulation of the reporter in the INM. We speculate that the relatively high-affinity NLS enables effective competition of membrane proteins with 'more abundant' soluble cargos, that is, those that use Kap60/Kap95 for nuclear accumulation (see Chapter 7).

Acknowledgements

We thank M. C. King, M. P. Rout, and D. J. Slotboom for discussion; V. Krasnikov for help with confocal microscopy; M. Graham for assistance with immunoelectron microscopy, and M. P. Rout for reagents. This work was supported by funding from the Netherlands Organization for Scientific Research (VIDI fellowship to L.M.V.; Top-subsidy grant 700.56.302 to B.P.).

References

1. Caputo, S., J.Couprie, I.Duband-Goulet, E.Konde, F.Lin, S.Braud, M.Gondry, B.Gilquin, H.J.Worman, and S.Zinn-Justin. 2006. The carboxyl-terminal nucleoplasmic region of MAN1 exhibits a DNA binding winged helix domain. *J. Biol. Chem.* **281**:18208-18215.
2. Chen, J., X.F.Zheng, E.J.Brown, and S.L.Schreiber. 1995. Identification of an 11-kDa FKBP12-rapamycin-binding domain within the 289-kDa FKBP12-rapamycin-associated protein and characterization of a critical serine residue. *Proc. Natl. Acad. Sci. U. S. A* **92**:4947-4951.
3. Conti, E. and J.Kuriyan. 2000. Crystallographic analysis of the specific yet versatile recognition of distinct nuclear localization signals by karyopherin alpha. *Structure.* **8**:329-338.
4. Deng, M. and M.Hochstrasser. 2006. Spatially regulated ubiquitin ligation by an ER/nuclear membrane ligase. *Nature* **443**:827-831.
5. Dingwall, C. and R.A.Laskey. 1991. Nuclear targeting sequences--a consensus? *Trends Biochem. Sci.* **16**:478-481.
6. Dingwall, C., S.V.Sharnick, and R.A.Laskey. 1982. A polypeptide domain that specifies migration of nucleoplasmin into the nucleus. *Cell* **30**:449-458.
7. Ellenberg, J., E.D.Siggia, J.E.Moreira, C.L.Smith, J.F.Presley, H.J.Worman, and J.Lippincott-Schwartz. 1997. Nuclear membrane dynamics and reassembly in living cells: targeting of an inner nuclear membrane protein in interphase and mitosis. *J. Cell Biol.* **138**:1193-1206.
8. Frenkiel-Krispin, D., B.Maco, U.Aebi, and O.Medalia. 2010. Structural analysis of a metazoan nuclear pore complex reveals a fused concentric ring architecture. *J. Mol. Biol.* **395**:578-586.
9. Funakoshi, T., M.Clever, A.Watanabe, and N.Imamoto. 2011. Localization of Pom121 to the inner nuclear membrane is required for an early step of interphase nuclear pore complex assembly. *Mol. Biol. Cell* **22**:1058-1069.
10. Graumann, K., S.L.Irons, J.Runions, and D.E.Evans. 2007. Retention and mobility of the mammalian lamin B receptor in the plant nuclear envelope. *Biol. Cell* **99**:553-562.
11. Grund, S.E., T.Fischer, G.G.Cabal, O.Antunez, J.E.Perez-Ortin, and E.Hurt. 2008. The inner nuclear membrane protein Src1 associates with subtelomeric genes and alters their regulated gene expression. *J. Cell Biol.* **182**:897-910.
12. Hahn, S., P.Maurer, S.Caesar, and G.Schlenstedt. 2008. Classical NLS proteins from Saccharomyces cerevisiae. *J. Mol. Biol.* **379**:678-694.
13. Haruki, H., J.Nishikawa, and U.K.Laemmli. 2008. The anchor-away technique: rapid, conditional establishment of yeast mutant phenotypes. *Mol. Cell* **31**:925-932.
14. Hinshaw, J.E., B.O.Carragher, and R.A.Milligan. 1992. Architecture and design of the nuclear pore complex. *Cell* **69**:1133-1141.
15. Hodel, A.E., M.T.Harreman, K.F.Pulliam, M.E.Harben, J.S.Holmes, M.R.Hodel, K.M.Berland, and A.H.Corbett. 2006. Nuclear localization signal receptor affinity correlates with in vivo localization in Saccharomyces cerevisiae. *J. Biol. Chem.* **281**:23545-23556.
16. Kadowaki, T., S.Chen, M.Hitomi, E.Jacobs, C.Kumagai, S.Liang, R.Schneiter, D.Singleton, J.Wisniewska, and A.M.Tartakoff. 1994. Isolation and characterization of Saccharomyces cerevisiae mRNA transport-defective (mtr) mutants 2. *J. Cell Biol.* **126**:649-659.
17. Keminer, O. and R.Peters. 1999. Permeability of single nuclear pores. *Biophys. J.* **77**:217-228.
18. King, M.C., C.P.Lusk, and G.Blobel. 2006. Karyopherin-mediated import of integral inner nuclear membrane proteins. *Nature* **442**:1003-1007.
19. Lanfermeijer, F.C., A.Picon, W.N.Konings, and B.Poolman. 1999. Kinetics and consequences of binding of nona- and dodecapeptides to the oligopeptide binding protein (OppA) of Lactococcus lactis. *Biochemistry* **38**:14440-14450.
20. Lange, A., L.M.McLane, R.E.Mills, S.E.Devine, and A.H.Corbett. 2010. Expanding the definition of the classical bipartite nuclear localization signal. *Traffic.* **11**:311-323.
21. Lott, K. and G.Cingolani. 2010. The importin beta binding domain as a master regulator of nucleocytoplasmic transport. *Biochim. Biophys. Acta.*
22. Lu, W., J.Gotzmann, L.Sironi, V.M.Jaeger, M.Schneider, Y.Luke, M.Uhlen, C.A.Szigyarto, A.Brachner, J.Ellenberg, R.Foisner, A.A.Noegel, and I.Karakesisoglou. 2008. Sun1 forms immobile macromolecular assemblies at the nuclear envelope. *Biochim. Biophys. Acta* **1783**:2415-2426.
23. Lusk, C.P., G.Blobel, and M.C.King. 2007. Highway to the inner nuclear membrane: rules for the road. *Nat. Rev. Mol. Cell Biol.* **8**:414-420.
24. Marelli, M., C.P.Lusk, H.Chan, J.D.Aitchison, and R.W.Wozniak. 2001. A link between the synthesis of nucleoporins and the biogenesis of the nuclear envelope. *J. Cell Biol.* **153**:709-724.
25. Margalit, A., A.Brachner, J.Gotzmann, R.Foisner, and Y.Gruenbaum. 2007. Barrier-to-autointegration factor--a BAFfling little protein. *Trends Cell Biol.* **17**:202-208.
26. Ostlund, C., J.Ellenberg, E.Hallberg, J.Lippincott-Schwartz, and H.J.Worman. 1999. Intracellular trafficking of

emerin, the Emery-Dreifuss muscular dystrophy protein. *J. Cell Sci.* **112**:1709-1719.

27. Ostlund, C., T.Sullivan, C.L.Stewart, and H.J.Worman. 2006. Dependence of diffusional mobility of integral inner nuclear membrane proteins on A-type lamins. *Biochemistry* **45**:1374-1382.
28. Pemberton, L.F. and B.M.Paschal. 2005. Mechanisms of receptor-mediated nuclear import and nuclear export. *Traffic.* **6**:187-198.
29. Shulga, N., N.Mosammaparast, R.Wozniak, and D.S.Goldfarb. 2000. Yeast nucleoporins involved in passive nuclear envelope permeability. *J. Cell Biol.* **149**:1027-1038.
30. Soullam, B. and H.J.Worman. 1995. Signals and structural features involved in integral membrane protein targeting to the inner nuclear membrane. *J. Cell Biol.* **130**:15-27.
31. Stewart, M. 2007. Molecular mechanism of the nuclear protein import cycle. *Nat. Rev. Mol. Cell Biol.* **8**:195-208.
32. Tapley, E.C., N.Ly, and D.A.Starr. 2011. Multiple mechanisms actively target the SUN protein UNC-84 to the inner nuclear membrane. *Mol. Biol. Cell* **22**:1739-1752.
33. Timney, B.L., J.Tetenbaum-Novatt, D.S.Agate, R.Williams, W.Zhang, B.T.Chait, and M.P.Rout. 2006. Simple kinetic relationships and nonspecific competition govern nuclear import rates in vivo. *J. Cell Biol.* **175**:579-593.
34. Turgay, Y., R.Ungricht, A.Rothballer, A.Kiss, G.Csucs, P.Horvath, and U.Kutay. 2010. A classical NLS and the SUN domain contribute to the targeting of SUN2 to the inner nuclear membrane. *EMBO J.* **29**:2262-2275.
35. van den Bogaart, G., A.C.Meinema, V.Krasnikov, L.M.Veenhoff, and B.Poolman. 2009. Nuclear transport factor directs localization of protein synthesis during mitosis. *Nat. Cell Biol.* **11**:350-356.
36. Wente, S.R. and M.P.Rout. 2010. The nuclear pore complex and nuclear transport. *Cold Spring Harb. Perspect. Biol.* **2**:a000562.
37. West, M., N.Zurek, A.Hoenger, and G.K.Voeltz. 2011. A 3D analysis of yeast ER structure reveals how ER domains are organized by membrane curvature. *J. Cell Biol.* **193**:333-346.
38. Worman, H.J. and J.C.Courvalin. 2000. The inner nuclear membrane. *J. Membr. Biol.* **177**:1-11.
39. Wu, W., F.Lin, and H.J.Worman. 2002. Intracellular trafficking of MAN1, an integral protein of the nuclear envelope inner membrane. *J. Cell Sci.* **115**:1361-1371.
40. Yewdell, W.T., P.Colombi, T.Makhnevych, and C.P.Lusk. 2011. Lumenal interactions in nuclear pore complex assembly and stability. *Mol. Biol. Cell* **22**:1375-1388.
41. Zuleger, N., D.A.Kelly, A.C.Richardson, A.R.Kerr, M.W.Goldberg, A.B.Goryachev, and E.C.Schirmer. 2011. System analysis shows distinct mechanisms and common principles of nuclear envelope protein dynamics. *J. Cell Biol.* **193**:109-123.
42. Zuleger, N., N.Korfali, and E.C.Schirmer. 2008. Inner nuclear membrane protein transport is mediated by multiple mechanisms. *Biochem. Soc. Trans.* **36**:1373-1377.

Chapter 4

Long unfolded linkers facilitate membrane protein import through the nuclear pore complex

Anne C. Meinema[1], Justyna K. Laba[1], Rizqiya A. Hapsari[1], Renee Otten[1], Frans A. A. Mulder[1], Annemarie Kralt[2], Bert Poolman[1], Liesbeth M. Veenhoff[1,2]

1 Department of Biochemistry, Groningen Biomolecular Sciences and Biotechnology Institute, Netherlands Proteomics Centre, Zernike Institute for Advanced Materials, University of Groningen, Nijenborgh 4, 9747 AG, Groningen, The Netherlands.

2 Department of Neuroscience, European Research Institute on the Biology of Ageing, University Medical Centre Groningen, Groningen, The Netherlands

Published in:

Meinema AC*, Laba JK*, Hapsari RA*, Otten R, Mulder FA, Kralt A, van den Bogaart G, Lusk CP, Poolman B, Veenhoff LM. Long unfolded linkers facilitate membrane protein import through the nuclear pore complex. *Science*. 2011 Jul 1; **333**(6038):90-3.

* These authors contributed equally to this work

Abstract

Active nuclear import of soluble proteins involves the recognition of a nuclear localization signal (NLS) on cargo by transport factors (karyopherins). In turn, the karyopherins shuttle the cargo through the nuclear pore complex (NPC) by binding to phenylalanine-glycine (FG)-rich domains of nucleoporins (Nups). Similarly, some membrane proteins carry an NLS as well and require also transport factors for their nuclear localization. How these membrane proteins cross the NPC to reach the inner nuclear membrane is presently unclear. Here, we found that an intrinsically-disordered linker of at least 120 residues, spanning the distance between the NLS and the transmembrane segment in transmembrane proteins, is required for nuclear transport. Using mutant strains, we show that membrane protein import specifically requires the GLFG-rich regions of FG-Nups, Nup145N, Nup100 and Nup57. We show that membrane reporters with an extralumenal domain up to 174 kDa are still imported to the INM, indicating a spacious transport path through the NPC. A membrane reporter with an N-terminal FKBP affinity-tag could be trapped at a complementary C-terminal FRB-moiety that was fused to Nsp1. The position of the FRB-domain on Nsp1 is on the pore side of the NPC scaffold and thus we conclude that the linker can span the distance between the pore membrane and the central channel. We propose an import mechanism for membrane proteins in which an unfolded linker slices through the NPC scaffold to enable binding between the transport factor and the FG-domains in the centre of the NPC.

Introduction

The nuclear envelope (NE) consists of an inner and outer nuclear membrane (INM, ONM) connected by the pore membrane (POM) at sites where the NPCs are embedded (Fig. 3.1). The ONM is continuous with the endoplasmic reticulum (ER). NPCs are composed of a membrane-anchored scaffold that stabilizes a cylindrical central channel, in which nucleoporins (Nups) with disordered phenylalanine–glycine (FG)-rich regions provide the selectivity barrier (Wente and Rout, 2010). In order for a membrane protein to move through the NPC, its transmembrane domains pass through the pore membrane (POM), while its extralumenal soluble domain(s) pass through the NPC by a mechanism yet to be clarified (Lusk *et al.*, 2007;Ohba *et al.*, 2004;Zuleger *et al.*, 2008;Antonin *et al.*, 2011). Some proteins reach the INM by diffusion through the pore membrane and adjacent lateral channels (Frenkiel-Krispin *et al.*, 2010;Hinshaw *et al.*, 1992;Malik *et al.*, 2010;Soullam and Worman, 1995) and accumulate by binding to nuclear structures (Ellenberg *et al.*, 1997;Ostlund *et al.*, 1999;Ostlund *et al.*, 2006;Wu *et al.*, 2002). Other membrane proteins, like Heh1 and Heh2 in yeast, have a nuclear localization signal (NLS) (King *et al.*, 2006). These proteins need binding to karyopherin 60 and 95 (Kap60 and Kap95 or karyopherin-α and karyopherin-ß1 in mammalian cells) for nuclear import into the INM and the RanGTP-gradient across the NE provides directionality to this transport.

Heh1 and Heh2 are members of the LEM (Lap2, Emerin, MAN1)-family of integral INM proteins (King *et al.*, 2006). These two membrane proteins share sequence identity in their HEH/LEM-domains at the N-terminus, the NLS, the MAN1-C-terminal Homology Domain (MCHD) and the lumenal domain (LD) between the first (TM1) and second transmembrane segment (TM2) (Fig. 4.1). The LD is positioned within the lumenal space between the INM and ONM, it interacts with components of the NPC (Yewdell *et al.*, 2011).

In chapter three we removed the HEH/LEM homology domain, LD, TM2 and MCHD in Heh2. The resulting membrane protein reporter, named h2NLS-L-TM, consisted of GFP to probe the reporter, the NLS of Heh2 (h2NLS), a linker domain (L) and the transmembrane helix (TM) to localize the reporter in the membrane (Fig. 2.1B). We showed that this membrane reporter protein still accumulated at the INM and concluded that the removed domains are not essential for nuclear targeting, even though they likely contribute to the nuclear accumulation by binding to nuclear binding partners. We observed that the membrane reporter h2NLS-L-TM could accumulate in the nucleus without being trapped to nuclear structures (Fig. 3.7A); this enabled us to study the mechanism of Kap-dependent nuclear targeting of membrane proteins. We concluded that membrane proteins need a high-affinity NLS (like the h2NLS) for strong accumulation in the nucleus (3.9B). In this chapter, we present studies on the role of the linker in nuclear targeting of membrane proteins.

Results

The linker between the NLS and TM is essential for nuclear accumulation of h2NLS-L-TM

The function of the linker domain, spacing the h2NLS and the first transmembrane segment in Heh1 and Heh2, was unknown. We truncated the linker in h2NLS-L-TM and measured the nuclear accumulation (as described in Chapter 3 and Chapter 5, Fig. 5.2), because the linker domain was not conserved (Fig. 4.1). Since this h2NLS-L-TM was not tethered in the nucleus, we could directly study the linker's contribution to the transport efficiency of the membrane reporter across the NPC. The reporter having a linker truncated to 135 residues accumulated at the INM, but the NE/ER ratio was markedly decreased from 34.1 ± 4.8 to 9.4 ± 0.7. Two other reporters, having a linker domain of 90 and 37 residues, respectively, did not accumulate at the INM (Fig. 4.2). Although the amino acid sequence of the linker domain is not conserved, the data indicate that the linker is important for nuclear import of h2NLS-L-TM.

The linkers of Heh2 and Heh1 are intrinsically disordered

To further investigate how the linker contributed to nuclear targeting of these membrane proteins, we determined the biochemical properties of the linker domain. A construct composed of the h2NLS-L (Heh2 84-309) fused to, in consecutive order, a TEV-cleavage site, GFP and a His-tag was expressed in *Lactococcus lactis*. The protein h2NLS-L-TEV-GFP-His was purified by nickel-sepharose and size-exclusion chromatograpy (Fig. 4.3A). The GFP was removed by TEV-cleavage and h2NLS-L was isolated in a second size-exclusion chromatography step. The elution volume of purified h2NLS-L (25.5 kDa) was compared to a standard curve and a large Stokes

```
                                                HEH/LEM
Heh1  MNSDLEYLEDGFDPNSMKVATLRRILVENNVDFPSNARKNALVGLFDEKVKPQIPQLRKM 60
Heh2  ------MDHRNLDPKTLKVSQLRRVLVENDVAFPANARKPVLVKLFEEKVR-QRLQSSPE 53
            . .:**:::**: ***:****:* **:**** .** **:***: *  *

Heh1  YLNVRPSDEGIVKMDRPSSSPSIASPRRSRRARREKSASPMAKQFKKNRILDDVSNDDDD 120
Heh2  ASKVRTSIQKVVKSGAKN-----ADRKKTLKSKKLESSSSESKTVK-------------- 94
        :**.* : :** .  .     *. ::: :::: :*:*. :* .*
                NLS                                          NLS
Heh1  DDDDDDDNDKKDDPLIVPSGTDTDEVDDEEDDVITSSSNKSDTNDFQQNSDTRKKRKDPD 180
Heh2  -DENVETNKRKRE---------------------QISTDNEAKMQIQEEKSPKKKRKKRS 132
       *:: : *.:* :                      *:::. . ::*::...:****. .
                                    Linker-domain
Heh1  SDDWSESNSKENKIDNKHLNLLSSDSEIEQDYQKAKKRKTSDLNQEHGNGSAILGKLSVK 240
Heh2  SKANKPPESPPQSKSDGKATSADLTSELETVEELHKKDSSDDKPRVKELPKPELPNLKVS 192
      *.  . .:*  :. .: : .  .  **:*   :  ** .:.*  : :   .. * :*.*.

Heh1  TPIKNTNRKPVSMDNFNDSLTSSGTENDPFVPNIRHNPKELGTANGTGHSTPLSKLKVSA 300
Heh2  N---------EFLAQLNKELASAATEN---------------------------------- 210
      .           : ::*..*:*:.***

Heh1  SFADKLPQKEVPSTILVPEVEQQEPSQSERTPSLFSSEGSGSESEAPLLPEITTPGPHQP 360
Heh2  --YDHSIKSTDLSSIRIETEEPVGPSTG----------------------AETRNESEV 245
        *:  :.   *:* :   *   ** .                        * .  :

Heh1  MGNTSNNVVEMIDTDSSNLVSDEDEVLVPTRIETPQLPTEKDVEKCEARVQELQEEVNEQ 420
Heh2  MENINLEVQPEVKEAKEELTKISETFDNQDEEDTSRLSSKKNIRSPKGRTRHFIANK--- 302
      * * . :*   :.  ..:*.. .: .    . :*.:*.::*:.. :.*.:.:  :
                                                TM1
Heh1  LEHENGSEFDVKQGSGKVGNRHKFKRALKFLSKSLLALFLFCIFI--VIPLLFGLWYREQ 478
Heh2  -------------------TKRGIDIMKPFIAHLFIWLWNGAIFLSIICPILFGLWYREQ 343
                        .:: :.    *::: :: *:  .**:  : *:*********
                                    Lumenal-domain
Heh1  RLLIGYCGHEVPSHRVSGNSFEFIQKLDNLLQDYRPKCIPCPPNGICYPYLKLKCKPDYK 538
Heh2  RIQVGYCGHEKPLKSLAISAFPQTERVDSVLQAYRPNCLECPEHGICSSFMNVECEPGYE 403
      *: :****** * : :: .:*   :::*.:** ***:*: ** :*** .:::::*:*.*:

Heh1  LAPSRLDFLEIIPAQGKCVKDDKKQQLVSEVVEKSLEFLRAKNAQISCGDGKDDIESGMT 598
Heh2  PKSSILETYGIIPFPKYCAKDESKEKEVDELVWKVNEYLKKKNAQHECGEGENLFESGET 463
        .* *:   ***    *.**:.*:: *.*:* *  *:*: **** .**:*:: :*** *

Heh1  EDALYQIFNEARAPWIRDDEFEDLWIQVIKDLTEEPEILWRQLSPTDNNIGGNSNNIIKT 658
Heh2  ETKLYDIFSHSRPSWESQREFNDHWKNVLEILKKKDDIIWLPLDFETNGKREKS------ 517
      *  **:**..:*..*  : **:* * :*:: *.:: :*:*  *.   *.   :*
                                                TM2
Heh1  NDVPRQKRHLPEKFISKTRNFRSTSKKYIGMKCRFEREIYQTYKKFQRPIWLMFLLIVIS 718
Heh2  -----------KSNNTNYIYRSTSKKWVTLQCHLEGDIQEYITKYGGSLFITLGVLFLI 565
                 *  ...  :******:: ::*::* :* :  .*:  .::: : ::.:
                                        MCHD
Heh1  KVIEIKLKNYYRKKARIEELVTQTMEKLKFQKIKSMSDPKENAYLSIVQLRDIFLSDIVD 778
Heh2  KKIQSTLDNYVQGEQIIEKLVKEAIDKLKDVKKNKGEEP----FLTTVQLRATLLSDIPN 621
      * *: .*.** : :  **:**.::::***  * :. .:*    :*: **** :**** :
                MCHD
Heh1  LKYKNQLWSEVVKYLEHNNS-NIKSNLTEIRGEIMKCWEWIGPMELNEPKDSAENKI 834
Heh2  IKEQNNLWAQTKEKIMKEQSENIELYLLEENGEIMTCWEWKE--------------- 663
      :* :*:**::. : : :::* **:  * * .****.****
```

Figure 4.1: Minimal conservation in the linker domain of Heh1 and Heh2. The sequence alignment of the amino acid sequences was performed with Clustal W (Larkin *et al.*, 2007). Similarity was found in the HEH/LEM-domain, the MAN1-C-terminal homology domain (MCHD) and the lumenal domain (LD). The transmembrane domains, in particular TM1, and the NLS-region show also some sequence similarity, but the linker domains are minimally conserved. An asterisk (*) indicates identical amino acids, whereas the dots (: and .) indicates analogous residues.

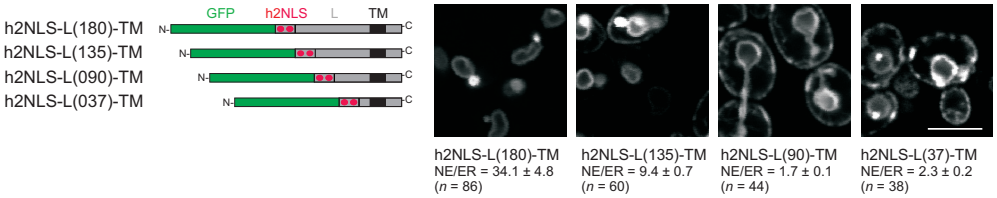

Figure 4.2: The linker domain is required for nuclear targeting of membrane proteins. Representation of h2NLS-L-TM and the three derived reporters with shortened linker domains. The length of the linker domain is indicated by the number of residues; the native linker of h2NLS-L-TM is 180 residues long. The corresponding confocal fluorescence images show the localization of the reporters in the KAP95-AA strain; the nuclear accumulation (NE/ER ratio) with SEM is indicated under the images. The scale bar is 5 µm.

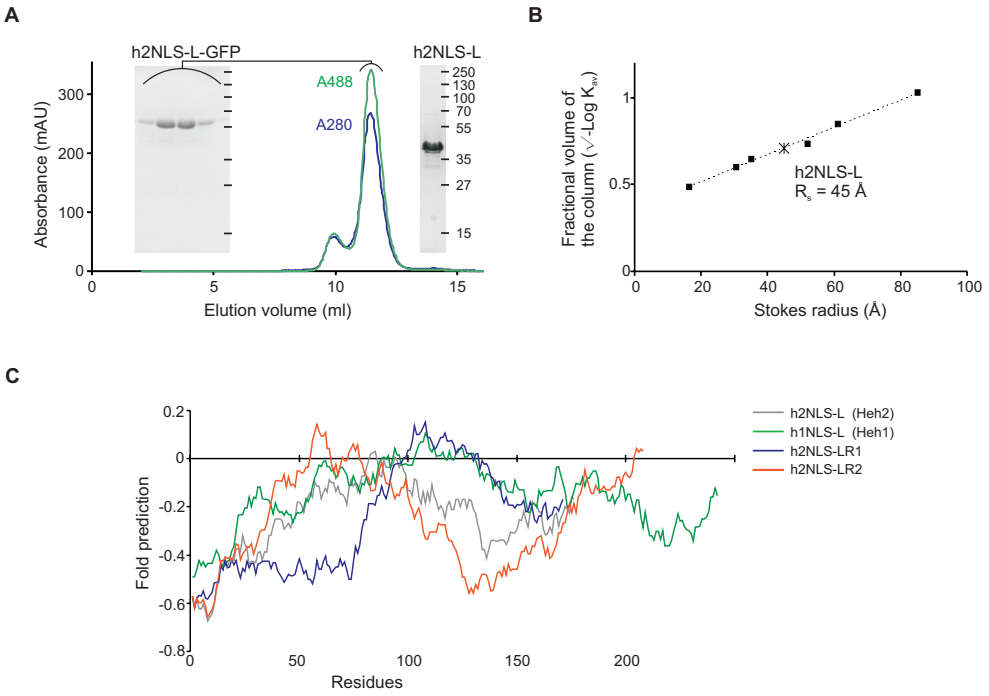

Figure 4.3: h2NLS-L has a large Stokes radius and is predicted to be intrinsically-disordered. **A)** The elution profile from size-exclusion chromatography (SEC) of h2NLS-L-GFP (containing a TEV-site and a His-tag, expressed in *L.lactis*) and a CBB-stained SDS-PAGE gel of peak fractions (left inset). The CBB-stained SDS-PAGE gel of h2NLS-L after removal of GFP by TEV-cleavage is also shown (right). **B)** The Stokes radius of the purified h2NLS-L domain (25.5 kDa) determined by SEC was 45 Å. The fractional volume (K_{av}) of the protein standards is plotted to the belonging Stokes radii as the calibration of the SEC-column. The fractional volume represents the fraction of the stationary gel volume that is available for diffusion of a given solute species; molecules elutes in order of decreasing molecular size. **C)** The output from the FoldIndex prediction algorithm (Prilusky *et al.*, 2005) for the propensity to fold gives a negative value when the peptide is predicted to be unstructured over a stretch of 51 amino acids. The fold prediction is plotted for h2NLS-L from Heh2 (gray), h1NLS-L from Heh1 (green), h2NLS-LR1 (blue) and h2NLS-LR2 (orange).

radius of 45 Å was found (Fig. 4.3B). The Stokes radius of an unfolded protein domain of a 25.5 kDa with an extended coil conformation is predicted to be 47 ± 17 Å; while for a similar protein but folded and globular, the radius is expected to be 22 ± 7 Å) (SD is indicated) (Wilkins *et al.*, 1999;Tcherkasskaya *et al.*, 2003). The experimental Stokes radius thus indicates an unfolded structure for h2NLS-L. An intrinsically-disordered linker domain in both Heh1 and Heh2 is also suggested by on-line structure prediction algorithms as FoldIndex (Prilusky *et al.*, 2005) and FoldUnfold (Galzitskaya *et al.*, 2006) (Fig. 4.3C).

To confirm that linker domain is indeed unstructured, we performed nuclear magnetic resonance (NMR) spectroscopy on h2NLS-L. The NMR spectra of (unlabeled) h2NLS-L were similar to the spectra of a typical intrinsically-disorded human protein called α-synuclein (Mulder *et al.*, 2010) and different from the folded mammalian calbindin-D_{9k} (Oktaviani *et al.*, 2011). The absence of stable secondary and tertiary structure was gauged from a lack of signal dispersion of the backbone amides for h2NLS-L in 1D ^{1}H-NMR spectra (Fig. 4.4A, shaded area). For com-

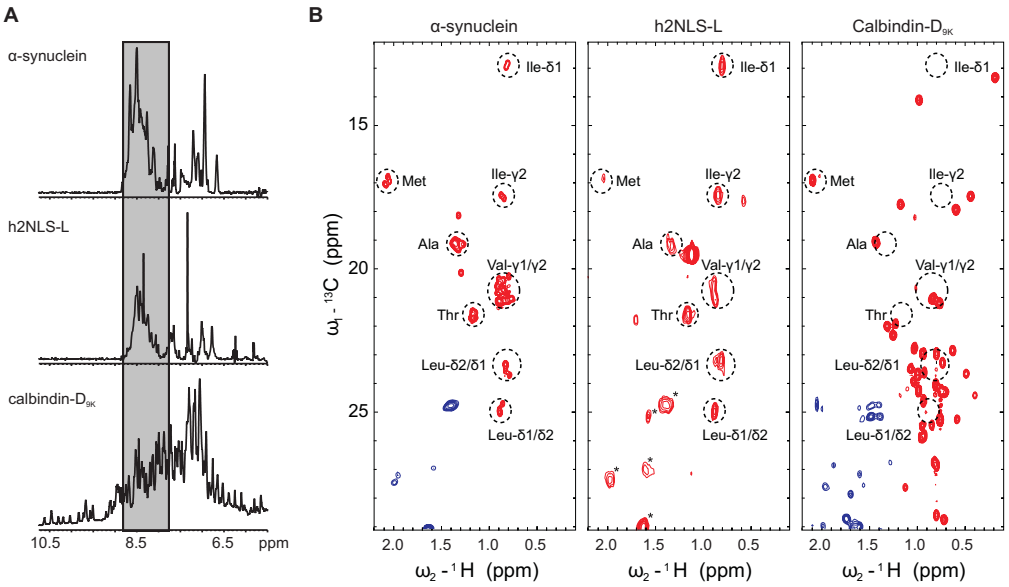

Figure 4.4: The intrinsically-disordered nature of h2NLS-L is revealed by NMR spectroscopy. **A)** 1D ^{1}H NMR of the backbone amides for (unlabeled) h2NLS-L, compared with the intrinsically-disordered protein human α-synuclein, and the folded protein calbindin-D9k. **B)** Methyl region of the [^{1}H-^{13}C]-Heteronuclear Single Quantum Coherence (HSQC) spectrum of the intrinsically-disordered protein human α-synuclein (left), h2NLS-L (middle), and the folded protein calbindin D_{9k} (right)(Mulder *et al.*, 2010). The dotted circles designate the typical positions of methyl groups of the different amino acid types in disordered proteins. Signals in blue or indicated with an asterisk originate from methylene- and methine-groups in the amino acid side chains. Dispersion of spectral correlations of methyl groups outside the regions shown is indicative of a folded protein/domain. Comparison of the spectrum of h2NLS-L with a disordered (middle) and folded (right) protein establishes the disordered nature of h2NLS-L.

parison, the 1D ^{1}H NMR spectra of α-synuclein and calbindin-D_{9k} are shown. The intrinsically-disordered nature of h2NLS-L is further confirmed by a lack of dispersion of the side chain methyl signals in a 2D [^{1}H-^{13}C]-Heteronuclear Single Quantum Coherence (HSQC) spectra (Fig. 4.4B), indicating a lack of persistent tertiary interactions. Comparison of both the 1D and the 2D spectra of h2NLS-L with the intrinsically-disordered protein human α-synuclein, and the folded protein calbindin-D_{9k} show that h2NLS-L is natively unstructured.

The nuclear accumulation of h2NLS-L-TM depends on the length of the linker, rather than on its amino acid sequence

We conclude that the linker domains of Heh1 and Heh2 are intrinsically-disordered and reasoned that the length and flexibility might be required during nuclear transport of membrane protein, while the amino acid sequence is less important. To test this hypothesis, we replaced the coding regions of the linker domain in h2NLS-L-TM for two synthetic sequences, LR1 and LR2. These were generated randomly but had the same relative amino acid abundance as L. LR1 and LR2 are also predicted to be unfolded (Fig. 4.3C). The randomized linker-containing reporters, h2NLS-LR1-TM and h2NLS-LR2-TM, were expressed in the Kap95-AA strain (see Chapter 3)

and efficiently transported to the INM (Fig. 4.5A, left). We confirmed that the nuclear transport of the reporters containing the synthetic linker is similarly dependent on Kap95 as h2NLS-L-TM (Fig. 3.4A), because the reporter leaked back from the INM to the ONM upon conditional cellular depletion of functional Kap95 by the addition of rapamycin (Fig. 4.5A, right). Systematic truncations of LR1 and LR2, together with the truncations of the native linker (L) (Fig. 4.2), resulted in three sets of reporters with variable linker lengths (see Chapter 5, Table 5.2 and 5.3). The shortest truncations of each linker set did not lead to accumulation of the reporters to the

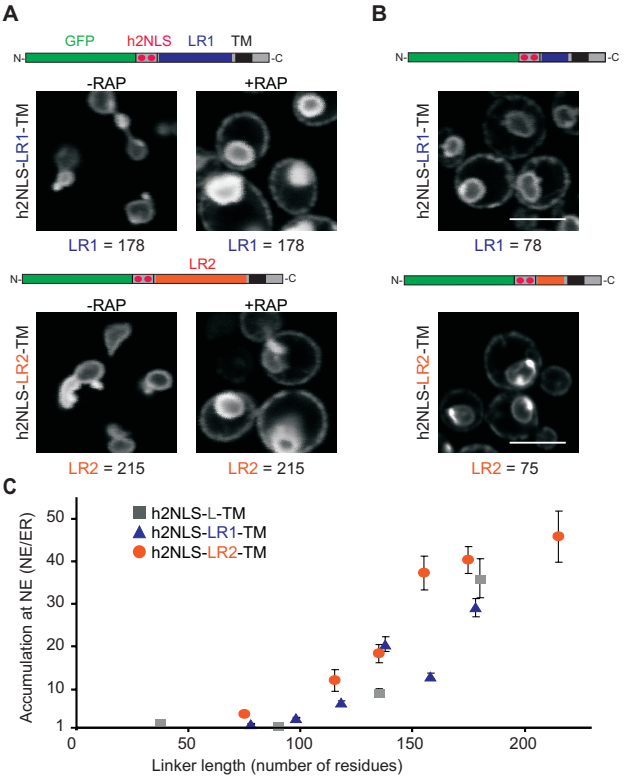

Figure 4.5: Membrane reporters containing synthetic unfolded linkers localize at the INM. A) Representation of reporters containing the longest linker of the randomized versions LR1 (blue) and LR2 (orange). The corresponding confocal fluorescence images, depicting the localization of the reporters in the KAP95-AA strain, are shown below the cartoons. Addition of rapamycin (+RAP) shows the distribution of the reporter over the NE-ER network. The linker length is indicated by the number of amino acids. **B)** Same as **A)** but the reporters contain the shorter versions of the randomized linker LR1 (blue) and LR2 (orange). The reporters are distributed equally over the NE-ER network. The scale bar is 5 µm. **C)** The accumulation at the NE of h2NLS-L-TM (■), h2NLS-LR1-TM (▲) and h2NLS-LR2-TM (●), and truncations thereof, is plotted against the length of the linker spacing the h2NLS and TM ($n \geq 20$). The SEM is indicated.

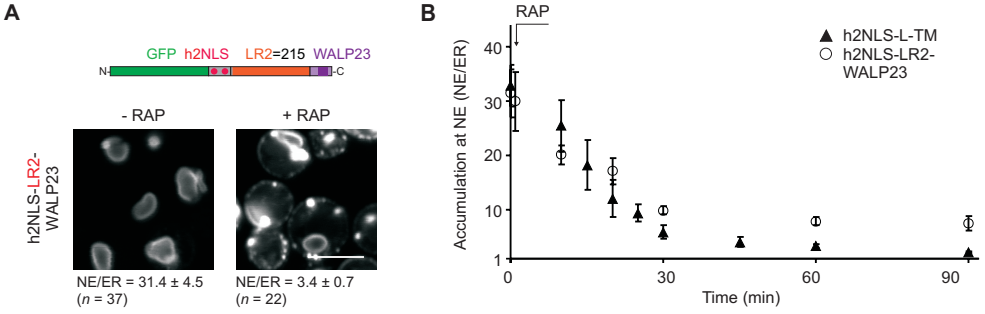

Figure 4.6: Membrane reporter with the synthetic transmembrane helix WALP23 is targeted to the INM. A) Representation of h2NLS-LR2 fused to the WALP23 TM-region and confocal fluorescence images of their localization in the absence and presence of rapamycin. The nuclear accumulation is indicated with the SEM. The scale bar is 5 µm. **B)** After adding of rapamycin (RAP), the reporter h2NLS-LR2-WALP23 leaked back to the ER with similar kinetics as NLS-L-TM. The SEM is indicated.

nucleus, rather they were randomly distributed over the NE-ER network similar to the h2NLS-lacking reporter, L-TM (Fig. 4.5B). We quantified the INM accumulation of each reporter construct and found a striking dependence of INM import on linker length irrespective of the linker sequence (Fig. 4.5C). A linker length of 120 amino acids was minimally required and with a length of more than 150 residues maximal nuclear import was observed. We conclude that the length rather than sequence or a specific structure of the linker between h2NLS and TM is important for nuclear transport of membrane proteins.

An ER-localized integral membrane protein could be targeted to the INM

We reasoned that the high-affinity h2NLS separated by a long linker domain from the TM could be a sorting signal to target membrane proteins to the INM. To test whether this "h2NLS - linker" can act as a general targeting signal for membrane proteins, we designed a reporter consisting of the h2NLS, a randomized linker (LR2) of 215 residues long and the synthetic transmembrane segment WALP23 (de Planque and Killian, 2003). This reporter was completely artificial, except for the bipartite h2NLS. Indeed, h2NLS-LR2(215)-WALP23 had a similar accumulation as the reporter containing the Heh2-derived TM (Fig. 4.6A). The accumulation of h2NLS-LR2(215)-WALP23 was Kap-mediated, because the reporter leaked back to the ER-network when Kap95 was sequestered to the plasma membrane upon addition of rapamycin (Fig. 4.6A). Even the efflux kinetics of h2NLS-LR2(215)-WALP23 were similar to h2NLS-L-TM, indicating that a different TM has no influence on the transport properties over the NPC (Fig. 4.6B). However, after the nuclear efflux of h2NLS-L-WALP23, fluorescence blobs were seen in the ER and the ONM, possibly caused by aggregation of the reporter.

To target an ER-localized protein to the INM, we subsequently fused h2NLS-LR1 (having a randomized linker of 138 residues) to a single TM of the ER protein Sec61, as well to the full-length version of Sec61, having 10 transmembrane spanning helices. After 2 hours of induction, the nuclear accumulation of h2NLS-LR1(138)-Sec61(TM1) and h2NLS-LR1(138)-Sec61 were compared to the nuclear accumulation of h2NLS-LR1(138)-TM, having the Heh2-derived TM (Fig. 4.7A). Interestingly, both the Sec61-fusions, with the first TM (Fig. 4.7B) and all 10 TMs of Sec61, (Fig. 4.7C) were targeted to the INM (left panels). The reporters with the Sec61-TMs without an h2NLS (middle panels) or containing a short linker (LR1 truncated to 78 residues, right panels) did not target to the INM. However, the accumulation of h2NLS-LR1(138) fused to full length Sec61 was lower than h2NLS-LR1(138) fused to the Heh2-derived TM or the Sec61 single TM. A reason for the lower nuclear accumulation could be that a part of the reporters fused to Sec61 is in complex with the Sec-translocon and thus functionally trapped in the ER. We conclude that the h2NLS-L is sufficient to target a synthetic TM and a full length ER-localized transmembrane protein to the INM, and this polypeptide can be considered as a sorting signal for INM-destined membrane proteins. And indeed, a similar "NLS-L-TM" domain structure could be found in Heh1. This sorting signal, h1NLS-L, could also transport the Heh2-derived TM to the nucleus (Fig. 4.8). Of note is that although the linker in Heh1 is longer (230 residues) than in Heh2 (180 residues) and the NLS-L sorting signals sequence homology (identity score <0.18), the proteins share the intrinsically-disordered nature in their linkers (Fig. 4.1).

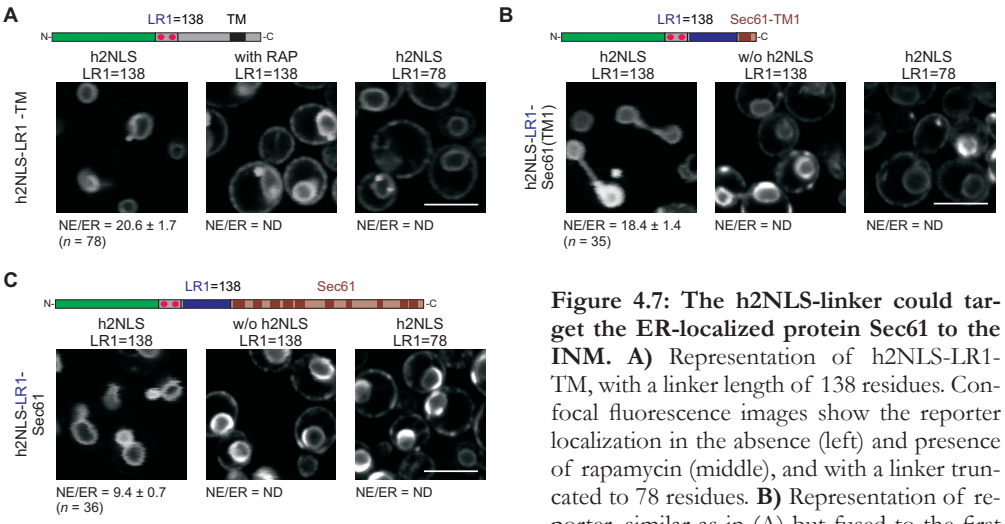

Figure 4.7: The h2NLS-linker could target the ER-localized protein Sec61 to the INM. A) Representation of h2NLS-LR1-TM, with a linker length of 138 residues. Confocal fluorescence images show the reporter localization in the absence (left) and presence of rapamycin (middle), and with a linker truncated to 78 residues. **B)** Representation of reporter, similar as in (A) but fused to the first TM of Sec61. The confocal images show the NE-localization of h2NLS-LR1(138)-Sec61(TM1) (left). The accumulation is lost without the h2NLS (middle) and upon shortening of the linker, LR1(78) (right). **C)** Same as **B)** but for full-length Sec61, having 10 TMs. The data indicate that, similar to h2NLS-LR1(138)-TM, an NLS and a long linker are required for targeting of full-length Sec61 to the INM. The scale bar is 5 μm.

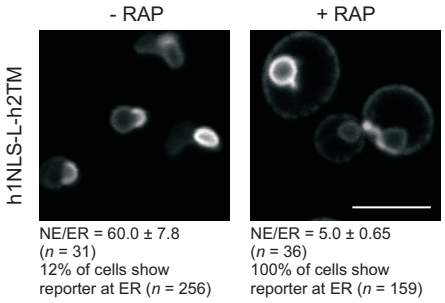

Figure 4.8: Heh1 is a homolog of Heh2 and has a similar "NLS-L-TM"-signature which convokes INM targeting. The h1NLS-L was fused to the TM of Heh2 and showed a strong nuclear accumulation of 60-fold at the NE. After adding rapamycin (RAP) the reporter leaked out of the nucleus, showing that the accumulation was Kap95-dependent. The scale bar is 5 μm.

Is the linker length needed to allow the h2NLS to reach in the central channel of the NPC?

We hypothesized that the length of the linker in the membrane proteins might be needed to position the Kap-bound NLS in the central channel of the NPC during nuclear transport. This would allow the Kaps to interact with the FG-Nups to carry the membrane protein across the NPC. To study if the h2NLS at the N-terminus of the reporter is indeed transported through the central channel, we performed three experiments. First, we determined if the nuclear transport of h2NLS-L-TM is dependent on the FG-Nups in the central channel. Secondly, we evaluated whether reporters with large extralumenal domains are imported. It has been reported that the 10 nm wide lateral channels along the POM allow passage of extralumenal domains of up to 60 kDa (Deng and Hochstrasser, 2006;Hinshaw *et al.*, 1992;Wu *et al.*, 2002), and obviously the wider central channel accommodates larger cargo. Thirdly, we trapped the h2NLS-containing N-terminus of the membrane reporter during its transit through the central channel at a FG-Nup within the NPC.

I) Nuclear transport of membrane proteins is dependent of a specific subset of nucleoporins.

We first determined the FG-Nup dependency of membrane protein transport across the NPC. We used yeast strains, generated by the Wente laboratory (Strawn *et al.*, 2004), in which the FG-regions of several nucleoporins were deleted, and we measured the nuclear accumulation of the reporters. We evaluated the accumulation of the soluble tcNLS-GFP within the nucleus to confirm that general classical transport was affected compared to wild type cells in the strains where FG-domains of subsets of nucleoporins were deleted. Specifically, we examined nuclear accumulation in SWY2950 (*nup100⊿GLFG nup145n⊿GLFG nup57⊿GLFG*, Fig. 4.9A, yellow), SWY3062 (*nup42⊿FG nup159⊿FG nup1⊿FxFG nup2⊿FxFG nup60⊿FxFG nsp1⊿FG⊿FxFG*, Fig. 4.9A, orange) and SWY3042 (*nup42⊿FG nup159⊿FG nup1⊿FxFG nup2⊿FxFG nup60⊿FxFG nup100⊿GLFG*, Fig. 4.9A, green). In all these strain, we found a strong decrease in nuclear accumulation of the soluble reporter tcNLS-GFP (2.7 – 8 fold, Fig. 4.9A). The decrease of soluble transport shows that indeed the classical transport pathway of Kap60/95-mediated transport through the NPC was affected in all three strains.

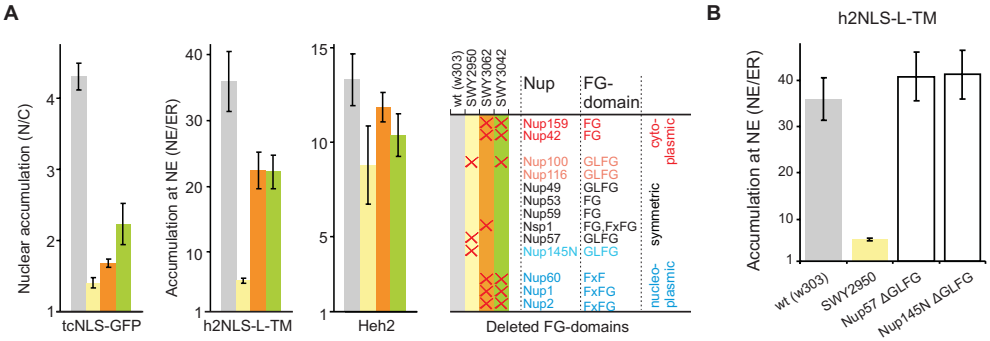

Figure 4.9: A subset of FG-Nups is needed for nuclear transport of h2NLS-L-TM. A) The nuclear accumulation of soluble tcNLS-GFP and the accumulation of the membrane reporters h2NLS-L-TM and Heh2 at the INM are compared in different FG-mutant strains (Strawn *et al.*, 2004) and the parental wild type strain w303 (white), after 2 hours induction. In the mutant strains, the following domains are deleted: SWY2950: *nup57⊿GLFG nup100⊿GLFG nup145n⊿GLFG* (yellow); SWY3062: *nup42⊿FG nup159⊿FG nup1⊿FxFG nup2⊿FxFG nup60⊿FxFG nsp1⊿FG ⊿FxFG* (orange) and SWY3042: *nup42⊿FG nup159⊿FG nup1⊿FxFG nup2⊿FxFG nup60⊿FxFG nup100⊿GLFG* (green). $n \geq 21$ and the SEM is indicated. **B)** The nuclear accumulation of h2NLS-L-TM in the strains where the GLFG-domains are deleted of the single Nup57 or Nup145N, were compared to the accumulation in SWY2950 (yellow bar), where the GLFG-domains of Nup100, Nup57 and Nup145N are deleted and wild-type cells (wt, w303, grey bar). $n \geq 24$ and the SEM is indicated.

However, we observed minimal reduction (~1.6-fold) in the nuclear accumulation of h2NLS-L-TM in the strains, in which the FxFG and FG regions were deleted (SWY3062 and SWY3042) (Fig. 4.9A). Only the strain that lacked the GLFG repeats of Nup100, Nup145 and Nup57 (SWY2950), which are anchored symmetrically to both the cytoplasmic and nucleoplasmic halves of the NPC scaffold (Alber *et al.*, 2007;Rout *et al.*, 2000), showed severe reduction of INM accumulation (Fig. 4.9A) when compared to the wild type, while minimal effects were seen with single deletions (Fig. 4.9B).We thus observe that the import of membrane reporters specifically requires the combination of GLFG-regions of the Nup100, Nup145 and Nup57, but to a lesser

extent the combination the FxFG and FG-regions of the Nup1, Nup2, Nup60, Nup42, Nup159 and Nsp1. It thus seems that the Kap60/95-mediated import of membrane proteins specifically requires the symmetrical GLFG-Nups, which are considered to localize in the central channel.

We then examined the nuclear accumulation of Heh2, after 2 hour induction in the strain that lacks the GLFG repeats of Nups 100, 145 and 57 (SWY2950). We did not observe a significant decrease in nuclear accumulation in this mutant strain (Fig. 4.9A, 4.10A). Heh2 maintains the nuclear accumulation, probably by a retention mechanism through interactions at the INM (Fig. 3.7A). We looked how fast the final accumulation levels were reached in the wild type and mutant strains after the induction of the expression of the reporters. Although the final nuclear accumulation was not affected, it took about 4 times longer to reach the same Heh2-accumulation level in the mutant strain as compared to the wild-type (Fig. 4.10A, C). We reason that the Nup-deletions caused reduced import kinetics and a slower passage through the NPC observed. This resulted in an increase in time to reach the final accumulation for Heh2 and a lower nuclear accumulation for h2NLS-L-TM (Fig. 4.10B, C). We concluded that the symmetrical GLFG-Nups are essential for the transport of both the membrane reporter protein and the full length Heh2. This suggests that the pathway of nuclear transport of the membrane protein is indeed through the central channel.

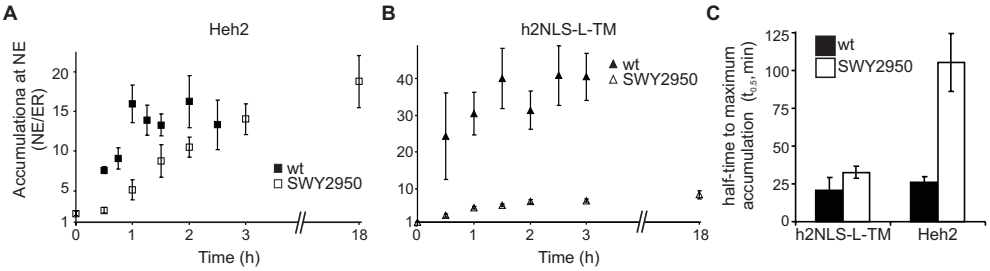

Figure 4.10: A reduced import rate in SWY2950 may cause a lower nuclear accumulation of h2NLS-L-TM and a slower import of Heh2. A) The accumulation at the NE of Heh2, expressed in the wild-type strain w303 (■) and SWY2950 (□, *nup57⊥GLFG nup100⊥GLFG nup145n⊥GLFG*), is plotted up to 3 hours after induction of expression. Heh2 reached wild type accumulation levels only after ~3 hours of induction. $n \geq 13$ and the SEM is indicated. **B)** Similar as in (A) but for h2NLS-L-TM in the wild-type strain w303 (▲) or the mutants strain SWY2950 (Δ). The accumulation of h2NLS-L-TM is 4 – 6 fold lower in the mutant strain than in the wild-type. $n \geq 11$ and the SEM is indicated. **C)** h2NLS-L-TM reached a stable accumulation at the INM with a half-time of 36 ± 10 min in the wild type strain (filled bars) and 52 ± 5 min in the mutant strain (open bars). Heh2 displayed a half-time of 26 ± 5 in the mutant and a half-time of 113 ± 22 min in the wild type cells. The SEM is indicated.

II) Membrane reporter proteins having an extralumenal N-terminal domain up to 174 kDa still accumulate in the INM

The finding, that the GLFG-Nups in the central channel of the NPC are required for nuclear transport of membrane proteins, supports the idea that the long linker is needed for the Kap-bound h2NLS to reach out from the pore membrane to interact with FG-Nups in the central channel. Since the central channel facilitates the transport of large soluble cargo, we tested if reporters with extralumenal soluble domains, larger than the proposed size limit of 60 kDa for

the lateral channel would also be imported. We stepwise enlarged the extralumenal soluble domain with copies of the Maltose Binding Protein (MBP), to get a series of 4 reporters, having an N-terminal extralumenal domains from 51 kDa to 174 kDa (Fig. 4.11). Surprisingly, all membrane reporters were imported to the INM, although the efficiency went down with increasing size (Fig. 4.11). Our data point toward passage of the extralumenal soluble domains of the membrane proteins through a spacious area of the NPC, such as the central channel.

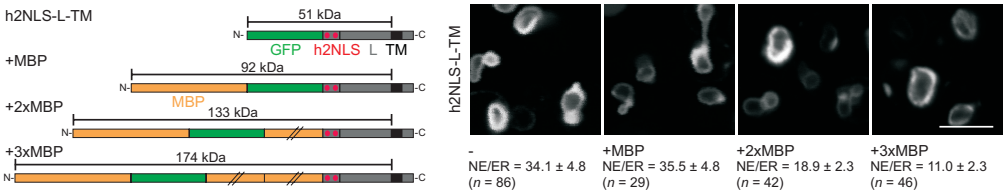

Figure 4.11: Reporters with extralumenal domain of up to 174 kDa are imported to the INM. Representation of h2NLS-L-TM and derived reporters with one, two or three additional MBP domains are shown. The localization of the reporters, with indicated nuclear accumulation, show that they are still imported at the INM. The SEM is indicated and the scale bar is 5 µm.

III) The membrane reporter protein was trapped with its N-terminus at Nsp1 in the central channel of the NPC.

Proof for the idea that the extralumenal soluble domains pass through the central channel came from experiments where we designed a trap for the reporters that are on transit through the NPC. We constructed a strain expressing FRB tagged FG-Nup Nsp1. The C-terminal FRB-tag on Nsp1 is anchored on the pore side of the scaffold of the NPC within the central cahnnel (Alber *et al.*, 2007;Rout *et al.*, 2000;Bailer *et al.*, 2001;Schrader *et al.*, 2008). The h2NLS-L-TM reporter, with FKBP at its N-terminus, was expressed to enable rapamycin-dependent trapping at Nsp1-FRB in the NPC (Fig. 4.12A). This rapamycin-dependent trapping can only occur when the N-terminus of the reporter is in close proximity of the FRB-tag at Nsp1 in the central channel of the pore. Without rapamycin, or in wild-type cells, the reporter distributed evenly over the NE, which was quantified from confocal images by measurement of the standard deviation of the fluorescence along the NE (Fig. 4.12). Upon addition of rapamycin, the standard deviation of fluorescence along the NE increased from ~27% to ~41%, and a typical punctate stain was observed, analogous to what is seen for NPC-localized proteins. Indeed, the deviation of fluorescence at the NE after rapamycin was added became similar to cells where Nsp1-GFP was expressed, suggesting that the reporter was trapped in the NPC (Fig. 4.12C).

Subsequently, we assessed if trapping of the reporter at the NPC affected nuclear transport. We used a reporter expressed at higher levels (with an additional N-terminal Protein A tag (PrA)) for these experiments and observed a blockage of INM import: after PrA-FKBP-h2NLS-L-TM was conditionally trapped at Nsp1-FRB in the NPC, we noticed a steady increase in fluorescence at the ER from newly synthesized proteins (Fig. 4.13A, RAP). We confirmed that the increase of fluorescence at the ER was not the result of INM-accumulated membrane proteins leaking back to the ER, because we did not see any increase in fluorescence at the ER when

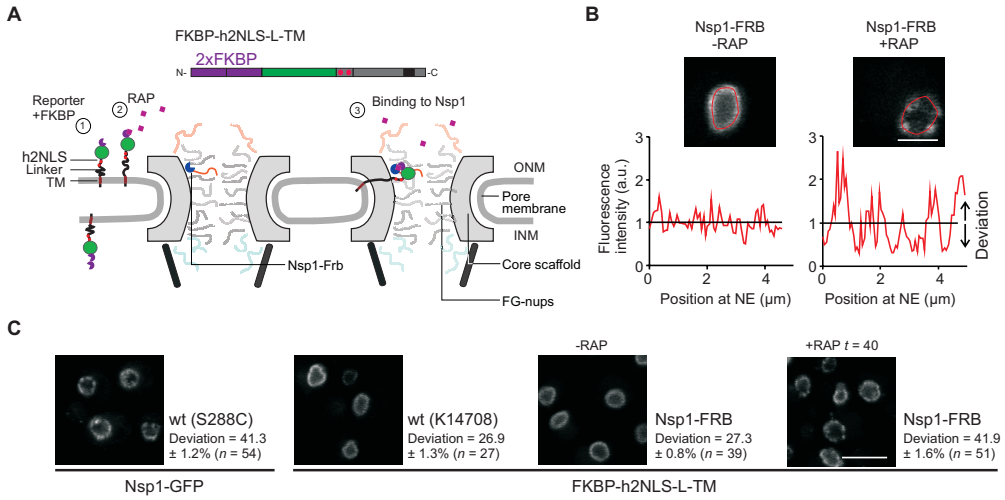

Figure 4.12: The membrane reporter FKBP-h2NLS-L-TM could be trapped at Nsp1-FRB in the central channel of the NPC. A) In order to trap the N-terminus of the reporter at the pore side of the nucleus, two copies of FKBP (2×FKBP) were fused to the N-terminus of the h2NLS-L-TM reporter (1). FRB was fused to the C-terminus of Nsp1, a FG-Nup that is present in multiple copies and anchored to the NPC scaffold by its C-terminal domain. Once rapamycin is added to the cell culture, it will bind to the FKBP at the reporter (2), enabling the FKBP to bind to FRB (3). **B)** Localization of a reporter with an N-terminal FKBP-tag in a strain expressing Nsp1-FRB before (left) and after addition of rapamycin (right). Trapping of FKBP-tagged reporter at NPCs is apparent from the punctate staining at the NE; the deviation in fluorescence at the NE is higher in the presence of rapamycin. The scale bars is 2 μm and SEM is indicated. **C)** Confocal fluorescence image of the localization of Nsp1-GFP at the NPC (deviation of fluorescence at the NE is indicated), showing a punctate stain at the NE, which is typical for NPC-localized proteins. The localization of FKBP-h2NLS-L-TM in a strain expressing Nsp1-FRB before addition of rapamycin (RAP) show a uniform stain at the NE, similar to the localization of the reporter in a wild-type (K14708) strain (Haruki *et al.*, 2008). Confocal images of FKBP-h2NLS-L-TM in Nsp1 after 40 min of incubation with rapamycin (RAP) show a similar punctate stain at the NE as for NPC-localized proteins (deviation of fluorescence at the NE is similar to Nsp1-GFP). The scale bar is 5 μm and SEM is indicated.

the expression of the reporter was inhibited with glucose at the moment that the reporter was trapped at Nsp1-FRB (Fig. 4.13A, Gluc/RAP). We quantified the percentage of cells in a large population having visible fluorescence at the ER during 80 minutes after addition of rapamycin (Fig. 4.13B). The percentage of cells having a detectable fluorescence signal in the ER was initially very small, namely 5 – 10 %. This is smaller than what was observed for h2NLS-L-TM, where > 60% of the cells has visible ER strain. The difference between the reporters is due to the 10-fold lower expression level of PrA-FKBP-tagged reporter in combination with a stronger nuclear accumulation than h2NLS-L-TM. It was not the result of different transport properties caused by the FRB-tagged Nsp1 as we see normal accumulation of the reporter h2NLS-L-TM (Fig. 4.13C). We clearly observed an increase in the percentage of cells having visible fluorescence signal at the ER after trapping the PrA-FKBP-reporter at Nsp1, but not for cells where the expression was inhibited with glucose (Fig. 4.13B, bars). As a result of emerging fluorescence signal at the ER, the NE/ER ratio decreased (Fig. 4.13B, line). With these reporters we did not see a punctuate NE

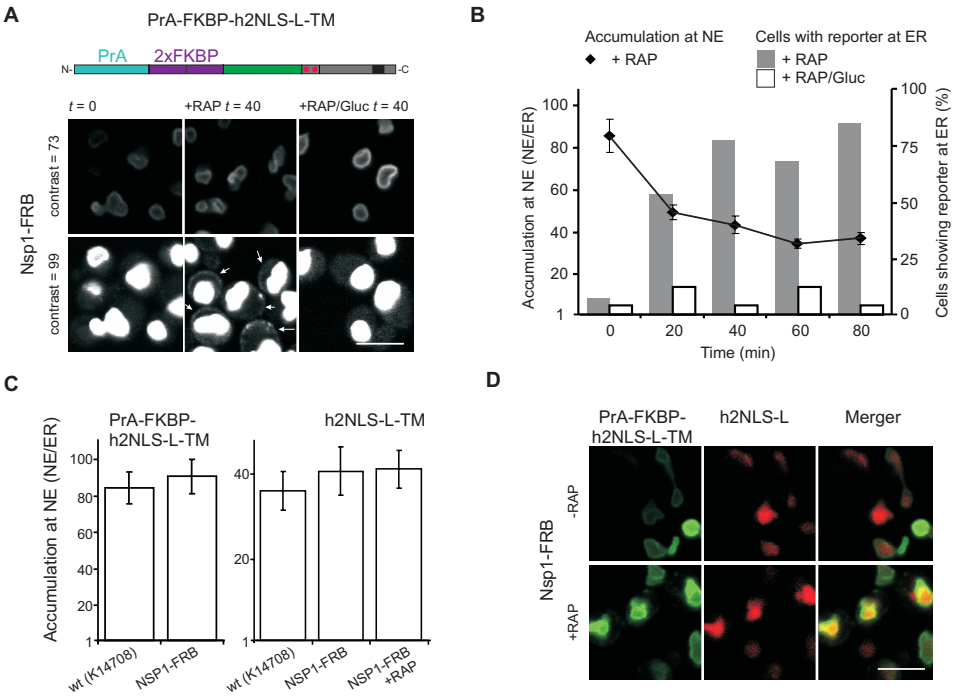

Figure 4.13: The membrane reporter FKBP-h2NLS-L-TM could be trapped at Nsp1-FRB in the central channel of the NPC. A) In order to trap the N-terminus of the reporter at the pore side of the nucleus, two copies of FKBP (2×FKBP) were fused to the N-terminus of the h2NLS-L-TM reporter (1). FRB was fused to the C-terminus of Nsp1, a FG-Nup that is present in multiple copies and anchored to the NPC scaffold by its C-terminal domain. Once rapamycin is added to the cell culture, it will bind to the FKBP at the reporter (2), enabling the FKBP to bind to FRB (3). **B)** Localization of a reporter with an N-terminal FKBP-tag in a strain expressing Nsp1-FRB before (left) and after addition of rapamycin (right). Trapping of FKBP-tagged reporter at NPCs is apparent from the punctate staining at the NE; the deviation in fluorescence at the NE is higher in the presence of rapamycin. The scale bars is 2 µm and SEM is indicated. **C)** Confocal fluorescence image of the localization of Nsp1-GFP at the NPC (deviation of fluorescence at the NE is indicated), showing a punctate stain at the NE, which is typical for NPC-localized proteins. The localization of FKBP-h2NLS-L-TM in a strain expressing Nsp1-FRB before addition of rapamycin (RAP) show a uniform stain at the NE, similar to the localization of the reporter in a wild-type (K14708) strain (Haruki *et al.*, 2008). Confocal images of FKBP-h2NLS-L-TM in Nsp1 after 40 min of incubation with rapamycin (RAP) show a similar punctate stain at the NE as for NPC-localized proteins (deviation of fluorescence at the NE is similar to Nsp1-GFP). The scale bar is 5 µm and SEM is indicated.

when the reporter was trapped at Nsp1-FRB, because the expression level of PrA-FKBP-tagged reporter was ~10 fold higher than the FKBP-tagged reporter used in Fig. 4.12; the subtle changes in fluorescence due to specific reporter localization of some reporters at the NPC was overruled by the fluorescence relatively large pool of reporters distributed over the NE. Trapping the reporter at Nsp1-FRB specifically blocked the nuclear transport of membrane proteins and not the nuclear transport of soluble proteins. This shows that the NPCs are still functional for transport of non-membrane reporters (Fig. 4.13D).

In summary, we could visualize that the FKBP-reporter was conditionally trapped at Nsp1-FRB in the NPC. This caused a punctated fluorescence stain at the NE, which is typical for NPC-localized proteins. As a consequence of the trapping in the NPC, we observed that the transport of newly synthesized membrane reporters was blocked. Since the N-terminus of the (PrA)-FKBP-reporter was trapped at Nsp1 in the central channel of the NPC, we conclude that h2NLS-containing N-terminus of the reporter must pass where Nsp1 is anchored to the NPC scaffold.

Discussion and Conclusions

Import to the inner nuclear membrane of the yeast membrane proteins Heh1 and Heh2 depends on the presence of an extralumenal NLS that is recognized by Kap60 plus a linker that spaces the distance with the first TM. The Heh2-derived reporter proteins accumulate at the INM, not because they are retained or trapped at the INM, but because Kap60/95-mediated import is faster than export. In this study, we unravel that the linker region is intrinsically-disordered. Import of the h2NS-L-TM reporters requires a minimum length of the linker domain of about 120 amino acids. Using randomized versions of the native linker domain, we show that the amino acid sequence is not important.

We concluded that the linker is needed to position the Kap-bound NLS in the central channel of the NPC while the transmembrane domain stays in the membrane. But is the linker long enough to span this distance? The cell cycle-dependent kinase inhibitor $P27^{Kip}$ has an intrinsically-disordered tail at the C-terminus of almost 100 residues (Galea *et al.*, 2008), for which was experimentally shown that it could adopt an extended or stretched conformation of ~14 nm (Galea *et al.*, 2008). By comparison, the linker domain of Heh2 consistS of 180 amino acids would thus be able to stretch to ~26 nm. This length is sufficient to extend the h2NLS from the pore membrane to the central channel of the NPC and allow Kap95/60 to interact with the different FG-Nups. Moreover, we assume that it takes little energy to stretch the linker, because intrinsically disordered domains are typically less stiff than folded domains (Miyagi *et al.*, 2008). The more elongated or stretched conformation of the linker may be promoted by the interaction of the NLS-bound Kaps with the FG-Nups.

The reporters that we use in our studies have a domain structure that categorizes them as tail anchored, as they have a carboxy-terminal transmembrane domain. They may belong to the ~5 % of membrane proteins that cannot be inserted by the co-translational pathway, employing the signal recognition particle (SRP)-dependent pathway and the Sec61 translocon (reviewed by (Osborne *et al.*, 2005;Stirling, 1999)). Instead, the Get3 cytosolic ATPase might be used for post-translational insertion in the ER (Cross *et al.*, 2009;Schuldiner *et al.*, 2008). In that case import could theoretically involve soluble chaperoned proteins and insertion could occur post-import. But a number of observations strongly argue against this explanation: first we have shown for h2NLS-L-TM that the nuclear import is dependent on Nup170 (Fig. 3.4), this is similar as Heh2 (King *et al.*, 2006) but different than for soluble proteins (Shulga *et al.*, 2000). Secondly, we found that for the transport of membrane proteins different FG-Nups were required than for the trans-

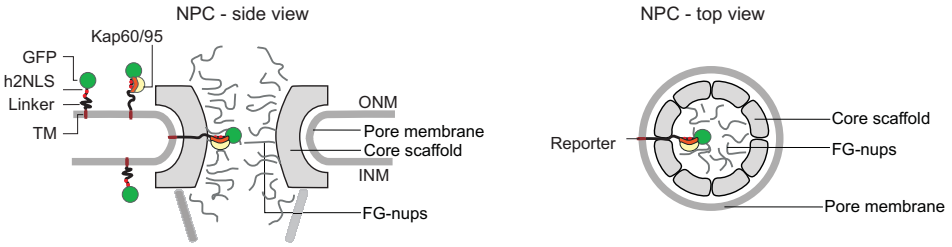

Figure 4.14: Model for active nuclear import of membrane proteins. Prior to transport over the NPC, Kap60/95 binds the high affinity h2NLS of the membrane reporter. It will not take much energy to stretch the intrinsically-disordered linker, to allow the Kap60/95 bound to the h2NLS, to interact with the FG-Nups in the central channel of the NPC. Facilitated diffusion of the h2NLS-containing soluble domain is through the central channel of the NPC, while transmembrane spanning segments diffuse through the pore membrane. As a consequence, conduits must exist to allow the linker to slice through the scaffold of the NPC.

port of soluble proteins (Fig. 9A). Thirdly, the multi-pass transmembrane domain of Sec61 can also be imported to the INM and translocation over the NPC is fully reversible. It is implausible to imagine the multi-pass membrane protein to be extracted from the membrane of the ER and reinserted into the INM or vice versa. Additional arguments are discussed in chapter 7.

Altogether, we conclude that the Kaps facilitate the transport of the soluble domain of the membrane proteins through the central channel while the TM domain remains embedded in the pore membrane. A corollary of this conclusion is that the linker will dodge between the NPC scaffold allowing the karyopherins to bind the FG-Nups (Fig. 4.14). The proposed transport route implies that, at least transiently, openings must exist between the space immediately aligning the POM and the central channel. These conduits between the POM and the central channel, which are called the lateral gates of the NPC, allow the linker to slice through the scaffold of the NPC. At present, structures of the NPC do not have the resolution to reveal such conduits, but its plasticity and the overall lattice-like scaffold structure observed in electron microscopy (Beck *et al.*, 2007;Frenkiel-Krispin *et al.*, 2010;Hinshaw *et al.*, 1992;Yang *et al.*, 1998) and computational structures (Alber *et al.*, 2007) are compatible with our model. The transport mechanism described here is likely to exist in parallel with a previously proposed route based on diffusion and nuclear retention (Ellenberg *et al.*, 1997;Malik *et al.*, 2010;Ostlund *et al.*, 1999;Soullam and Worman, 1995;Wu *et al.*, 2002;Zuleger *et al.*, 2008).

Acknowledgements

We thank M. C. King, M. P. Rout, and D. J. Slotboom for discussion; We thank S. R. Wente, and U. K. Laemmli for strains. This work was supported by funding from the Netherlands Organization for Scientific Research (VIDI fellowship to L.M.V. and F.A.A.M.; Top-subsidy grant 700.56.302 to B.P.).

References

1. Alber, F., S.Dokudovskaya, L.M.Veenhoff, W.Zhang, J.Kipper, D.Devos, A.Suprapto, O.Karni-Schmidt, R.Williams, B.T.Chait, A.Sali, and M.P.Rout. 2007. The molecular architecture of the nuclear pore complex. *Nature* **450**:695-701.
2. Antonin, W., R.Ungricht, and U.Kutay. 2011. Traversing the NPC along the pore membrane: targeting of membrane proteins to the INM. *Nucleus.* **2**:87-91.
3. Bailer, S.M., C.Balduf, and E.Hurt. 2001. The Nsp1p carboxy-terminal domain is organized into functionally distinct coiled-coil regions required for assembly of nucleoporin subcomplexes and nucleocytoplasmic transport. *Mol. Cell Biol.* **21**:7944-7955.
4. Beck, M., V.Lucic, F.Forster, W.Baumeister, and O.Medalia. 2007. Snapshots of nuclear pore complexes in action captured by cryo-electron tomography. *Nature* **449**:611-615.
5. Cross, B.C., I.Sinning, J.Luirink, and S.High. 2009. Delivering proteins for export from the cytosol. *Nat. Rev. Mol. Cell Biol.* **10**:255-264.
6. de Planque, M.R. and J.A.Killian. 2003. Protein-lipid interactions studied with designed transmembrane peptides: role of hydrophobic matching and interfacial anchoring. *Mol. Membr. Biol.* **20**:271-284.
7. Deng, M. and M.Hochstrasser. 2006. Spatially regulated ubiquitin ligation by an ER/nuclear membrane ligase. *Nature* **443**:827-831.
8. Ellenberg, J., E.D.Siggia, J.E.Moreira, C.L.Smith, J.F.Presley, H.J.Worman, and J.Lippincott-Schwartz. 1997. Nuclear membrane dynamics and reassembly in living cells: targeting of an inner nuclear membrane protein in interphase and mitosis. *J. Cell Biol.* **138**:1193-1206.
9. Frenkiel-Krispin, D., B.Maco, U.Aebi, and O.Medalia. 2010. Structural analysis of a metazoan nuclear pore complex reveals a fused concentric ring architecture. *J. Mol. Biol.* **395**:578-586.
10. Galea, C.A., A.Nourse, Y.Wang, S.G.Sivakolundu, W.T.Heller, and R.W.Kriwacki. 2008. Role of intrinsic flexibility in signal transduction mediated by the cell cycle regulator, p27 Kip1. *J. Mol. Biol.* **376**:827-838.
11. Galzitskaya, O.V., S.O.Garbuzynskiy, and M.Y.Lobanov. 2006. FoldUnfold: web server for the prediction of disordered regions in protein chain. *Bioinformatics.* **22**:2948-2949.
12. Haruki, H., J.Nishikawa, and U.K.Laemmli. 2008. The anchor-away technique: rapid, conditional establishment of yeast mutant phenotypes. *Mol. Cell* **31**:925-932.
13. Hinshaw, J.E., B.O.Carragher, and R.A.Milligan. 1992. Architecture and design of the nuclear pore complex. *Cell* **69**:1133-1141.
14. King, M.C., C.P.Lusk, and G.Blobel. 2006. Karyopherin-mediated import of integral inner nuclear membrane proteins. *Nature* **442**:1003-1007.
15. Larkin, M.A., G.Blackshields, N.P.Brown, R.Chenna, P.A.McGettigan, H.McWilliam, F.Valentin, I.M.Wallace, A.Wilm, R.Lopez, J.D.Thompson, T.J.Gibson, and D.G.Higgins. 2007. Clustal W and Clustal X version 2.0. *Bioinformatics.* **23**:2947-2948.
16. Lusk, C.P., G.Blobel, and M.C.King. 2007. Highway to the inner nuclear membrane: rules for the road. *Nat. Rev. Mol. Cell Biol.* **8**:414-420.
17. Malik, P., N.Korfali, V.Srsen, V.Lazou, D.G.Batrakou, N.Zuleger, D.M.Kavanagh, G.S.Wilkie, M.W.Goldberg, and E.C.Schirmer. 2010. Cell-specific and lamin-dependent targeting of novel transmembrane proteins in the nuclear envelope. *Cell Mol. Life Sci.* **67**:1353-1369.
18. Miyagi, A., Y.Tsunaka, T.Uchihashi, K.Mayanagi, S.Hirose, K.Morikawa, and T.Ando. 2008. Visualization of intrinsically disordered regions of proteins by high-speed atomic force microscopy. *Chemphyschem.* **9**:1859-1866.
19. Mulder, F.A.A., M.Lundqvist, and R.M.Scheek. 2010. Nuclear Magnetic Resonance Spectroscopy Applied to (Intrinsically) Disordered Proteins. John Wiley & Sons, Inc., Hoboken, NJ, USA..
20. Ohba, T., E.C.Schirmer, T.Nishimoto, and L.Gerace. 2004. Energy- and temperature-dependent transport of integral proteins to the inner nuclear membrane via the nuclear pore. *J. Cell Biol.* **167**:1051-1062.
21. Oktaviani, N.A., R.Otten, K.Dijkstra, R.M.Scheek, E.Thulin, M.Akke, and F.A.Mulder. 2011. 100% complete assignment of non-labile (1)H, (13)C, and (15)N signals for calcium-loaded Calbindin D(9k) P43G. *Biomol. NMR Assign.* **5**:79-84.
22. Osborne, A.R., T.A.Rapoport, and B.B.van den. 2005. Protein translocation by the Sec61/SecY channel. *Annu. Rev. Cell Dev. Biol.* **21**:529-550.
23. Ostlund, C., J.Ellenberg, E.Hallberg, J.Lippincott-Schwartz, and H.J.Worman. 1999. Intracellular trafficking of emerin, the Emery-Dreifuss muscular dystrophy protein. *J. Cell Sci.* **112**:1709-1719.
24. Ostlund, C., T.Sullivan, C.L.Stewart, and H.J.Worman. 2006. Dependence of diffusional mobility of integral inner nuclear membrane proteins on A-type lamins. *Biochemistry* **45**:1374-1382.
25. Prilusky, J., C.E.Felder, T.Zeev-Ben-Mordehai, E.H.Rydberg, O.Man, J.S.Beckmann, I.Silman, and J.L.Sussman.

2005. FoldIndex: a simple tool to predict whether a given protein sequence is intrinsically unfolded. *Bioinformatics.* **21**:3435-3438.

26. Rout, M.P., J.D.Aitchison, A.Suprapto, K.Hjertaas, Y.Zhao, and B.T.Chait. 2000. The yeast nuclear pore complex: composition, architecture, and transport mechanism. *J. Cell Biol.* **148**:635-651.
27. Schrader, N., P.Stelter, D.Flemming, R.Kunze, E.Hurt, and I.R.Vetter. 2008. Structural basis of the nic96 subcomplex organization in the nuclear pore channel. *Mol. Cell* **29**:46-55.
28. Schuldiner, M., J.Metz, V.Schmid, V.Denic, M.Rakwalska, H.D.Schmitt, B.Schwappach, and J.S.Weissman. 2008. The GET complex mediates insertion of tail-anchored proteins into the ER membrane. *Cell* **134**:634-645.
29. Shulga, N., N.Mosammaparast, R.Wozniak, and D.S.Goldfarb. 2000. Yeast nucleoporins involved in passive nuclear envelope permeability. *J. Cell Biol.* **149**:1027-1038.
30. Soullam, B. and H.J.Worman. 1995. Signals and structural features involved in integral membrane protein targeting to the inner nuclear membrane. *J. Cell Biol.* **130**:15-27.
31. Stirling, C.J. 1999. Protein targeting to the endoplasmic reticulum in yeast. 1997 Fleming Lecture. *Microbiology* **145 (Pt 5)**:991-998.
32. Strawn, L.A., T.Shen, N.Shulga, D.S.Goldfarb, and S.R.Wente. 2004. Minimal nuclear pore complexes define FG repeat domains essential for transport. *Nat. Cell Biol.* **6**:197-206.
33. Tcherkasskaya, O., E.A.Davidson, and V.N.Uversky. 2003. Biophysical constraints for protein structure prediction. *J. Proteome. Res.* **2**:37-42.
34. Wente, S.R. and M.P.Rout. 2010. The nuclear pore complex and nuclear transport. *Cold Spring Harb. Perspect. Biol.* **2**:a000562.
35. Wilkins, D.K., S.B.Grimshaw, V.Receveur, C.M.Dobson, J.A.Jones, and L.J.Smith. 1999. Hydrodynamic radii of native and denatured proteins measured by pulse field gradient NMR techniques. *Biochemistry* **38**:16424-16431.
36. Wu, W., F.Lin, and H.J.Worman. 2002. Intracellular trafficking of MAN1, an integral protein of the nuclear envelope inner membrane. *J. Cell Sci.* **115**:1361-1371.
37. Yang, Q., M.P.Rout, and C.W.Akey. 1998. Three-dimensional architecture of the isolated yeast nuclear pore complex: functional and evolutionary implications. *Mol. Cell* **1**:223-234.
38. Yewdell, W.T., P.Colombi, T.Makhnevych, and C.P.Lusk. 2011. Lumenal interactions in nuclear pore complex assembly and stability. *Mol. Biol. Cell* **22**:1375-1388.
39. Zuleger, N., N.Korfali, and E.C.Schirmer. 2008. Inner nuclear membrane protein transport is mediated by multiple mechanisms. *Biochem. Soc. Trans.* **36**:1373-1377.

Chapter 5

Methods for studying transport of membrane protein transport across the nuclear pore complex

- Material and methods belonging to chapter 3 and 4 -

Anne C. Meinema[1], Justyna K. Laba[1], Rizqiya A. Hapsari[1], Renee Otten[1], Frans A. A. Mulder[1], Annemarie Kralt[2], Geert van den Bogaart[1‡], C. Patrick Lusk[3], Bert Poolman[1], Liesbeth M. Veenhoff[1,2†]

1 Departments of Biochemistry and Biophysical Chemistry, Groningen Biomolecular Sciences and Biotechnology Institute, Netherlands Proteomics Centre, Zernike Institute for Advanced Materials, University of Groningen, Nijenborgh 4, 9747 AG, Groningen, The Netherlands.

2 Department of Neuroscience, European Research Institute on the Biology of Ageing, University Medical Centre Groningen, Groningen, The Netherlands

3 Department of Cell Biology, Yale School of Medicine, New Haven, CT, USA, 06519

‡ Present address: Department of Neurobiology, Max Planck Institute for Biophysical Chemistry, Am Faßberg 11, 37077 Göttingen, Germany

Published in:

Meinema AC*, Laba JK*, Hapsari RA*, Otten R, Mulder FA, Kralt A, van den Bogaart G, Lusk CP, Poolman B, Veenhoff LM. Long unfolded linkers facilitate membrane protein import through the nuclear pore complex. *Science*. 2011 Jul 1; **333**(6038):90-3.

* These authors contributed equally to this work

Introduction

The directional transport of membrane proteins across the nuclear pore complex (NPC) toward the inner nuclear membrane (INM) is mediated by karyopherins (Kap60 and Kap95) and depends on nuclear RanGTP. We have shown that a high-affinity interaction between Kap60 and the nuclear localization signal of Heh2 (h2NLS) is required for efficient targeting of a membrane protein to the INM (Chapter 3). The h2NLS is spaced from the transmembrane segment by a long intrinsically-disordered linker domain (L) and a minimal linker length of 120 residues is required for the transport to the INM (Chapter 4). We discussed that this linker enables the NLS-bound Kaps to interact with the FG-nups in the central channel of the nuclear pore complex (NPC), while the transmembrane domain remains in the pore membrane. The linker domain slices through the NPC's scaffold during the translocation.

This chapter presents the materials and methods belonging to these chapters (3 and 4). The different yeast strains used to study the nuclear transport are listed in Table 5.1 and the generation of the Kap95 anchor away (KAP95-AA) and the NSP1-FRB strain are described (see *Strains*). The use of the KAP95-AA strain in the Kap95-depletion assay is explained and the method to trapping the reporter protein at Nsp1 in the NPC is detailed (see *fluorescence microscopy* and Fig. 5.2). All the reporters used in this study were expressed from plasmids, which are listed in Table 5.2. The design and construction of the plasmids are described in the section *plasmids*. The polypeptide sequences of the reporters are listed in Table 5.3 and the expression of the reporters was confirmed on Western blots (Fig. 5.1). The subcellular localization was routinely addressed by fluorescence laser scanning microscopy; the intensity of the reporters was quantified with a pixel analysis of fluorescent images (see *Fluorescence microscopy*). INM localization of the reporters was confirmed by immuno-electron microscopy (see *Immuno-Electron Microscopy*). h2NLS-L-GFP was expressed in *Lactococcus lactis* and purified for characterization with size-exclusion chromatography (SEC) and nuclear magnetic resonance (NMR) (see *Characterization of h2NLS-L*). Kap60IBB and tcNLS-GFP were purified from *Escherichia coli* and binding of Kap60ΔIBB to the h2NLS-L-GFP and tcNLS-GFP assayed in a bead-binding assay (*Karyopherin-cargo binding assay*).

Materials and methods

Strains

The *E.coli* strain MC1061 was used for DNA manipulation and expression was controlled by the arabinose-promoter. The *L.lactis* strain NZ9000 was used for production of h2NLS-L-GFP using the nisin A-promoter system. The *KAP95*-gene in the *S.cerevisiae* HHY110 strain and *NSP1* in strain K14708 were tagged with *FRB* to obtain the KAP95-AA and NSP1-FRB strains, respectively, as described in (Haruki *et al.*, 2008). The *FRB::KanMx* cassette in pFA6a-FRB-KanMX6 was amplified by PCR (primers for KAP95-AA: forward (frw): 5'- aagat gggct agaga gcaac agaag cgtca attat ccttа GGTCG ACGGA TCCCC GGGTT, reverse (rvs): 5'-ATGGA AAAGA ACCAA AATCA GCTTG TAAGT TCTAT CGTAA tcgat gaatt cgagc tcgtt; primers for NSP1-FRB: frw: 5'- ctcca cctct ctgga aaaac aaatc aactc gataa agaaa GGTCG ACGGA TCCCC GGGTT,

rvs: 5'- gtcaa ataag tgtag aatag aggga atttt ttctt ttaga TCGAT GAATT CGAGC TCGTT; uppercase: annealing sequence, lower case: primer overhang, *Phusion* polymerase (Finnzymes, Espoo, Finland)). See Table 5.1 for a list of the strains used in this study. The chromosomal integration of the cassettes after transformation was confirmed by colony PCR and Western blotting (Fig. 5.1).

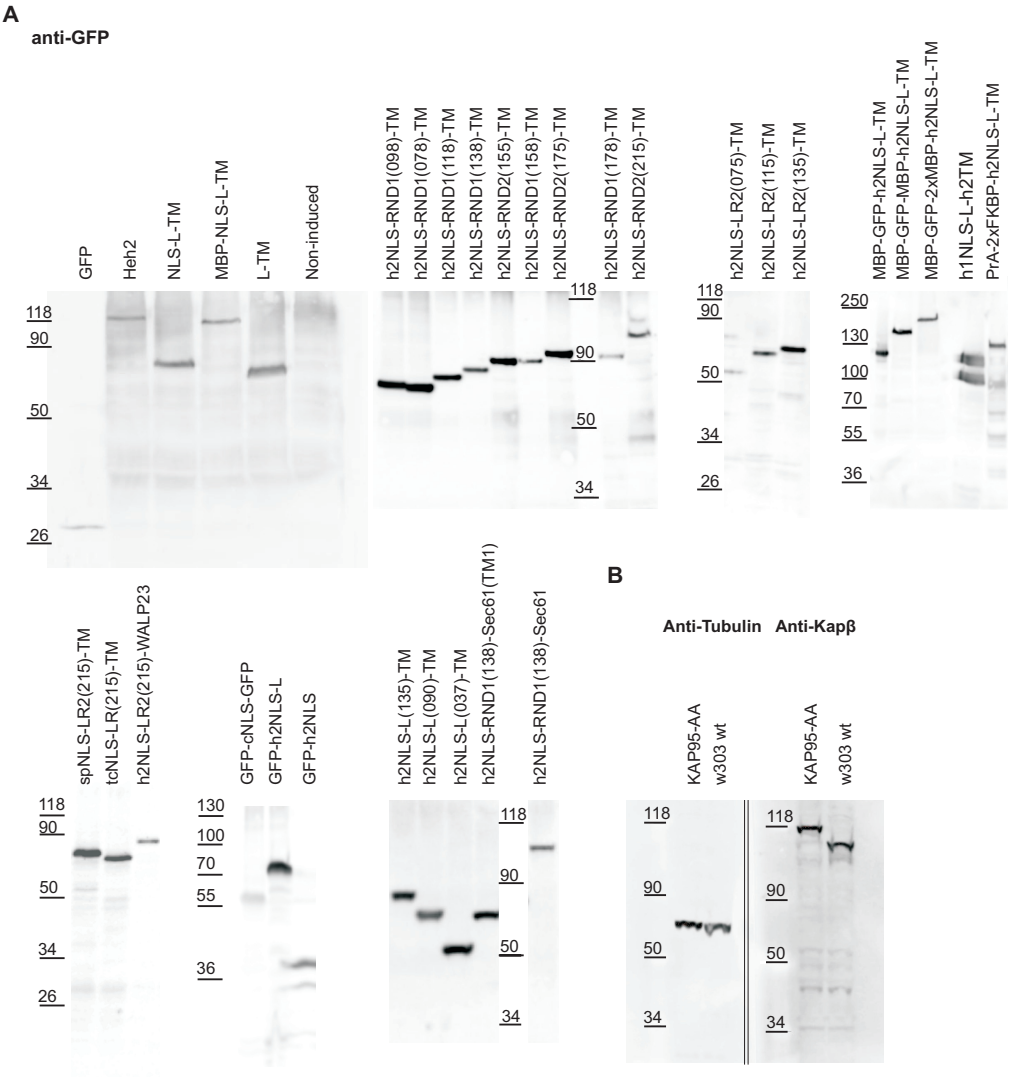

Figure 5.1: Western blot of whole cell extracts showing the expression of various proteins. A) Cells were grown to 10^7 cells per mL, and, after 2 hours of induction with 0.1% (w/v) D-galactose, whole cell lysates were prepared. For immuno-detection, an anti-GFP antibody was used. **B)** The concentration of Kap95 was determined in wild-type and KAP95-AA strains, expressing h2NLS-L-TM. Cells were grown to 10^7 cells per mL, an equivalent of 7×10^6 cells was loaded onto the gel. The increase in molecular weight is due to the presence of the 14 kDa FRB-tag. The expression in S. cerevisiae w303 of Kap95-tagged with FRB is similar to that of wild-type Kap95. Tubulin levels were used as a loading control.

Plasmids

See Table 5.2 for a list of plasmids and Table 5.3 for the amino acid sequences of all constructs. All DNA constructs were confirmed by sequencing and full length expression of the various gene constructs was determined by Western blotting (Fig. 5.1).

The plasmid pACM021-GFP was obtained by replacing the *Met25* promoter of pUG34 (Niedenthal *et al.*, 1996) for a *Gal1* promoter, which was amplified from pYes3/CT (Invitrogen) and ligated into the *Xba*I and *Sac*I sites (primers used: frw: 5'-gcatc tagaG GTTTT TTCTC CTTGA CGTTA AAGTA TAGAG G and rvs: 5'-gcaga gctcA CGGAT TAGAA GCCGC CGAGC). A ligation-independent cloning (LIC) cassette was inserted in the pACM021-GFP, which was adapted from (Aslanidis and de Jong, 1990;Geertsma and Poolman, 2007) and optimized for the expression vector in yeast by replacing the *Swa*I for a *Stu*I restriction site and ligated into the *Spe*I and the *Bam*HI sites as hybridized oligonucleotides (5'-CTAGT CATGG TGAGA ATTTA TTAGG CCTTC CCACC CTCCC AG; 5'- GATCC TGGGA GGGTG GGAAG GCCTA ATAAA TTCTC ACCAT GA). The coding sequence of Heh2, h2NLS-L-TM and L-TM were amplified by PCR from genomic DNA of *BY4742* (primers used, respectively: frw: 5'-atggt gagaa tttat taggt ATGGA CCACA GAAAC CTTGA TCCGA AAACG C and rvs: 5'- tggga gggtg ggaag gtcat taTTC TTTCC ACTCC CAACA TGTCA TG; frw: 5'- atggt gagaa tttat taggt caagg tGTCA AAGAT GAAAA TGTTG AAACT AACAA GAG and rvs: 5'- tggga gggtg ggaag gtcat taTCG ATAAG CTTGC AACAC TGAAT CTAC; frw: 5'-atggt gagaa tttat taggt caagg tCCAC CAGAG TCTCC TCCAC AATCT AAG and rvs: 5'- tggga gggtg ggaag gtcat taTCG ATAAG CTTGC AACAC TGAAT CTAC). The PCR-fragments were inserted in the expression vector pACM021-GFP-Lic by ligation-independent cloning to obtain the plasmids pACM022-GFP-Heh2, pACM023-GFP-h2NLS-L-TM and pACM024-GFP-L-TM.

The linker domain L of Heh2 (amino acids 146 – 294) was replaced by two random sequences of 149 and 186 residues with identical amino acid composition as in the Heh2 linker. The sequences were generated by RandSeq tool on ExPASy.org with user specified amino acid composition of Ala(5.4%), Arg(4.0%), Asn(6.0%), Asp(6.7%), Cys(0%), Gln(2.0%), Glu(16.1%), Gly(2.7%), His(1.3%), Ile(4.0%), Leu(8.7%), Lys(10.7%), Met(0.7%), Phe(1.3%), Pro(5.4%), Ser(12.15), Thr(7.4%), Trp(0%), Tyr(0.7%), and Val(4.7%). The linkers replaced 154 amino acids in the linker of the h2NLS-L-TM reporter, while keeping 8 amino acids C-terminal of the h2NLS and 18 amino acids N-terminal of the transmembrane helix (TM). The amino acid sequences were for LR1(178): ASEES APSKK LQFDE VNSKN EELEE EREDG KDTEL SEQHN VSYPK TLEDP DANPL EALFE PSRIE SKTDE NIITS VSRVD KRGGS PNRVL GITSA KIVTL RELDA EEPTL QATAT ETNDN ESLSK SKLKE SNTHE PEKKD KLSSK KMVI and for LR2(215): NEYDR ATHVT LSSLD QVVPR NLGLS KVPIE KNEEA TSPSL ELEKN VKQSG SILVS DSTSE KEEIQ KFMLV ASKLD HEANN EGVKR DERGE PNFPK AEEED LAKES PPSTT SPEENE KTKRS ESESN ESRLS DSTDT KTKQK ELPSK AKKEN TAIKI TEKRV RDLLI TEEDI DTDLA ALEEG SPNSD. Both are predicted to be unfolded by a number of prediction algorithms, e.g. FoldIndex (Prilusky *et al.*, 2005) (Fig. 4.3C). The gene fragments for h2NLS-LR1(178)-TM and h2NLS-LR2(215)-TM were ordered as synthetic

DNA (GeneArt, Regensburg, Germany) and subsequently the fragments were ligated into the *BamHI* and *EcoRI* sites of pACM21-GFP; the linkers were truncated by PCR-based mutagenesis (adapted from Quik Change protocol, Stratagene, La Jolla, USA)(primers used: frw LR1(158): 5'-GAAGA ATTGG AAGAA GAAAG AGAAG ATG; frw LR1(138): 5'-GTTTC TTATC CAAAA ACTTT CGAAG ATCC; frw LR1(118): 5'-CCATC AAGAA TTGAA TCTAA AACTG ATG; frw LR1(098): 5'-AAAAG AGGTG GTTCT CCAAA TAGAG TTTTG; frw LR1(078): 5'-AGAGA ATTGG ATGCT GAAGA ACCAA C; frw LR2(175): 5'-GAATT GGAAA AAAAT GTTAA ACAAT CTGG; frw LR2(155): 5'-AAAGA AGAAA TTCAA AAATT TATGT TG-GTT G; frw LR2(135): 5'-GAAGG TGTTA AAAGA GATGA AAGAG GTG; frw LR2(115): 5'-TTGGC TAAAG AATCT CCACC ATCTAC; frw LR2(075): 5'- AAAGA ATTGC CATCT AAAGC TAAAG ATTTG; rvs RND: 5'-GACGT CAGAT TGTGG AGGAG ACTC). The truncation of the native linker in h2NLS-L-TM was similar as written above, we used the primers: frw L(135): 5'-GTATC AAACG AATT TTTAG CTCAA CTAAA TAAAG; frw L(090): GGAGC AGAAA CAAGA AATGA AAGTG AG; frw L(037): CGAAG TCCAA AAGGT CG-CAC C; rvs: 5'-AGATT GTGGA GGAGA CTCTG GTGG. The amino acid sequences of the fragments are listed in Table 5.3.

To construct pACM053-GFP-tcNLS-LR2(215)-TM and pACM054-GFP-sp h2NLS-LR2(215)-TM, the coding sequence of h2NLS in pACM034-GFP-h2NLS-LR2(215)-TM was replaced for the coding sequence of respectively the tcNLS (PKKKR KVGPK KKRK) or the sp h2NLS; this is a single-partite version of the h2NLS that lacks the first KRKR basic region (PKKKR KKRSS KANK). The coding sequence for the NLSs were ordered as single stranded oligonucleotides (tc NLS: 5'- GATCC CCAAA AAAGA AGAGA AAGGT AGGGC CCAAA AAGAA GAGAA AGGTA GCTAG CGACG T and 5'- CGCTA GCTAC CTTTC TCTTC TTTTT GGGCC CTACC TTTCT CTTCT TTTTT GGG; sp h2NLS: 5'- GATCC GTCAA AGATG AAAAT GTTGA AACTA ACGGG CCCAA AAAGA AAAGA AAGAA AAGAT CTAGT AAGGC CAATA AACCA CCAGA GTCTC CTCCA CAATC TGACG T and 5'- CA-GAT TGTGG AGGAG ACTCT GGTGG TTTAT TGGCC TTACT AGATC TTTTC TTTCT TTTCT TTTTG GGCCC GTTAG TTTCA ACATT TTCAT CTTTG ACG). The oligonucle-otides are annealed and ligated in the vector at *Bam*HI and *Aat*II.

To construct pACM050-GFP-h2NLS-L(176) and pACM051-GFP-h2NLS-L(033), the sequence coding for the transmembrane domain was removed in pACM23-GFP-L-TM and pACM27-GFP-L(037)-TM, respectively, by PCR-based mutagenesis (adapted from Quik Change protocol, Stratagene, La Jolla, USA). We used the primers frw: 5'- CCTTC CCACC CTCCC AGGAT C and rvs: 5'- ttatc atgaC GGTTT CATAA TATCT ATCCC TCTTT TAGTT TTG. To construct pACM052-GFP-tcNLS-GFP, the coding sequence of tcNLS and an extra gene of GFP were ligated into pUG34 (Niedenthal *et al*., 1996), at respectively *Bam*HI and *Eco*RI and *Eco*RI and *Eco*RV. The coding sequence of the tcNLS was ordered as single stranded oligonucle-otides (5'- GGATC CCCAA AAAAG AAGAG AAAGG TAGAT CCAAA AAAGA AGAGA AAGGT AGCTA GCGAA TTC and 5'- GAATT CGCTA GCTAC CTTTC TCTTC TTTTT TGGAT CTACC TTTCT CTTCT TTTTT GGGGA TCC) and annealed. The gene coding for

GFP was amplified by PCR from pUG34 (frw: 5'- gccga attcA TGTCT AAAGG TGAAG AATTA TTCAC TGGTG TTG, rvs: 5'- gccga tatcA GCGGA TTTGT ACAAT TCATC CATAC CATGG GTAAT ACC).

The gene coding for WALP23 (de Planque and Killian, 2003) was ordered as synthetic DNA (GeneArt, DNVGE PALSR KITKK PKGWW LALAL ALALA LALAL ALWWA TARGD HMFSE PILVQ). The transmembrane domain of *Heh2* was replaced in vector pACM034-GFP-h2NLS-LR2(215)-TM for the *WALP23*-sequence, using the restriction sites *Kas*I and *Eco*RI.

The transmembrane domain in pACM030-GFP-h2NLS-LR1(138)-TM was replaced by *Sec61* as written for the *WALP23*-sequence. Full-length *Sec61* (25-471), encoding a protein with 10 transmembrane segments (reviewed in (Robson and Collinson, 2006)), was amplified without N-terminal XXRR-like ER membrane retention signal (Teasdale and Jackson, 1996) (frw: 5'-attgg cgccA GGAAG GTTCC ATACA ATCAG AAACT TATCT G) and lacks a potential C-terminal KDEL-signal (Teasdale and Jackson, 1996) (rvs: 5'-cgggga attct catta GTTCT TAGTA AACCC ACCTT CCTTG GC); The transmembrane domain for pACM030-GFP-h2NLS-LR1(138)-Sec61TM1 was amplified using the primer: frw: 5'-attgg cgccA GGAAG GTTCC ATACA ATCAG AAACT TATCT G and rvs: 5'-attga attct catta TAGCC AGTAC AGAGG GTCGG AAGTC. The *Sec61* fragments were amplified from pBG1805-Sec61 (Open Biosystems, Huntsville, USA). To construct pACM046-GFP-h2NLS-LR1(078)-Sec61 and pACM047-GFP-h2NLS-LR1(078)-Sec61TM1, the linker LR(138) was truncated as written before. To construct pACM048-GFP-LR1(138)-Sec61 and pACM049-GFP-LR1(138)-Sec61TM1, the sequence coding for the h2NLS was exchanged for a oligonucleotide without NLS. This oligonucleotide was ordered as single stranded DNA (5'- gatcc GTCAA AGATG AAAAT GTTGA AACTA ACCCC GGGGA ACAAA TTAGT ACGCC TAGGT CTAGT AAGGC CAATA AACCA CCAGA GTCTC CTCCA CAATC Tgacg t and 5'- cAGAT TGTGG AGGAG ACTCT GGTGG TTTAT TGGCC TTACT AGACC TAGGC GTACT AATTT GTTCC CCGGG GTTAG TTTCA ACATT TTCAT CTTTG ACg) annealed and ligated in the vectors at *Bam*HI and *Aat*II,

To construct the MBP-reporters, the restriction site *Sac*II was introduced 5' of the GFP gen and *Asc*I was made 3' of the *GFP* gene. Therefore, *GFP* was replaced by a fragment of *GFP* that was amplified with primers containing 5' the *Sac*II and *Asc*I sites (primers: 5'-cagtc tagac cgcgg agatc tccta ggATG TCTAA AGGTG AAGAA TTATT TACTG GTGTT GTC, 5'- ccgtc tagag catgc TTTGT ACAAT TCATC CATAC CATGG GTAAT AC). To construct pACM040-MBP-GFP-h2NLS-L-TM, the gene for maltose binding protein was amplified from a plasmid published in (van den Bogaart *et al.*, 2009) (primers: 5'- cggcc gcggA TGAAA ATCGA AGAAG GTAAA CTGGT AATCT G, 5'- cgacc gcggA GTCTG TGCAG CTGCC AGGG) and ligated (T4 Ligase, Fermentas, Burlington, Canada) into the *SacII* restriction site. To construct pACM041-MBP-GFP-MBP-h2NLS-L-TM and pACM042-MBP-GFP-2×MBP-h2NLS-L-TM, the gene encoding maltose binding protein was amplified, using a forward primer containing an *Asc*I restriction site (frw: 5'- cttgg cgcgc ctaAT GAAAA TCGAA GAAGG TAAAC TGGTA ATC) and a reverse primer containing a *Mlu*I restriction site (rvs: 5'- ccgac gcgtA GTCTG AGCAG CTGCC AGGGC), and the fragment was ligated in the *Asc*I site.

To construct pACM055-mCh-h2NLS-L(175) the gene of GFP was exchanged for the gene of mCherry in pACM050-GFP-h2NLS-L(176). The mCherry was amplified by PCR (frw: GGTCT AGAAT GGTGA GCAAG GGCGA GG; rvs: 5'- GCTCT AGATT ACTTG TACAG CTCGT CCATG CC) from pcDNA3.1-mCherry (Invitrogen, Carlsbad, CA) and ligated in the *Xba*I-sites of the plasmid.

To construct pRAH01-h1NLS-L-h2TM, the NLS-L encoding fragment of *Heh*1 was amplified by PCR from genomic DNA of *BY4742* (primers: frw: cggga tccAC CAATG ATTTTCAG-CA AAATT CC, rvs: attgg cgccG TTCCC GACCT TCCCA GATCC). The h2NLS-LR2(205) encoding region in pACM023 was replaced by the h1NLS-L fragment, using the *Bam*HI and *Kas*I sites.

To construct pJKL01-2×FKBP12-GFP-Lic-h2NLS-L-TM a tandem version of *FKBP* (2×FKBP), containing the restriction sites *Sac*II, *Aat*II *and, Stu*I at the 5'-site and *Sac*II at the 3'-site, was ordered as synthetic DNA (GeneArt, Regensburg, Germany; PRMDV RPGAG VQVET ISPGD GRTFP KRGQT CVVHY TGMLE DGKKF DSSRD RNKPF KFMLG KQEVI RG-WEE GVAQM SVGQR AKLTI SPDYAY GATGH PGIIP PHATL VFDV ELLKL ETRGV QVETI SPGDG RTFPK RGQTC VVHYT GMLED GKKFD SSRDR NKPFK FMLGK QE-VIR GWEEG VAQMS VGQRA KLTIS PDYAY GATGH PGIIPP HATLV FDVEL LKLET GAPR). The 2×FKBP12 encoding fragment was ligated into the *Sac*II site of pACM023-GFP-Lic-h2NLS-L-TM. To construct pJKL02-PrA-2FKBP12-GFP-Lic-h2NLS-L-TM, *PrA* was subsequently amplified from pBXa-His5 and ligated in the restriction sites *Aat*II and *Stu*I (frw: 5'-cg-gaa tgacg tcGGT GAAGC TCAAA AACTT AATGA CTC, rvs: 5'- ccgaa taggc ctAGG ATCGT CTTTA AGACT TTGGA TGAAG C).

To produce tcNLS-GFP and to purify the protein from *Escherichia coli*, an arabinose-inducible expression vector was used. The fragment coding for the tcNLS containing LIC competent overhangs was ordered as single stranded oligo's (5'-ATGGG TGGTG GATTT GC-TAT GCCAA AAAAG AAGAG AAAGG TAGAT CCAAA AAAGA AGAGA AAGGT AGCTA GCATG GGTGGT GGATTT AAATTT ATACT TCCAAG GG; 5'- TTGGA AG-TAT AAATT TTCCC TTGGA AGTAT AAATT TAAAT CCACC ACCCA TGCTA GCTAC CTTTC TCTTC TTTTTT GGATC TACCT TTCTCT TCTTTT TTGGC ATAG), annealed and inserted in pBADcLIC-GFP using ligation-independent cloning (Geertsma and Poolman, 2007). The plasmid for expression in *E.coli* of Kap60 with the StrepII sequence (WSHPQFEK) at the C-terminus (p1BAD-Kap60-Strep) was made by ligation of a fragment of *Kap60* in p1BAD between *Spe*I and *Asc*I. *Kap60* was amplified from genomic DNA of *BY4742* (primers: frw: 5'-gacta gtatg gataA TGGTA CAGAT TCTTC CACG; rvs: 5'-ggcgc gcctt atttt tcgaa ttgag gatga gacca GTTAA AATTG AATTG TTGGT TGACA TTAGA AC).

The vector for expression of h2NLS-L-GFP in *Lactococcus lactis* (pNZ-h2NLS-L-GFP-His) was made by PCR amplification of the h2NLS-L encoding fragment (5'-atggg tggtg gattt gctat gGAAT CAAGT TCTAG TGAGA GTAAA ACTGT CAAAG, 5'-ttgga agtat aaatt ttcAA TATCT ATCCC TCTTT TAGTT TTGTT GGC) and inserted into pREcLIC by using ligation-independent cloning (LIC) as described (Geertsma and Poolman, 2007), yielding plasmid pRE-

h2NLS-L-GFP-His. This pRE vector was converted into pNZ-h2NLS-L-GFP-His by Vector Backbone Exchange (VBEx) with pERL as described (Geertsma and Poolman, 2007) to express h2NLS-L-GFP in *L. lactis*.

Fluorescence Microscopy

Growth conditions: Yeast strains were grown at 30°C in synthetic defined medium without L-histidine, supplemented with 2% (w/v) filter-sterilized D-raffinose and 0.01 % (w/v) adenine, unless indicated otherwise. The reporter proteins were expressed from low-copy plasmids under the control of the *GAL1* promoter by 1-2 hours induction with 0.1% (w/v) D-galactose, unless indicated otherwise. Exponentially growing cells were kept in the SD growth medium at 30°C.

Image acquisition: Imaging was performed on a laser-scanning confocal microscope, as described previously (van den Bogaart *et al.*, 2007), and on a commercial LSM 710 confocal microscope (Carl Zeiss MicroImaging, Jena, Germany), using an objective C-Apochromat 40/1.2NA, a solid state laser (488 nm) for excitation and ZEN2010B software. The pixel dwell times for laser-scanning ranged from 0.2 to 0.5 ms with a pixel step of 50 nm. When measuring cells containing a high accumulation of reporter at either the inner nuclear membrane (INM) or in the nucleoplasm, a longer dwell time of 0.5 ms was used, such that the low fluorescence intensity at the ER and in the cytoplasm could be quantified.

Data analysis and NE/ER-ratios: For each cell, the distribution of pixel intensities at the nuclear envelope (NE) and at the cortical endoplasmic reticulum (ER) was determined, and the ratio of the average intensities at both locations, the NE/ER ratio, was calculated for at least 20 cells (Fig. 2). These NE/ER ratios were stable between 1 and 3 hours after induction (Chapter 3, Fig. 3). In all cases, only cells showing a clear ER or a higher than background intensity in the cytoplasm were analyzed, using home-made software or ZEN2010B. In all strains expressing the h2NLS-L-TM-derived reporters, >60% of the cells could be quantified; in the other cells the signal at the ER was too low to determine an NE/ER ratio. The fraction of cells that showed no signal at the ER was very high for h1NLS-L-h2TM (88%) and PrA-FKBP-GFP-h2NLS-L-TM (~90%), so the average NE/ER ratio should be considered as a lower limit, in these cases. We emphasize that in these cells the accumulation of membrane proteins in the INM is even more compelling, but we are unable to give a precise NE/ER ratio. The differences between the reporters are explained by differences in expression levels; at lower expression levels the fluorescence at the ER is too close to background levels. We measured the average fluorescence intensity of PrA-FKBP-GFP-h2NLS-L-TM by confocal microscope and compared it to h2NLS-L-TM, and indeed we found that on average the expression level was 10× lower (n = 40). As mentioned in chapter 4, FKBP-GFP-h2NLS-L-TM, was even lower expressed than PrA-FKBP-GFP-h2NLS-L-TM. Obviously, in all cases, after depleting the cells of Kap95 or trapping cargo, a larger (up to 100%) percentage of the cells could be quantified (Fig. 4.5 – 4.8 and 4.13A). In the case of the soluble reporter h2NLS-GFP, an N/C-ratio was determined (nucleus/cytoplasm). The nuclear accumulation was so strong that only a small fraction of cells showed no cytoplasmic staining and thus the underestimation of the accumulation of h2NLSGFP is significant (Fig. 3.8).

Nuclear efflux of membrane reporter protein. KAP95-AA expresses an allele of *KAP95* fused to the *FRB* fragment of *TOR1* and a plasma membrane 'anchor' fused to FKBP12 (PMA1-FKBP12) (Haruki *et al.*, 2008). The addition of rapamycin drives the formation of a ternary complex of FKBP12 with FRB with nanomolar affinity (Chen *et al.*, 1995), allowing to conditionally trap Kap95-FRB at the plasma membrane and thereby inhibit Kap95-mediated import. After 2 hours of expression of the reporters in exponentially growing cells, 2 µg/mL of rapamycin was added to trigger Kap95-FRB interaction with Pma1-FKBP to abolish the Kap95-mediated nuclear import (Fig. 3.5A). The absence of Kap95-facilitated import will result in a loss of nuclear accumulation for free moving cargo (not trapped). This can be measured as temporary net efflux of cargo from the nucleus. During the experiment, the cells were kept at 30°C and for every time point a new fresh sample was prepared. We measured the fluorescence intensity at the NE and at the ER and divided NE/ER to find the accumulation value (Fig. 5.2). The total fluorescence intensity in the cells did not change after adding rapamycin to the cells (Fig. 3.7B).

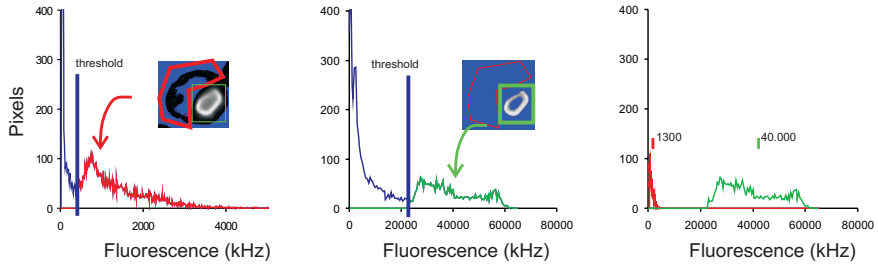

Figure 5.2: Membrane reporter proteins accumulate at INM. Image analysis to determine the accumulation levels in a typical confocal image of a cell expressing h2NLS-L-TM, the area of the nucleus (red box) and the ER were selected (green box) as indicated. The corresponding distributions of the pixel fluorescence intensities in the entire selected areas are plotted in a histogram for the ER (left) and the NE (middle). The histogram shows two populations of pixels: the low fluorescence intensity pixels correspond to background and out-of-focus signal and the high intensity pixels to the focused signal at the membranes of the cell. A mask was created to exclude all the low intensity pixels. Therefore a minimum threshold was set between these populations. The values of the pixels not excluded by the mask in the image are plotted in the graphs: in red for the focused signal at the ER (left) and green for the INM (middle), and combined in one graph (right). The accumulation is defined as the mean fluorescence intensity in the NE (in this case 40,000) divided by the mean fluorescence intensity in the ER (here 1,300, thus the NE/ER-ratio was 31). The differences in NE/ER-ratios of one experiment in a double blind test was <10% (n = 26).

Immuno-Electron Microscopy

Samples from KAP95-AA strains expressing h2NLS-L-TM were fixed in 4% paraformaldehyde and 0.1% glutaraldehyde in 100 mM HEPES for 1 hour at room temperature, rinsed in PBS and re-suspended in 10% gelatin. Blocks were placed in 2.3 M sucrose overnight at 4°C, transferred to aluminum pins and dropped into liquid nitrogen. The frozen block was trimmed on a Leica Cryo-EMUC6 UltraCut and 65 nm thick sections were collected and placed on a nickel formvar/carbon coated grid. The grids were treated with 100 mM ammonium chloride and blocked with 1% fish skin gelatin in PBS. Grids were incubated with an anti-GFP antibody (gift of M. Rout) for 30 minutes. After washing, the grids were incubated with 10nm gold-conjugated

antibodies for an additional 30 minutes. All grids were washed in PBS and post-fixed with 1% gluteraldehyde followed by uranyl acetate treatment. Grids were all viewed with a FEI Tecnai Biotwin TEM at 80kV. Images were acquired using a Morada CCD and iTEM (Olympus) software (Fig. 3.5A, B).

Characterization of h2NLS-L

Purification of h2NLS-L. Purified h2NLS-L was obtained by expression of h2NLS-L-GFP (containing a His-tag) in *Lactococcus lactis* NZ9000 (Kuipers *et al.*, 1997) grown on M17 medium (Oxoid, Basingstoke, United Kingdom) supplemented with 0.5% glucose and 5 μg/mL chloramphenicol at a constant pH (6.5) and temperature (30°C). Expression was induced at an OD of 0.7 by the addition of nisin A to a 1:10,000 (v/v) dilution of the supernatant from a stationary-phase (OD of 1.5) of a *L. lactis* NZ9700 culture (Kuipers *et al.*, 1993). Cells were harvested after 3.5 hours and washed once with 50 mM potassium phosphate pH 7.0. After cryogenic lysis (Alber *et al.*, 2007), the frozen, ground cells were resuspended in buffer (100 mM sodium phosphate (NaPi) pH 7.0, 0.1 mM $MgCl_2$, 18 mg/mL PMSF, 0.3 mg/mL pepstatin A plus 10% glycerol) with 150 mM NaCl, and 5 μg/mL DNase, using a Polytron Pt-K (Kinematica Swiss). Cell debris was removed by centrifugation for 20 minutes at 20,000×g at 4°C. h2NLS-L-GFP-His was purified on Ni-Sepharose (Fast Flow; GE Healthcare) after washing with 20 column volumes lysis buffer with 300 mM NaCl plus 15 mM imidazole and 20 column volumes lysis buffer with 300 mM NaCl plus 50 mM imidazole. The protein was eluted in 100 mM NaPi pH 7.0, 0.1 mM $MgCl_2$, 10% glycerol plus 300 mM imidazole, and peak fractions were loaded (0.5 mL/min) onto a size-exclusion chromatography (SEC) Superdex-200 column equilibrated with 50 mM potassium phosphate pH 7.0 plus 200 mM NaCl. After SEC, the protein was stable for days at 4°C. Peak fractions were concentrated on Vivaspin 30 kDa cut-off filters (GE Healthcare) to 4.8 mg/mL in 50 mM Tris-HCl pH 8.0, 1 mM DTT plus 1 mM EDTA. GFP-His was cleaved off using 60 μg/mL TEV-protease, overnight at 4°C (TEV-protease was produced as described by Waugh, D. S. on http://mcl1.ncifcrf.gov/waugh_tech.html). Non-cleaved h2NLS-L-GFP-His and GFP-His were removed by incubation with Ni-Sepharose. The flow-through and wash fractions containing 50 mM KPi (pH 7.0) plus 15 mM imidazole were combined and subsequently, h2NLS-L was concentrated on pre-washed Vivaspin 3 kDa cut-off filters to 1.4 mg/mL (55 μM). The resulting h2NLS-L in ~12.5 mM Tris-HCl, 37.5 mM KPi (pH 7.0), 6 mM imidazole, 0.4 mM EDTA plus 0.4 mM DTT was supplemented with D_2O to contain 93/7% v/v H_2O/D_2O.

NMR. NMR experiments were performed on a Varian Unity Inova spectrometer operating at 600 MHz, equipped with a triple-resonance room temperature probe. Data for unlabeled h2NLS-L and $^{15}N/^{13}C$-labeled α-synuclein were acquired at 10°C; in the case of $^{15}N/^{13}C$-labeled calbindin D_{9k}, the temperature was set to 28°C. One-dimensional ^1H spectra were recorded using a water-flip-back scheme for the intrinsically disordered proteins, while presaturation of the water resonance was applied for calbindin D_{9k}. The [^1H–^{13}C]–HSQC experiment on unlabeled h2NLS-L was recorded with 128 (^{13}C) × 1024 (^1H) complex data points (10.7 × 128 ms maximum evolution times, respectively) averaging 160 scans per FID, giving rise to a net acquisition time of 13

hours. A constant-time [^{1}H–^{13}C]–HSQC experiment was acquired on α-synuclein, using 200 (^{13}C) × 512 (^{1}H) complex data points (25 × 64 ms maximum evolution times, respectively) averaging 2 scans per FID, giving rise to a net acquisition time of 15 minutes. For calbindin D_{9k}, the same experiment was recorded, but with 160 (^{13}C) × 512 (^{1}H) complex data points (16 × 64 ms maximum evolution times, respectively) averaging 2 scans per FID (Mulder *et al.*, 2010).

Determination of the Stokes radius using SEC. The Stokes radius of h2NLS-L, as obtained after TEV-cleavage of h2NLS-L-GFP, was calibrated using size-exclusion chromatography (SEC) standards (thyroglobulin (669 kDa, Rs = 85 Å), ferritin (440 kDa, Rs = 61 Å), catalase (232 kDa, Rs = 52 Å), albumin (67 kDa, Rs = 35 Å), ovalbumin (43 kDa, Rs = 30.5 Å), ribonuclease (13.7 kDa, Rs = 16.4 Å)). SEC was performed in 50 mM potassium phosphate pH 7.0 plus 200 mM NaCl. The partition coefficient of the proteins was determined with $K_{av} = (V_e\text{-}V_0) / (V_c\text{-}V_0)$, and the Stokes radius calculated by linear regression of the standard curve; where V_e is the elution volume, V_0 is the void volume and V_c is the geometric column volume. A theoretical value for the Stokes radius was calculated with $Rh = (4.75 \pm 1.11)N^{0.29 \pm 0.02}$ and $Rh = (0.75 \pm 0.05)M^{0.33 \pm 0.02}$ for a globular folded protein and $Rh = (2.21 \pm 1.07)N^{0.57 \pm 0.02}$ and $Rh = (0.19 \pm 0.01)M^{0.54 \pm 0.02}$ for a unfolded protein (Tcherkasskaya *et al.*, 2003;Wilkins *et al.*, 1999). Where *R*h is the hydrodynamic or Stokes radius of h2NLS-L, *N* the number of residues in the protein domain (227 amino acids) and *M* the molar mass in Dalton (25592.03 Da).

Karyopherin-cargo binding assay

Kap60, under the control of the arabinose-promoter (PBAD), was expressed in *E. coli* MC1061 by induction with 10^{-3}% (w/v) arabinose for approximately 2 hours at 30°C. Cells were lysed in 50 mM potassium phosphate pH 7.0, 100 mM NaCl, 1 mM EDTA, 2 mM DTT, 18 mg/mL PMSF plus 0.3 mg/mL pepstatin A and purified using a two-step purification protocol with first Strep-Tactin Superflow (Qiagen) and second SEC Sephadex 200 in 50 mM sodium phospate pH 8.0 plus 300 mM NaCl. GFP with C-terminal His_{10} and N-terminal tandem cNLS (tcNLS) sequences was purified by Ni-Sepharose and SEC. h2NLS-L-GFP purification was performed as described in the NMR section. A significant fraction of Kap60 was proteolysed, and the fraction lacking the IBB domain was used in the binding assay. The cleavage site was confirmed with linear mode MALDI MS on a 4800 mass analyzer.

The binding affinity of Kap60ΔIBB to h2NLSL-GFP and tcNLS-GFP was measured using a solid phase binding assay (Fanara *et al.*, 2000;Hahn *et al.*, 2008). Fresh fractions of Kap60ΔIBB (2× excess of binding capacity of the beads) from SEC were incubated with Strep-Tactin magnetic beads (Qiagen) for 30 minutes. These bead-containing suspensions were divided into 5 µL tube reactions (approximately containing 1 µg = 16.6 µmol of Kap60ΔIBB each). Cargoes (h2NLS-L-GFP and tcNLS-GFP-His) were added at different concentrations in TBT buffer (20 mM K/HEPES, pH 7.4, 110 mM KOAc, 2mM MgCl2 plus 0.1% Tween-20) and incubated overnight at 4°C. Beads were washed twice with 50 mM NaH_2PO_4, pH 8.0, 300 mM NaCl plus 0.05% Tween

20 and eluted in 20 μL of the same buffer, supplemented with 10 mM biotin, 0.5% SDS plus 5 mM DTT. Elution fractions were incubated for 5 minutes at room temperature and separated on 12.5% SDS-PAGE gels. In-gel fluorescence of GFP, representing the amount of bound cargo was quantified using ImageJ software (U. S. National Institutes of Health, Bethesda, MD, USA). Fractional saturation curves were fitted with simple binding kinetics (Lanfermeijer *et al.*, 1999).

Western blots

Exponentially growing cells were lysed in NaOH and β-mercaptoethanol and TCA-precipitated. The samples were separated on SDS-PAGE gels and transferred to a PVDF membrane. For detection of GFP we used anti-GFP antibody (Merck, Darmstadt, Germany) at a dilution of 1:2,000 (v/v) and a secondary with anti-rabbit-alkaline phosphatase conjugate at 1:10,000 (v/v) (Sigma-Aldrich, St. Louis, USA). For the detection of tubulin, we used anti-Tubulin at 1:1,000 (v/v) (AbCam, Cambridge, UK) with anti-rat-alkaline phosphatase conjugate at 1:10,000 (v/v) (Sigma-Aldrich). To detect Kap95 we used anti-Kap95 at 1:1000 (v/v) (Santa Cruz Biotechnology, Santa Cruz, USA) with anti-goat-alkaline phosphatase conjugate at 1:10,000 (Sigma-Aldrich). Pre-stained molecular weight marker (Fermentas) was used.

Tables

Table 5.1: S. cerevisiae strains

Name	Description	Source
w303	*mata/α leu2-3,112 trp1-1 can1-100 ura3-1 ade2-1 his3-11,15*	
BY4742 (Brachmann *et al.*, 1998)	*matα his3Δ1 leu2Δ0 lys2Δ0 ura3Δ0*	Invitrogen
HHY110	*w303, matα tor1-1 fpr1::NAT PMA1-2xFKBP12::TRP1*	(Haruki *et al.*, 2008)
K14708	*w303, matα tor1-1 fpr1::NAT*	(Haruki *et al.*, 2008)
KAP95-AA	*HHY110, KAP95-FRB::KanMX*	This study
NSP1-FRB	*K14708, NSP1-FRB::KanMX*	This study
Mtr1-1	*mtr1-1*	(Kadowaki *et al.*, 1994)
Nup170Δ (Winzeler *et al.*, 1999)	*BY4743, Homo 2N, NUP170::KanMX*	Open Biosystems
SWY2950	*nup100ΔGLFG nup145ΔGLFG nup57ΔGLFG*	(Strawn *et al.*, 2004)
SWY3042	*nup42ΔFG nup159ΔFG nup60ΔFxF nup1ΔFxFG nup2ΔFxFG nup100ΔGLFG*	(Strawn *et al.*, 2004;Strawn *et al.*, 2004)
SWY3062	*nup42ΔFG nup159ΔFG nup60ΔFxF nup1ΔFxFG nup2ΔFxFG nsp1ΔFGΔFxFG*	(Strawn *et al.*, 2004)

Table 5.2: Plasmids

Name	Description	Source
pACM021-GFP	pUG34 *Gal1* promoter (in stead of *Met25*)	(Niedenthal *et al.*, 1996),
pACM022-GFP-Heh2	*GFP-Heh2* under *GAL1* promoter (HIS, *Cen*)	This study
pACM023-GFP-h2NLS-L-TM	As above, coding for Heh2 (93-378)	This study
pACM024-GFP-L-TM	As above, coding for Heh2 (138-378)	This study
pACM25-GFP-L(135)-TM	As pAC023-GFP-h2NLS-L-TM, truncated L containing 135 residues	This study
pACM26-GFP-L(090)-TM	As pAC023-GFP-h2NLS-L-TM, truncated L containing 90 residues	This study
pACM27-GFP-L(037)-TM	As pAC023-GFP-h2NLS-L-TM, truncated L containing 37 residues	This study

Table 5.2: Plasmids

Name	Description	Source
pACM028-GFP-h2NLS-LR1(178)-TM	pAC023-GFP-Lic-h2NLS-L-TM where the L is replaced for a artificial linker LR1, containing 178 residues	This study
pACM029-GFP-h2NLS-LR1(158)-TM	As above, truncated LR1 containing 158 residues	This study
pACM030-GFP-h2NLS-LR1(138)-TM	As above, truncated LR1 containing 138 residues	This study
pACM031-GFP-h2NLS-LR1(118)-TM	As above, truncated LR1 containing 118 residues	This study
pACM032-GFP-h2NLS-LR1(098)-TM	As above, truncated LR1 containing 98 residues	This study
pACM033-GFP-h2NLS-LR1(078)-TM	As above, truncated LR1 containing 78 residues	This study
pACM034-GFP-h2NLS-LR2(215)-TM	pAC023-GFP-h2NLS-L-TM where the L is replaced for a artificial linker LR2, containing 205 residues	This study
pACM035-GFP-h2NLS-LR2(175)-TM	As above, truncated LR2 containing 175 residues	This study
pACM036-GFP-h2NLS-LR2(155)-TM	As above, truncated LR2 containing 155 residues	This study
pACM037-GFP-h2NLS-LR2(135)-TM	As above, truncated LR2 containing 135 residues	This study
pACM038-GFP-h2NLS-LR2(115)-TM	As above, truncated LR2 containing 115 residues	This study
pACM039-GFP-h2NLS-LR2(075)-TM	As above, truncated LR2 containing 75 residues	This study
pACM040-MBP-GFP-h2NLS-L-TM	Heh2 (93-378) fused to MBP-GFP	This study
pACM041-MBP-GFP-MBP-h2NLS-L-TM	Heh2 (93-378) fused to MBP-GFP-MBP	This study
pACM042-MBP-GFP-2xMBP-h2NLS-L-TM	Heh2 (93-378) fused to MBP-GFP-MBP-MBP	This study
pACM043-GFP-h2NLS-LR2(215)-WALP23	pAC034-GFP-h2NLS-LR2(215)-TM where the TM is replaced for WALP23	This study
pACM044-GFP-h2NLS-LR1(138)-Sec61	pAC030-GFP-h2NLS-LR1(138)-TM where the TM is replaced for full-length Sec61 (Residues 25-471)	This study
pACM045-GFP-h2NLS-LR1(138)-Sec61TM1	As above, Sec61 but with only N-terminal TM (Residues 25-42)	This study
pACM046-GFP-h2NLS-LR1(078)-Sec61	pACM044-GFP-h2NLS-LR1(138)-Sec61 where the linker is truncated to 78 residues	This study
pACM047-GFP-h2NLS-LR1(078)-Sec61TM1	pACM045-GFP-h2NLS-LR1(138)-Sec61TM1 where the linker is truncated to 78 residues	This study
pACM048-GFP-LR1(138)-Sec61	pACM044-GFP-h2NLS-LR1(138)-Sec61 where the h2NLS is removed	This study
pACM049-GFP-LR1(138)-Sec61TM1	pACM045-GFP-h2NLS-LR1(138)-Sec61TM1 where the h2NLS is removed	This study
pACM050-GFP-h2NLS-L(176)	pAC023-GFP-h2NLS-L-TM, where the TM is removed	This study
pACM051-GFP-H2NLS-L(033)	pACM050-GFP-h2NLS-L(176), where L is truncated to 33 residues	This study
pACM052-GFP-tcNLS-GFP	pACM021-GFP, where tcNLS and GFP are inserted	This study
pACM053-GFP-tcNLS-LR2(215)-TM	pACM034-GFP-h2NLS-LR2(215)-TM where the h2NLS is replaced for tcNLS	This study
pACM054-GFP-sp h2NLS-LR2(215)-TM	pACM034-GFP-h2NLS-LR2(215)-TM where the h2NLS is replace for the single partite sp h2NLS	This study
pACM055-mCh-h2NLS-L(175)	pACM050-GFP-h2NLS-L(176), where GFP is replaced for mCherry	This study
pFA6a-FRB-KanMX6	Cassette for amplification of FRB and KanMx with F2 and R1 primer binding sites	(Haruki *et al*., 2008)
pJKL01-2xFKBP12-GFP-Lic-h2NLS-L-TM	pAC023-GFP-h2NLS-L-TM where 2xFKBP12 is N-terminally fused to h2NLS-L-TM	This study
pJKL02-PrA-2xFKBP12-GFP-Lic-h2NLS-L-TM	pJKL01-2xFKBP12-GFP-Lic-h2NLS-L-TM where PrA is N-terminally fused to 2xFKBP12-h2NLS-L-TM	This study
pRAH01-h1NLS-L-h2TM	pAC023-GFP-h2NLS-L-TM where NLS-L of Heh2 is replaced for NLS-L of Heh1	This study
p1BAD-Kap60-Strep	Vector for expression of Kap60 with Strep-tag in *E.coli*	This study
pBADcLic-tcNLS-GFP	Vector for expression of tcNLS-GFP in *E. coli*	This study
pNZ-h2NLS-L-GFP-His	Vector for expression of h2NLS-L-GFP in *L. lactis*	This study

Table 5.3: The amino acid sequences of the reporters

Name[1]	Sequence[2]
GFP	MSKGEELFTGVVPILVELDGDVNGHKFSVSGEGEGDATYGKLTLKFICTTGKLPVPWPTLVTTFGYGVQCFARYPD HMKQHDFFKSAMPEGYVQERTIFFKDDGNYKTRAEVKFEGDTLVNRIELKGIDFKEDGNILGHKLEYNYNSHNV YIMADKQKNGIKVNFKIRHNIEDGSVQLADHYQQNTPIGDGPVLLPDNHYLSTQSALSKDPNEKRDHMVLLEFV TAAGITHGMDELYKSRTSHGENLLGQG
h2NLS-L(180)-TM[3] -L(135) -L(090) -L(037)	VKDENVETNKRKREQISTDNEAKMQIQEEKSPKKKRKKRSSKANKPPESPPQS>KSDGKATSADLTSELETVEELH KKDSSDDKPRVKELPKPELPNLK<VSNEFLAQLNKELASAATENYDHSIKSTDLSSIRIETEEPVGPST<GAETRNESE VMENINLEVQPEVKEAKEELTKISETFDNQDEEDTSRLSSKKNI<RSPKGRTRHFIANKTKRGIDIMKPFIAHL*FIWL WNGAIFLSIICPILFGLWY*REQRIQVGYCGHEKPLKSLAISAFPQTERVDSVLQAYR
L-TM[3]	PPESPPQSKSDGKATSADLTSELETVEELHKKDSSDDKPRVKELPKPELPNLKVSNEFLAQLNKELASAATENYDH SIKSTDLSSIRIETEEPVGPSTGAETRNESEVMENINLEVQPEVKEAKEELTKISETFDNQDEEDTSRLSSKKNIRSPK GRTRHFIANKTKRGIDIMKPFIAHL*FIWLWNGAIFLSIICPILFGLWY*REQRIQVGYCGHEKPLKSLAISAFPQTER VDSVLQAYR
PrA-2×FKBP12[4] 2×FKBP12	>GEAQKLNDSQAPKADAQQNNFNKDQQSAFYEILNMPNLNEAQRNGFIQSLKDDPSQSTNVLGEAKKLNESQ APKADNNFNKEQQNAFYEILNMPNLNEEQRNGFIQSLKDDPSQSANLLSEAKKLNESQAPKADNKFNKKQQNA FYEILHLPNLNEEQRNGFIQSLKDDPSQSANLLAEAKKLNDAQAPKADNKFNKEQQNAFYEILHLPNLTEEQRNGF IQSLKDDP<RPGAGVQVETISPGDGRTFPKRGQTCVVHYTGMLEDGKKFDSSRDRNKPFKFMLGKQEVIRGWEE GVAQMSVGQRAKLTISPDYAYGATGHPGIIPPHATLVFDVELLKLETRGVQVETISPGDGRTFPKRGQTCVVHYTG MLEDGKKFDSSRDRNKPFKFMLGKQEVIRGWEEGVAQMSVGQRAKLTISPDYAYGATGHPGIIPPHATLVFDVEL LKLET
h2NLS-LR1(178)-TM[3] -LR1(158) -LR1(138) -LR1(118)	VKDENVETN**KRKR**EQISTDNEAKMQIQEEKS**PKKKRKKRSSKANK**PPESPPQSDV>ASEESAPSKKLQFDEVSKN <EELEEEREDGKDTELSEQHN<VSYPKTLEDPDANPLEALFE<PSRIESKTDENIITSVSRVD<KRGGSPNRVLGITSA KIVTL<RELDAEEPTLQATATETNDNESLSKSKLKESNTHEPEKKDKLSSKKMVIGANKTKRGIDIMKPFIAHL*FIWL WNGAIFLSIICPILFGLWY*REQRIQVGYCGHERPLKSLAISAFPQTERVDSVLQAYRP
h2NLS-LR2(215)-TM[3] -LR2(175) -LR2(155) -LR2(135) -LR2(115)	VKDENVETN**KRKR**EQISTDNEAKMQIQEEKS**PKKKRKKRSSKANK**PPESPPQSDV>NEYDRATHVTLSSLDQVV PR<NLGLSKVPIEKNEEATSPSL<ELEKNVKQSGSILVSDSTSE<KEEIQKFMLVASKLDHEANN<EGVKRDERGEPN FPKAEEED<LAKESPPSTTSPEENEKTKRSESESNESRLSDSTDTKTKQ<KELPSKAKDLKENTAIKITEKRVRLITEEDI DTDLAALEEGSPNSDGANKTKRGIDIMKPFIAHL*FIWLWNGAIFLSIICPILFGLWY*REQRIQVGYCGHERPLKSLAI SAFPQTERVDSVLQAYRP
sp h2NLS-LR2(215)-TM[3]	VKDENVETNG**PKKKRKKRSSKANK**PPESPPQSDVNEYDRATHVTLSSLDQVVPRNLGLSKVPIEKNEEATSPSLEL EKNVKQSGSILVSDSTSEKEEIQKFMLVASKLDHEANNEGVKRDERGEPNFPKAEEEDLAKESPPSTTSPEENEKTK RSESESNESRLSDSTDTKTKQKELPSKAKDLKENTAIKITEKRVRLITEEDIDTDLAALEEGSPNSDGANKTKRGIDIM KPFIAHL*FIWLWNGAIFLSIICPILFGLWY*REQRIQVGYCGHERPLKSLAISAFPQTERVDSVLQAYRP
tcNLS-LR2(215)-TM[3]	**PKKKRK**VG**PKKKRK**VASDVNEYDRATHVTLSSLDQVVPRNLGLSKVPIEKNEEATSPSLELEKNVKQSGSILVSDST SEKEEIQKFMLVASKLDHEANNEGVKRDERGEPNFPKAEEEDLAKESPPSTTSPEENEKTKRSESESNESRLSDSTD TKTKQKELPSKAKDLKENTAIKITEKRVRLITEEDIDTDLAALEEGSPNSDGANKTKRGIDIMKPFIAHL*FIWLWNGA IFLSIICPILFGLWY*REQRIQVGYCGHERPLKSLAISAFPQTERVDSVLQAYRP
h2NLS-LR2(215)-WALP23[3]	VKDENVETN**KRKR**EQISTDNEAKMQIQEEKS**PKKKRKKRSSKANK**PPESPPQSDVNEYDRATHVTLSSLDQVPR NLGLSKVPIEKNEEATSPSLELEKNVKQSGSILVSDSTSEKEEIQKFMLVASKLDHEANNEGVKRDERGEPNFPKAE EEDLAKESPPSTTSPEENEKTKRSESESNESRLSDSTDTKTKQKELPSKAKDLKENTAIKITEKRVRLITEEDIDTDLAA LEEGSPNSDGADNVGEPALSRKITKKPKG*WWLALALALALALALALWWAT*ARGDHMFSEPILVQ
h2NLS-LR1(138)-Sec61[3] -LR1(078)	VKDENVETN**KRKR**EQISTDNEAKMQIQEEKS**PKKKRKKRSSKANK**PPESPPQSDV>VSYPKTFEDPDANPLEALF EPSRIESKTDENIITSVSRVDKRGGSPNRVLGITSAKIVTL<RELDAEEPTLQATATETNDNESLSKSKLKESNTHEPEK KDKLSSKKMVIGARKVPYNQK*LIWTGVSLLIFLILGQIPLYGIV*SSETSDPLYWLAMLASNR*GTLLELGVSPIITSSMIF* QFLQGTQLLQIRPESKQDRE*LFQIAQKVCAIILILGQALVVVM*TGNYGAPSD*LGLPICLLLIFQLMFASLIVMLL*DELL SK*GYGLGSGISLFTATNIAEQIFW*RAFAPTTVNSGRGKEFEGAVIAFFHLLAVRKDKKRALVEAFYRTNLPN*MFQVL MTVAIFLFVLYLQGF*RYELPIRSTKVRGQIGIYPIKLFYTSNTP*IMLQSALTSNIFLI*SQILFQKYPTNPLIRLIGVWGIRP GTQGPQMALSGLAYYIQPLMSLSEALLDPIKTI*VYITFVLGSCAVFS*KTWIEISGTSPRDIAKQFKDQGMVINGKRE TSIYRELKK*IIPTAAAFGGATIGALSVG*SDL*LGTLGSGASILMATTTIYGYY*EAAAKEGGFTKN
h2NLS-LR1(138)-Sec61TM1[3] -LR1(078)	VKDENVETN**KRKR**EQISTDNEAKMQIQEEKS**PKKKRKKRSSKANK**PPESPPQSDV>VSYPKTFEDPDANPLEALF EPSRIESKTDENIITSVSRVDKRGGSPNRVLGITSAKIVTL<RELDAEEPTLQATATETNDNESLSKSKLKESNTHEPEK KDKLSSKKMVIGARKVPYNQK*LIWTGVSLLIFLILGQIPLYGIV*SSETSDPLYWL
LR1(138)-Sec61[3]	VKDENVETNPGEQISTPRSSKANKPPESPPQSDVVSYPKTFEDPDANPLEALFEPSRIESKTDENIITSVSRVDKRGG SPNRVLGITSAKIVTLRELDAEEPTLQATATETNDNESLSKSKLKESNTHEPEKKDKLSSKKMVIGARKVPYNQK*LIW TGVSLLIFLILGQIPLYGIV*SSETSDPLYWLAMLASNR*GTLLELGVSPIITSSMIF*QFLQGTQLLQIRPESKQDRE*LFQIA QKVCAIILILGQALVVVM*TGNYGAPSD*LGLPICLLLIFQLMFASLIVMLL*DELLSK*GYGLGSGISLFTATNIAEQIFW*RA FAPTTVNSGRGKEFEGAVIAFFHLLAVRKDKKRALVEAFYRTNLPN*MFQVLMTVAIFLFVLYLQGF*RYELPIRSTKV RGQIGIYPIKLFYTSNTP*IMLQSALTSNIFLI*SQILFQKYPTNPLIRLIGVWGIRPGTQGPQMALSGLAYYIQPLMSLSE ALLDPIKTI*VYITFVLGSCAVFS*KTWIEISGTSPRDIAKQFKDQGMVINGKRETSIYRELKK*IIPTAAAFGGATIGALSVG* SDL*LGTLGSGASILMATTTIYGYY*EAAAKEGGFTKN
LR1(138)-Sec61TM1[3]	VKDENVETNPGEQISTPRSSKANKPPESPPQSDVVSYPKTFEDPDANPLEALFEPSRIESKTDENIITSVSRVDKRGG SPNRVLGITSAKIVTLRELDAEEPTLQATATETNDNESLSKSKLKESNTHEPEKKDKLSSKKMVIGARKVPYNQK*LIW TGVSLLIFLILGQIPLYGIV*SSETSDPLYWL

Table 5.3: The amino acid sequences of the reporters

Name[1]	Sequence[2]
MBP[5]	MKIEEGKLVIWINGDKGYNGLAEVGKKFEKDTGIKVTVEHPDKLEEKFPQVAATGDGPDIIFWAHDRFGGYAQSG LLAEITPDKAFQDKLYPFTWDAVRYNGKLIAYPIAVEALSLIYNKDLLPNPPKTWEEIPALDKELKAKGKSALMFNLQ EPYFTWPLIAADGGYAFKYENGKYDIKDVGVDNAGAKAGLTFLVDLIKNKHMNADTDYSIAEAAFNKGETAMTIN GPWAWSNIDTSKVNYGVTVLPTFKGQPSKPFVGVLSAGINAASPNKELAKEFLENYLLTDEGLEAVNKDKPLGAV ALKSYEEELAKDPRIAATMENAQKGEIMPNIPQMSAFWYAVRTAVINAASGRQTVDAALAAAQT
GFP-h2NLS-L[3] GFP-h2NLS	VKDENVETN**KRKR**EQISTDNEAKMQIQEEKS**PKKKRKKRSSKANK**PPESPPQS>KSDGKATSADLTSELETVEELH KKDSSDDKPRVKELPKPELPNLKVSNEFLAQLNKELASAATENYDHSIKSTDLSSIRIETEEPVGPSTGAETRNESEV MENINLEVQPEVKEAKEELTKISETFDNQDEEDTSRLSSKKNI<RSPKGRTRHFIANKTKRGIDIMKPS
mCh-h2NLS-L	MVSKGEEDNMAIIKEFMRFKVHMEGSVNGHEFEIEGEGEGRPYEGTQTAKLKVTKGGPLPFAWDILSPQFMYGS KAYVKHPADIPDYLKLSFPEGFKWERVMNFEDGGVVTVTQDSSLQDGEFIYKVKLRGTNFPSDGPVMQKKTMG WEASSERMYPEDGALKGEIKQRLKLKDGGHYDAEVKTTYKAKKPVQLPGAYNVNIKLDITSHNEDYTIVEQYERAE GRHSTGGMDELYKACSRTSHGENLLGQGVKDENVETN**KRKR**EQISTDNEAKMQIQEEKS**PKKKRKKRSSKANK** PPESPPQSKSDGKATSADLTSELETVEELHKKDSSDDKPRVKELPKPELPNLKVSNEFLAQLNKELASAATENYDHS IKSTDLSSIRIETEEPVGPSTGAETRNESEVMENINLEVQPEVKEAKEELTKISETFDNQDEEDTSRLSSKKNIRSPKG RTRHFIANKTKRGIDIMKP
GFP-tcNLS-GFP	MSKGEELFTGVVPILVELDGDVNGHKFSVSGEGEGDATYGKLTLKFICTTGKLPVPWPTLVTTFGYGVQCFARYPD HMKQHDFFKSAMPEGYVQERTIFFKDDGNYKTRAEVKFEGDTLVNRIELKGIDFKEDGNILGHKLEYNYNSHNVY IMADKQKNGIKVNFKIRHNIEDGSVQLADHYQQNTPIGDGPVLLPDNHYLSTQSALSKDPNEKRDHMVLLEFVTA AGITHGMDELYKSRTSGS**PKKKRKV**D**PKKKRKV**ASEFMSKGEELFTGVVPILVELDGDVNGHKFSVSGEGEGDAT YGKLTLKFICTTGKLPVPWPTLVTTFGYGVQCFARYPDHMKQHDFFKSAMPEGYVQERTIFFKDDGNYKTRAEVK FEGDTLVNRIELKGIDFKEDGNILGHKLEYNYNSHNVYIMADKQKNGIKVNFKIRHNIEDGSVQLADHYQQNTPIG DGPVLLPDNHYLSTQSALSKDPNEKRDHMVLLEFVTAAGITHGMDELYK
h1NLS-L-h2TM[3]	TNDFQQNSDT**RKKRK**DPDSDDWSESNSKENKIDNKHLNLLSSDSEIEQDYQ**KAKKRK**TSDLNQEHGNGSAILGK LSVKTPIKNTNRKPVSMDNFNDSLTSSGTENDPFVPNIRHNPKELGTANGTGHSTPLRKLKVSASFADKLPQKEVP STILVPEVEQQEPSQSERTPSLFSSEGSGSESEAPLLPEITTPGPHQPMGNTSNNVVEMIDTDSSNLVSDEDEVLVP TRIETPQLPTEKDVEKCEARVQELQEEVNEQLEHENGSEFDVKQGSGKVGNGANKTKRGIDIMKPFIAHL*FIWLW NGAIFLSIICPILFGLWY*REQRIQVGYCGHERPLKSLAISAFPQTERVDSVLQAYRP
tcNLS-GFP[6]	M**PKKKRKV**D**PKKKRKV**ASenlyfqgQFSKGEELFTGVVPILVELDGDVNGHKFSVSGEGEGDATYGKLTLKFICTTG KLPVPWPTLVTTLTYGVQCFSRYPDHMKRHDFFKSAMPEGYVQERTISFKDDGNYKTRAEVKFEGDTLVNRIELK GIDFKEDGNILGHKLEYNYNSHNVYITADKQKNGIKANFKIRHNIEDGSVQLADHYQQNTPIGDGPVLLPDNHYL STQSALSKDPNEKRDHMVLLEFVTAAGITHGMDELYKTShhhhhhhhhh
h2NLS-L-GFP[6]	MESSSSESKTVKDENVETN**KRKR**EQISTDNEAKMQIQEEKS**PKKKRKKRSSKANK**PPESPPQSKSDGKATSADLT SELETVEELHKKDSSDDKPRVKELPKPELPNLKVSNEFLAQLNKELASAATENYDHSIKSTDLSSIRIETEEPVGPSTG AETRNESEVMENINLEVQPEVKEAKEELTKISETFDNQDEEDTSRLSSKKNIRSPKGRTRHFIANKTKRGIDIenlyfq gQFSKGEELFTGVVPILVELDGDVNGHKFSVSGEGEGDATYGKLTLKFICTTGKLPVPWPTLVTTLTYGVQCFSRYP DHMKRHDFFKSAMPEGYVQERTISFKDDGNYKTRAEVKFEGDTLVNRIELKGIDFKEDGNILGHKLEYNYNSHNV YITADKQKNGIKANFKIRHNIEDGSVQLADHYQQNTPIGDGPVLLPDNHYLSTQSALSKDPNEKRDHMVLLEFVT AAGITHGMDELYKTShhhhhhhhhh

[1] Truncations of each parental sequence are indicated.
[2] Residues between > and < are deleted in truncations. NLS-regions are **bold**; transmembrane domains are *italic*.
[3] These reporters contain N-terminal GFP, which is not shown in the sequence.
[4] PrA-FKBP and FKBP are constructed N-terminally of GFP in h2NLS-L-TM.
[5] MBP is constructed C-terminally of GFP in MBP-h2NLS-L-TM, the second and the third MBP is inserted N-terminally of GFP.
[6] tcNLS-GFP is expressed in *E.coli* and h2NLS-L-GFP in *L.lactis*. The TEV-cleavage site (enlyfqg) and the His-tag (hhhhhhhhhh) are underlined.

Acknowledgements

We thank V. Krasnikov for help with confocal microscopy; and M. Graham for assistance with immunoelectron microscopy. We thank S. R. Wente, U. K. Laemmli, and M. P. Rout for reagents and strains. This work was supported by funding from the Netherlands Organization for Scientific Research (VIDI fellowship to L.M.V. and F.A.A.M.; Top-subsidy grant 700.56.302 to B.P.).

References

1. Alber, F., S.Dokudovskaya, L.M.Veenhoff, W.Zhang, J.Kipper, D.Devos, A.Suprapto, O.Karni-Schmidt, R.Williams, B.T.Chait, A.Sali, and M.P.Rout. 2007. The molecular architecture of the nuclear pore complex 1. *Nature* **450**:695-701.
2. Aslanidis, C. and P.J.de Jong. 1990. Ligation-independent cloning of PCR products (LIC-PCR). *Nucleic Acids Res.* **18**:6069-6074.
3. Brachmann, C.B., A.Davies, G.J.Cost, E.Caputo, J.Li, P.Hieter, and J.D.Boeke. 1998. Designer deletion strains derived from Saccharomyces cerevisiae S288C: a useful set of strains and plasmids for PCR-mediated gene disruption and other applications. *Yeast* **14**:115-132.
4. Chen, J., X.F.Zheng, E.J.Brown, and S.L.Schreiber. 1995. Identification of an 11-kDa FKBP12-rapamycin-binding domain within the 289-kDa FKBP12-rapamycin-associated protein and characterization of a critical serine residue. *Proc. Natl. Acad. Sci. U. S. A* **92**:4947-4951.
5. de Planque, M.R. and J.A.Killian. 2003. Protein-lipid interactions studied with designed transmembrane peptides: role of hydrophobic matching and interfacial anchoring. *Mol. Membr. Biol.* **20**:271-284.
6. Fanara, P., M.R.Hodel, A.H.Corbett, and A.E.Hodel. 2000. Quantitative analysis of nuclear localization signal (NLS)-importin alpha interaction through fluorescence depolarization. Evidence for auto-inhibitory regulation of NLS binding. *J. Biol. Chem.* **275**:21218-21223.
7. Geertsma, E.R. and B.Poolman. 2007. High-throughput cloning and expression in recalcitrant bacteria. *Nat. Methods* **4**:705-707.
8. Hahn, S., P.Maurer, S.Caesar, and G.Schlenstedt. 2008. Classical NLS proteins from Saccharomyces cerevisiae. *J. Mol. Biol.* **379**:678-694.
9. Haruki, H., J.Nishikawa, and U.K.Laemmli. 2008. The anchor-away technique: rapid, conditional establishment of yeast mutant phenotypes. *Mol. Cell* **31**:925-932.
10. Kadowaki, T., S.Chen, M.Hitomi, E.Jacobs, C.Kumagai, S.Liang, R.Schneiter, D.Singleton, J.Wisniewska, and A.M.Tartakoff. 1994. Isolation and characterization of Saccharomyces cerevisiae mRNA transport-defective (mtr) mutants. *J. Cell Biol.* **126**:649-659.
11. Kuipers, O.P., M.M.Beerthuyzen, R.J.Siezen, and W.M.de Vos. 1993. Characterization of the nisin gene cluster nisABTCIPR of Lactococcus lactis. Requirement of expression of the nisA and nisI genes for development of immunity. *Eur. J. Biochem.* **216**:281-291.
12. Kuipers, O.P., P.G.de Ruyter, M.Kleerebezem, and W.M.de Vos. 1997. Controlled overproduction of proteins by lactic acid bacteria. *Trends Biotechnol.* **15**:135-140.
13. Lanfermeijer, F.C., A.Picon, W.N.Konings, and B.Poolman. 1999. Kinetics and consequences of binding of nona- and dodecapeptides to the oligopeptide binding protein (OppA) of Lactococcus lactis. *Biochemistry* **38**:14440-14450.
14. Mulder, F.A.A., M.Lundqvist, and R.M.Scheek. 2010. Nuclear Magnetic Resonance Spectroscopy Applied to (Intrinsically) Disordered Proteins. John Wiley & Sons, Inc., Hoboken, NJ, USA..
15. Niedenthal, R.K., L.Riles, M.Johnston, and J.H.Hegemann. 1996. Green fluorescent protein as a marker for gene expression and subcellular localization in budding yeast. *Yeast* **12**:773-786.
16. Prilusky, J., C.E.Felder, T.Zeev-Ben-Mordehai, E.H.Rydberg, O.Man, J.S.Beckmann, I.Silman, and J.L.Sussman. 2005. FoldIndex: a simple tool to predict whether a given protein sequence is intrinsically unfolded. *Bioinformatics.* **21**:3435-3438.
17. Robson, A. and I.Collinson. 2006. The structure of the Sec complex and the problem of protein translocation. *EMBO Rep.* **7**:1099-1103.
18. Strawn, L.A., T.Shen, N.Shulga, D.S.Goldfarb, and S.R.Wente. 2004. Minimal nuclear pore complexes define FG repeat domains essential for transport. *Nat. Cell Biol.* **6**:197-206.
19. Tcherkasskaya, O., E.A.Davidson, and V.N.Uversky. 2003. Biophysical constraints for protein structure prediction. *J. Proteome. Res.* **2**:37-42.
20. Teasdale, R.D. and M.R.Jackson. 1996. Signal-mediated sorting of membrane proteins between the endoplasmic reticulum and the golgi apparatus. *Annu. Rev. Cell Dev. Biol.* **12**:27-54.
21. van den Bogaart, G., N.Hermans, V.Krasnikov, A.H.de Vries, and B.Poolman. 2007. On the decrease in lateral mobility of phospholipids by sugars. *Biophys. J.* **92**:1598-1605.
22. van den Bogaart, G., A.C.Meinema, V.Krasnikov, L.M.Veenhoff, and B.Poolman. 2009. Nuclear transport factor directs localization of protein synthesis during mitosis. *Nat. Cell Biol.* **11**:350-356.
23. Wilkins, D.K., S.B.Grimshaw, V.Receveur, C.M.Dobson, J.A.Jones, and L.J.Smith. 1999. Hydrodynamic radii of native and denatured proteins measured by pulse field gradient NMR techniques. *Biochemistry* **38**:16424-16431.
24. Winzeler, E.A., D.D.Shoemaker, A.Astromoff, H.Liang, K.Anderson, B.Andre, R.Bangham, R.Benito, J.D.Boeke, H.Bussey, A.M.Chu, C.Connelly, K.Davis, F.Dietrich, S.W.Dow, B.M.El, F.Foury, S.H.Friend, E.Gentalen, G.Giaever, J.H.Hegemann, T.Jones, M.Laub, H.Liao, N.Liebundguth, D.J.Lockhart, A.Lucau-Danila, M.Lussier, N.M'Rabet, P.Menard, M.Mittmann, C.Pai, C.Rebischung, J.L.Revuelta, L.Riles, C.J.Roberts, P.Ross-MacDonald, B.Scherens, M.Snyder, S.Sookhai-Mahadeo, R.K.Storms, S.Veronneau, M.Voet, G.Volckaert, T.R.Ward, R.Wysocki, G.S.Yen, K.Yu, K.Zimmermann, P.Philippsen, M.Johnston, and R.W.Davis. 1999. Functional characterization of the S. cerevisiae genome by gene deletion and parallel analysis. *Science* **285**:901-906.

Chapter 6

Quantitative analysis of membrane protein transport across the nuclear pore complex

Anne C. Meinema[1], Bert Poolman[1]and Liesbeth M. Veenhoff[1,2]

1 Department of Biochemistry, Groningen Biomolecular Sciences and Biotechnology Institute, Netherlands Proteomics Centre, Zernike Institute for Advanced Materials, University of Groningen, Nijenborgh 4, 9747 AG, Groningen, The Netherlands.

2 Department of Neuroscience, European Research Institute on the Biology of Ageing, University Medical Centre Groningen, University of Groningen, The Netherlands

This chapter is submitted for publication.

Abstract

Nuclear transport of the *Saccharomyces cerevisiae* membrane proteins Src1/Heh1 and Heh2 across the NPC, is facilitated by a long intrinsically disordered linker between the nuclear localization signal (NLS) and the transmembrane domain. We proposed that the linker allows interaction of the NLS-associated karyopherins with the FG-Nups in the central channel of the NPC. Here, we present a quantitative analysis of Kap60/95-mediated import and passive efflux of membrane reporter proteins derived from Heh2, including data on the mobility of the reporter proteins in different membrane compartments. Although slower, even membrane proteins with extralumenal domains up to 174 kDa terminal to the linker and NLS, passively leak out of the nucleus via the NPC. We propose that also during efflux, the unfolded linker facilitates the passage of extralumenal domains through the central channel of the NPC.

Introduction

Transport of cargo between the cytoplasm and the nucleus is mediated by the nuclear pore complex (NPC). For import, nuclear import factors, belonging to the family of karyopherins (Kaps), bind specifically a nuclear localization signal (NLS) on cargo molecules (reviewed in (Pemberton and Paschal, 2005)). The basic classical NLSs (cNLS), as a single partite or a bipartite sequence (Dingwall and Laskey, 1991), are recognized by the adapter proteins Kap60 (Importin-α or Kap-α in higher eukaryotes), and for nuclear transport it additionally requires Kap95 (importin-β1 or Kap-β1 in higher eukaryotes). Kap95 interacts with the phenylalanine-glycine (FG)-repeats of the FG-nucleoporins and carries the Kap60-Kap95-cargo-complex across the NPC. Once the complex reaches the nuclear side of the NPC, binding to nuclear localized RanGTP leads to dissociation of the cargo, whereby the Kaps are recycled back to the cytoplasm (reviewed in: (Wente and Rout, 2010;Kahms *et al.*, 2011)). The kinetics of facilitated import and passive leak across the NPC (nuclear efflux), together with possible retention at either the nuclear or cytoplasmic compartment determine the localization of proteins.

Integral membrane proteins with a function at the inner nuclear membrane (INM) of the nuclear envelope (NE) are also transported via the NPC. The outer nuclear membrane (ONM) is continuous with the INM via the sharply curved pore membrane (POM), at sites where the NPCs are anchored (Powell and Burke, 1990). Different mechanisms have been proposed for translocation of integral membrane proteins via the POM across the NPC (reviewed by (Antonin *et al.*, 2011;Burns and Wente, 2012;Lusk *et al.*, 2007;Zuleger *et al.*, 2012)).

Early publications supported a diffusion/retention model (Worman and Courvalin, 2000), in which membrane proteins traverse the NPC by diffusion (Soullam and Worman, 1995;Powell and Burke, 1990;Soullam and Worman, 1993) and accumulate at the INM by binding to nuclear structures (Ellenberg *et al.*, 1997;Graumann *et al.*, 2007;Ostlund *et al.*, 1999;Wu *et al.*, 2002). This

diffusion across the NPC was thought to occur through the narrow lateral or peripheral channels along the POM (Hinshaw *et al.*, 1992;Zuleger *et al.*, 2008;Soullam and Worman, 1995). It has been reported that these ~10 nm wide channels allows passage of molecules of up to ~60 kDa (Soullam and Worman, 1995;Wu *et al.*, 2002). While for most membrane proteins studied so far, nuclear retention is an important determinant, specific domains or signals that contribute to targeting to or across the NPCs have been reported in recent years.

Important was the discovery of actual NLS sequences in the yeast Src1/Heh1 and Heh2 proteins (King *et al.*, 2006). These bipartite NLS sequences are bound by Kap60 and import of the proteins to the INM is dependent on Kap95 and the gradient of RanGTP across the NE, just as it is for transport of soluble cargo. Similar NLS sequences that attract Kapβ via Kapα have been identified in other membrane proteins, including the human SUN2 (Turgay *et al.*, 2010), *Caenorhabditis elegans* Unc-84 (Tapley *et al.*, 2011), and the human Pom121 (Funakoshi *et al.*, 2011). The NLSs are not the only sequences that contribute to the targeting of these proteins. Unc-84, e.g. has besides two cNLSs, an INM sorting motif, consisting of three lysines at the cytoplasmic side of a transmembrane helix, and a conserved region called the SUN-nuclear envelop localization signal. SUN2 targeting relies on a functional cNLS, a Golgi retrieval signal and a luminal SUN domain to contribute to targeting to the INM (Turgay *et al.*, 2010).

We have recently shown in *Saccharomyces cerevisiae* that Kap-mediated nuclear transport suffices to accumulate membrane reporter proteins in the INM, i.e., without a need for nuclear retention (Meinema *et al.*, 2011). We designed reporter proteins, having the minimal features required for INM-targeting. From the N-terminus, the reporter, named GFP-h2NLS-L-TM, consisted of: 1) GFP, 2) the high-affinity NLS of Heh2 (h2NLS) to ensure strong interaction with Kap60 (and Kap95), 3) an intrinsically-disordered linker between the NLS and the TM with a minimal length of 120 residues, and 4) a transmembrane α-helical segment (TM) that anchors the reporter to the membrane. Different from native Heh2, the accumulation of the reporters at the INM is solely based on the rates of nuclear import and efflux across the NPC.

Also reporters with synthetic linkers, a synthetic TM segment or the TM domain of Sec61 were efficiently targeted to the INM (Meinema *et al.*, 2011). These experiments showed that the primary sequences of the transmembrane segments, flanking regions and the linker are not important for targeting to the INM. In fact, these experiments argue against Heh2 having a so-called INM sorting motif, consisting of a cluster of positively charged residues within 4 – 8 residues of the cytoplasmic end of the transmembrane helix (Braunagel *et al.*, 2004;Saksena *et al.*, 2004;Saksena *et al.*, 2006) as was previously proposed (Liu *et al.*, 2010). Our Sec61-derived and synthetic reporters contain positively-charged residues in cytosolic loops, flanking transmembrane helices, to ensure correct insertion in the ER (Harley and Tipper, 1996;Heijne, 1986;Heijne, 1986). It is however unlikely that these positively charged residues would act as alternative INM sorting motifs, particularly as genuine Sec61 is an ER resident protein. We concluded that nuclear import of these membrane proteins requires only an intrinsically disordered linker domain of at least 120 residues and the h2NLS and their movement in the ER is diffusion mediated.

Our previous study revealed details on Kap60/95-facilitated import of GFP-h2NLS-L-TM reporters through the NPC. We proposed that the linker is needed, to position the Kap-bound NLS in the vicinity of the FG-Nups in the central channel, while the transmembrane segment(s) reside(s) in the pore membrane. A corollary of this model is that radial conduits in the scaffold of the NPC must exist to provide space for the linker. However, little was known of how these proteins, particularly those with large soluble domains, leave the INM compartment. Here, we show that also these membrane reporters can exit the INM and travel back to the ONM and ER. We present quantitative information on the kinetics of membrane protein import and passive efflux across the NPC and the lateral diffusion of the reporters in the different membrane compartments. We discuss our findings in the light of the architecture of the NPC.

Results

Terminology

We use the terms nuclear import (and export) for metabolic energy and karyopherin-dependent transport across the NPC. For equilibration, independent of metabolic energy and karyopherins, we use the terms passive nuclear influx and efflux. Mobility of proteins in the membrane is referred to as lateral diffusion and assumed to be 2D Brownian diffusion.

Transport factor binds h2NLS-reporter in ER

The movement of membrane proteins to the INM involves both lateral diffusion to the NPC through the network of ER-ONM membranes and translocation across the NPC. The translocation of membrane proteins across the NPC to the INM is Kap-mediated import or Kap-independent passive influx. The movement of INM-localized membrane proteins back to the ER involves Kap-independent passive efflux across the NPC and lateral diffusion through the ER-ONM network. To determine the kinetics of nuclear import and efflux of membrane proteins in *Saccharomyces cerevisiae*, we used the Heh2-based membrane reporter GFP-h2NLS-L-TM (referred to as h2NLS-L-TM in (Meinema *et al.*, 2011)). First, we show that Kap95 binds the NLS of the reporter protein when present in the ER by imaging the localization of chromosomally expressed Kap95-GFP. Normally, Kap95-GFP is homogeneously distributed in the cytoplasm with some accumulation at the NE (Fig. 6.1A)(Seedorf *et al.*, 1999). A co-expressed mCherry (mCh)-tagged reporter, mCh-h2NLS-L-TM, is efficiently imported into the INM (Fig. 6.1B). In most cells is thus just a small fraction of the reporter present at the peripheral ER. To reduce INM-accumulation of the reporter, we co-expressed mCh-h2NLS-L(37)-TM with Kap95-GFP. This reporter with a shortened linker of 37 residues does not accumulate in the INM and remains at the peripheral ER (Meinema *et al.*, 2011). We found indeed that in 80% of the cells where mCh-reporter localized at the peripheral ER, Kap95-GFP co-localized with the reporter ($n = 78$) (Fig. 6.1C). As a further control, we show that mCh-L-TM, a reporter without the h2NLS, did not show co-localization with Kap95-GFP in any of the analyzed cells ($n > 150$) (Fig. 6.1D). We

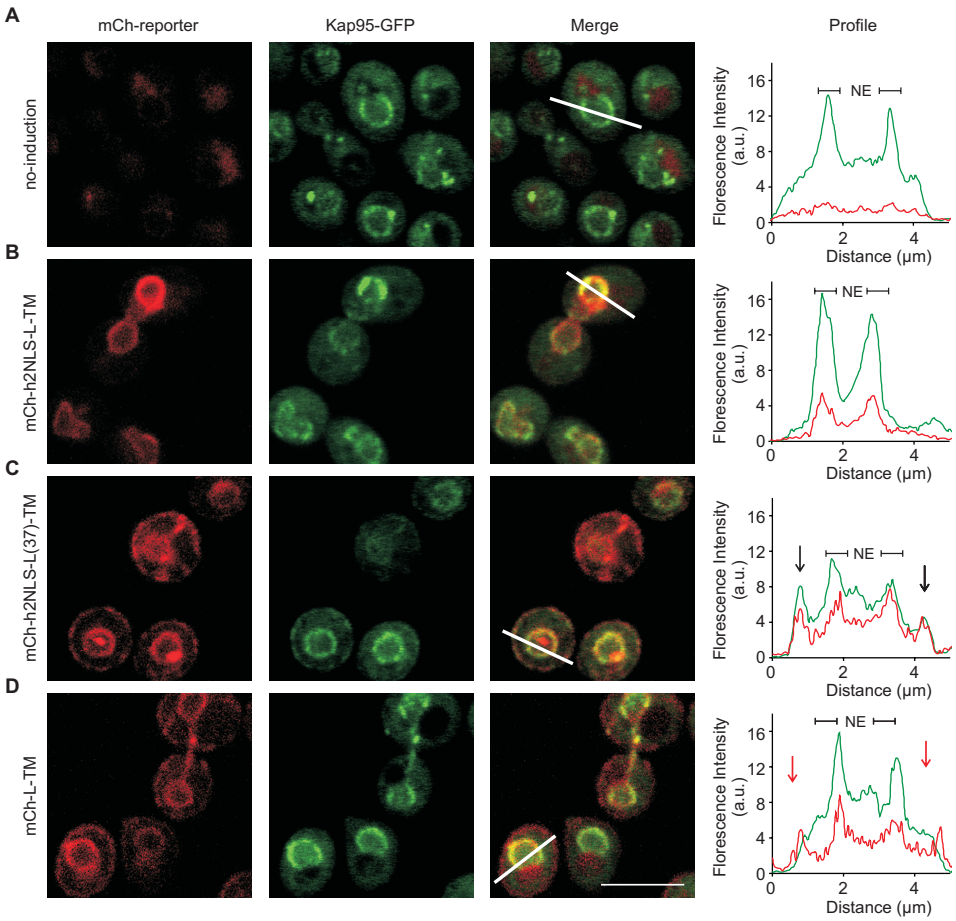

Figure 6.1: **Kap95-GFP co-localizes with GFP-h2NLS-containing membrane reporter at the ER.** Confocal images of cells expressing Kap95-GFP **(A)** and cells in which Kap95-GFP is co-expressed with mCherry-tagged GFP-h2NLS-L-TM **(B)** GFP-h2NLS-L(37)-TM having a linker of 37 residues **(C)**, or GFP-L-TM **(D)**. In (A) the expression of mCh-h2NLS-L-TM was not induced. The profile of the fluorescence intensity along a 5 pixel wide line through one of the cells is plotted on the right. The NE is indicated and the arrows point when there is co-localization at the ER (black) or when only the mCh-reporter is visible at the ER (red). Scale bar is 5 μm.

conclude that the high-affinity NLS of the membrane proteins attract both Kap60 and Kap95 while diffusing in the ER, that is, prior to gating the NPC. The data is consistent with the strong binding of Kap60 to h2NLS measured *in vitro*, K_D < 1 nM (Meinema *et al.*, 2011) and the cellular concentrations of Kap60 and Kap95 in the micromolar range (Ghaemmaghami *et al.*, 2003;Hahn and Schlenstedt, 2011).

The *in vitro* affinity of the h2NLS for Kap60 lacking the importin-β binding domain is very high, even if we compare it with other classical single partite NLSs or the bipartite NLSs (Hahn *et al.*, 2008;Lange *et al.*, 2010). We co-expressed the soluble cargo tcNLS-mCh, i.e. mCherry with two copies of the classical SV40 NLS (Dingwall and Laskey, 1991), with GFP-h2NLS-L-TM to measure the effect of competition for the pool of Kap60 and Kap95 *in vivo*. As a control, we

expressed rgNLS-mCh, i.e. mCherry with the NLS of Nab2,(Lee and Aitchison, 1999;Timney *et al.*, 2006); rgNLS-mCh makes use of Kap104 rather than Kap60/95 for nuclear import. The INM accumulation of GFP-h2NLS-L-TM did not change upon co-expression with tcNLS-mCh or rgNLS-mCh (Fig. 6.2A), but all nuclear accumulation of tcNLS-mCh was lost when GFP-h2NLS-L-TM was co-expressed (Fig. 6.2B). As anticipated nuclear accumulation of rgNLS-mCh was not affected by GFP-h2NLS-L-TM (Fig. 6.2C). The expression level of GFP-h2NLS-L-TM (~13,000 copies/cell) was similar to tcNLS-mCh (~14,000 copies/cell) or rgNLS-mCh (~15,000 copies/cell) (Fig. 6.3). Thus, in the cell h2NLS-membrane cargo competes effectively with tcNLS-soluble cargo for binding to Kap60.

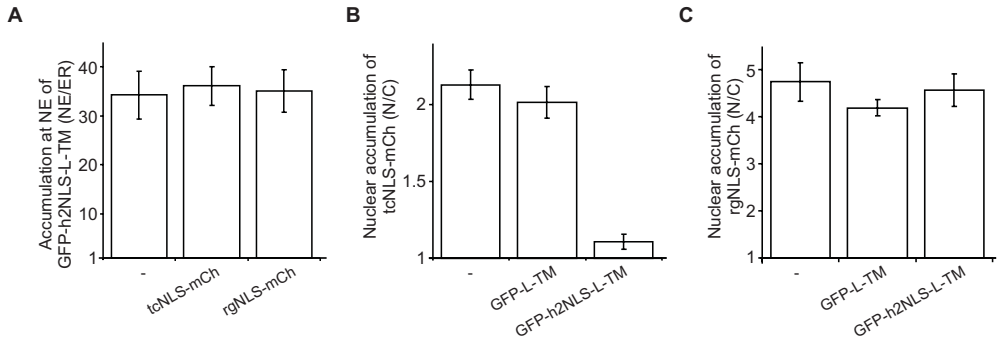

Figure 6.2: Nuclear transport of GFP-h2NLS-L-TM is not reduced upon co-expression of competitive cargo, tcNLS-mCherry. A) The level of accumulation of GFP-h2NLS-L-TM at the INM, without co-expression (-), with co-expression of tcNLS-mCherry (tcNLS-mCh), or rgNLS-mCh ($n \geq 20$). **B)** The level of nuclear accumulation of tcNLS-mCh without co-expression (-), with co-expression of GFP-L-TM and with co-expression of GFP-h2NLS-L-TM ($n \geq 44$). **C)** The level of nuclear accumulation of rgNLS-mCh without co-expression (-), with co-expression of GFP-L-TM and with co-expression of GFP-h2NLS-L-TM ($n \geq 52$). SEM is indicated.

Lateral diffusion of membrane proteins in the ER, INM and ONM

Next, we analyzed the lateral mobility of the membrane reporters in the ER, the INM and the ONM, using fluorescent recovery after photobleaching (FRAP) (Fig. 6.4A). We determined the diffusion coefficient (*D*) of GFP-h2NLS-GFP-L-TM, GFP-L-TM and MBP-GFP-h2NLS-L-TM. We compared the mobility of these reporters with that of ER-resident Sec translocon protein Sec61 and the full length INM-resident Heh2, both tagged with GFP. The reporter GFP-MBP-h2NLS-L-TM has an N-terminal maltose-binding protein (MBP) to increase the mass of the extralumenal domain by 40 kDa. In order to have a sufficient concentration of reporters in the ER, we made use of the KAP95-AA strain (Meinema *et al.*, 2011). In this strain and when rapamycin (RAP) is present, an FRB-tagged version of Kap95 is tethered to the plasma membrane by high affinity binding to Pma1-FKBP (Haruki *et al.*, 2008). Addition of rapamycin rapidly depletes the cells of functional Kap95-FRB, and, as a consequence, the reporters equilibrate over the INM, ONM and ER (Meinema *et al.*, 2011). FRAP experiments were performed at the different locations along the NE-ER network and the recovery traces were fitted to an empirical equation describing the lateral diffusion of membrane proteins in one dimension through membranes (Ellenberg *et al.*, 1997)(Fig. 6.4B).

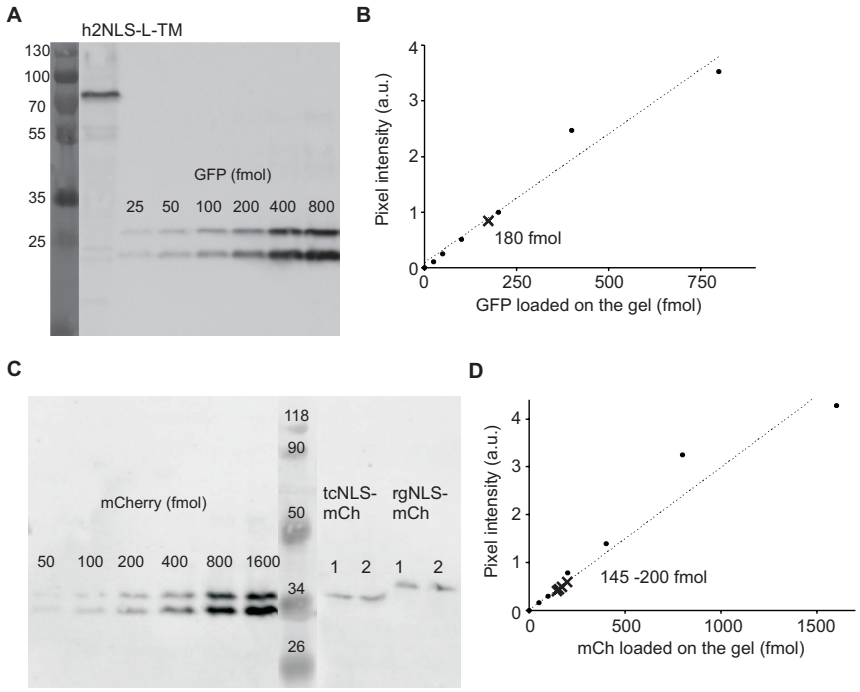

Figure 6.3: The expression levels of the membrane reporter GFP-h2NLS-L-TM. A) The copy number of GFP-h2NLS-L-TM was obtained from quantitative Western blots using an antibody against GFP or mCherry. The culture was grown to a density of $1.7 \cdot 10^7$ cells/ml and the expression of GFP-h2NLS-L-TM was induced for 2 hours with 0.1% (w/v) D-galactose. An equivalent of $8.3 \cdot 10^6$ cells was loaded on a SDS-PAA gel together with a dilution series from 25 to 800 fmol of purified GFP, and the proteins. **B)** We used chemiluminescence to detect the proteins and densitometry to quantify the protein levels. We found 180 fmol GFP-h2NLS-L-TM in $8.3 \cdot 10^6$ cells, corresponding to a copy number of 13,000 copies of GFP-h2NLS-L-TM per cell. **C)** Similar as (A) but now for tcNLS-mCh and rgNLS-mCh co-expressed either with GFP-h2NLS-L-TM (1) or GFP-L-TM (2). The culture was grown to a density of $1.4 \cdot 10^7$ cells/ml. An equivalent of $7.2 \cdot 10^6$ cells was loaded on a SDS-PAA gel, together with a dilution series from 50 to 1,600 fmol of purified mCh. **D)** Similar as (B) but now for tcNLS-mCh and rgNLS-mCh co-expressed either with GFP-h2NLS-L-TM or GFP-L-TM. We found 145 fmol tcNLS-mCh when co-expressed with GFP-h2NLS-L-TM and 169 fmol tcNLS-mCh when co-expressed with GFP-L-TM, corresponding to copy numbers of 12,000 and 15,000 per cell, respectively. We found 150 fmol rgNLS-mCh when co-expressed with GFP-h2NLS-L-TM and 198 fmol rgNLS-mCh when co-expressed with GFP-L-TM, corresponding to copy numbers of 13,000 and 17,000 per cell, respectively.

The diffusion coefficient of all reporters and Sec61-GFP present in the ER was similar and about 0.16 $\mu m^2/s$; the mobile fraction was in all cases >80% (Fig. 6.4C, Table 6.1). The mobility of the membrane proteins was thus not sensitive to the mass of the soluble domains, that, in case of GFP-Heh2, GFP-h2NLS-L-TM and MBP-GFP-h2NLS-L-TM, will also have included bound-Kap60.

We measured the lateral diffusion in the INM by photobleaching the fluorescence of GFP-Heh2, GFP-h2NLS-L-TM and MBP-GFP-h2NLS-L-TM at the NE. These reporters are highly accumulated in the INM (NE/ER-ratio = 32.8) and the recovery kinetics will thus be dominated by the diffusion of the INM-localized molecules. Fluorescence recovery due to transport across

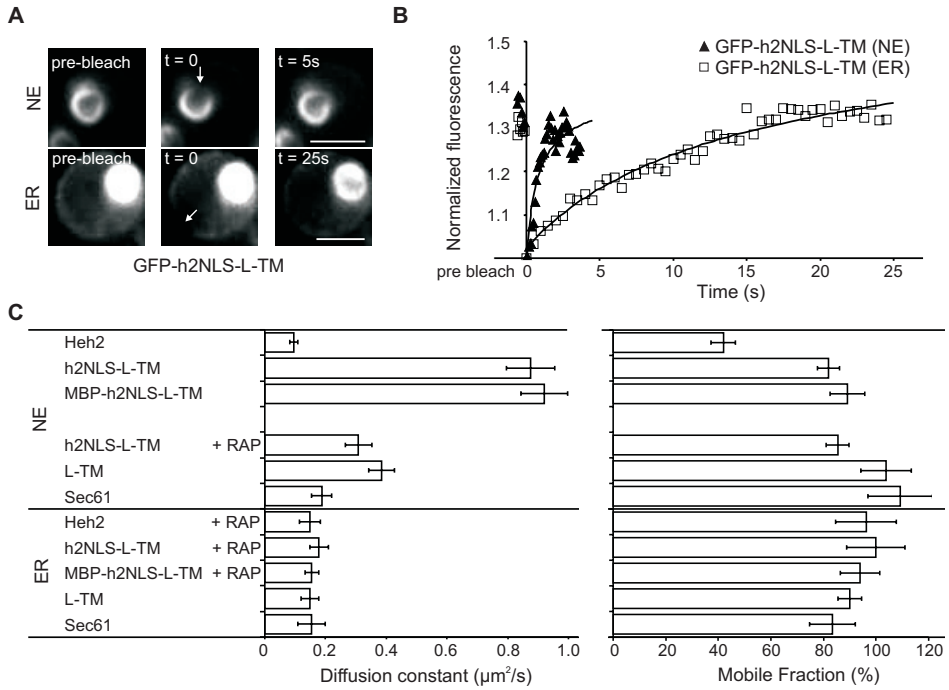

Figure 6.4: Mobility of reporters at the NE and ER. A) Confocal images showing fluorescence recovery after photobleaching of reporter localized at the NE (top) and at the ER (bottom). **B)** An example of a time-trace of fluorescence intensity in the bleached spot, for GFP-h2NLS-L-TM in the NE and ER. **C)** Representation of diffusion coefficients of reporters in the INM (accumulated at the NE), in the ONM (not accumulated at the NE) and in the ER. All reporters are tagged with GFP, scale bar is 2 μm, SEM is indicated.

Table 6.1: Diffusion coefficients of membrane proteins

	Reporter[1]	*D* (μm²/s)[2]	Mobile fraction (%)[2]	*n*
	Heh2	0.09 ± 0.01	42 ± 5	20
	h2NLS-L-TM	0.87 ± 0.08	82 ± 4	58
At INM	MBP-h2NLS-L-TM	0.92 ± 0.08	89 ± 7	29
	L-TM	0.31 ± 0.04	85 ± 4	38
	h2NLS-L-TM + RAP	0.38 ± 0.04	104 ± 10	15
At ONM	Sec61	0.19 ± 0.03	109 ± 12	6
	Heh2 + RAP	0.15 ± 0.03	96 ± 11	26
	h2NLS-L-TM + RAP	0.18 ± 0.03	100 ± 11	20
	MBP-h2NLS-L-TM + RAP	0.15 ± 0.02	94 ± 8	23
	L-TM	0.15 ± 0.03	90 ± 4	28
At ER	Sec61	0.15 ± 0.05	84 ± 9	7

[1] All reporters are fused to GFP
[2] SEM is indicated.

the NPC has little effect on the kinetics of recovery, as it is much slower. Unexpectedly, we found a 5-fold higher diffusion coefficient for GFP-h2NLS-L-TM (D = 0.87 ± 0.08 μm²/s) and MBP-GFP-h2NLS-L-TM (D = 0.92 ± 0.08 μm²/s) in the INM than when these reporters were present in the ER. In stark contrast with these high mobility values is the slow diffusion of INM resident Heh2 (D = 0.09 ± 0.01 μm²/s). The mobility of GFP-Heh2 is an order magnitude lower than that of GFP-h2NLS-L-TM and MBP-GFP-h2NLS-L-TM and the mobile fraction was ~40%, while the mobility and mobile fraction of GFP-Heh2 in the ER was similar to that of the other reporters. These findings are consistent with the observation that the majority of GFP-Heh2 is trapped at the INM (King *et al.*, 2006;Yewdell *et al.*, 2011), while the membrane reporters are not retained by nuclear structures (Meinema *et al.*, 2011).

We measured the lateral mobility of proteins in the ONM by photobleaching the NE in cells expressing GFP-L-TM or Sec61-GFP. These proteins are not accumulated in the INM. In addition, we used GFP-h2NLS-L-TM in the rapamycin-treated KAP95-AA strain to prevent INM accumulation of the reporter and thus have a good signal at the ONM and ER. In the absence of functional Kap95, GFP-h2NLS-L-TM is thus distributed throughout the entire network of the INM, ONM and ER (Meinema *et al.*, 2011), like GFP-L-TM. We found that the diffusion coefficient of GFP-Sec61 at the ONM is similar to that of the reporters at the ER (D = 0.19 ± 0.03 μm²/s). The diffusion coefficient of GFP-L-TM (D = 0 .31 ± 0.04 μm²/s) and GFP-h2NLS-L-TM (+RAP; D = 0.38 ± 0.04 μm²/s) are higher than that of Sec61 (D = 0.19 ± 0.03 μm²/s), which might relate to some contribution from the mobility of INM-localized reporters. We conclude that lateral diffusion in the ONM and ER is slower than in the INM.

The diffusion coefficient of soluble GFP in the cytoplasm of yeast was established at 13.6 ± 1.3 μm²/s (n = 20). This is consistent with values measured in other cell-types (Nenninger *et al.*, 2010;Swaminathan *et al.*, 1997), but almost two orders of magnitude faster than the mobility of proteins in the ER-ONM network.

Overall efflux kinetics

To measure the kinetics of membrane protein transport we tested the three assays that have been described for measurement of transport of soluble cargo in yeast. The first is a steady state assay using selective FRAP (sFRAP, Chapter 2). Here, one selectively photobleaches the nucleus and measures the recovery of fluorescence as a consequence of transport (import, influx and efflux) through the NPC (van den Bogaart *et al.*, 2009;Goodwin and Kenworthy, 2005). The second is the Kap95-depletion method. Here, the cell is depleted of functional Kap95 upon addition of rapamycin and one measures the net efflux of cargo after the import is abolished (Haruki *et al.*, 2008). The third is a metabolic poison assay were cells are treated with sodium azide plus 2-deoxyglucose to deplete the cells of metabolic energy and disrupt the RanGTP-gradient over the NPC (Schwoebel *et al.*, 2002;Shulga *et al.*, 1996). Immediately after poisoning net efflux can be measured and when all accumulation is lost, the metabolic poisons can be washed away, and net import can be measured. To validate the three methods, we first measured import and passive efflux of soluble GFP-tcNLS-GFP using the Kap-depletion or the metabolic poison assay methods (Fig. 6.5A) and compared it with results from a sFRAP assay (Fig. 6.5B) (van den Bogaart *et al.*,

2009). Using the Kap95-depletion assay or the metabolic poison assay we directly measured the overall efflux rate constant (k_{out}) and calculated the overall import rate constant (k_{in}) from the k_{out} and the steady state accumulation of GFP-tcNLS-GFP (Fig. 6.5A). Indeed, at steady state, the N/C ratio is equal to k_{in}/k_{out}. In the sFRAP assay, the recovery of fluorescence in the nucleus and cytosol are fitted to yield k_{in} and k_{out} (van den Bogaart *et al.*, 2009). With all three methods, we obtained similar rate constants (k_{out} of $1.2 – 2.0 \cdot 10^{-2}$ s^{-1} and k_{in} of 0.10 – 0.16 s^{-1}, Fig. 6.5C) and concluded that they are valid approaches to study NPC transport kinetics of soluble proteins. The Kap95-depletion assay offers advantages over sFRAP when nuclear accumulation is high and the pool of the cytosol-localized proteins is small which can prohibit sFRAP measurements. The Kap95-depletion method offers advantages over the metabolic poison assay as it perturbs the cell more specifically (it does not interfere with energy metabolism and ion homeostasis), but unfortunately it is not reversible.

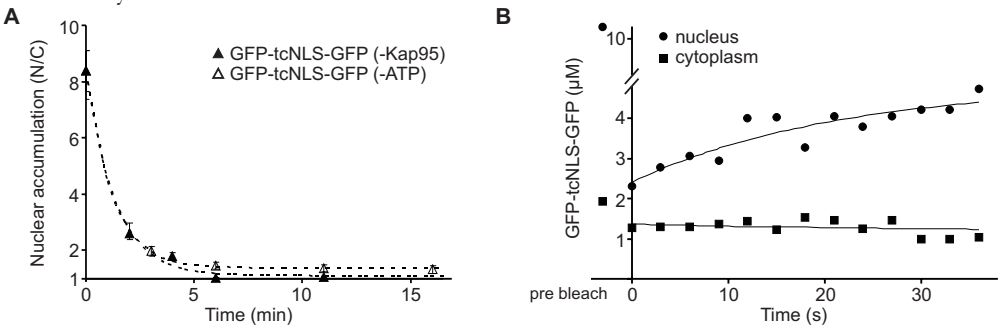

C

Nuclear transport of GFP-tcNLS-GFP

Method	k_{out} ($\cdot 10^{-2}$ s^{-1})	k_{in} (s^{-1})	*n*
sFRAP	2.0 ± 0.35	0.16 ± 0.029	22
Efflux (-ATP)	1.3 ± 0.15	0.11 ± 0.015	>27
Efflux (-Kap95)	1.2 ± 0.1	0.10 ± 0.011	>22

Figure 6.5: Comparison of Kap95-depletion and metabolic poison transport assays and selective-FRAP. **A)** Nuclear efflux of soluble GFP-tcNLS-GFP in the Kap95-depletion assay (▲, for each time point, $n \geq 27$) and poison assay (Δ, for each time point, $n \geq 22$) fitted with a single exponent (dashed line). **B)** Recovery traces of fluorescence from GFP-tcNLS-GFP in the nucleus (●) and cytoplasm (■) after selective photobleaching in the nucleus. Fitted as described in (van den Bogaart *et al.*, 2009). **C)** Nuclear import and efflux rate constants of GFP-tcNLS-GFP, measured in different assays as indicated. *n* is the number of cells measured at each time point during nuclear efflux. In the selective-FRAP (sFRAP) assay, *n* is the number of individual selective FRAP measurements.

We first aimed to measure the nuclear import of membrane proteins using sFRAP by selectively photobleaching the NE and determining the recovery of fluorescence as a quantitative measure of transport. However, due to the high accumulation of GFP-h2NLS-L-TM in the NE, a major fraction of the pool of reporter proteins was photobleached. This made the analysis very difficult. Instead, we measured the nuclear efflux rate constant of the membrane reporter GFP-h2NLS-L-TM and calculated the import rate constant, based on the efflux rate constant and the nuclear accumulation. To measure the nuclear efflux of GFP-h2NLS-L-TM in the Kap95-depletion assay, the membrane reporter was first expressed in the Kap95-AA strain and accumulated at the INM. Upon addition of rapamycin, Kap60/95-mediated nuclear import stops, resulting in a temporary net flux of GFP-h2NLS-L-TM from the INM to the ONM and ER. We plotted the

NE/ER-ratio of the reporter over time and fitted the data to a single exponential. We found an overall efflux rate constant (k_{out}) of $0.83 \cdot 10^{-3} \pm 0.16 \cdot 10^{-3}$ s^{-1} (Fig. 6.6A). Our results demonstrate that the efflux of GFP-h2NLS-L-TM is much slower in ATP-depleted cells than in Kap95-depleted cells: k_{out} of $0.15 \cdot 10^{-3} \pm 0.02 \cdot 10^{-3}$ s^{-1} (Fig. 6.6A). The Kap95-depletion and poison assays did not show these marked differences for transport of the soluble cargo GFP-tcNLS-GFP (Fig. 6.5A). We determined whether the ATP-dependence is specific to membrane protein efflux or may be related to just the presence of the long, unfolded linker.

We thus compared the efflux of GFP-tcNLS-GFP with a soluble reporter having the 176 amino acid-long unfolded linker of Heh2, GFP-h2NLS-L, and a reporter having a shorter linker of only 33 amino acids, GFP-h2NLS-L(33). These reporters accumulated in the nucleus more than 200-fold, due to the high affinity h2NLS (Fig. 6.2 and (Meinema *et al.*, 2011)). A fast and mono-exponential efflux was observed for all three reporters after the cells were depleted of Kap95 (Fig. 6.6B, C). The efflux of the larger GFP-h2NLS-L was somewhat slower than GFP-h2NLS-L(33), as expected. However, a marked difference was observed when the cells were depleted of ATP. Initially, the efflux of GFP-h2NLS-L was fast but it leveled off after a few minutes (Fig. 6.6B). The data could not be fitted with a mono-exponential decay fit ($R^2 < 0.6$) but was fitted by a two-term exponential decay model, which yielded two first-order rate constants for efflux. The efflux of GFP-h2NLS-L(33) in ATP-depleted cells could be fitted by a mono-exponential decay. The efflux rate constant of the initial fast phase for GFP-h2NLS-L did not differ significantly from the value in the Kap95-depletion assay (Fig. 6.6C). We conclude that the linkers do not affect the nuclear efflux of soluble reporters when the cells contain normal ATP levels, but do so under energy-depleted conditions.

What could be the molecular basis for these observations? Upon ATP depletion, the Kap-cargo complexes do not dissociate from the nuclear face of the NPC in the absence of a RanGTP-gradient (Görlich *et al.*, 1996;Ribbeck *et al.*, 1999). Kap-cargo stuck in the NPC would obstruct further nuclear efflux (Kutay *et al.*, 1997). Indeed, when we image the localization of Kap60-GFP and Kap95-GFP, we see that they concentrate at the NPCs upon addition of sodium-azide plus 2-deoxygluces. In wild-type cells, Kap60-GFP and Kap95-GFP show the punctate fluorescence stain, typical for NPC-localized proteins (Fig. 6.6D). After ATP depletion, the ratio of fluorescence at the NPC over the intensity in the cytoplasm (NPC/C) increased 7- and 5-fold for Kap60 and Kap95, respectively (Fig. 6.6E). We thus confirm previous data (Ribbeck *et al.*, 1999) and show that the Kap-cargo complexes accumulate at the NPC in ATP-depleted cells. The NPC-accumulated Kap-cargo might particularly hinder the nuclear efflux of molecules with large Stokes radii, such as the linker-containing reporters. The high-affinity h2NLS on the soluble reporters may be bound by NPC-resident Kaps, which provides an extra means of retention in the NPC during nuclear efflux. In conclusion, as we see similar effects of ATP depletion for the efflux of soluble and transmembrane reporters, it is most likely that the slow efflux of GFP-h2NLS-L-TM in the absence of ATP is simply due to the presence of the h2NLS-L domain with large Stokes radius and not specific for membrane transport. The ATP-depletion assay is thus not suitable to determine efflux rate constants of h2NLS-L-TM.

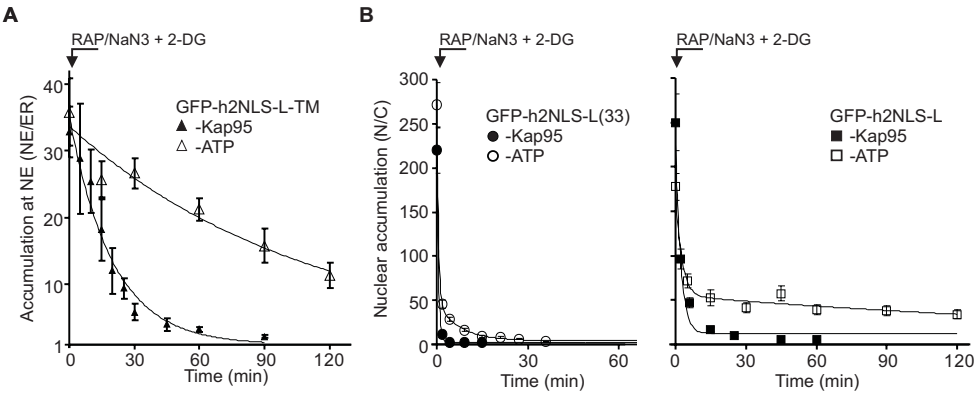

C

		-Kap95		-ATP			
	Size (kD)	k_{out} (s^{-1})	R^2	k_{out} (s^{-1})	$k_{out}1$ (s^{-1})	$k_{out}2$ (s^{-1})	R^2
GFP-h2NLS-L(33)	37	$18 \cdot 10^{-3}$	0.999	$11 \cdot 10^{-3}$	-	-	0.998
GFP-h2NLS-L	53	$7.7 \cdot 10^{-3}$	0.987	-	$6.5 \cdot 10^{-3}$	$0.067 \cdot 10^{-3}$	0.987

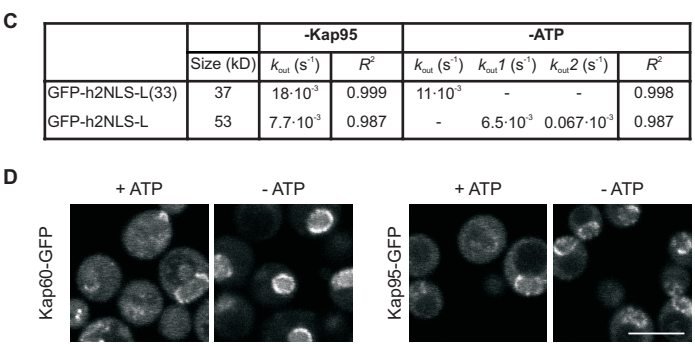

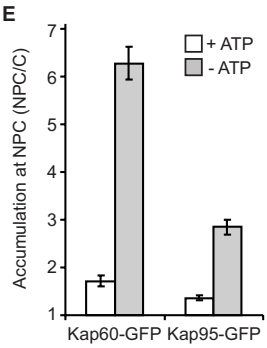

Figure 6.6: Measurements of nuclear efflux of membrane and soluble reporter proteins by depleting the cells of Kap95 or ATP. A) After the expression of GFP-h2NLS-L-TM, the cells were depleted of functional Kap95 (▲, data from (Meinema *et al.*, 2011)) or ATP (Δ) after rapamycin (RAP) or sodium azide plus 2-deoxyglucose (NaN_3 + 2-DG) was added. The nuclear accumulation (NE/ER) was plotted as a function of time and fitted to a single exponent (dashed line). ($n < 8$ for each time point). **B)** Similar as (A), cells were depleted of functional Kap95 (data from (Meinema *et al.*, 2011)) or depleted of ATP, after expression of GFP-h2NLS-L(33) (●/○) or GFP-h2NLS-L (■/□). The nuclear accumulation (N/C) is plotted as a function of time and fitted to a single exponent (dashed line) ($n < 14$). The nuclear efflux of GFP-h2NLS-L in the metabolic poison assay (□) was fitted with a two-term decay model. **C)** The nuclear efflux rate constants measured in the Kap95-depletion assay and in the poison assay and the R^2 for each fit. **D)** Confocal images of Kap60-GFP and Kap95-GFP, under normal conditions (+ATP) and depletion of ATP (-ATP). **E)** The accumulation at the NPC of Kap60-GFP and Kap95-GFP under normal conditions (open bars) and in cells depleted of ATP (gray bars). Scale bar is 5 μm, SEM is indicated.

Efflux of reporters with large extralumenal domains

Where does the NLS-terminal region of membrane reporters pass through the NPC during efflux? To address this question we increased the number of soluble domains and thus the mass at the N-terminus. If the extralumenal domains of the reporters travel through the narrow lateral channel facing the POM, one would expect a slowing of the efflux with increasing mass. In fact, the upper size limit for transit through the lateral channel in yeast or vertebrate NPCs is thought to be ~60 kDa (Deng and Hochstrasser, 2006;Soullam and Worman, 1995;Wu *et al.*,

2002). We observed that reporters with extralumenal domains of 174 kDa are capable to travel from the INM to ONM/ER (Fig. 6.7A). The rate constants for efflux were constant (k_{out} ~$0.9 \cdot 10^{-3}$ s^{-1}) up to an extralumenal domain mass of 92 kDa and decreased to $0.15 \cdot 10^{-3}$ s^{-1} at 174 kDa (i.e. three additional MBP-domains). The expression of the reporters MBP-GFP-MBP-h2NLS-L-TM and MBP-GFP-2×MBP-h2NLS-L-TM showed spots with high fluorescence intensity at the NE in a fraction (<20%) of the cells, which did not disappear upon addition of rapamycin. These sites may correspond to reporter aggregation at the INM and/or ONM, and as a result, the efflux rate constant will be underestimated. In parallel with a 5-fold reduced exit rate, the nuclear accumulation (NE/ER ratio) decreased with increasing number of soluble domains (Fig. 6.7B). This implies that the overall import was affected more than the efflux (Fig. 6.7B, C). Altogether, the efflux kinetics of the reporter with multiple extralumenal domains is not compatible with passage through 10 nm wide lateral channels (Hinshaw *et al.*, 1992) and argue for a spacious exit

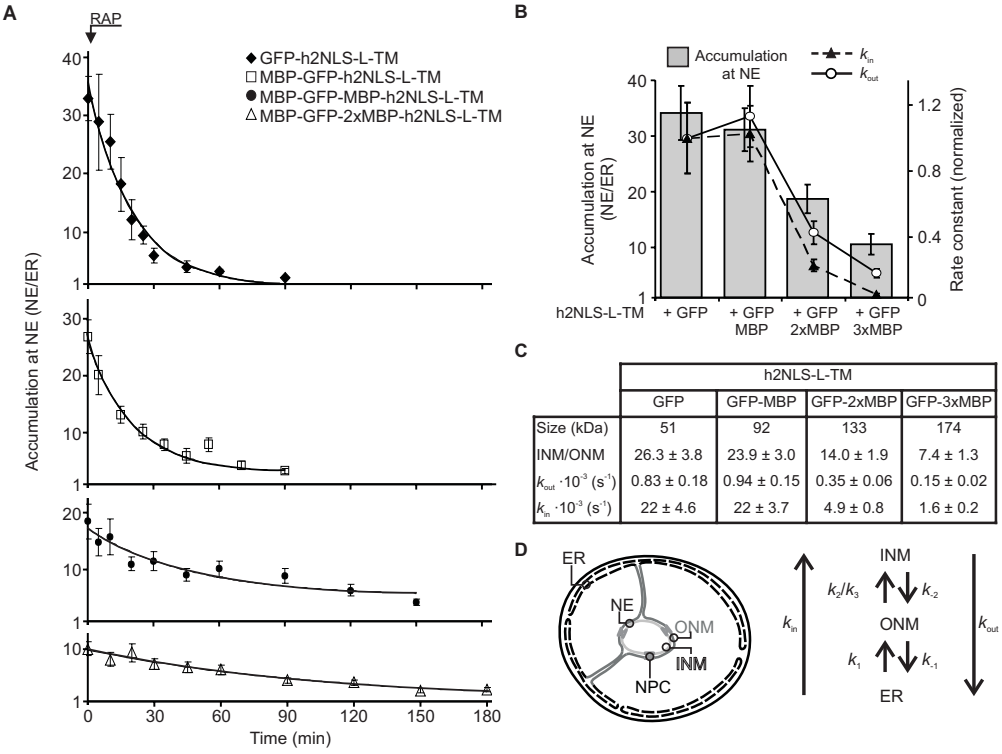

Figure 6.7: Large extralumenal domains can transit via the central channels of the NPC. A) The nuclear accumulation (NE/ER) of GFP-h2NLS-L-TM (♦, data from (Meinema *et al.*, 2011)) and of reporters with one (□), two (●) or three (Δ) additional extralumenal MBPs is plotted as a function of time upon addition of rapamycin and fitted with a single exponent. **B)** The nuclear accumulation (NE/ER) at steady state of GFP-h2NLS-L-TM and the derived variants with one, two or three additional extralumenal MBPs (bars, data from (Meinema *et al.*, 2011)); the overall efflux rate constants (k_{out}, ○, solid line) and overall import rate constants (k_{in}, ▲, dashed line) derived from (A) are also plotted. **C)** The overall efflux rate constants (k_{out}) and the calculated overall import rate constants (k_{in}). **D)** For the overall flux of membrane proteins to the INM, we distinguish lateral diffusion through ER and ONM to the NPCs (k_1), diffusion across the NPC (influx) (k_2) or Kap-facilitated import (k_3). For the overall efflux, we distinguish diffusion across the NPC (efflux) (k_{-2}) and lateral diffusion from ONM to ER (k_{-1}). See discussion for details. SEM is indicated.

route, alike that is used during import.

Discussion

The yeast membrane protein Src1/Heh1 and Heh2 pass the NPC via an import mechanism that depends on the binding interactions between Kap95 and FG-Nups to cross the central channel of the NPC (King *et al.*, 2006;Meinema *et al.*, 2011). A long intrinsically disordered linker spacing the h2NLS and the transmembrane domain facilitates the interactions between NLS-associated Kaps and FG-Nups. We now present a quantitative analysis of Kap60/95-mediated import and efflux of membrane cargos, including data on the mobility of the reporter proteins in the different membrane compartments.

Lateral diffusion in the INM, ONM and ER

Our estimates of lateral diffusion of membrane proteins in the ER of yeast (Fig. 6.4, Table 6.1) are a little lower than those in the mammalian ER, where values ranging from 0.3 to 0.5 $\mu m^2/s$ were measured (Ellenberg *et al.*, 1997;Nehls *et al.*, 2000;Ostlund *et al.*, 1999). The diffusion coefficient of GFP-Heh2 at the INM is comparable with earlier findings of full length membrane proteins trapped at the INM (Ellenberg *et al.*, 1997;Ostlund *et al.*, 1999) and concur with those of proteins tested in HeLa cells (Zuleger *et al.*, 2011). The diffusion of the free moving membrane reporters in the ER was observed to be 5-6 times slower than in the INM (Fig. 6.4). Overall, the diffusion in the ONM and ER of the yeast cell was thus lower than in the INM, presumably reflecting a higher macromolecular crowding in the ONM and ER and/or a different viscosity of the membrane (e.g. lipid composition). This observation, that the diffusion of membrane reporters in the INM is faster than in the ER, is in marked contrast with the finding that the diffusion of full length membrane proteins was faster in the ER than in the INM of HeLa cells (Zuleger *et al.*, 2011). When the areas of the bleaching spots are taken into account, the half-time of recovery in the ER of HeLa cells corresponds to diffusion coefficients that are similar to those in the ER of yeast. The differences between our work in yeast and that of Zuleger are likely caused by (transient) interactions of the full-length proteins with other nuclear structures in the HeLa cells. Our reporters were designed to assure free diffusion.

Quantitative analysis of active and passive transport of membrane cargo.

Throughout the manuscript we refer to the NE/ER-ratio as the experimental value that allows direct comparison of the accumulation levels of different cargo's, or of the same cargo under different conditions. The measured efflux rate constants and the below derived import rate constants are the overall rate constants of a number of different steps (Fig. 6.7D): For movement towards the INM we distinguish: lateral diffusion through the ER to the NPCs (k_1), and passive influx to the INM for proteins without an NLS (k_2) or active import facilitated by karyopherins (for proteins bearing an NLS) (k_3). For the outward pathway from the INM, we distinguish nuclear efflux to the ONM (k_{-2}) and lateral diffusion in the ONM/ER away from the NPCs (k_{-1}). The kinetics of Kap60/95 association and dissociation in the ER and ONM will not likely influ-

ence the overall import (and efflux) kinetics; Kap60/Kap95 associates with the h2NLS when the reporter is still located in the ER (Fig. 6.1) and competition between membrane and soluble cargo takes place (Fig. 6.2). The measured efflux rate constant reflects thus k_{-1} and k_{-2} while the below calculated overall import rate constant reflects k_3 and k_1.

The diffusion of membrane proteins in the ER was almost two orders of magnitude slower than the diffusion in the cytosol of yeast. For the lateral diffusion of GFP-h2NLS-L-TM through the membranes of the ER, a diffusion coefficient of $D = 0.16$ μm^2/s was measured. The diffusion through the membranes (k_1 and k_{-1}) may thus have a significant influence on the overall import. Indeed, if we estimate that the reporter diffuses on average 3.5 μm from a position in the ER to an NPC (see material and methods for this estimation), it would take ~20 seconds based on a 2D random walk. This number is indeed in the same range as the half time for import (~38 seconds) that can be calculated on the basis of the $k_{in} = 1.8 \cdot 10^{-2}$ s^{-1} (see below).

The nuclear accumulation of GFP-h2NLS-L-TM is the resultant of, on the one hand, the import rate constant (k_3) and the protein concentration in the ER-ONM, and on the other hand, the efflux rate constant (k_{-2}) plus the protein concentration in the INM. Thus, to derive import rate constants from the measured efflux rate constants and the NE/ER ratio's, we needed to estimate the concentrations of the reporters at the INM and the ONM. We considered a simplified view of what we know the structure of the ER at the periphery of a yeast cell looks like (West *et al.*, 2011) and assume it consists on average of cisternae of two closely positioned bilayers enclosing the lumenal space, alike the NE. Furthermore, we assume that 40% of the periphery is covered with ER (between 20 – 40 % (West *et al.*, 2011)). Lastly, we assume that the concentrations of the reporter in the two membranes of the ER and in the ONM are identical. With these assumptions we can convert our measured NE/ER ratio of 2.3 of GFP-L-TM (Meinema *et al.*, 2011) into an INM/ONM-ratio of 0.8. GFP-h2NLS-L-TM with a measured NE/ER ratio of 34 converts to an INM/ONM ratio of 26. Based on the measured efflux rate constant of $0.83 \cdot 10^{-3}$ s^{-1} and the INM/ONM ratio of 26 we calculated an import rate constant for GFP-h2NLS-L-TM of ~$2.2 \cdot 10^{-2}$ s^{-1} (Fig. 6.7C).

Based on the INM/ONM ratio of 26, we can conclude that efflux over the NPC is at least an order of magnitude slower than Kap-mediated import. The slow diffusion through the membranes and approximately equally slow overall import leads us to speculate that exit of membrane proteins via the NPC is slow and rate-limiting for the overall efflux. For Kap-mediated import, the actual transport through the NPC is likely not rate-limiting as diffusion through the ER-ONM is slow.

Comparing transport of soluble and membrane cargo through the NPC

On the basis of Western blot analysis (Fig. 6.3), we estimated that about $13 \cdot 10^3$ membrane reporter molecules are present per cell. Taking into account the accumulation ratios and estimates of the surface area of the INM, ONM and ER membranes (see materials and methods for details), we find ~$0.4 \cdot 10^2$ molecules/μm^2 in the ONM and ER and ~$8.8 \cdot 10^2$ molecules/μm^2 in the INM. Assuming a density of 12 NPCs per μm^2 (Timney *et al.*, 2006;Winey *et al.*, 1997), the flux of GFP-h2NLS-L-TM over the NPC is ~0.06 molecules/NPC·s.

How do these fluxes compare to those of soluble nuclear transport? For the soluble reporter GFP-tcNLS-GFP, we found an import rate constant of 0.16 ± 0.03 s^{-1} (Fig. 6.4). We estimated ~$1.5 \cdot 10^5$ soluble GFP-tcNLS-GFP copies in the cytoplasm, yielding a flux of soluble reporters over the NPC of 13 ± 2.2 molecules/NPC·s, which is in good agreement with earlier studies in yeast (Timney *et al.*, 2006). If the GFP-tcNLS-GFP reporter would be present at an equal number of copies per cell as GFP-h2NLS-L-TM, the flux would have been 1.5 molecules/NPC·s. This is more than an order of magnitude faster than the flux of ~0.06 molecules/NPC·s for GFP-h2NLS-L-TM, which shows that the molecular transport of membrane proteins to the nucleus is significantly slower than that of soluble proteins when comparing cargo's transported by Kap60/95 and similar in abundance.

In conclusion, comparing the transport kinetics of Kap60/95-facilitated import of the integral membrane reporter GFP-h2NLS-L-TM and soluble GFP-tcNLS-GFP we see two major differences. For the membrane reporter we show that 1) the affinity of Kap60 for the h2NLS is high and as a consequence we see little effect of competition with other lower affinity cargo and 2) the lateral diffusion in the ER is slow and may significantly affect the overall nuclear import kinetics. For the soluble reporters 1) the tcNLS and other NLS's have a lower affinity for Kap60 than h2NLS and finding a Kap in competition with many other proteins may be determining the overall import rate (Timney *et al.*, 2006) and 2) the diffusion of soluble cargo in the cytoplasm is relatively fast and not rate-limiting for the nuclear import (Smith *et al.*, 2002;Timney *et al.*, 2006). The relatively slow but robust accumulation of membrane cargo is compatible with reported roles of actively imported INM proteins, such as NPC-assembly and maintenance of nuclear organization and structures (Funakoshi *et al.*, 2011;Grund *et al.*, 2008;Mekhail *et al.*, 2008;Rodriguez-Navarro *et al.*, 2002;Talamas and Hetzer, 2011;Tapley *et al.*, 2011;Turgay *et al.*, 2010;Yavuz *et al.*, 2010;Yewdell *et al.*, 2011).

Mechanism of transport across NPC of membrane cargo

Taking into account our recently published and new data, we discuss a possible mechanism and path for transport of membrane proteins through the NPC. Our previously published data supported that the extralumenal domains of the investigated INM-destined membrane proteins are transported through the central channel of the NPC (Meinema *et al.*, 2011). Most conclusive is that we show that the terminus of the linker can be trapped at the Nsp1-anchor site. Our present data suggests that the extralumenal domains terminal to the linker can travel back to the ONM through the same channel. Namely, we found that membrane reporters could leak back from the nucleus to the ER, while having extralumenal domains with overall masses far above the reported upper size limit for proteins diffusing through the lateral channel facing the POM (Fig. 6.7A). Vice versa, we expect that the reporter with large extralumenal domains terminal to the linker can also reach the INM by influx, with similar slow kinetics. We had proposed that the NPCs have a central channel that is continuous with narrow conduits through the scaffold, lateral gates. These gates enable the linker to slice through the scaffold of the NPC. Since these lateral gates have not been detected in electron microscopy studies (Hinshaw *et al.*, 1992;Yang *et al.*, 1998;Frenkiel-Krispin *et al.*, 2010;Stoffler *et al.*, 2003;Akey and Radermacher, 1993), we assume they are narrow,

likely dynamic and possibly existing after restructuring of the NPC (Solmaz *et al.*, 2011), but wide enough for a linker to slice through. One possibility is that such gates are formed in-between the 8-fold rotational symmetry units, the spokes, of the NPC (Akey and Radermacher, 1993;Hinshaw *et al.*, 1992).

During nuclear import of membrane proteins, the karyopherin-bound NLS interacts with FG-repeat binding sites in the NPC, which may favor a stretched or extended conformation of the flexible linker. We infer that it would not cost much energy to promote this extended conformation, as intrinsically disordered domains can already adopt a wide range of conformations (Galea *et al.*, 2008) and are typically less stiff than folded domains (Miyagi *et al.*, 2008). With both ends of the molecule "bound", the TM domain embedded in the membrane and the NLS bound to the FG-repeats via Kap60 and Kap95, the linker can dodge into the lateral gates. The length of the linker may give the karyopherin enough freedom to scavenge the entire width of the central channel and interact with the numerous FG-repeats. The RanGTP-gradient gives direction to the flux of Kap-cargo to the nuclear site of the NPC. Without karyopherins attached to the NLS, entry into the NPC, and residence of the extralumenal domain in the central channel, will be much less likely to occur, as there is no mechanism that promotes a stretched linker. Due to the intrinsic dynamics of the linker, it will still occasionally adopt an extended conformation, and the soluble domains terminal of the linker can enter the NPC central channel and allow efflux of the reporter. Future studies will have to show if the interpretation of our data is correct. Key will be to show the existence of the lateral gates connecting the space immediately adjacent to the nuclear envelope and the central channel with more direct methods.

Materials and Methods

Strains and plasmids

All experiments were performed in the *S. cerevisiae* KAP95-AA strain (Meinema *et al.*, 2011), except for the selective-FRAP measurements (Fig. 6.5), which were done in BY4742 ((Brachmann *et al.*, 1998) Invitrogen, Carlsbad, California) and the (co-)localization experiments (Fig. 6.1, 6D), which were done in the ATCC201388 ((Howson *et al.*, 2005;Huh *et al.*, 2003), Invitrogen, Carlsbad, California). The correct integration of GFP in the strains Sec61-GFP, Kap60-GFP and Kap95-GFP (Invitrogen, Carlsbad, California) was confirmed by PCR.

Most reporter proteins were expressed in yeast from low-copy number plasmids that are based on pUG34 and pUG36 (Niedenthal *et al.*, 1996), and the genes were under control of the *GAL1* promoter, except for GFP-tcNLS-GFP that was expressed under control of a constitutive *MET25* promoter. The soluble cargo proteins rgNLS-mCh and tcNLS-mCh were expressed in yeast from a 2μ-plasmid under the control of the *TPI1*-promoter, based on pBT016-Nab2NLS-GFP-PrA (Timney *et al.*, 2006). See Table 6.2 and 6.3 for a list of the strains and the plasmids used in this study.

Table 6.2: S.cerevisiae strains

Name	Description	Source
BY4742	MATα his3Δ1 leu2Δ0 lys2Δ0 ura3Δ0	Invitrogen
KAP95-AA	w303, matα tor1-1 fpr1::NAT PMA1-2xFKBP12::TRP1 KAP95-FRB::KanMX	(Haruki *et al.*, 2008;Meinema *et al.*, 2011)
Sec61-GFP	MATα his3Δ1 leu2Δ0 met15Δ0 ura3Δ0 SEC61-GFP::HIS3	Invitrogen
Kap60-GFP	MATα his3Δ1 leu2Δ0 met15Δ0 ura3Δ0 KAP60-GFP::HIS3	Invitrogen
Kap95-GFP	MATα his3Δ1 leu2Δ0 met15Δ0 ura3Δ0 KAP95-GFP::HIS3	Invitrogen

Plasmid construction To obtain the expression vector pACM062-mCh-h2NLS-L(180)-TM and pACM063-mCh-L(180)-TM, the coding sequence of h2NLS-L(180)-TM and L(180)-TM were isolated from pACM023-GFP-h2NLS-L-TM and pACM024-GFP-L-TM, respectively (Meinema *et al.*, 2011) and ligated into the *Xba*I and *Bam*HI sites of pUG36(Niedenthal *et al.*, 1996). Subsequently, the coding sequence of GFP was replaced for that of mCherry (mCh), which was amplified by PCR from pcDNA3.1-mCherry (Invitrogen, Carlsbad, California) (primers used: frw: 5'-ggtct agaAT GGTGA GCAAG GGCGA GG, rvs: gctct agaTT ACTTG TACAG CTCGT CCATG CC uppercase: annealing sequence, lower case: primer overhang, *Phusion* polymerase (Finnzymes, Espoo, Finland) and ligated in the *Xba*I site. The linker of pACM062-mCh-h2NLS-L(180)-TM was truncated to obtain pACM061-mCh-h2NLS-L(37)-TM by PCR-based mutagenesis (adapted from Quik Change protocol, Stratagene, La Jolla, California) (primers used frw: CGAAG TCCAA AAGGT CGCAC C and rvs: 5'-AGATT GTGGA GGAGA CTCTG GTGG). To construct pACM065-GFP-tcNLS-GFP, first the coding sequence of tcNLS, ordered as complementary single stranded oligonucleotides (5'- GGATC CCCAA AAAAG AAGAG AAAGG TAGAT CCAAA AAAGA AGAGA AAGGT AGCTA GCGAA TTC and 5'- GAATT CGCTA

GCTAC CTTTC TCTTC TTTTT TGGAT CTACC TTTCT CTTCT TTTTT GGGGA TCC), was annealed and ligated into pUG34(Niedenthal *et al.*, 1996) at *Bam*HI and *Eco*RI. Subsequently, a second GFP gene was ligated at *Eco*RI and *Eco*RV. The gene coding for GFP was amplified by PCR from pUG34 (frw: 5'- gccga attcA TGTCT AAAGG TGAAG AATTA TTCAC TGGTG TTG, rvs: 5'- gccga tatcA GCGGA TTTGT ACAAT TCATC CATAC CATGG GTAAT ACC). The rgNLS in pACM066-rgNLS-mCh was replaced for a tcNLS to yield pACM067-tcNLS-mCh. The tcNLS was ordered as complementary single stranded oligonucleotides (5'-AATTC ATGCC AAAAA AGAAG AGAAA GGTAG ATCCA AAAAA GAAGA GAAAG GTAGC TAGCG and 5'-GATCC GCTAG CTACC TTTCT CTTCT TTTTT GGATC TACCT TTCTC TTCTT TTTTG GCATG), annealed and ligated in the *Eco*RI and *Bam*HI site of pACM066-rgNLS-mCh. All DNA constructs were confirmed by sequencing.

Table 6.3: Plasmids

Name	Description	Source
pUG34	*Met25* promoter, His3 selection marker, *GFP*	(Niedenthal *et al*., 1996)
PUG36	*Met25* promoter, Ura3 selection marker, *GFP*	(Niedenthal *et al*., 1996)
pACM022-GFP-Heh2	*GFP-HEH2* under *Gal1* promoter, His3 selection marker	(Meinema *et al*., 2011)
pACM023-GFP-h2NLS-L-TM	As above, Heh2[aa93-378]	(Meinema *et al*., 2011)
pACM024-GFP-L-TM	As above, Heh2[aa138-378]	(Meinema *et al*., 2011)
pACM040-MBP-GFP-h2NLS-L-TM	As above, Heh2[aa93-378] fused to *MalE-GFP*	(Meinema *et al*., 2011)
pACM041-MBP-GFP-MBP-h2NLS-L-TM	As above, Heh2[aa93-378] fused to *MalE-GFP-MalE*	(Meinema *et al*., 2011)
pACM042-MBP-GFP-2xMBP-h2NLS-L-TM	As above, Heh2[aa93-378] fused to *MalE-GFP-MalE-MalE*	(Meinema *et al*., 2011)
pACM062-mCh-h2NLS-L(180)-TM	pUG36, GFP replaced for mCh with h2NLS-L-TM under Gal1 promoter	This study
pACM061-mCh-h2NLS-L(37)-TM	As pACM062-mCh-h2NLS-L(180)-TM, but linker truncated to 37 residues	This study
pACM063-mCh-L(180)-TM	pUG36, GFP replaced for mCh with Heh2[aa138-378] under *Gal1* promoter	This study
pACM065-GFP-tcNLS-GFP	pUG34 where tcNLS and GFP are inserted	This study
pACM066-rgNLS-mCh	2µ plasmid, NLS of Nab2 fused with mCh, under TPI-promoter, Leu2 selection marker	(van den Bogaart *et al*., 2009)
pACM067-tcNLS-mCh	2µ plasmid, tcNLS fused with mCh, under TPI-promoter, Leu2 selection marker	This study
pACM050-GFP-h2NLS-L(176)	pAC023-GFP-h2NLS-L-TM, where the gene fragment coding for the TM segment was removed	(Meinema *et al*., 2011)
pACM051-GFP-H2NLS-L(033)	pACM050-GFP-h2NLS-L(176), where L was truncated to 33 residues	(Meinema *et al*., 2011)

Fluorescence Microscopy

Growth conditions. Yeast strains were grown at 30°C in synthetic dropout medium without histidine, leucine or uracil, supplemented with 2% (w/v) filter-sterilized D-raffinose plus 0.01 % (w/v) adenine. The genes encoding reporter proteins were expressed from low-copy plasmids under the control of the *GAL1* promoter by 1-2 hours induction with 0.1% (w/v) D-galactose, except for MBP-GFP-MBP-h2NLS-L-TM (3 hour of induction) and MBP-GFP-2MBP-h2NLS-L-TM (4 hour of induction). The cells with constructs under control of the constitutive MET25 or TPI1-promoter were grown in medium supplemented with 2% (w/v) D-glucose.

Image acquisition: All imaging and selective-FRAP experiment were performed on a home-build laser-scanning confocal microscope or a commercial LSM 710 confocal microscope as described previously (Meinema *et al.*, 2011). Data was analyzed with home-made software and the ZEN2010B package (Carl Zeiss, Jena, Germany). To quantify the protein mobility in the membranes, an epi-fluorescence microscope was used, which is based on an inverted microscope Observer D1 (Carl Zeiss, Jena, Germany). The laser beam (488 nm, argon ion laser, Melles Griot, Carlsbad, CA, USA) was focused by a Zeiss C-Apochromat infinity-corrected 1.2 NA 63× water immersion objective and directed to the sample. The fluorescence emission was detected by a Cool-Snap HQ2 CCD camera (Photometrics, Tucson, AZ, USA) and recorded in MetaMorph (Molecular Devices, Downingtown, USA).

Data analysis and NE/ER-ratios. Since the resolution of optical microscopy does not discriminate the INM from ONM, we used the NE/ER ratio as a measure for accumulation at the INM. The NE/ER ratio is an experimental value that allows direct comparison of import efficiencies. The NE/ER ratio was calculated as the average pixel intensity at the nuclear envelope (NE) divided by the average pixel intensity at the peripheral or plasma membrane associated endoplasmic reticulum as described before (Meinema *et al.*, 2011).

The nuclear transport of membrane proteins across the NPC is between the ER-ONM network and the INM. We assume that the concentrations at the ER and ONM are the same. The changes in membrane protein density at the INM ($[A]_{INM}$) and ER-ONM ($[A]_{ER/ONM}$) can be written as:

$$\frac{d[A]_{INM}(t)}{dt} = k_{in}[A]_{ER/ONM} - k_{out}[A]_{INM} \quad (1)$$

$$\frac{d[A]_{ER/ONM}(t)}{dt} = -k_{in}[A]_{ER/ONM} + k_{out}[A]_{INM} \quad (2)$$

where k_{in} and k_{out} are the import and the efflux rate constants, respectively, and t is the time. At steady state is the reporter concentrations at the INM ($[A]_{INM}$) and the ONM ($[A]_{ONM}$) determined by the ratio of k_{in}/k_{out} (equation (3))

$$\frac{[A]_{INM}}{[A]_{ER/ONM}} = \frac{k_{in}}{k_{out}} \quad (3)$$

The INM/ONM ratio, the ratio of the reporter concentrations at the INM and the ONM, is calculated from the experimental NE/ER ratios, the measured ratio of fluorescence levels at the NE and the ER. First, for the purpose of our calculations we consider that the ER consist on average of two closely positioned bilayers forming cisternea (flattened membrane disks) enclosing a lumen that is continuous with the NE lumen. This is obviously a simplification as the structure of the ER is more complex, consisting of cisternae (flattened membrane disks) and tubules (tube structures) (West *et al.*, 2011). Second, proteins can diffuse throughout the entire network, and we assume that the concentration of membrane reporters in ONM and ER are equal. Third, to estimate the concentrations of the reporters and the surface area of the ER membranes, we take

into account that 40% of the plasma membrane is covered with peripheral ER at the contour of a yeast cell (20% - 40% in (West *et al.*, 2011;Schuck *et al.*, 2009). At our resolution, we see the ER as a continuous membrane system and the actual concentration of fluorescent reporters is thus 2.5 times the measured concentration of reporters. The calculation thus are performed as follows: We measured for GFP-h2NLS-L-TM an NE/ER-ratio of 34, thus for the fluorescence *intensities* (*i*) in the membranes we can write: *i*(NE):*i*(ER) = 34:1. Not taking into account the 2.5 times underestimation of the concentration at the ER and ONM we would write *i*(INM): *i*(ONM): *i*(ER) = 33.5:0.5:1. But correcting for this underestimation of the concentration of reporters at the ER and ONM, we can write for the ratio of *concentrations* of reporters in the INM and ONM: INM/ONM ratio = (*i*(NE):*i*(ER) – (0.5*2.5)) / 0.5*2.5) =26. For GFP-L-TM, with a measured NE/ER-ratio of 2.3, we arrive at an INM/ONM-ratio of 0.84.

Diffusion of soluble protein. We used the LSM710 confocal microscope to measure the diffusion coefficient of GFP in the cytoplasm of yeast. We positioned the focused laser beam (wavelength: 488 nm) in the cytoplasm of a yeast cell and photobleached a small spot for 3.31 ms with 100% of the output power of a 15 mW solid state laser to obtain 40 - 50% of the initial intensity. The recovery was measured by taking images of 0.5 × 0.5 μm in 3.78 ms for a period of 200 ms using 0.4% of the output power of the laser. The recovery trace was fitted to a single exponent to find the half-time of recovery. The diffusion coefficient was obtained according to equation (1), derived from (Axelrod *et al.*, 1976):

$$D = \frac{w^2}{4t_{0.5}} \qquad (4)$$

where D is the diffusion coefficient, w the radius of the beam and $t_{0.5}$ the half-time of recovery. To determine the diameter of the beam, we bleached a similar spot in poly(methyl methacrylate) (PMMA) doped with Rhodamine B, imaged a frame of 5 × 5 μm and measured the diameter (d) of the beam as the full width at half minimum (FWHM) of the spot, yielding d = 2.0 ± 0.2 μm (n = 16).

Lateral diffusion of membrane proteins. For quantitative estimates of protein mobility in the membrane, FRAP-measurements were performed. The laser was focused for 30 - 50 ms to photobleach the fluorescent signal at the membrane to 40-50% of the initial intensity, using ~ 10% of the output power of a 10 mW argon ion laser. Immediately after the photobleaching, a time series of 50 images was recorded every 100 ms for fast diffusing reporters at the INM or 500 ms for the more slow lateral diffusion in the ONM and ER. The diameter (d) of the photobleached spot was defined as the full width of half minimum (FWHM) of the intensity level immediately after photobleaching and determined as d = 1.8 ± 0.1 μm (n = 38).

The fluorescence intensity was determined by pixel analysis in the centre of the photobleached spot (d = 0.7 μm), using MetaMorph (Molecular Devices, Downingtown, USA). A significant fraction of total fluorescence at the NE was photobleached, since we photobleached a spot corresponding to 20 – 40% of the size of NE. To find the mobile fraction, we corrected for this reduction of the total fluorescence by plotting the ratio of the intensity in the bleached

spot over the intensity in a reference spot with the same size at the same membrane compartment. The photobleaching as a result of imaging during the recovery was negligible (~4%). Therefore, uncorrected data could be fitted according to earlier publications (Ellenberg *et al.*, 1997) to obtain a measure for the lateral diffusion coefficient *D* (expressed in $\mu m^2/s$).

We estimated how much time a membrane protein would need on average to diffuse from the ER to the nucleus. We used equation (5) for the mean squared displacement, describing the average distance (*r*) a particle travels in time (*t*) based on Brownian motion of a random walk in a two dimensional system of the plane of a membrane.

$$\left\langle r^2(t)\right\rangle = 4Dt \tag{5}$$

D is the coefficient for lateral diffusion and *t* is the time interval. We measured the volume of a yeast cell as 49 ± 2 μm^3 (*n* = 381) (van den Bogaart *et al.*, 2009), consistent with (Tyson *et al.*, 1979). Assuming a circumference of a yeast cell of ~15 μm, we estimated the average travel distance (*r*) through the peripheral ER aligning the plasma membrane to be ~3.5 μm.

Selective-FRAP. Selective-FRAP was used to quantify the nuclear transport of soluble proteins (as reviewed in (Goodwin and Kenworthy, 2005)). The import and efflux rate constants of soluble proteins were calculated as described before (van den Bogaart *et al.*, 2009).

Reporter efflux assays. (i) The Kap95-depletion assay: After 2 hours of membrane reporter expression in exponentially growing KAP95-AA cells, 2 μg/ml of rapamycin was added to trigger Kap95-FRB interaction with Pma1-FKBP. Kap95 depletion disables further Kap95-mediated nuclear import, resulting in a net efflux of INM-accumulated reporter (Haruki *et al.*, 2008;Meinema *et al.*, 2011). (ii) The poison assay: The cells were harvested and resuspended in glucose-free medium supplemented with 10 mM sodium azide plus 10 mM 2-deoxy-D-glucose. This treatment dissipates the ATP pool and thereby the Ran-GTP gradient across the nuclear envelope. For both assays, images at t = 0 were recorded, i.e. before adding rapamycin or sodium azide/2-deoxy-D-glucose, and time series were recorded for a period of 90 to 180 minutes. The cells were kept at 30°C during the course of the experiment. For every time point new microscopy slides were prepared from one culture, the data thus represents averages of multiple cells, as described in (Shulga *et al.*, 1996;Worman and Courvalin, 2000).

We plotted the nuclear accumulation as the NE/ER ratio and fitted the data with a single exponential decay function. We simplified equation (1) to obtain equation (6) as the passive inward flux is negligible during the efflux experiment.

$$d\frac{[\mathrm{A}]_{\mathrm{INM}}}{[\mathrm{A}]_{\mathrm{ONM/ER}}} = -k_{\mathrm{out}}\frac{[\mathrm{A}]_{\mathrm{INM}}}{[\mathrm{A}]_{\mathrm{ONM/ER}}}\mathrm{d}t \tag{6}$$

or a two-term exponential decay function:

$$d\frac{[\mathrm{A}]_{\mathrm{INM}}}{[\mathrm{A}]_{\mathrm{ONM/ER}}} = \left(-k_{\mathrm{out}\,1}\frac{[\mathrm{A}]_{\mathrm{INM}}}{[\mathrm{A}]_{\mathrm{ONM/ER}}} - k_{\mathrm{out}\,2}\frac{[\mathrm{A}]_{\mathrm{INM}}}{[\mathrm{A}]_{\mathrm{ONM/ER}}}\right)\mathrm{d}t \tag{7}$$

Calculation of import rate constants and membrane protein fluxes through the NPC. The import rate constant was calculated from the steady state accumulation of the membrane reporter and the efflux rate constant as estimated in the Kap95-depletion, using equation (4). The import rate constant was used to calculate the flux of reporter through the NPC (in units of molecules/s·NPC), which requires an estimate of the number of reporters per cell, the total surface area of the ER-ONM and the INM, and the number of NPCs per nucleus. Quantitative Western blotting yielded a copy number of GFP-h2NLS-L-TM in the Kap95-AA strain of ~13,000 per cell (Fig. 6.3A, B). On the basis of the geometry of the cell, we estimated the average radius of the cell and nucleus as $r = 2.3 \pm 0.1$ μm and $r = 1.00 \pm 0.05$ ($n = 381$), respectively, as described in (van den Bogaart *et al.*, 2009). Assuming the ER as a double membrane and aligned with the outline of the cell and covering ~40% of the plasma membrane (West *et al.*, 2011;Schuck *et al.*, 2009), we estimated the surface area of the ER-ONM to be ~64 μm^2 and that of the INM ~12 μm^2, which is consistent with earlier data (Prinz *et al.*, 2000;Strambio-De-Castillia *et al.*, 1995). The density of NPCs in the NE of yeast is on average 12 NPCs/μm^2 (Timney *et al.*, 2006;Winey *et al.*, 1997). Given the accumulation of GFP-h2NLS-L-TM at the INM, and assuming equal concentrations of reporter in ONM and ER, we calculated a membrane protein density for GFP-h2NLS-L-TM of 879 molecules/μm^2 at the INM and 39 molecules/μm^2 at the ER-ONM in the Kap95-AA strain.

Acknowledgements

We thank V. Krasnikov for help with microscopy, G. van den Bogaart, P. Popken and A. Kralt for help with data analysis. This work was supported by funding from the Netherlands Organization for Scientific Research NWO (VIDI fellowship to L.M.V. and top-subsidy grant 700.56.302 to B.P.).

References

1. Akey, C.W. and M.Radermacher. 1993. Architecture of the Xenopus nuclear pore complex revealed by three-dimensional cryo-electron microscopy. *J. Cell Biol.* **122**:1-19.
2. Antonin, W., R.Ungricht, and U.Kutay. 2011. Traversing the NPC along the pore membrane: targeting of membrane proteins to the INM. *Nucleus.* **2**:87-91.
3. Axelrod, D., D.E.Koppel, J.Schlessinger, E.Elson, and W.W.Webb. 1976. Mobility measurement by analysis of fluorescence photobleaching recovery kinetics. *Biophys. J.* **16**:1055-1069.
4. Brachmann, C.B., A.Davies, G.J.Cost, E.Caputo, J.Li, P.Hieter, and J.D.Boeke. 1998. Designer deletion strains derived from Saccharomyces cerevisiae S288C: a useful set of strains and plasmids for PCR-mediated gene disruption and other applications. *Yeast* **14**:115-132.
5. Braunagel, S.C., S.T.Williamson, S.Saksena, Z.Zhong, W.K.Russell, D.H.Russell, and M.D.Summers. 2004. Trafficking of ODV-E66 is mediated via a sorting motif and other viral proteins: facilitated trafficking to the inner nuclear membrane. *Proc. Natl. Acad. Sci. U. S. A* **101**:8372-8377.
6. Burns, L.T. and S.R.Wente. 2012. Trafficking to uncharted territory of the nuclear envelope. *Curr. Opin. Cell Biol.*
7. Deng, M. and M.Hochstrasser. 2006. Spatially regulated ubiquitin ligation by an ER/nuclear membrane ligase. *Nature* **443**:827-831.
8. Dingwall, C. and R.A.Laskey. 1991. Nuclear targeting sequences--a consensus? *Trends Biochem. Sci.* **16**:478-481.
9. Ellenberg, J., E.D.Siggia, J.E.Moreira, C.L.Smith, J.F.Presley, H.J.Worman, and J.Lippincott-Schwartz. 1997. Nuclear membrane dynamics and reassembly in living cells: targeting of an inner nuclear membrane protein in interphase and mitosis. *J. Cell Biol.* **138**:1193-1206.
10. Frenkiel-Krispin, D., B.Maco, U.Aebi, and O.Medalia. 2010. Structural analysis of a metazoan nuclear pore complex reveals a fused concentric ring architecture. *J. Mol. Biol.* **395**:578-586.
11. Funakoshi, T., M.Clever, A.Watanabe, and N.Imamoto. 2011. Localization of Pom121 to the inner nuclear membrane is required for an early step of interphase nuclear pore complex assembly. *Mol. Biol. Cell* **22**:1058-1069.
12. Galea, C.A., A.Nourse, Y.Wang, S.G.Sivakolundu, W.T.Heller, and R.W.Kriwacki. 2008. Role of intrinsic flexibility in signal transduction mediated by the cell cycle regulator, p27 Kip1. *J. Mol. Biol.* **376**:827-838.
13. Ghaemmaghami, S., W.K.Huh, K.Bower, R.W.Howson, A.Belle, N.Dephoure, E.K.O'Shea, and J.S.Weissman. 2003. Global analysis of protein expression in yeast. *Nature* **425**:737-741.
14. Goodwin, J.S. and A.K.Kenworthy. 2005. Photobleaching approaches to investigate diffusional mobility and trafficking of Ras in living cells. *Methods* **37**:154-164.
15. Görlich, D., N.Pante, U.Kutay, U.Aebi, and F.R.Bischoff. 1996. Identification of different roles for RanGDP and RanGTP in nuclear protein import. *EMBO J.* **15**:5584-5594.
16. Graumann, K., S.L.Irons, J.Runions, and D.E.Evans. 2007. Retention and mobility of the mammalian lamin B receptor in the plant nuclear envelope. *Biol. Cell* **99**:553-562.
17. Grund, S.E., T.Fischer, G.G.Cabal, O.Antunez, J.E.Perez-Ortin, and E.Hurt. 2008. The inner nuclear membrane protein Src1 associates with subtelomeric genes and alters their regulated gene expression. *J. Cell Biol.* **182**:897-910.
18. Hahn, S., P.Maurer, S.Caesar, and G.Schlenstedt. 2008. Classical NLS proteins from Saccharomyces cerevisiae. *J. Mol. Biol.* **379**:678-694.
19. Hahn, S. and G.Schlenstedt. 2011. Importin beta-type nuclear transport receptors have distinct binding affinities for Ran-GTP. *Biochem. Biophys. Res. Commun.* **406**:383-388.
20. Harley, C.A. and D.J.Tipper. 1996. The role of charged residues in determining transmembrane protein insertion orientation in yeast. *J. Biol. Chem.* **271**:24625-24633.
21. Haruki, H., J.Nishikawa, and U.K.Laemmli. 2008. The anchor-away technique: rapid, conditional establishment of yeast mutant phenotypes. *Mol. Cell* **31**:925-932.
22. Heijne, G. 1986. The distribution of positively charged residues in bacterial inner membrane proteins correlates with the trans-membrane topology. *EMBO J.* **5**:3021-3027.
23. Hinshaw, J.E., B.O.Carragher, and R.A.Milligan. 1992. Architecture and design of the nuclear pore complex. *Cell* **69**:1133-1141.
24. Howson, R., W.K.Huh, S.Ghaemmaghami, J.V.Falvo, K.Bower, A.Belle, N.Dephoure, D.D.Wykoff, J.S.Weissman, and E.K.O'Shea. 2005. Construction, verification and experimental use of two epitope-tagged collections of budding yeast strains. *Comp Funct. Genomics* **6**:2-16.
25. Huh, W.K., J.V.Falvo, L.C.Gerke, A.S.Carroll, R.W.Howson, J.S.Weissman, and E.K.O'Shea. 2003. Global analysis of protein localization in budding yeast. *Nature* **425**:686-691.
26. Kahms, M., J.Huve, R.Wesselmann, J.C.Farr, V.Baumgartel, and R.Peters. 2011. Lighting up the nuclear pore complex. *Eur. J. Cell Biol.* **90**:751-758.
27. King, M.C., C.P.Lusk, and G.Blobel. 2006. Karyopherin-mediated import of integral inner nuclear membrane proteins. *Nature* **442**:1003-1007.

28. Kutay, U., E.Izaurralde, F.R.Bischoff, I.W.Mattaj, and D.Gorlich. 1997. Dominant-negative mutants of importin-beta block multiple pathways of import and export through the nuclear pore complex. *EMBO J.* **16**:1153-1163.
29. Lange, A., L.M.McLane, R.E.Mills, S.E.Devine, and A.H.Corbett. 2010. Expanding the definition of the classical bipartite nuclear localization signal. *Traffic.* **11**:311-323.
30. Lee, D.C. and J.D.Aitchison. 1999. Kap104p-mediated nuclear import. Nuclear localization signals in mRNA-binding proteins and the role of Ran and Rna. *J. Biol. Chem.* **274**:29031-29037.
31. Liu, D., X.Wu, M.D.Summers, A.Lee, K.J.Ryan, and S.C.Braunagel. 2010. Truncated isoforms of Kap60 facilitate trafficking of Heh2 to the nuclear envelope. *Traffic.* **11**:1506-1518.
32. Lusk, C.P., G.Blobel, and M.C.King. 2007. Highway to the inner nuclear membrane: rules for the road. *Nat. Rev. Mol. Cell Biol.* **8**:414-420.
33. Meinema, A.C., J.K.Laba, R.A.Hapsari, R.Otten, F.A.Mulder, A.Kralt, G.van den Bogaart, C.P.Lusk, B.Poolman, and L.M.Veenhoff. 2011. Long unfolded linkers facilitate membrane protein import through the nuclear pore complex. *Science* **333**:90-93.
34. Mekhail, K., J.Seebacher, S.P.Gygi, and D.Moazed. 2008. Role for perinuclear chromosome tethering in maintenance of genome stability. *Nature* **456**:667-670.
35. Miyagi, A., Y.Tsunaka, T.Uchihashi, K.Mayanagi, S.Hirose, K.Morikawa, and T.Ando. 2008. Visualization of intrinsically disordered regions of proteins by high-speed atomic force microscopy. *Chemphyschem.* **9**:1859-1866.
36. Nehls, S., E.L.Snapp, N.B.Cole, K.J.Zaal, A.K.Kenworthy, T.H.Roberts, J.Ellenberg, J.F.Presley, E.Siggia, and J.Lippincott-Schwartz. 2000. Dynamics and retention of misfolded proteins in native ER membranes. *Nat. Cell Biol.* **2**:288-295.
37. Nenninger, A., G.Mastroianni, and C.W.Mullineaux. 2010. Size dependence of protein diffusion in the cytoplasm of Escherichia coli. *J. Bacteriol.* **192**:4535-4540.
38. Niedenthal, R.K., L.Riles, M.Johnston, and J.H.Hegemann. 1996. Green fluorescent protein as a marker for gene expression and subcellular localization in budding yeast. *Yeast* **12**:773-786.
39. Ostlund, C., J.Ellenberg, E.Hallberg, J.Lippincott-Schwartz, and H.J.Worman. 1999. Intracellular trafficking of emerin, the Emery-Dreifuss muscular dystrophy protein. *J. Cell Sci.* **112**:1709-1719.
40. Pemberton, L.F. and B.M.Paschal. 2005. Mechanisms of receptor-mediated nuclear import and nuclear export. *Traffic.* **6**:187-198.
41. Powell, L. and B.Burke. 1990. Internuclear exchange of an inner nuclear membrane protein (p55) in heterokaryons: in vivo evidence for the interaction of p55 with the nuclear lamina. *J. Cell Biol.* **111**:2225-2234.
42. Prinz, W.A., L.Grzyb, M.Veenhuis, J.A.Kahana, P.A.Silver, and T.A.Rapoport. 2000. Mutants affecting the structure of the cortical endoplasmic reticulum in Saccharomyces cerevisiae. *J. Cell Biol.* **150**:461-474.
43. Ribbeck, K., U.Kutay, E.Paraskeva, and D.Gorlich. 1999. The translocation of transportin-cargo complexes through nuclear pores is independent of both Ran and energy. *Curr. Biol.* **9**:47-50.
44. Rodriguez-Navarro, S., J.C.Igual, and J.E.Perez-Ortin. 2002. SRC1: an intron-containing yeast gene involved in sister chromatid segregation. *Yeast* **19**:43-54.
45. Saksena, S., Y.Shao, S.C.Braunagel, M.D.Summers, and A.E.Johnson. 2004. Cotranslational integration and initial sorting at the endoplasmic reticulum translocon of proteins destined for the inner nuclear membrane. *Proc. Natl. Acad. Sci. U. S. A* **101**:12537-12542.
46. Saksena, S., M.D.Summers, J.K.Burks, A.E.Johnson, and S.C.Braunagel. 2006. Importin-alpha-16 is a translocon-associated protein involved in sorting membrane proteins to the nuclear envelope. *Nat. Struct. Mol. Biol.* **13**:500-508.
47. Schuck, S., W.A.Prinz, K.S.Thorn, C.Voss, and P.Walter. 2009. Membrane expansion alleviates endoplasmic reticulum stress independently of the unfolded protein response. *J. Cell Biol.* **187**:525-536.
48. Schwoebel, E.D., T.H.Ho, and M.S.Moore. 2002. The mechanism of inhibition of Ran-dependent nuclear transport by cellular ATP depletion. *J. Cell Biol.* **157**:963-974.
49. Seedorf, M., M.Damelin, J.Kahana, T.Taura, and P.A.Silver. 1999. Interactions between a nuclear transporter and a subset of nuclear pore complex proteins depend on Ran GTPase. *Mol. Cell Biol.* **19**:1547-1557.
50. Shulga, N., P.Roberts, Z.Gu, L.Spitz, M.M.Tabb, M.Nomura, and D.S.Goldfarb. 1996. In vivo nuclear transport kinetics in Saccharomyces cerevisiae: a role for heat shock protein 70 during targeting and translocation. *J. Cell Biol.* **135**:329-339.
51. Smith, A.E., B.M.Slepchenko, J.C.Schaff, L.M.Loew, and I.G.Macara. 2002. Systems analysis of Ran transport. *Science* **295**:488-491.
52. Solmaz, S.R., R.Chauhan, G.Blobel, and I.Melcak. 2011. Molecular architecture of the transport channel of the nuclear pore complex. *Cell* **147**:590-602.
53. Soullam, B. and H.J.Worman. 1993. The amino-terminal domain of the lamin B receptor is a nuclear envelope targeting signal. *J. Cell Biol.* **120**:1093-1100.
54. Soullam, B. and H.J.Worman. 1995. Signals and structural features involved in integral membrane protein targeting to the inner nuclear membrane. *J. Cell Biol.* **130**:15-27.

55. Stoffler, D., B.Feja, B.Fahrenkrog, J.Walz, D.Typke, and U.Aebi. 2003. Cryo-electron tomography provides novel insights into nuclear pore architecture: implications for nucleocytoplasmic transport. *J. Mol. Biol.* **328**:119-130.

56. Strambio-De-Castillia, C., G.Blobel, and M.P.Rout. 1995. Isolation and characterization of nuclear envelopes from the yeast Saccharomyces. *J. Cell Biol.* **131**:19-31.

57. Swaminathan, R., C.P.Hoang, and A.S.Verkman. 1997. Photobleaching recovery and anisotropy decay of green fluorescent protein GFP-S65T in solution and cells: cytoplasmic viscosity probed by green fluorescent protein translational and rotational diffusion. *Biophys. J.* **72**:1900-1907.

58. Talamas, J.A. and M.W.Hetzer. 2011. POM121 and Sun1 play a role in early steps of interphase NPC assembly. *J. Cell Biol.* **194**:27-37.

59. Tapley, E.C., N.Ly, and D.A.Starr. 2011. Multiple mechanisms actively target the SUN protein UNC-84 to the inner nuclear membrane. *Mol. Biol. Cell* **22**:1739-1752.

60. Timney, B.L., J.Tetenbaum-Novatt, D.S.Agate, R.Williams, W.Zhang, B.T.Chait, and M.P.Rout. 2006. Simple kinetic relationships and nonspecific competition govern nuclear import rates in vivo. *J. Cell Biol.* **175**:579-593.

61. Turgay, Y., R.Ungricht, A.Rothballer, A.Kiss, G.Csucs, P.Horvath, and U.Kutay. 2010. A classical NLS and the SUN domain contribute to the targeting of SUN2 to the inner nuclear membrane. *EMBO J.* **29**:2262-2275.

62. Tyson, C.B., P.G.Lord, and A.E.Wheals. 1979. Dependency of size of Saccharomyces cerevisiae cells on growth rate. *J. Bacteriol.* **138**:92-98.

63. van den Bogaart, G., A.C.Meinema, V.Krasnikov, L.M.Veenhoff, and B.Poolman. 2009. Nuclear transport factor directs localization of protein synthesis during mitosis. *Nat. Cell Biol.* **11**:350-356.

64. Wente, S.R. and M.P.Rout. 2010. The nuclear pore complex and nuclear transport. *Cold Spring Harb. Perspect. Biol.* **2**:a000562.

65. West, M., N.Zurek, A.Hoenger, and G.K.Voeltz. 2011. A 3D analysis of yeast ER structure reveals how ER domains are organized by membrane curvature. *J. Cell Biol.* **193**:333-346.

66. Winey, M., D.Yarar, T.H.Giddings, Jr., and D.N.Mastronarde. 1997. Nuclear pore complex number and distribution throughout the Saccharomyces cerevisiae cell cycle by three-dimensional reconstruction from electron micrographs of nuclear envelopes. *Mol. Biol. Cell* **8**:2119-2132.

67. Worman, H.J. and J.C.Courvalin. 2000. The inner nuclear membrane. *J. Membr. Biol.* **177**:1-11.

68. Wu, W., F.Lin, and H.J.Worman. 2002. Intracellular trafficking of MAN1, an integral protein of the nuclear envelope inner membrane. *J. Cell Sci.* **115**:1361-1371.

69. Yang, Q., M.P.Rout, and C.W.Akey. 1998. Three-dimensional architecture of the isolated yeast nuclear pore complex: functional and evolutionary implications. *Mol. Cell* **1**:223-234.

70. Yavuz, S., R.Santarella-Mellwig, B.Koch, A.Jaedicke, I.W.Mattaj, and W.Antonin. 2010. NLS-mediated NPC functions of the nucleoporin Pom121. *FEBS Lett.* **584**:3292-3298.

71. Yewdell, W.T., P.Colombi, T.Makhnevych, and C.P.Lusk. 2011. Lumenal interactions in nuclear pore complex assembly and stability. *Mol. Biol. Cell* **22**:1375-1388.

72. Zuleger, N., D.A.Kelly, A.C.Richardson, A.R.Kerr, M.W.Goldberg, A.B.Goryachev, and E.C.Schirmer. 2011. System analysis shows distinct mechanisms and common principles of nuclear envelope protein dynamics. *J. Cell Biol.* **193**:109-123.

73. Zuleger, N., A.R.Kerr, and E.C.Schirmer. 2012. Many mechanisms, one entrance: membrane protein translocation into the nucleus. *Cell Mol. Life Sci.*

74. Zuleger, N., N.Korfali, and E.C.Schirmer. 2008. Inner nuclear membrane protein transport is mediated by multiple mechanisms. *Biochem. Soc. Trans.* **36**:1373-1377.

Chapter 7

The transport of integral membrane proteins across the nuclear pore complex in perspective

- Conclusions and discussion -

This chapter is based on a manuscript in press: The transport of integral membrane proteins across the nuclear pore complex. *Nucleus.* 2012.

Abstract

Specific membrane proteins destined for the inner nuclear membrane (INM) are actively transported across the nuclear pore complex (NPC). A long intrinsically-disordered linker attached to these proteins is essential to position the Kap-bound nuclear localization signal (NLS) in the central channel of the NPC while the transmembrane domain is in the pore membrane. This means that the linker dodges into the scaffold of the NPC and implies the existence of lateral gates connecting the space aligning the pore membrane and the central channel. We discuss here that the need for lateral gates is not in contradiction with existing data but merely conflicts with the many cartoons drawn of the NPC. We also discuss that the charge in the intrinsically disordered linker might promote the passage through the lateral gates. Although this import pathway seems to be conserved in other species, membrane proteins other than Heh1 and Heh2 that are actively targeted to the INM, have so far not been found in a genome wide screen in yeast. The specific function of the studied proteins, Heh1 and Heh2, may require high nuclear accumulation without intranuclear retention. We speculate that Heh1 and Heh2 might be involved in defining the orientation of the NPC during the assembly of new NPCs.

Introduction

The nuclear envelope (NE) segregates the content of the nucleus from the cytoplasm in eukaryotes, and thus separates the sites of DNA-replication and transcription from that of translation. This enables a higher degree of regulation of these processes than present in prokaryotes, and is likely needed to maintain the complexity of a eukaryotic cell (Field and Dacks, 2009). As a consequence of the compartmentalization, an efficient mechanism for selective transport between cytoplasm and nucleus is required. All this transport is mediated by the nuclear pore complexes (NPCs), which are embedded in the double membranes of the nuclear envelope. The NPC has indeed an important role in fundamental cellular processes, like the regulation of gene expression and signal transduction (Chen and Thorner, 2007;Johnson *et al.*, 2004).

The selectivity of the nuclear transport resides in the presence of a nuclear localization signal (NLS) or a nuclear export signal (NES) on cargo proteins. Only proteins destined for the nucleus feature an NLS, while proteins exported out of the nucleus feature an NES. Those signals are recognized by transport factors, which are collectively called karyopherins (Kaps, or importins in mammals). Cargo featuring the classical SV40 NLS (Dingwall and Laskey, 1991) is imported into the nucleus by two Kaps. The yeast Kap60 (Kapα) binds the classical NLS on the cargo molecule. Kap95 (Kapβ) in turn, interacts with the NPC-components in the central channel (FG-Nups), while associated with the Kap60-cargo complex. At the nuclear side of the NPC, the complex is dissociated in the presence of RanGTP. As such, the cargo is delivered to the nucleus and the Kaps are shuttled back to the cytoplasm and made available for the next round of transport (reviewed in (Stewart, 2007)).

Similar to soluble proteins, membrane proteins destined for the INM, like the yeast Heh1/Src1 and Heh2 bear an NLS and need karyopherin for selective transport ((King *et al.*, 2006) and chapter 3). We conclude that during translocation across the pore, the transmembrane segment remains in the membranes while the NLS-bound karyopherin interacts with the FG-Nups in the central channel of the NPC (chapter 4). A long and flexible linker between the NLS and the transmembrane helix allows the NLS-bound karyopherins to scavenge for FG-Nups within the NPC (chapter 4). Consequently, the linker will slice through the scaffold of the NPC, utilizing the proposed lateral gates, which likely exist between the spokes of the NPC (chapters 4 and 6). In this thesis, we conclude that the transport of soluble cargo across the NPC is fast relative to transport of membrane proteins. We measured *in vivo* a flux of actively transported soluble proteins, such as GFP fused to a tandem of the classical NLS (GFP-tcNLS), of 30 – 50 molecules/(NPC·s), when the cargo protein is expressed at 10^5 copies per cell (chapter 2 and 6). The flux of membrane proteins actively transported over the NPC was significant smaller, and amounted to ~ 0.1 molecules/NPC·s when estimated at a level of expression that was ~10-fold lower than for GFP-tcNLS. Thus, we conclude that the transport rate of soluble cargo is an order of magnitude faster than that of membrane proteins, if corrected for the copy number (as discussed in chapter 6). This may reflect the dodging of the linker into the scaffold, a thermodynamically unfavorable step (as discussed in chapters 4 and 6). Alternatively, it is possible that the higher viscosity of the membranes, as compared to the (crowded) aqueous environment of the cytosol and nucleus, causes the slower transport.

Nuclear import and efflux

In a living cell, soluble and membrane cargo are actively imported into the nucleus and the naked cargo (after the Kaps are stripped off in the nucleus) can leak back to the cytoplasm. All nuclear import and export plus the diffusion of soluble and membrane proteins occurs via the NPC. The NPC is clearly a crowded intersection for traffic between the cytoplasm and the nucleus. One could argue that traffic is slowed down at such congestion sites and cargo molecules may have to wait for another. On the basis of the diffusion coefficient of GFP in the cytoplasm (chapter 6), we estimate that soluble GFP could travel the distance of the 100 – 200 nm long channel in the NPC within 3 – 5 ms. The facilitated diffusion of cargo across the NPC is 3 – 6× slower than the 3D Brownian diffusion in the cytoplasm; the hindered diffusion of non-cargo is even >30× slower (Cardarelli and Gratton, 2010;Yang *et al.*, 2004), which suggests that the NPC is indeed a congestion point for traffic between the cytoplasm and nucleoplasm.

To evaluate the role of the high-affinity NLS in nuclear transport, as was found in Heh1 and Heh2 (Chapter 3), we will try to deduce some "priority rules" for nuclear trafficking across the NPC. Nuclear transport can be described by a simple pump-leak model (Timney *et al.*, 2006): cargo is selectively pumped into the nucleus and can leak back down the concentration gradient, both via the NPC. The ratio of the import and efflux rate constants determines the steady-state level of nuclear accumulation. We consider the affinity of the Kaps for the NLS a key factor in determining the priority for transport through the NPC. Cargos bearing a high-affinity NLS will have a competitive advantage for binding a Kap and thus for entering the NPC.

We observed that membrane proteins need a high-affinity NLS for efficient accumulation in the INM (Fig. 3.9B). The high-affinity NLS assures strong interaction between the membrane protein and the Kaps (Fig. 3.9A). We reasoned that the high-affinity binding is needed to compete with other cargos for the available Kaps. This advantage in competition may compensate for the generally lower concentrations of membrane proteins as compared to soluble proteins. The copy number of membrane proteins in general, and Heh1 and Heh2 in particular (1250 – 2100 copies per cell (Ghaemmaghami *et al.*, 2003)) is low. Furthermore, we observed that the import of membrane proteins is at least an order of magnitude slower than that of soluble proteins (chapter 6); membrane proteins may thus spend more time in or at the NPC. Naked cargo present within the NPC can compete for the Kap60/95 and chase off karyopherins from proteins with a lower affinity NLS. Without a strong binding to the Kaps, a membrane protein might lose its Kaps to a more abundant soluble cargo while within the NPC. We infer that having a high-affinity NLS on membrane proteins ensures high concentrations in the nucleus, despite lower copy numbers and slower nuclear import compared to other cargos in the cell.

The transport of high abundant soluble cargo across the NPC has priority to non-cargo or naked cargo, which was shown in NPC mimics and modeling studies (Jovanovic-Talisman *et al.*, 2009;Zilman *et al.*, 2010). In fact the diffusion of cargo across the NPC is facilitated and diffusion of non-cargo is hindered (Peters, 2009). Thus, at the congestion points where cargo and non-cargo compete for the available space in the pore, the Kap-cargo has "right of way" because its affinity for the FG-Nups. The passive or hindered diffusion of naked cargo out of the nucleus across the NPC depends on the space available in the central channel of the NPC, which in turn is influenced by the amount of Kap-cargo that transits the pore. Thus, high affinity NLS-cargo would go before low-affinity NLS-cargo, and low-affinity NLS-cargo would go before naked cargo.

We conclude that any cargo having an NLS gets transported preferentially and that the priority is determined by the affinity of the Kap for the NLS. A high-affinity allows less well expressed cargos to compete with more abundant proteins having a lower affinity NLS. Modification of the NLS allows the affinity and thus the priority for transport to be regulated. Such rules of priority allow the transport across NPC to adapt to situations were more or less nuclear transport is needed, without losing the selectivity of the translocation reaction.

Membrane reporters stay in the membrane during transport

The nuclear transport of the membrane proteins Heh1 and Heh2 resembles that of soluble proteins: it requires RanGTP, Kaps and FG-Nups, and the NLS-encoding domain passes through the central channel (Chapter 3, 4 and (King *et al.*, 2006)). Therefore, we challenged the option that Heh1 and Heh2 might be translocated across the NPC like a soluble protein. There is a precedent for this possibility, as the membrane-anchored yeast spindle pole body protein Nbp1 is transported across the NPC as a soluble protein. Once the transport factor Kap123 is removed after transport into the nucleus, an amphipatic helix gets exposed to enable interaction with the INM (Kupke *et al.*, 2011).

We studied the nuclear transport pathway of Heh1 and Heh2 with the membrane reporter h2NLS-L-TM, having one transmembrane segment at the C-terminus. While polytopic membrane proteins are generally co-translationally integrated in the ER via the signal receptor particle (SRP) and Sec61 translocation pathway (reviewed in (Osborne *et al.*, 2005;Renthal, 2010;Stirling, 1999)), some tail-anchored membrane proteins use post-translational membrane insertion mechanism (reviewed in (Cross *et al.*, 2009;Renthal, 2010;Schuldiner *et al.*, 2008)). If the transmembrane domain is close to the C-terminus of the polypeptide, the translation is terminated before the SRP recognizes the hydrophobic element, and the protein dissociates from the ribosome. To insert the tail-anchored protein post-translationally into the ER, the hydrophobic transmembrane domain is shielded and stabilized by dimeric Get3 prior to insertion into the ER via the ER-localized membrane receptors Get1 and Get2 (Auld *et al.*, 2006;Mariappan *et al.*, 2011;Mateja *et al.*, 2009;Schuldiner *et al.*, 2008). Theoretically, Get1 and Get2 are small enough to diffuse across the NPC via the pore membrane and could facilitate the post-translational integration of the nuclear accumulated soluble h2NLS-L-TM directly into the INM. However, our data indicate first that h2NLS-L-TM is integrated in the ER and second that the nuclear transport across the NPC occurs via the pore membrane:

i) We trapped the reporter at Nsp1 within the NPC and could specifically block nuclear transport of membrane proteins (Fig. 4.13). Subsequently, we observed a steady concentration increase of newly synthesized h2NLS-L-TM specifically at the ER and not at the INM (Fig. 4.13A, B). We thus conclude that h2NLS-L-TM is integrated in the ER, alike the native Heh1 and Heh2.

ii) After h2NLS-L-TM is integrated in the ER, subsequent extraction from the membranes and re-insertion into the INM after nuclear transport as soluble proteins is very unlikely. The energy costs for displacing a transmembrane spanning segment from the membrane are high. The hydropathy estimates of Goldman-Engelman-Steitz (GES) or Kyte and Doolittle (KD) give a number for the energy associated with the transfer of each type of amino acid side-chain from oil to water (Fig. 7.1A, (Engelman *et al.*, 1986;Kyte and Doolittle, 1982)). The energic costs to extract the first transmembrane segment of Heh2, as was used in the reporter h2NLS-L-TM, are ~170 kJ/mol (Fig. 7.1B). The hydrolysis of ATP releases 30 – 50 kJ/mol (Alberts *et al.*, 2002); the extraction of one protein from the membrane would cost thus the equivalent of several ATPs. For the reporter fusions with Sec61, having 10 transmembrane spanning segments, it is even harder to imagine that they would be extracted from the ER/ONM membrane and inserted into the INM after translocation (as in Fig. 4.7C). Most of all, in the absence of solublizing or stabilizing agents, membrane proteins would aggregate once extracted from the membrane.

iii) Finally, the transport characteristics of soluble and membrane proteins are markedly different. We observed that the translocation of h2NLS-L-TM through the NPC is disrupted in a Nup170-deletion strain (Fig. 3.4B), similar as Heh2 (King *et al.*, 2006), while the transport of soluble cargo is not affected (Fig. 7.1C and (Shulga *et al.*, 2000)). Also the nuclear transport of membrane proteins is specifically dependent on particular FG-Nups (Fig. 4.9), h2NLS-L-TM thus utilizes a different import route than soluble cargos.

Altogether, we conclude that it is highly implausible that integral membrane proteins are transported to the nucleus as soluble cargo with the hydrophobic domain shielded during translocation and reinserted into INM after transport through the NPC.

A

Amino acid		$\Delta G_{oil \rightarrow water}$ (kJ/mol) GES	KD
Ala	A	6.7	7.5
Arg	R	-51.5	-18.8
Asn	N	-20.1	-14.7
Asp	D	-38.5	-14.7
Cys	C	8.4	10.5
Gln	Q	-17.2	-14.7
Glu	E	-34.3	-14.7
Gly	G	4.2	-1.7
His	H	-12.6	-13.4
Ile	I	13.0	18.8
Leu	L	11.7	15.9
Lys	K	-36.8	-16.3
Met	M	14.2	8.0
Phe	F	15.5	11.7
Pro	P	-0.8	-6.7
Ser	S	2.5	-3.3
Thr	T	5.0	-2.9
Trp	W	8.0	-3.8
Tyr	Y	-2.9	-5.4
Val	V	10.9	17.6

B

Reporter	# of TM segments	$\Delta G_{oil \rightarrow water}$ (kJ/mol) GES	KD
Heh1	2 of Heh1	315.3	378.1
Heh2	2 of Heh2	272.6	256.7
h2NLS-L-TM	First of Heh2	184.2	166.2
h2NLS-LR2(215)-WALP23	WALP23	202.6	193.0
h2NLS-LR1(138)-Sec61TM1	First of Sec61	162.4	194.7

C

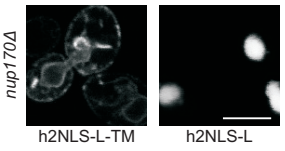

Figure 7.1: Transmembrane segments are not likely extracted from the membrane during nuclear transport. A) The high energy costs for the extraction of integral membrane proteins from the lipid bilayer. The hydropathy table showing the free energies (ΔG), needed to transfer amino acid side chains present in α-helices from the lipid bilayer (the oil phase) to the cytoplasm (the water phase), as estimated by Goldman-Engelman-Steitz (GES) or Kyte and Doolittle (KD) (Engelman *et al.*, 1986;Kyte and Doolittle, 1982). **B)** The calculated free energies (ΔG) needed to extract the all the transmembrane (TM) segments of the reporters from the lipid bilayer (the oil phase) to the cytoplasm (the water phase), based on the GES and KD estimates (A). **C)** Confocal fluorescence images in cells where Nup170 is knocked out (*nup170⊿*) show mislocalization of h2NLS-L-TM but the soluble h2NLS-L is accumulated in the nucleus. The scale bar is 5 μm.

The properties of the linker

The transmembrane domains thus remain in the pore membrane during the import of membrane proteins to the INM. The distance between the NLS and the transmembrane segment of Heh1 and Heh2 is spaced by a long and flexible linker of minimally 120 residues (Fig. 4.5C). We have shown that this linker is intrinsically disordered and exists in an extended conformation (Fig. 4.4). This is needed to allow the NLS-bound Kap60/95 to interact with the FG-Nups in the central channel of the NPC (Fig. 4.9 - 4.13). It has been shown that intrinsically-disordered domains can easily adopt a wide range of lengths (Galea *et al.*, 2008) and it will not cost much energy to stretch such a domain (Chapter 4, (Kriwacki and Yoon, 2011;Miyagi *et al.*, 2008)). We assume that stretching the linker is thermodynamically favored by the enthalpy gain from binding of NLS-bound Kap60/95 to the multiple FG-repeat binding sites in the central channel of the NPC. We replaced the native linker (L) for two randomized versions (LR1, LR2) and measured that the NE/ER-accumulation was not decreased (Fig. 4.5C). The linker length rather than its sequence is essential for nuclear transport. Since the randomized linkers LR1 and LR2 have the same amino acid composition as the native linker L, we cannot conclude if a particular amino acid composition is required for transport. The occurrence of specific amino acids can determine the flexibility and compactness of an intrinsically-unfolded domain: glutamic acid, serine and to some extent proline and aspartic acid can promote the formation of an extended coil, while asparagine and glycine and to some extent glutamine and threonine contribute to a more collapsed unfolded coil (Yamada *et al.*, 2010). We thus compared the composition of the linkers in Heh1 and Heh2 with compositions of the average *S. cerevisiae* proteins (Nakamura *et al.*, 2000). We found indeed that the linkers in Heh1 and Heh2 are relatively abundant in glutamic acid, serine and proline; the ratio of extended coil promoting residues over those favoring a collapsed coil (Ratio E/C) reveal

that both linkers contain more extended coil promoting residues than an 'average' yeast protein (Fig. 7.2A). Further, the linkers have a net negative charge and contain more charged residues than average. The transport efficiency plotted as the NE/ER ratio seems to correlate with the charge content of different linkers (Fig. 7.2B): we clustered the linkers with similar size and observe, particularly in the cluster with reporters having a ~180 residues long linker, that the import efficiency is higher when more charged residues are present in the linker. The charge content might be needed to stimulate the extended conformation by electric repulsion and/or to slice through the scaffold of the NPC. The overall negative charge might also prevent association with the negatively charged surface of the membranes; the ER and presumably the pore membrane contain a significant fraction of the anionic lipid phosphatidylserine.

We tried to make the linker less flexible and introduced stretches of 5-6 prolines, to promote the formation of a polyproline type II (PPII) helix in the linker. In helical polyproline type II conformations, the rise per residue in the helix is 3.1 Å, due to the trans-isomeric orientation of the peptide bond. This is similar to the spacing of 3.6 Å between neighboring Cα's in the backbone of proteins. The PPII helix thus promotes an extended conformation of the peptide. This secondary structure of the PPII helix is less flexible than a normal amino acid chain (Adzhubei and Sternberg, 1993;Stryer and Haugland, 1967). We measured the accumulation of the reporter with a linker of 34% (LP1) or 44% (LP2) proline residues and found a small but significant reduction in the import efficiency (Fig. 7.2C).

Owing to trans/cis isomerization of the polyproline helix into an polyproline type I (PPI) conformation, the linker can adapt a more collapsed conformation with a rise per residue in the helix of 1.9 Å (Doose *et al.*, 2007). Although the conversion from a PPII to PPI helix is thermodynamically unfavorable due to the more condensed conformation (Adzhubei and Sternberg, 1993), a subpopulation of the reporters might have stretches in the PPI conformation thereby affecting their effective linker length. Besides, the polyproline linkers have a lower content of glutamic acid and serine and an overall lower charge content, which might result in a more collapsed coil. The lower charge content might also reduce effective slicing of the linker between the Nups. Since we have not assessed the Stokes radii or flexibility of these linkers experimentally, we do not know if the reduced import efficiency is caused by lower flexibility, a lower overall charge of the linker or the formation of a more collapsed conformation (see future outlook).

Implications for the structure of the NPC

The intrinsically-disordered linkers between the NLS and TM in Heh1 and Heh2 are flexible, have a high content of charged residues and overall net negative charge, and as discussed above these properties may promote effective slicing through the scaffold of the NPC. However, in existing models, the scaffold of the NPC is depicted as a donut-shape composed of concentric rings. The lateral gates between the spokes or openings in the scaffold rings were never observed in EM-studies, but even the most detailed images of the NPC obtained by 3D EM-tomography may have too limited resolution to observe such features (~60 Å resolution (Beck *et*

A

Amino acid	Charge at pH 6	Propterties	Promote conformation	L (Heh2) n	L (Heh2) %	L (Heh1) n	L (Heh1) %	LR1 n	LR1 %	LR2 n	LR2 %	LP1 n	LP1 %	LP2 n	LP2 %	Average %
R	+	hydrophilic		8	4	7	3	7	4	9	4	6	3	6	3	4.4
D	-	hydrophilic	extended coil	11	6	11	5	12	7	15	7	10	5	7	4	5.8
K	+	hydrophilic	extended coil	19	11	17	7	19	11	23	11	11	6	9	5	7.3
E	-	hydrophilic	extended coil	25	14	26	11	25	14	31	14	18	10	16	9	6.5
N		hydrophilic	collapsed coil	10	6	17	7	10	6	12	6	8	4	7	4	6.1
Q		hydrophilic	collapsed coil	4	2	11	5	4	2	5	2	2	1	2	1	3.9
H	+	hydrophilic		4	2	6	3	3	2	3	1	2	1	2	1	2.1
Y		hydrophobic		1	1	0	0	1	1	1	0	1	1	1	1	3.4
P		hydrophobic	extended coil	13	7	19	8	13	7	15	7	62	34	80	44	4.4
S		hydrophilic		20	11	28	12	20	11	25	12	13	7	10	5	8.9
G			collapsed coil	5	3	15	6	6	3	7	3	4	2	3	2	5.1
T		hydrophilic	collapsed coil	13	7	16	7	12	7	15	7	8	4	6	3	5.9
A		hydrophobic		10	6	7	3	10	6	12	6	6	3	6	3	5.6
W		hydrophobic		0	0	0	0	0	0	0	0	0	0	0	0	1
C		hydrophobic		0	0	1	0	0	0	0	0	0	0	0	0	1.3
V		hydrophobic		7	4	17	7	8	4	10	5	8	4	6	3	5.7
L		hydrophobic		14	8	19	8	14	8	17	8	10	5	10	5	9.5
I		hydrophobic		10	6	7	3	9	5	10	5	9	5	8	4	6.5
M		hydrophobic		2	1	3	1	2	1	2	1	2	1	2	1	2.1
F		hydrophobic		4	2	7	3	3	2	3	1	3	2	2	1	4.5
				180	101	234	99	178	101	215	100	183	98	183	99	100
			Relative charge	-0.028 pAA		-0.030 pAA		-0.045 pAA		-0.051 pAA		-0.049 pAA		-0.033 pAA		0.015 pAA
			Charged residues	37 %		29 %		37 %		38 %		26 %		22 %		26 %
			Hydrophilic residues	63 %		59 %		63 %		64 %		43 %		36 %		51 %
			Ratio E/C	2.1		1.2		2.2		2.2		5		6.2		1.1

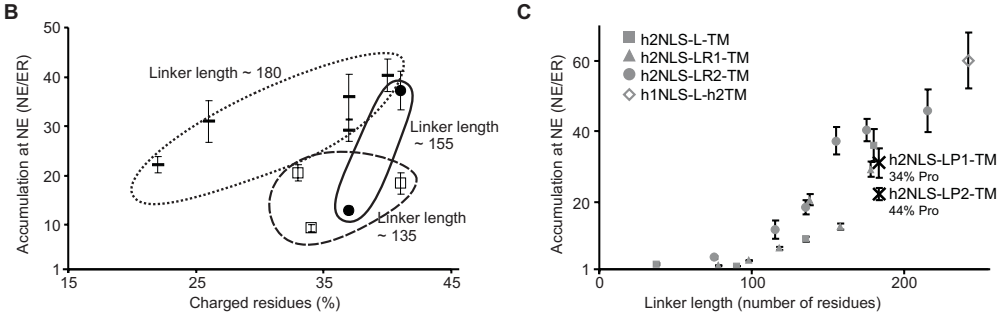

Figure 7.2: Presence of charge and extended coil promoting residues in the linker might be essential for nuclear membrane protein transport. A) The table shows the absolute (*n*) and relative (%) occurrence of the amino acids in the linkers (L) of Heh1 and Heh2, the randomized Heh2 linkers (LR1 and LR2), the Heh2 linker with 34% or 44% proline occurrence (LP1 and LP2) and in the average of yeast proteins (Nakamura *et al.*, 2000). The physical properties of the amino acids, like the charge under physiologic conditions in a yeast cell (at pH ~6 (Conway and Downey, 1950;Pena *et al.*, 1995), the hydrophobicity, and their contribution to form an extended or collapsed random coil, are listed. The relative charge is the total net charge of the peptide expressed per residue, the number of extended coil promoting residues per collapsed coil promoting residues is indicated as a ratio (Ratio E/C). **B)** Same as figure 4.5B (grey), showing the nuclear accumulation of reporters at the INM. The nuclear accumulation of h2NLS-LP1-TM and h2NLS-LP2-TM, having respectively 34% and 44% of the amino acids in the linker replaced for short stretches of 5 – 6 prolines, is plotted in the graph (black, ×). SEM is indicated. **(C)** The nuclear accumulation (NE/ER) of different reporters is plotted to percentage of charged residues (lysine, arginine, histidine, aspartic acid, glutamic acid) within the linker. The data points are clustered for reporters having a similar linker length. SEM is indicated.

al., 2007;Frenkiel-Krispin *et al.*, 2010)). Can we reconcile our transport model with current data describing the NPC structure? The model asks for flexibility between the spokes of the NPC and a modular construction without permanent interactions between the spokes. We will discuss recent literature to judge if there is any data contradicting the existence of lateral gates.

The structure and architecture of the NPC have been investigated intensively with electron microscopy (EM) (Akey and Radermacher, 1993;Beck *et al.*, 2007;Fahrenkrog and Aebi, 2003;Frenkiel-Krispin *et al.*, 2010). A model of the yeast NPC was made on the basis of a large array of experimental data and subsequent computational modeling (Alber *et al.*, 2007b;Alber *et al.*, 2007a;Cronshaw *et al.*, 2002;Rout *et al.*, 2000). In the EM-studies, the nuclear pore complex is

shown as a spoke-ring complex with an eight-fold rotational symmetry along the nucleocytoplasmic axis through the central channel and a two-fold symmetry in the plane of the membrane. The eight-fold rotational symmetry of the NPC, is based on a distinct electron density pattern of the spokes along the NPC (Gall, 1967;Hinshaw *et al.*, 1992). In both the vertebrate and yeast NPC, one can clearly observe that the protein density is lower between the spokes (Fig. 7.3A, B, adapted from (Yang *et al.*, 1998)). These EM-studies also revealed a high structural plasticity within the NPC. The NPCs can differ in in their radial size and occasionally NPCs with more than eight spokes were seen (Hinshaw and Milligan, 2003). The radial flexibility in the NPC became further obvious from the observed size differences of single spokes within one NPC, causing asymmetric octagonals (Beck *et al.*, 2007;Frenkiel-Krispin *et al.*, 2010). The variation in spokes sizes was explained by spoke compaction and extension or changing distances between spokes. This might be needed to facilitate the transport of large particles across the NPC and allows dilation or shrinkage of the complex (Akey, 1995;Pante and Kann, 2002). Consistent with flexibility between the spokes, sliding modules were shown within the NPC scaffold. Antiparallel oriented α-helical hairpins in different Nups alternating their hydrogen bond network to enable iris-like adjustments of the NPC were proposed (Melcak *et al.*, 2007). These publications show that the NPC is not static or rigid at all, but has radial flexibility, resulting from dynamics between the spokes.

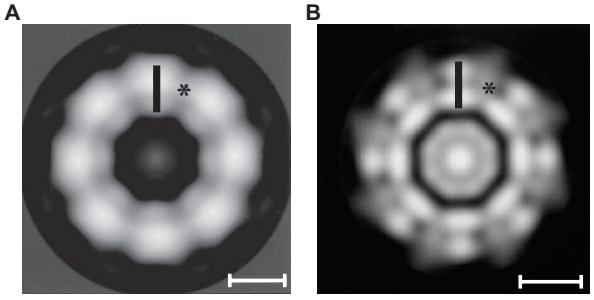

Figure 7.3: The distinct spokes are clearly visible in electron microscopic images of the vertebrate and yeast NPC. A) Electron microscopic image of a plane through the vertebrate NPC, perpendicular on the nucleoplasmic axis, adapted with permission from (Yang *et al.*, 1998). The distinct pattern of alternating high (|) and low (*) protein density along the scaffold of the pore, mark the spokes. **B)** Similar as (A) but for the yeast NPC. Scale bar is 30 nm, image is adapted with permission from (Yang *et al.,* 1998).

What do we actually know about the interactions between the spokes? From the architectural model of the yeast NPC we learn that the scaffold is composed of two equal outer and two equal inner rings at the cytoplasmic and nucleoplasmic sides. The outer rings in yeast is formed by an 8-fold arrangement of a subcomplex of 7 proteins, called the Nup84 complex and consists of Nup133, Nup120, Nup85, Nup84, Nup145N, Sec13 and Seh1. The inner rings consist of a complex of 4 proteins, i.e. Nup157, Nup170, Nup188 and Nup192. These rings, together with the membrane Nups, Pom152, Pom34 and Ndc1, form the structural core or the scaffold of the NPC (Alber *et al.*, 2007b). The scaffold provides stability to the NPC and maintains the sharply curved bending in the pore membrane (Devos *et al.*, 2004). The FG-Nups, which facilitate the transport, are attached to the inner side of the scaffold, facing the central channel. All the 8 spokes are similar in composition and each consists of different subcomplexes, indicating a modular architecture of the NPC. But are the subcomplexes of different spokes connected to each other within rings or not? The existence of stable subcomplexes was biochemically dem-

onstrated in recent years: (i) the 400 Å long and Y-shaped Nup84 complex of the outer rings is stable and could be isolated as intact single heptamers and visualized by 2D-EM (Lutzmann *et al.*, 2002;Siniossoglou *et al.*, 2000). There is no evidence that these Nup84 complexes have a tendency to oligomerize, which would have been indicative for spoke-to-spoke interactions via the Nup84 complexes. (ii) The Nsp1-complex, the Nup60-Nup2 dimer and the Nup82 complex are small subcomplexes containing FG-Nups (Hurwitz *et al.*, 1998;Grandi *et al.*, 1993;Dilworth *et al.*, 2001). These small complexes are localized in the central channel and interactions with complexes in the neighboring spokes are not reported. (iii) The Ndc1 complex is an assembly with two other membrane proteins, Pom152 and Pom34, and it is inserted in the pore membrane to anchor the NPC (Onischenko *et al.*, 2009). These membrane proteins form distinct patches in the membrane, Ndc1 and Pom34 have regions located at the pore side of the membrane, whereas the Pom152 domains reach the lumen of the NE and form a stable ring structure around the NPC (Alber *et al.*, 2007b;Alber *et al.*, 2007a). In fact, of all the Nups, only Pom152 forms a continuous ring by homotypic interactions of the lumenal domains (Strambio-de-Castillia *et al.*, 1995). These lumenal rings will obviously not affect the movement of the linker since they exist at the other side of the pore membrane in the lumen of the NE. (iv) Recently, Nup170/157 and Nup192/188 of the inner rings were purified from the eukaryotic thermophile *Chaetomium thermophilum* and *in vitro* reconstituted as a subcomplex (Amlacher *et al.*, 2011). Flexible interactions were shown with the Ndc1 complex on one side and via the linker Nups Nic96 and Nup53 with the Nsp1 subcomplex on the other side. The inner ring complex thus connects the membrane anchor with the FG-Nups, which allows the FG-repeat filaments to protrude into the central channel.

Collectively, these studies show that: A) the NPC forms a modular architecture of different subcomplexes within each spoke. B) Several subcomplexes are stable and can be isolated or reconstituted, and they do not need other interactions for their own stability. C) There is no data that points to stable spoke-to-spoke interactions. D) The subcomplex of Nup170/157 and Nup192/188 bridges the membrane proteins with FG-Nups. The stability of one such spoke seems to be formed by interactions within the spoke. We judge that the available data on the structure of the NPC does not contradict the proposed lateral gates that connect the space close to the pore membrane and the central channel. It is mostly the cartoons (and descriptions) of the NPC that have suggested a solid scaffold structure built of continuous rings.

Screen of INM-proteins

The NPC with its modular composition and high flexibility is fit to allow the nuclear transport of membrane proteins. But how many proteins in yeast make use of this pathway? To answer this question, we searched the entire yeast genome for more INM-targeted integral membrane proteins having the appropriate targeting signal including a linker domain (Chapter 4). The targeting consensus consists of an NLS spaced from the first (or last) transmembrane helix by an intrinsically-unfolded linker. We defined the components of the consensus as the parameters in our screen as follows:

We searched for proteins having a putative classical NLS sequence by simply looking for at least 3 positive residues in a row (K, R). This prediction is based on the 'pat4' definition as is used in the protein localization predictor PSORTII (Nakai and Horton, 1999), where minimally 3 out of 4 residues are positively charged. Although Heh1 and Heh2 contain high-affinity NLSs, we observed that less strong NLSs could target membrane proteins to the INM, but at lower efficiency (Fig. 3.9B). Thus, we chose to search with the minimal definition of an NLS to avoid missing INM targeted proteins.

The linker (L) between the NLS and the first transmembrane segment was defined to be minimally 80 and maximally 250 residues long and unfolded over at least 80 residues. Although our data on the Heh2-based reporters suggest that the linker is at least 120 residues long (Fig. 4.5C), we searched a somewhat wider range of linker lengths. The position of the transmembrane segment in the protein was predicted by the TMHMM server v.2 (Krogh *et al.*, 2001). The polypeptide counted as disordered when it scored negative for the foldability in a sequence of >80 residues in the linker, as was calculated with FoldIndex© (Prilusky *et al.*, 2005). The orientation of the protein, also predicted by the TMHMM server v.2, must be such that the NLS points into the cytoplasm/nucleoplasm instead of the lumen of the ER. The option that the NLS is present between two transmembrane segments was allowed in the search, but only if it had a sufficiently long linker at both sides of the NLS and the appropriate orientation.

The script, custom made in Python 3.3.2 (Ghandi, T. unpublished data), identified 35 proteins out of a total of 5749 (verified and uncharacterized) translated open reading frames in the *Saccharomyces* genome database (www.yeastgenome.org) that met our criteria, including Heh1 and Heh2. To determine if these NLS-linker (NLS-L) domains comprised genuine targeting, we amplified the coding sequences of the putative NLS-L from the yeast genome and cloned them in an expression vector in front of the coding sequence of the Heh2 transmembrane segment (h2TM) (Hapsari, RA; Kralt, A; Laba, JK; Meinema, AC; unpublished data). In the cases where more regions of positive residues were present in a protein at the appropriate distance from a transmembrane segment, more sequences with different length were amplified from the same gene. In total, we cloned 45 putative NLS-L coding sequences. We expressed the constructs with a C-terminal NLS (L-NLS) after an inversed version of h2TM. The amino acid sequence of the transmembrane segment was inversed to have the orientation of construct in the membranes of the ER such that the NLS is present at the cytoplasmic/nucleoplasmic side. We expressed these constructs in yeast and measured the localization with confocal microscopy. 38 of the putative NLS-L domains expressed well in yeast and just 3 of these reporters showed distinct nuclear accumulation, in addition to those of Heh1 and Heh2. However, the nuclear accumulation was not strong (NE/ER ~ 5 – 8 ×) and only visible after a very long induction period of 15 – 18 hours and only in a subset of cells. To test if the nuclear accumulation was specific and Kap-dependent, we depleted the strains of Kap95, but we did not see significant nuclear efflux within 1 – 2 hours. The nuclear accumulation was thus Kap95-independent and likely not caused by selective nuclear targeting. All together, we conclude that the nuclear accumulation of these reporters was an artifact, likely caused by random aggregation at the NE. Among the reporters that did not ex-

press well, were many reporters with the NLS at the C-terminus and fused to the inverted Heh2 transmembrane segment. These constructs were likely not properly inserted into the membrane and possibly among them there are proteins that are imported to the INM alike Heh1 and Heh2. Particularly, Nur1, which is localized at the INM and has a confirmed NLS would be a clear candidate (Fig. 7.4, (Mekhail *et al.*, 2008;King *et al.*, 2006)). Possibly the picture will change with better search criteria and after solving the expression problems.

Other membrane proteins at the INM

Although we did not find other INM-localized proteins that are actively targeted to the INM in yeast, recently three candidates were found in other organisms. For the human Pom121 and Sun2 and the *Caenorhabditis elegans* Unc-84, it was shown that these proteins localize at the INM and that the transport across the NPC to the INM is dependent on an NLS, similar to Heh1

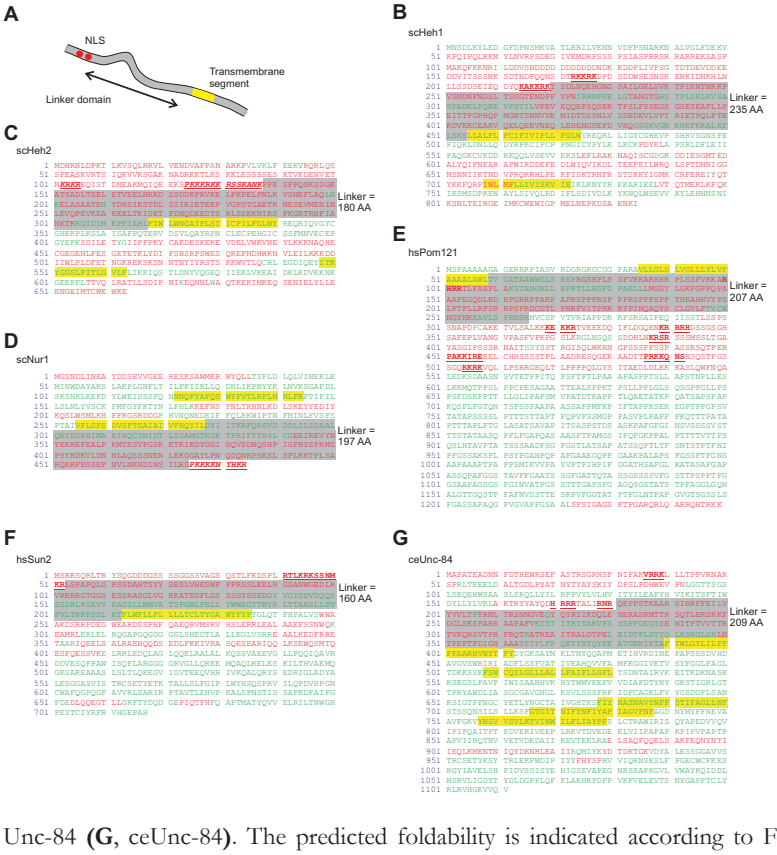

Figure 7.4: Eukaryotic proteins with putative NLS-L-TM configuration. A) Representation of the NLS-L-TM configuration within a membrane protein, having at one end the NLS (red dots), the other end the transmembrane segment (yellow) and a linker domain (gray) in between. The NLS-L-TM configurations are indicated in respectively the yeast Heh1 **(B**, scHeh1**)** and Heh2 **(C**, scHeh2**)** and predicted for respectively the yeast Nur1 **(D**, scNur1**)**, the human Pom121 **(E**, hsPom121**)**, the human Sun2 **(F**, hsSun2**)** and the *Caenorhabditis elegans* Unc-84 **(G**, ceUnc-84**)**. The predicted foldability is indicated according to FoldIndex© (Prilusky *et al.*, 2005), where the disordered segments are red and folded segments green. The NLS, as predicted by PSORTII (Nakai and Horton, 1999) and experimentally determined(Funakoshi *et al.*, 2011;Turgay *et al.*, 2010;Yavuz *et al.*, 2010;Tapley *et al.*, 2011;Mekhail *et al.*, 2008;Tapley *et al.*, 2011), is bold and underlined; the transmembrane segments, as predicted by the TMHMM server v.2 (Krogh *et al.*, 2001), is highlighted yellow; the linker between the NLS and transmembrane segment is highlighted gray and its length is indicated.

and Heh2 (King *et al.*, 2006). Pom121 and Sun2 have a clear bipartite NLS, interact with Kapβ via Kapα and their INM-localization was dependent on RanGTP (Funakoshi *et al.*, 2011;Turgay *et al.*, 2010;Yavuz *et al.*, 2010). The localization of the Sun protein Unc-84 was partly dependent on the presence of two stretches of cNLS segments (Tapley *et al.*, 2011). More proteins have been observed at the INM, but their accumulation is thought to be driven by binding to nuclear structures, like the lamina (Malik *et al.*, 2010;Soullam and Worman, 1995). The three INM-localized proteins Pom121, Sun2 and Unc-84 share no identity at the amino acid level with Heh1, Heh2 and Nur1, but they do share the 'NLS-L-TM'-feature (Fig. 7.4). The region between the NLS and the first transmembrane helix is predicted to be mainly unfolded in these proteins (Prilusky *et al.*, 2005), and the linker domains are long enough for nuclear targeting (>120 residues). Based on these considerations, we infer that these mammalian membrane proteins may well be targeted to the INM according to the model we have presented for the transport of Heh1 and Heh2 (Fig. 4.14).

Roles of Heh1 and Heh2

Although the transport mechanism for membrane proteins across the NPC might be conserved among different species, we could not confirm the 'NLS-L-TM'-feature for other yeast proteins. We thus wondered why this feature could be specific for Heh1 and Heh2. Likely many INM-localized proteins do not have an NLS and diffuse across the NPC via the lateral channels to accumulate in the INM by specific interactions with intranuclear structures (Chapter 1). Heh2 does not accumulate in the INM without an NLS (King *et al.*, 2006), although it is immobilized at the INM (Chapter 3). The NLS in Heh1 and Heh2 is clearly essential for accumulation in the nucleus and promotes a high concentration at the INM (Chapter 3). We discussed in this chapter that the high affinity NLS might be needed to assure these high nuclear concentrations in a competitive environment, while the protein is low abundant and its transport is less efficient. The functions of Heh1 and Heh2 might require a strong nuclear accumulation. However, their exact function is not well described. Heh1 and Heh2 are homologues of the mammalian proteins Man1 and Lem2 (Fig. 1.2), which are members of the LEM-domain containing family (Lap2, Emerin, Man1) (King *et al.*, 2006;Lin *et al.*, 2000). The well-conserved LEM and Man1 homology domains, which are present respectively at the N- and C-termini of Heh1 and Heh2 (Chapter 1), bind DNA, chromatin binding factors or the lamina in metazoans (Gruenbaum *et al.*, 2005;Mans *et al.*, 2004). The function of Heh1 is related to chromatin organization, regulation of gene expression and genome stability (Grund *et al.*, 2008;Mekhail *et al.*, 2008;Rodriguez-Navarro *et al.*, 2002). Recently, it was shown that both Heh1 and Heh2 contribute at discrete and different steps to the initiation of the assembly of new NPCs (Yewdell *et al.*, 2011). It was suggested that Heh1 could form a lumenal bridge with the pore membrane protein Pom152 and would function in the formation of the NPCs inner ring, while Heh2 could have a role in the formation of the outer ring. If Heh1 and Heh2 are indeed responsible for the initiation of the NPC assembly, than the strong accumulation at the INM might be essential to determine the orientation of the NPC in the NE. Heh1 and Heh2 accumulated in the nucleus could mark the INM and assure initiation of NPC formation at the correct membrane of the NE. Leaving a significant portion of Heh1 and

Heh2 at the ONM could theoretically lead to the start of NPC assembly at the wrong side of the NE, resulting in non-functional NPCs. The strong nuclear accumulation of Heh2 is not achieved by nuclear retention without an NLS; thus the intranuclear interactions of Heh1 and Heh2 to chromatin are likely not strong enough. We speculate that the membrane proteins need to diffuse within the INM to define new sites for pore formation. The nuclear accumulated Heh1 and Heh2 might thus form a docking site for other components of the NPC and the formation of the large complexes of pre-pores might prevent the nuclear efflux of Heh1 and Heh2.

Future outlook

In this thesis, we studied the transport of integral membrane proteins across the NPC between the ONM and the INM. We present a new model explaining how this transport mechanistically occurs. The importance of the long and intrinsically-disordered linker domain between NLS and TM in integral membrane proteins was highlighted. The model also sheds new light on the architecture of the NPC. Many new questions have arisen due to this work and we will propose a few future directions of which some are currently pursued.

A corollary of our model is that lateral gates must exist between the spokes in the NPC-scaffold. Two experiments could confirm this hypothesis: in the first, one could try to cross-link the outer ring subunits with each other and then probe transport efficiency of h2NLS-L-TM across the NPC. In a second experiment, the reporter protein would have to be expressed first, followed by cross-linking of the subunits of the outer ring and measurement of nuclear efflux in the Kap95 depletion assay. The cross-linked outer rings would close the lateral gates and strongly reduce the nuclear accumulation in experiment 1 and nuclear efflux in experiment 2. Such data would be consistent with the existence of lateral gates. The subunits could be cross-linked with the FRBP-Rap-FRB technique (Haruki *et al.*, 2008).

As discussed in this chapter, the linker is expected to slice between the spokes through the lateral gate of the NPC. The linkers in Heh1 and Heh2 are more charged than average. We wonder if the relatively high charge (and/or the reduced hydrophobicity) in the linker would promote slicing of the linker through the scaffold of the NPC. I first propose to model the known X-ray structures of the Nup84-complex components in the observed Y-shape (as done before (Hoelz *et al.*, 2011)) and plot the distribution of charge and hydrophobicity on the surface of the entire complex. Since the entire Y-shaped complex could be isolated and was stable in a hydrophilic environment, I expect that the surface of the subunit is hydrophilic and likely charged, while the contact sites between the Nups in the subcomplex might be hydrophobic. Electrostatic stabilization of the linker between the subunits of the spokes might favor the dodging of the linker domain into the scaffold of the NPC. To study the role of the charge in the linker domain for the passage of membrane proteins across the NPC, I propose to replace the native linker for a zwitterionic linker, one with positive charges and one without charges. However, changing the charge in an unfolded region may change the Stokes radius or compactness. It is thus important to make the linker long enough to maintain the distance between the NLS and TM and measure the Stokes radius of the linkers used.

By size-exclusion chromatography and NMR, it was shown that the linker domain is intrinsically unstructured and adopts an extended coil conformation. The linker might thus be highly flexible (Chapter 3). We tried to reduce the flexibility and introduced polyproline patches separated by small fragments of the native linker. This data was difficult to interpret, because we did not know how these regions would arrange with respect to each other or if the linker would form a PPI conformation (see above). The Stokes radius of the linker would in both cases be reduced causing a reduced import efficiency. We have observed that beyond 180 residues the contribution of the linker length to transport efficiency is negligible. Therefore I propose to add a long stretch of 30 – 50 consecutive prolines to the linker and keep the total linker length ~220 residues long. The linker will be kept long enough, so that a possible increased compactness of the polyproline stretch (into e.g. PPI-conformation) will not influence transport significantly. I propose to add the stretch of prolines immediately adjacent to the first transmembrane segment, to study the effect of flexibility of slicing the pore and to add the prolines immediately adjacent to the NLS to study the effect of flexibility and dynamics of the linker within the central channel. Less intramolecular dynamics of the linker might reduce the freedom of the NLS-bound Kaps to interact efficiently with the FG-Nups and reduce the import efficiency. A linker with 30 – 50 prolines might be difficult to express and handle. The longest polyproline linker, expressed in cells, was up to 15 residues, as far as we know (Arora *et al.*, 2002). The expression and stability of the reporter having such a long PPII linker must thus be carefully checked. Furthermore, the three dimensional organization of such a long PPII linker is unknown, and it thus needs to be purified and analyzed by biophysical methods.

Finally, in the genomic screen of yeast we did not find proteins other than Heh1 and Heh2 that are actively transported to the INM. In higher eukaryotes, three more proteins have been found, Pom121, Sun2 and Unc-84 (Funakoshi *et al.*, 2011;Tapley *et al.*, 2011;Turgay *et al.*, 2010;Yavuz *et al.*, 2010). To confirm that the nuclear transport of these membrane proteins in metazoans is according to our model, we propose to express the yeast reporter h2NLS-L-TM in mammalian cells and study its localization with microscopy. We expect that it will accumulate at the INM in a Kapα and Kapβ dependent manner, and its localization at the INM will be dependent on the presence of the unfolded linker. Furthermore, we would like to express the NLS-L-TM of Pom121 in mammalian cells and replace the linker for a randomized linker and truncate the linker to prove that the linker in higher eukaryotes is also essential.

We expect that the elucidation of the mechanism of membrane protein transport from the ER to the INM will provide further insights in the architecture of the NPC and the function of the NE. Now that Heh1 and Heh2 seem involved in the assembly of the NPC, our model might contribute to a further understanding of the biogenesis of the nuclear pores.

Acknowledgements

We thank T. Ghandi, R.A. Hapsari, A. Kralt, J.K. Laba for the collaboration on the screen for putative INM proteins in yeast.

References

1. Adzhubei, A.A. and M.J.Sternberg. 1993. Left-handed polyproline II helices commonly occur in globular proteins. *J. Mol. Biol.* **229**:472-493.
2. Akey, C.W. 1995. Structural plasticity of the nuclear pore complex. *J. Mol. Biol.* **248**:273-293.
3. Akey, C.W. and M.Radermacher. 1993. Architecture of the Xenopus nuclear pore complex revealed by three-dimensional cryo-electron microscopy. *J. Cell Biol.* **122**:1-19.
4. Alber, F., S.Dokudovskaya, L.M.Veenhoff, W.Zhang, J.Kipper, D.Devos, A.Suprapto, O.Karni-Schmidt, R.Williams, B.T.Chait, M.P.Rout, and A.Sali. 2007a. Determining the architectures of macromolecular assemblies. *Nature* **450**:683-694.
5. Alber, F., S.Dokudovskaya, L.M.Veenhoff, W.Zhang, J.Kipper, D.Devos, A.Suprapto, O.Karni-Schmidt, R.Williams, B.T.Chait, A.Sali, and M.P.Rout. 2007b. The molecular architecture of the nuclear pore complex. *Nature* **450**:695-701.
6. Alberts, B., A.Johnson, J.Lewis, M.Raff, K.Roberts, and P.Walter. 2002. Molecular Biology of the Cell. Garland Science, New York.
7. Amlacher, S., P.Sarges, D.Flemming, N.van, V, R.Kunze, D.P.Devos, M.Arumugam, P.Bork, and E.Hurt. 2011. Insight into structure and assembly of the nuclear pore complex by utilizing the genome of a eukaryotic thermophile. *Cell* **146**:277-289.
8. Arora, P.S., A.Z.Ansari, T.P.Best, M.Ptashne, and P.B.Dervan. 2002. Design of artificial transcriptional activators with rigid poly-L-proline linkers. *J. Am. Chem. Soc.* **124**:13067-13071.
9. Auld, K.L., A.L.Hitchcock, H.K.Doherty, S.Frietze, L.S.Huang, and P.A.Silver. 2006. The conserved ATPase Get3/Arr4 modulates the activity of membrane-associated proteins in Saccharomyces cerevisiae. *Genetics* **174**:215-227.
10. Beck, M., V.Lucic, F.Forster, W.Baumeister, and O.Medalia. 2007. Snapshots of nuclear pore complexes in action captured by cryo-electron tomography. *Nature* **449**:611-615.
11. Cardarelli, F. and E.Gratton. 2010. In vivo imaging of single-molecule translocation through nuclear pore complexes by pair correlation functions. *PLoS. One.* **5**:e10475.
12. Chen, R.E. and J.Thorner. 2007. Function and regulation in MAPK signaling pathways: lessons learned from the yeast Saccharomyces cerevisiae. *Biochim. Biophys. Acta* **1773**:1311-1340.
13. Conway, E.J. and M.Downey. 1950. pH values of the yeast cell. *Biochem. J.* **47**:355-360.
14. Cronshaw, J.M., A.N.Krutchinsky, W.Zhang, B.T.Chait, and M.J.Matunis. 2002. Proteomic analysis of the mammalian nuclear pore complex. *J. Cell Biol.* **158**:915-927.
15. Cross, B.C., I.Sinning, J.Luirink, and S.High. 2009. Delivering proteins for export from the cytosol. *Nat. Rev. Mol. Cell Biol.* **10**:255-264.
16. Devos, D., S.Dokudovskaya, F.Alber, R.Williams, B.T.Chait, A.Sali, and M.P.Rout. 2004. Components of coated vesicles and nuclear pore complexes share a common molecular architecture. *PLoS. Biol.* **2**:e380.
17. Dilworth, D.J., A.Suprapto, J.C.Padovan, B.T.Chait, R.W.Wozniak, M.P.Rout, and J.D.Aitchison. 2001. Nup2p dynamically associates with the distal regions of the yeast nuclear pore complex. *J. Cell Biol.* **153**:1465-1478.
18. Dingwall, C. and R.A.Laskey. 1991. Nuclear targeting sequences--a consensus? *Trends Biochem. Sci.* **16**:478-481.
19. Doose, S., H.Neuweiler, H.Barsch, and M.Sauer. 2007. Probing polyproline structure and dynamics by photoinduced electron transfer provides evidence for deviations from a regular polyproline type II helix. *Proc. Natl. Acad. Sci. U. S. A* **104**:17400-17405.
20. Engelman, D.M., T.A.Steitz, and A.Goldman. 1986. Identifying nonpolar transbilayer helices in amino acid sequences of membrane proteins. *Annu. Rev. Biophys. Biophys. Chem.* **15**:321-353.
21. Fahrenkrog, B. and U.Aebi. 2003. The nuclear pore complex: nucleocytoplasmic transport and beyond. *Nat. Rev. Mol. Cell Biol.* **4**:757-766.
22. Field, M.C. and J.B.Dacks. 2009. First and last ancestors: reconstructing evolution of the endomembrane system with ESCRTs, vesicle coat proteins, and nuclear pore complexes. *Curr. Opin. Cell Biol.* **21**:4-13.
23. Frenkiel-Krispin, D., B.Maco, U.Aebi, and O.Medalia. 2010. Structural analysis of a metazoan nuclear pore complex reveals a fused concentric ring architecture. *J. Mol. Biol.* **395**:578-586.
24. Funakoshi, T., M.Clever, A.Watanabe, and N.Imamoto. 2011. Localization of Pom121 to the inner nuclear membrane is required for an early step of interphase nuclear pore complex assembly. *Mol. Biol. Cell* **22**:1058-1069.
25. Galea, C.A., A.Nourse, Y.Wang, S.G.Sivakolundu, W.T.Heller, and R.W.Kriwacki. 2008. Role of intrinsic flexibility in signal transduction mediated by the cell cycle regulator, p27 Kip1. *J. Mol. Biol.* **376**:827-838.
26. Gall, J.G. 1967. Octagonal nuclear pores. *J. Cell Biol.* **32**:391-399.
27. Ghaemmaghami, S., W.K.Huh, K.Bower, R.W.Howson, A.Belle, N.Dephoure, E.K.O'Shea, and J.S.Weissman. 2003. Global analysis of protein expression in yeast. *Nature* **425**:737-741.
28. Grandi, P., V.Doye, and E.C.Hurt. 1993. Purification of NSP1 reveals complex formation with 'GLFG' nucleoporins and a novel nuclear pore protein NIC96. *EMBO J.* **12**:3061-3071.

29. Gruenbaum, Y., A.Margalit, R.D.Goldman, D.K.Shumaker, and K.L.Wilson. 2005. The nuclear lamina comes of age. *Nat. Rev. Mol. Cell Biol.* **6**:21-31.
30. Grund, S.E., T.Fischer, G.G.Cabal, O.Antunez, J.E.Perez-Ortin, and E.Hurt. 2008. The inner nuclear membrane protein Src1 associates with subtelomeric genes and alters their regulated gene expression. *J. Cell Biol.* **182**:897-910.
31. Haruki, H., J.Nishikawa, and U.K.Laemmli. 2008. The anchor-away technique: rapid, conditional establishment of yeast mutant phenotypes. *Mol. Cell* **31**:925-932.
32. Hinshaw, J.E., B.O.Carragher, and R.A.Milligan. 1992. Architecture and design of the nuclear pore complex. *Cell* **69**:1133-1141.
33. Hinshaw, J.E. and R.A.Milligan. 2003. Nuclear pore complexes exceeding eightfold rotational symmetry. *J. Struct. Biol.* **141**:259-268.
34. Hoelz, A., E.W.Debler, and G.Blobel. 2011. The structure of the nuclear pore complex. *Annu. Rev. Biochem.* **80**:613-643.
35. Hurwitz, M.E., C.Strambio-de-Castillia, and G.Blobel. 1998. Two yeast nuclear pore complex proteins involved in mRNA export form a cytoplasmically oriented subcomplex. *Proc. Natl. Acad. Sci. U. S. A* **95**:11241-11245.
36. Johnson, H.M., P.S.Subramaniam, S.Olsnes, and D.A.Jans. 2004. Trafficking and signaling pathways of nuclear localizing protein ligands and their receptors. *Bioessays* **26**:993-1004.
37. Jovanovic-Talisman, T., J.Tetenbaum-Novatt, A.S.McKenney, A.Zilman, R.Peters, M.P.Rout, and B.T.Chait. 2009. Artificial nanopores that mimic the transport selectivity of the nuclear pore complex. *Nature* **457**:1023-1027.
38. King, M.C., C.P.Lusk, and G.Blobel. 2006. Karyopherin-mediated import of integral inner nuclear membrane proteins. *Nature* **442**:1003-1007.
39. Kriwacki, R.W. and M.K.Yoon. 2011. Cell biology. Fishing in the nuclear pore. *Science* **333**:44-45.
40. Krogh, A., B.Larsson, G.von Heijne, and E.L.Sonnhammer. 2001. Predicting transmembrane protein topology with a hidden Markov model: application to complete genomes. *J. Mol. Biol.* **305**:567-580.
41. Kupke, T., C.L.Di, H.M.Muller, A.Neuner, F.Adolf, F.Wieland, W.Nickel, and E.Schiebel. 2011. Targeting of Nbp1 to the inner nuclear membrane is essential for spindle pole body duplication. *EMBO J.* **30**:3337-3352.
42. Kyte, J. and R.F.Doolittle. 1982. A simple method for displaying the hydropathic character of a protein. *J. Mol. Biol.* **157**:105-132.
43. Lin, F., D.L.Blake, I.Callebaut, I.S.Skerjanc, L.Holmer, M.W.McBurney, M.Paulin-Levasseur, and H.J.Worman. 2000. MAN1, an inner nuclear membrane protein that shares the LEM domain with lamina-associated polypeptide 2 and emerin. *J. Biol. Chem.* **275**:4840-4847.
44. Lutzmann, M., R.Kunze, A.Buerer, U.Aebi, and E.Hurt. 2002. Modular self-assembly of a Y-shaped multiprotein complex from seven nucleoporins. *EMBO J.* **21**:387-397.
45. Malik, P., N.Korfali, V.Srsen, V.Lazou, D.G.Batrakou, N.Zuleger, D.M.Kavanagh, G.S.Wilkie, M.W.Goldberg, and E.C.Schirmer. 2010. Cell-specific and lamin-dependent targeting of novel transmembrane proteins in the nuclear envelope. *Cell Mol. Life Sci.* **67**:1353-1369.
46. Mans, B.J., V.Anantharaman, L.Aravind, and E.V.Koonin. 2004. Comparative genomics, evolution and origins of the nuclear envelope and nuclear pore complex. *Cell Cycle* **3**:1612-1637.
47. Mariappan, M., A.Mateja, M.Dobosz, E.Bove, R.S.Hegde, and R.J.Keenan. 2011. The mechanism of membrane-associated steps in tail-anchored protein insertion. *Nature* **477**:61-66.
48. Mateja, A., A.Szlachcic, M.E.Downing, M.Dobosz, M.Mariappan, R.S.Hegde, and R.J.Keenan. 2009. The structural basis of tail-anchored membrane protein recognition by Get3. *Nature* **461**:361-366.
49. Mekhail, K., J.Seebacher, S.P.Gygi, and D.Moazed. 2008. Role for perinuclear chromosome tethering in maintenance of genome stability. *Nature* **456**:667-670.
50. Melcak, I., A.Hoelz, and G.Blobel. 2007. Structure of Nup58/45 suggests flexible nuclear pore diameter by intermolecular sliding. *Science* **315**:1729-1732.
51. Miyagi, A., Y.Tsunaka, T.Uchihashi, K.Mayanagi, S.Hirose, K.Morikawa, and T.Ando. 2008. Visualization of intrinsically disordered regions of proteins by high-speed atomic force microscopy. *Chemphyschem.* **9**:1859-1866.
52. Nakai, K. and P.Horton. 1999. PSORT: a program for detecting sorting signals in proteins and predicting their subcellular localization. *Trends Biochem. Sci.* **24**:34-36.
53. Nakamura, Y., T.Gojobori, and T.Ikemura. 2000. Codon usage tabulated from international DNA sequence databases: status for the year 2000. *Nucleic Acids Res.* **28**:292.
54. Onischenko, E., L.H.Stanton, A.S.Madrid, T.Kieselbach, and K.Weis. 2009. Role of the Ndc1 interaction network in yeast nuclear pore complex assembly and maintenance. *J. Cell Biol.* **185**:475-491.
55. Osborne, A.R., T.A.Rapoport, and B.B.van den. 2005. Protein translocation by the Sec61/SecY channel. *Annu. Rev. Cell Dev. Biol.* **21**:529-550.
56. Pante, N. and M.Kann. 2002. Nuclear pore complex is able to transport macromolecules with diameters of about 39 nm. *Mol. Biol. Cell* **13**:425-434.
57. Pena, A., J.Ramirez, G.Rosas, and M.Calahorra. 1995. Proton pumping and the internal pH of yeast cells, measured

with pyranine introduced by electroporation. *J. Bacteriol.* **177**:1017-1022.

58. Peters, R. 2009. Translocation through the nuclear pore: Kaps pave the way. *Bioessays* **31**:466-477.
59. Prilusky, J., C.E.Felder, T.Zeev-Ben-Mordehai, E.H.Rydberg, O.Man, J.S.Beckmann, I.Silman, and J.L.Sussman. 2005. FoldIndex: a simple tool to predict whether a given protein sequence is intrinsically unfolded. *Bioinformatics.* **21**:3435-3438.
60. Renthal, R. 2010. Helix insertion into bilayers and the evolution of membrane proteins. *Cell Mol. Life Sci.* **67**:1077-1088.
61. Rodriguez-Navarro, S., J.C.Igual, and J.E.Perez-Ortin. 2002. SRC1: an intron-containing yeast gene involved in sister chromatid segregation. *Yeast* **19**:43-54.
62. Rout, M.P., J.D.Aitchison, A.Suprapto, K.Hjertaas, Y.Zhao, and B.T.Chait. 2000. The yeast nuclear pore complex: composition, architecture, and transport mechanism. *J. Cell Biol.* **148**:635-651.
63. Schuldiner, M., J.Metz, V.Schmid, V.Denic, M.Rakwalska, H.D.Schmitt, B.Schwappach, and J.S.Weissman. 2008. The GET complex mediates insertion of tail-anchored proteins into the ER membrane. *Cell* **134**:634-645.
64. Shulga, N., N.Mosammaparast, R.Wozniak, and D.S.Goldfarb. 2000. Yeast nucleoporins involved in passive nuclear envelope permeability. *J. Cell Biol.* **149**:1027-1038.
65. Siniossoglou, S., M.Lutzmann, H.Santos-Rosa, K.Leonard, S.Mueller, U.Aebi, and E.Hurt. 2000. Structure and assembly of the Nup84p complex. *J. Cell Biol.* **149**:41-54.
66. Soullam, B. and H.J.Worman. 1995. Signals and structural features involved in integral membrane protein targeting to the inner nuclear membrane. *J. Cell Biol.* **130**:15-27.
67. Stewart, M. 2007. Molecular mechanism of the nuclear protein import cycle. *Nat. Rev. Mol. Cell Biol.* **8**:195-208.
68. Stirling, C.J. 1999. Protein targeting to the endoplasmic reticulum in yeast. 1997 Fleming Lecture. *Microbiology* **145 (Pt 5)**:991-998.
69. Strambio-de-Castillia, C., G.Blobel, and M.P.Rout. 1995. Isolation and characterization of nuclear envelopes from the yeast Saccharomyces. *J. Cell Biol.* **131**:19-31.
70. Stryer, L. and R.P.Haugland. 1967. Energy transfer: a spectroscopic ruler. *Proc. Natl. Acad. Sci. U. S. A* **58**:719-726.
71. Tapley, E.C., N.Ly, and D.A.Starr. 2011. Multiple mechanisms actively target the SUN protein UNC-84 to the inner nuclear membrane. *Mol. Biol. Cell* **22**:1739-1752.
72. Timney, B.L., J.Tetenbaum-Novatt, D.S.Agate, R.Williams, W.Zhang, B.T.Chait, and M.P.Rout. 2006. Simple kinetic relationships and nonspecific competition govern nuclear import rates in vivo. *J. Cell Biol.* **175**:579-593.
73. Turgay, Y., R.Ungricht, A.Rothballer, A.Kiss, G.Csucs, P.Horvath, and U.Kutay. 2010. A classical NLS and the SUN domain contribute to the targeting of SUN2 to the inner nuclear membrane. *EMBO J.* **29**:2262-2275.
74. Yamada, J., J.L.Phillips, S.Patel, G.Goldfien, A.Calestagne-Morelli, H.Huang, R.Reza, J.Acheson, V.V.Krishnan, S.Newsam, A.Gopinathan, E.Y.Lau, M.E.Colvin, V.N.Uversky, and M.F.Rexach. 2010. A bimodal distribution of two distinct categories of intrinsically disordered structures with separate functions in FG nucleoporins. *Mol. Cell Proteomics.* **9**:2205-2224.
75. Yang, Q., M.P.Rout, and C.W.Akey. 1998. Three-dimensional architecture of the isolated yeast nuclear pore complex: functional and evolutionary implications. *Mol. Cell* **1**:223-234.
76. Yang, W., J.Gelles, and S.M.Musser. 2004. Imaging of single-molecule translocation through nuclear pore complexes. *Proc. Natl. Acad. Sci. U. S. A* **101**:12887-12892.
77. Yavuz, S., R.Santarella-Mellwig, B.Koch, A.Jaedicke, I.W.Mattaj, and W.Antonin. 2010. NLS-mediated NPC functions of the nucleoporin Pom121. *FEBS Lett.* **584**:3292-3298.
78. Yewdell, W.T., P.Colombi, T.Makhnevych, and C.P.Lusk. 2011. Lumenal interactions in nuclear pore complex assembly and stability. *Mol. Biol. Cell* **22**:1375-1388.
79. Zilman, A., T.S.Di, T.Jovanovic-Talisman, B.T.Chait, M.P.Rout, and M.O.Magnasco. 2010. Enhancement of transport selectivity through nano-channels by non-specific competition. *PLoS. Comput. Biol.* **6**:e1000804.

Transport van membraaneiwitten naar de celkern

- Nederlandse samenvatting voor mensen buiten het vakgebied -

Inleiding

Levende organismen, zoals mensen, dieren en planten bestaan uit cellen. De cel wordt gezien als het kleinste levende onderdeel van een organisme. De mens bestaat uit ongeveer 50 biljoen cellen (dat zijn er 50 keer miljoen keer miljoen), maar er zijn ook hele kleine organismen, die uit één cel bestaan. Dat zijn onder andere de bacterie en gist.

De inhoud van de cel wordt omgeven door het celmembraan en bestaat uit het cytoplasma. Dit is een waterige omgeving waar alle onderdelen van de cel zich bevinden. Uitgezonderd bacteriën, hebben alle cellen in het cytoplasma een celkern (Fig. 1A). De inhoud van de kern wordt door een kernmembraan afgescheiden van het cytoplasma. Het kernmembraan bestaat uit twee membranen, de binnen- en buitenmembraan van de kern. In de kern wordt het erfelijke materiaal, het DNA, van de cel opgeslagen en beschermd. Het erfelijke materiaal is opgedeeld in genen, dat zijn de stukken DNA die coderen voor eiwitten. In de kern bevinden zich bijvoorbeeld ook alle factoren die nodig zijn voor de transcriptie van de genen – zo wordt het proces genoemd waar genen worden omgezet naar RNA. Het RNA wordt vervolgens vanuit de kern naar het cytoplasma getransporteerd waar het wordt getransleerd - zo wordt het proces genoemd waar een ribosoom van losse aminozuren een specifiek eiwit maakt, zoals dat op het RNA gecodeerd is. Eiwitten zijn grote, complexe moleculen die als functionele onderdelen van de cel alle cellulaire processen mogelijk maken. Hun specifieke vouwing in combinatie met de driedimensionale verdeling van de aminozuren over het molecuul, maken de eiwitten uitermate geschikt voor zeer uiteenlopende taken in de cel.

De factoren die nodig zijn voor de transcriptie van DNA in de celkern, worden in het cytoplasma gemaakt en moeten de kern in worden getransporteerd, terwijl het RNA de kern uit moet worden getransporteerd. In een levende cel vindt er dus veel transport plaats tussen de kern en het cytoplasma. Dit gebeurt via de poriën in de twee kernmembranen. Deze poriën, die de inhoud van de kern met het cytoplasma verbinden, zijn geen eenvoudige gaten waar zonder meer van alles doorheen kan stromen. Ze worden opgevuld door een eiwitcomplex in een verbluffende samenstelling. Dit eiwitcomplex in de kernporie wordt het nuclear pore complex (NPC) genoemd (Fig. 1B). De stabiele structuur van de NPC heeft een driedimensionale vorm die grofweg vergelijkbaar is met een donut (Fig. 1C en D), waarbij het transport tussen kern en cytoplasma via het gat in het midden van de donut gaat. De NPC-eiwitten in de donutring bieden de stabiliteit aan het complex en zorgen ervoor dat het binnenmembraan aaneengesloten is met het buitenmembraan van de kern zodat er een porie ontstaat door beide membranen. Tegelijk verankeren ze het complex in die porie. De NPC-eiwitten aan de binnenkant van de

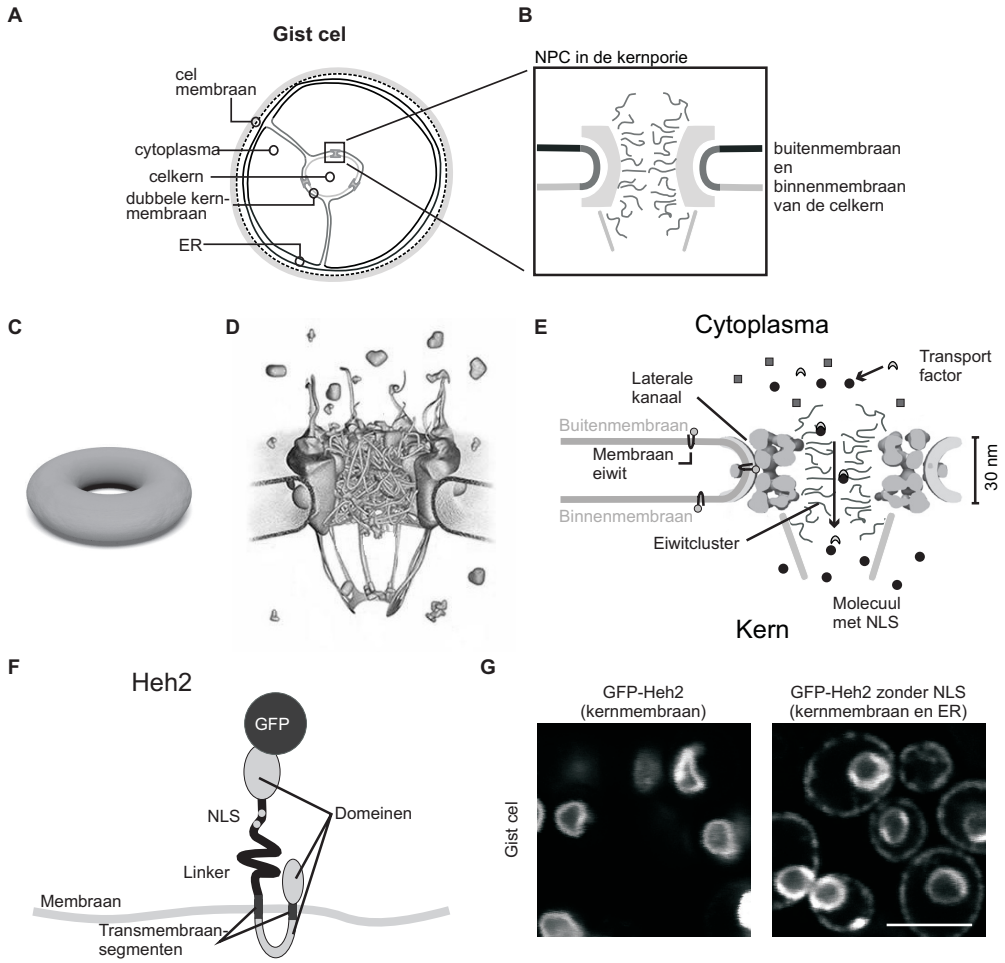

Figuur 1. De studie van membraan eiwitten in gist. A). De geometrie van een gistcel. Het celmembraan omgeeft het cytoplasma; vlak onder het celmembraan bevindt zich het endoplasmatisch reticulum (ER). Het ER is verbonden met het buitenmembraan van de celkern en via de kernporiën met het binnenmembraan. Op deze manier ontstaat er een opening door beide membranen. **B)**. In een kernporie zit een nuclear pore complex (NPC) verankerd. **C)**. De stabiele structuur van het NPC heeft grofweg een ringvorm vergelijkbaar met een donut. **D)**. De ring zit aan de buitenkant vast in de membranen van de kern, precies in de kernporie. De binnenkant van de ring is gevuld met een eiwitcluster. **E)**. Alleen moleculen met een lokalisatiesignaal voor de kern (NLS, bal) worden gebonden door een transportfactor (maan) en via de NPC naar de kern getransporteerd. Andere moleculen worden tegen gehouden (vierkant). Membraaneiwitten kunnen via de laterale kanalen in de NPC naar het binnenmembraan van de kern diffunderen. **F)**. Heh2 is gelabeld met een groene fluorescentie eiwit (GFP) en heeft verschillende domeinen. Het lokalisatiesignaal (NLS) dat het eiwit naar de kern stuurt is middels een linker verbonden aan de transmembraansegmenten. **G)**. De lokalisatie van Heh2 kon worden geobserveerd aan de hand van de fluorescentie van GFP. Heh2 met lokalisatiesignaal voor de kern werd alleen in het binnenmembraan van de kern gezien (links), maar zonder het lokalisatiesignaal zit het in het ER en in het buitenmembraan van de kern. De schaallijn is 5 μm.

donut, feitelijk in het gat, zitten aan de ene kant vast aan de structuur van het NPC maar vullen met de andere kant het gat (Fig. 1D). Op deze manier is het donut-gat gevuld met een eiwitcluster dat grote moleculen, zoals eiwitten en RNA, tegenhoud. Kleine moleculen, zoals water en zouten, kunnen gemakkelijk door de barrière van het eiwitcluster heen bewegen, maar grote moleculen moeten worden getransporteerd met behulp van een transportfactor (Fig. 1E). De transportfactor is een eiwit dat wel door de barrière in het NPC kan bewegen doordat het specifieke interacties met het eiwitcluster kan maken. Daarnaast kan het grote moleculen binden, maar alleen als deze moleculen een lokalisatie signaal voor de celkern hebben (een NLS).

De transportfactor "draagt" de moleculen (zoals eiwitten en RNA) dus over de barrière van het NPC; de moleculen kunnen dan vanuit het cytoplasma naar de kern of vanuit de kern naar het cytoplasma getransporteerd worden. Als de transportfactor met het molecuul in de kern is aangekomen, worden ze losgekoppeld en gaat de transportfactor terug naar het cytoplasma om een ander molecuul te transporteren. Het molecuul blijft achter in de kern. Op deze manier worden dus alleen eiwitten die nodig zijn in de kern gebracht en eiwitten die schadelijk zijn buiten gehouden. Het is namelijk essentieel voor eiwitten om het juiste lokalisatiesignaal te hebben die zorgen dat het eiwit op het juiste moment op de juiste plaats in de cel is.

Simpelweg kan de kern worden gezien als een middeleeuwse vestingstad in oorlogstijd. De kernmembraan is dan de ondoordringbare muur en de kernporie is de stadspoort waardoor het verkeer de stad in en uit gaat. Het NPC met het eiwitcluster is dan een stevige deur in de stadspoort, die altijd gesloten is. De moleculen met een lokalisatiesignaal, die middels een transportfactor de kern in worden gebracht, worden herkend door de portier die aan de stadspoort de wacht houdt; ze worden herkend aan hun adreslabel. De portier opent de deur voor hen en zij worden door hem binnengeleid.

Onderzoeksvraag

De meeste eiwitten die worden geproduceerd, zijn oplosbaar in het cytoplasma. Echter, een deel van de eiwitten is niet oplosbaar en wordt gedurende de translatie geïntegreerd in intracellulaire membranen. Een membraaneiwit bestaat uit minimaal één transmembraansegment die voor de verankering in het membraan zorgt, daarnaast heeft het vaak goed gevouwen en oplosbare eiwit domeinen aan het anker vast. Het genoemde netwerk van intracellulaire membranen wordt het endoplasmatisch reticulum (ER) genoemd (Fig. 1A). Het ER is onder andere betrokken bij de distributie van membraaneiwitten in de cel en dus ook naar de kernmembranen. De membranen van het ER zijn verbonden met het buitenmembraan van de celkern en via het NPC met het binnenmembraan van de celkern (Fig. 1A).

Toen ik als promovendus aan mijn wetenschappelijke onderzoek begon, was er weinig bekend over het transport van membraaneiwitten vanuit het ER naar het binnenmembraan van de celkern. Het was algemeen geaccepteerd dat membraaneiwitten vanuit het ER via het NPC de kern binnen konden stromen middels diffusie (willekeurige beweging) (Fig. 1E). De membranen zitten aan de buitenkant van de donutvorm van het NPC. Membraaneiwitten kunnen dus logischerwijs

niet via het gat in het midden van het NPC de kern in stromen. Aan de buitenkant van de donutvorm, daar waar het complex in de membranen zit verankerd, werden nauwe kanaaltjes geobserveerd, die laterale kanalen werden genoemd (Fig. 1E). De membraaneiwitten kunnen door deze laterale kanalen langs de membranen aan de buitenkant van het NPC de kern in bewegen. Aangekomen in de celkern, bevinden de membraaneiwitten zit nu in het binnenmembraan van de celkern. Hier zouden deze eiwitten dan specifiek gebonden worden door eiwitten of structuren die daar aanwezig zijn. Op deze manier kunnen sommige membraaneiwitten zich in de kern verzamelen, namelijk alleen die 1) klein genoeg zijn om door de laterale kanalen te diffunderen en 2) die gebonden worden door een bindingspartner in de kern.

Het verhaal bleek echter wat minder eenvoudig toen destijds werd aangetoond dat sommige membraaneiwitten ook een lokalisatiesignaal (NLS) voor de kern bezaten. In dit onderzoek, dat werd uitgevoerd in gistcellen, werd aangetoond dat membraaneiwitten op een vergelijkbare manier als andere (oplosbare) eiwitten gebruik maken van transportfactoren. Deze doorbraak deed bij ons verschillende nieuwe vragen rijzen, met één hoofdvraag: hoe is dit transport verenigbaar met het idee dat het NPC de vorm heeft van een donut (Fig. 1C en D)? Namelijk, gedurende het transport van membraaneiwitten over het NPC, bevindt het eiwit zich in het membraan, die zich aan de buitenkant van de donutvorm bevindt, terwijl de transportfactor bindt aan het eiwitcluster, dat zich in het midden van de donutvorm bevindt. Kortom, we vroegen ons af: hoe kan de transportfactor membraaneiwitten de kern in transporteren? We formuleerden drie hypotheses: 1) De transportfactor gaat in dit geval ook langs de buitenkant, via het laterale kanaal. 2) Het membraaneiwit komt even uit het membraan en gaat door het eiwitcluster heen. 3) De transportfactor gaat door het midden terwijl het membraaneiwit langs de buitenkant gaat en de donutring wordt "doorsneden". Wij waren erg nieuwsgierig hoe dit transport van membraaneiwitten van het ER naar de celkern kon plaatsvinden.

Experimenten

In dit onderzoek maakten we gebruik van gistcellen. Gistcellen hebben een celkern, evenals menselijke en zoogdierlijke cellen, maar zijn veel eenvoudiger te bestuderen en te manipuleren. Daarnaast was dit transport voor het eerst aangetoond in gistcellen, we konden dus eenvoudig gebruik maken van de kennis en het materiaal uit het voorgenoemde onderzoek. Gebaseerd op dit eerdere onderzoek kozen we voor het membraaneiwit Heh2 om het transport naar het binnenmembraan van de kern te bestuderen (Fig. 1F). We labelden het membraaneiwit met het groene fluorescentie eiwit GFP om de lokalisatie van het eiwit onder de microscoop te volgen (Fig. 1G. Vervolgens verwijderden we allerlei domeinen van het eiwit en bestudeerden of het eiwit nog steeds naar de kern ging (Fig. 1G, links) of niet (Fig. 1G, rechts). Wij konden bevestigen dat het membraaneiwit inderdaad een lokalisatiesignaal (NLS) had dat herkend werd door een transportfactor. We ontdekten dat de binding tussen de transportfactor en het lokalisatiesignaal van het membraaneiwit bijzonder sterk was. Verder zagen we dat het eiwit normaal gesproken bindt aan factoren in de kern, maar dat het eiwit ook zonder die interacties kon ophopen in de kern.

Tenslotte vonden we dat het domein tussen het lokalisatiesignaal en het transmembraansegment essentieel was voor het transport naar de kern (Fig. 1F). Echter, toen we dit domein gingen zuiveren en analyseren, bleek het volledig ongevouwen en erg flexibel te zijn. Verder onderzoek wees uit dat meer dan de exacte samenstelling, de lengte van dit domain belangrijk was. We namen aan dat dit domein een linker was, die de afstand spant tussen de lokalisatiesignaal (NLS) en transmembraansegment (Fig. 1F). We koppelden deze combinatie van NLS-linker aan een membraaneiwit dat standaard niet in het binnenmembraan van de kern lokaliseerd maar in het ER, en zagen dat dit eiwit vervolgens naar de kern werd gestuurd. Dit gebeurde alleen als de linker lang genoeg was en het lokalisatiesignaal aanwezig was. We concludeerden dus dat de linker een essentieel onderdeel is van het lokalisatiesignaal voor membraaneiwitten; het lokalisatiesignaal voor membraaneiwitten is kennelijk complexer dan dat voor oplosbare eiwitten. Tenslotte, deze aanwijzingen deden ons vermoeden dat de linker nodig zou zijn om de NLS met transport factor van het membraan naar het eiwitcluster in het midden van het NPC te krijgen; het transmembraansegment kan dan in het membraan blijven zitten (aan de buitenkant van de donutvorm) terwijl de transportfactor aan het lokalisatiesignaal van het membraaneiwit door het NPC kan (in het gat van de donutvorm). Om deze hypothese te bevestigen hebben we verschillende experimenten gedaan: in het meest overtuigende experiment konden we de ene kant van het membraaneiwit binden aan het eiwitcluster in het midden van het NPC, terwijl het andere uiteinde zich in de membranen bevond.

Conclusie

Al met al kwamen we tot een vrij compleet model dat de import van membraaneiwitten naar de celkern kan beschrijven (Fig. 2). Vanwege de sterke binding tussen het lokalisatiesignaal op het membraaneiwit en de transportfactor, ontstaat deze binding reeds wanneer de membraaneiwit zich in het ER bevindt. Middels diffusie bereiken het membraaneiwit en transportfactor het NPC in de buitenmembraan van de kern. Door de dynamiek en flexibiliteit van de linker kan het zich makkelijk uitstrekken zodat de transportfactor, dat gebonden is aan het lokalisatiesignaal van het membraaneiwit, in de buurt kan komen van het eiwitcluster. Er ontstaan een interacties tussen de transportfactor en het eiwitcluster in het midden van het NPC. Deze interacties zorgen ervoor dat de transportfactor door het NPC wordt getransporteerd, zoals dat gebeurt met oplosbare eiwitten. Doordat het transportfactor aan het lokalisatiesignaal gebonden zit, en dat met een linker is verbonden met de rest van het membraaneiwit, wordt het membraaneiwit meegetrokken over de NPC "getrokken" terwijl het in het membraan blijft zitten. De linker is flexibel genoeg om door de structuur van het NPC heen te "wiebelen", zodat de ring in wezen doorsneden wordt. Op basis van dit model stellen wij voor dat er, wellicht tijdelijk, openingen of gleufjes dwars door de ring heen worden gevormd.

We kunnen de analogie van de kern met een stad in oorlogstijd aanvullen met dit model. Dan zijn de membranen beekjes die door het land om de stad stromen en membraaneiwitten vlotjes die willekeurig met de stroom meedrijven. De laterale kanalen langs het NPC zijn dan

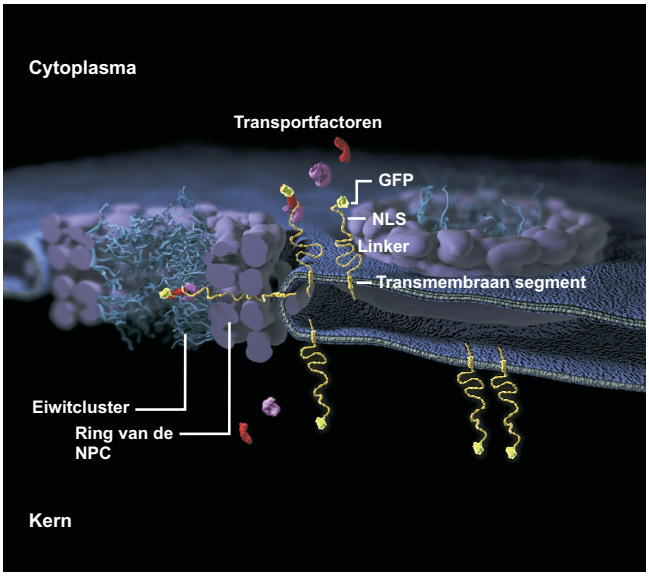

Figuur 2. Model voor het transport van membraaneiwitten over de NPC. Voor het transport bindt de transportfactor aan het lokalisatiesignaal voor de kern (NLS). De linker wordt uitgerekt, zodat de transportfactor met het eiwitcluster in het NPC kan binden. De linker beweegt door de structuur van de NPC, wellicht door gleufjes in de ring. Eenmaal in de kern laat de transportfactor het membraaneiwit weer los en gaat terug naar het cytoplasma om een volgend eiwit naar de kern te brengen. Deze artist impression van het NPC is gemaakt door Graham Johnson.

tunnels die naast de poort zitten zodat het water van de beekjes onder de muur door de stad in en uit kan stromen. Sommige membraaneiwitten kunnen de kern in bewegen, terwijl andere een lokalisatiesignaal nodig hebben. Dus sommige vlotjes kunnen zomaar de stad in stromen terwijl andere door de portier de stad binnen gehaald moeten worden. Uit ons model blijkt dan dat de portier niet het beekje inspringt om al zwemmend het vlotje door de tunnels onder de muur door te trekken.Ook haalt hij de vlotje niet uit de beek om ze de stad in te dragen en ze binnen weer terug in het water te plaatsen; de portier blijft op het droge en het vlot in het water. Namelijk, aan het vlot zit een touw met aan het uiteinde een adreslabel dat door de portier wordt herkent. De portier opent vervolgens de deur en loopt door de poort de stad binnen terwijl hij het touw vasthoudt. In de zijkant van de poort zit een gleuf waar het touw doorheen glijt zodat het vlot de stad wordt ingetrokken. In een cel betekent dit dat de transportfactor aan de NLS bindt, dat zich aan de uiteinde van de linker zich bevindt. De transportfactor gaat door het midden van het NPC en trekt het transmembraaneiwit via de linker door de membraan langs het NPC De linker snijdt dus door de structuur van de NPC en dit is alleen mogelijk als het NPC niet een gesloten ringvorm heeft. Het is namelijk nog onbekend hoe deze gleufjes er uit zien en of ze misschien alleen tijdelijk bestaan.

In perspectief

Dit model biedt allereerst een vernieuwd inzicht in het transport voor membraaneiwitten naar het binnenmembraan van de kern. Daarnaast impliceert ons model dat het NPC niet een statische donut is, maar meer als dynamisch moet worden beschouwd. En tot slot, dat er zeer lange ongevouwen domeinen in eiwitten kunnen bestaan, die zeker van belang zijn bij het functioneren

van het eiwit in de cel. Deze fundamentele biologische informatie kan relevant zijn voor medische toepassingen, aangezien fouten in membraaneiwitten aan het binnenmembraan van de kern of mislokalisatie van dergelijke eiwitten in verband worden gebracht met ernstige ziektebeelden.

We hebben een aantal humane eiwitten gevonden, die een duidelijke overeenkomst hebben met het door ons bestudeerde eiwit in gist Heh2; ze bezitten eveneens een klassiek lokalisatiesignaal dat aan het uiteinde van een linkerdomein zit. Voor de toekomende tijd verwacht ik dus dat een vergelijkbaar onderzoek in humane cellen wordt gedaan. Daarnaast wordt wellicht het bestaan van de door ons gesuggereerde kanaaltjes door de ringstructuur van het NPC beter onderzocht. Stapje voor stapje ontstaat er meer begrip van de complexe en vooral wonderlijke wereld binnen in een cel.

List of publications

Meinema AC, Poolman B, Veenhoff LM. Quantitative analysis of membrane protein transport across the nuclear pore complex. 2012. Submitted.

Meinema AC, Poolman B, Veenhoff LM. The transport of integral membrane proteins across the nuclear pore complex. *Nucleus*. 2012. In press.

Meinema AC*, Laba JK*, Hapsari RA*, Otten R, Mulder FA, Kralt A, van den Bogaart G, Lusk CP, Poolman B, Veenhoff LM. Long unfolded linkers facilitate membrane protein import through the nuclear pore complex. *Science*. 2011 Jul 1; **333**(6038):90-3.

Veenhoff LM, **Meinema AC**, Poolman B. A karyopherin acts in localized protein synthesis. *Cell Cycle*. 2010 Apr 1; **9**(7):1281-5.

van den Bogaart G*, **Meinema AC***, Krasnikov V, Veenhoff LM, Poolman B. Nuclear transport factor directs localization of protein synthesis during mitosis. *Nat Cell Biol*. 2009 Mar; **11**(3):350-6.

* Authors contributed equally to this work

Nawoord

Groningen, 2 april 2012

'Als er over vier jaar een proefschrift klaar moet liggen, kan ik het best direct beginnen'. Met die instelling begon ik op 3 september 2007 aan mijn promotieonderzoek. En vandaag, ruim vier-en-een-half jaar later, is het boekje geschreven, ligt er een vriezerlade vol met giststammen en DNA-constructen, is mijn laptop volledig versleten, maar met een harde schijf vol data en zijn veel leuke resultaten gepresenteerd en gepubliceerd. Dit avontuur van het wetenschappelijke onderzoek heb ik altijd vergeleken met een bergwandeling zonder kaart of kompas.

Toen ik begon had ik slechts een vaag idee welke kant ik op wilde; ik exploreerde wat en beliep betreden paden; ik herhaalde metingen die door anderen waren gedaan en oefende met technieken. Dit deel van de wandeling bracht me noch niet echt verder. Hoewel ik genoot van de makkelijk begaanbare wegen, wilde ik toch omhoog om meer te zien. In het voorjaar/zomer van 2008 deed ik nieuwe experimenten en verkreeg al snel een set data (Fig. 6.4 en tabel 6.1), leerde ik hoe ik data kon kwantificeren (Fig. 5.2) en kwam het onderzoek in versnelling. De wandeling ging nu echt omhoog. Het ging stapje voor stapje, maar toch, na elke nieuwe meting werden de inzichten beter; we kwamen als het ware steeds hoger op de berg en het uitzicht werd steeds duidelijker. Maar wat tijdens elke bergwandeling zonder kaart geldt, gold ook voor ons: de top die je ziet, is de top van de berg niet, de top ligt veel verder nog buiten het blikveld. Elke keer als we dachten dat we er bijna waren, werd ons verhaal niet geaccepteerd voor publicatie en moesten we weer verder. Om de echte top te bereiken, moesten we volhouden, elke keer twijfelend of we het wel zouden halen, of we niet een makkelijkere route moesten nemen.

De grote doorbraak kwam na één van de vele brainstormsessies met Liesbeth. We besloten een toen onbekend maar essentieel domein in ons eiwit te vervangen voor een volkomen willekeurige eiwitsequentie en zagen dat dit eiwit nog steeds naar de celkern werd getransporteerd (Fig. 4.5). Dit leverde vele nieuwe inzichten op, en hierdoor werd duidelijk welke richting we moesten inslaan. Een dergelijke zoektocht zonder kaart op kompas brengt je soms op verrassende plaatsen, maar dit gaat nooit via de kortste weg. Dus was de hulp van collega's en de goede samenwerking erg waardevol en essentieel voor deze expeditie. Ik ben uiteindelijk blij dat de berg is beklommen en het resulteerde in een mooie publicaties en dit proefschrift.

Ik wil dus iedereen hartelijk bedanken die een bijdrage heeft geleverd aan het onderzoek en de verwezelijking van het proefschrift. Een paar namen wil ik in het bijzonder noemen:

Allereerst wil ik mijn copromotor Liesbeth Veenhoff bedanken. Ik heb een hele goede tijd gehad onder jouw enthousiaste supervisie. Ik waardeerde de vrijheid die ik kreeg om mijn proeven te doen, terwijl je altijd beschikbaar was voor advies en discussie. De lange gesprekken die dan ontstonden, waarin we speculeerden over mogelijke modellen, vond ik erg interessant.

Bert – Bedankt dat ik in je lab de ruimte en mogelijkheden kreeg om dit werk te doen. De manier waarop je mensen vrijheid en verantwoordelijkheden gaf werkte motiverend. Ik heb veel gehad aan je suggesties een kritische commentaren.

Justyna and Astri – Thanks a lot for the collaboration. It was fun to work together on the project of membrane protein transport across the NPC. I enjoyed the time you were a student and I was really pleased to see you coming back to the lab. Thank you as well for being my paranimfs during the defense.

Geert van den Bogaart – Ik wil jou bedanken voor de hulp bij de data-analyse, de software die je schreef en de samenwerking gedurende mijn eerste maanden as promovendus.

Frans Mulder en Renée Otten – Dat jullie middels NMR lieten zien dat het linker domein in Heh2 inderdaad intrinsiek ongevouwen was, leverde het onderzoek een flinke boost op. Dank je wel voor de goede samenwerking.

Patrick Lusk and Megan King – Thanks for the valuable discussions and good comments on the manuscripts.

Victor Krasnikov – You always kept the microscopes up and running, so that I could do all the experiments I wanted, thanks for that. Further I appreciated your help with data analysis.

Ria en Gea – Fijn dat jullie het lab altijd draaiende hielden.

De leescommissie, Maarten Fornerod, Peter Lansdorp en Peter van Haastert, wil ik bedanken voor het lezen en beoordelen van mijn proefschrift.

Arend-Jan Suk en Frans Bianchi – Bedankt voor jullie inzet tijdens het studentenproject.

Thanks to al my collegues for the nice atmosphere in the lab.

Ik wil mijn familie en vrienden bedanken voor alle interesse en support.

Annemarie, ik wil jou bedanken voor de liefde en het geluk van de afgelopen jaren. Bijzonder vind ik dat we onze interesse voor macro- en microbiologische natuur delen en ons samen zo vaak verwonderen over de schoonheid van de schepping. Ik geniet van het leven met jou en met onze kleine Lise!

Ik wil mijn God en Vader bedanken voor de kracht en wijsheid die ik heb ontvangen in dit werk. Het is fasinerend om de natuur te kunnen bestuderen!

Anne Meinema